Theoretical and Photochemical studies of Some Group 6 Organometallic complexes

by

Mohammed Abid Hassan Alamiry B.Sc., M.Sc.

A thesis submitted to Dublin City University for the Degree of Doctor of Philosophy

Under the supervision of Prof. Conor Long

School of Chemical Sciences
Dublin City University

February 2005

DECLARATION

I hereby certify that this thesis, which I now submit for assessment on the programme of study leading to the award of Doctor of Philosophy is entirely my own work and has not been taken from the others save and to the extent that work has been cited and acknowledged within the text of my work

Signed: 

Date: 16.05.2005

Student ID No. 51187205

Mohammed Alamiry

Dedication

This thesis is dedicated to the soul of my brother (Mahdi), Mum, Dad, my wife Jenny, my baby Yasmin, brothers and sisters

Acknowledgements

I would like to say a most sincere thank you to all the following people, Professor Conor Long for his constant support, generous help, and guidance during the past few years. Very big thanks to Dr. Mary Pryce for her support and help. Special thanks to Johny who never hesitate to give help at any time even when he was very busy. All members past and present of CLRG research group, namely Karl, Jennifer, Kevin, Clare and Tony. My deep thanks are to everybody in the Lab. X-246 who made the past few years enjoyable and unforgettable. Special thanks are due to Noel, Bill, Fiona Lynch, Fiona Farell, Stefania, Declan and Wesely for their helps and supports. My thanks to All members of the chemistry department, especially the technicians Mick, Damen, Maurce, and Ambrose, who were always at hand when a problem arose.

A word of thanks to my close friends outside DCU Professor Ali H. Alwan and his family, Ali Hussain (UCD), Professor Fahad A. Hussien, Dr. Hamid J. Jafar, Dr. Safa Albaiaty, and Numan J. Salaman

Finally, to my wife (Jenny) and my family for their never-ending patience with the seemingly endless student life I have undertaken. Without their love and support these past few years would have been a lot more difficult. A special thanks to anyone else I have forgotten.

Abstract

Mohammed Abid Hassan Alamiry

Theoretical and Photochemical studies of Some Group 6

Organometallic complexes

This thesis consists of six chapters. Chapter 1 reviews the bonding considerations of carbonyl compounds, pyridine, and arene ligands, and recent considerations of the photochemical techniques and theoretical calculations applied to the complexes under this study.

Chapter 2 describes the photochemistry of $M(CO)_5L$, M = Cr, or W; L = Pyridine, acetylpyridine, cyanopyridine, or triphenylphosphine. This chapter also presents the steady state photolysis, laser flash photolysis and the matrix isolation studies on these complexes. Generally, the steady state photolysis of most of these complexes resulted in either ligand loss or CO loss photoproducts. In contrast with the published literature, no photochemical change was observed upon the photolysis of either $W(CO)_5Py$ or $W(CO)_5Acpy$ in the presence of excess of the ligand (0.01 M) with different broad band irradiations. Monochromatic irradiations (354.7 nm) give the tetracarbonyl complexes as precipitates from the cyclohexane solution. The photolysis of $M(CO)_5PPh_3$; M = Cr or W under CO atmosphere, resulted the formation of the corresponding hexacarbonyl, while the photolysis in the presence of excess PPh_3 ligand resulted tetracarbonyl photoproducts trans-$Cr(CO)_4(PPh_3)_2$ and cis-$W(CO)_4(PPh_3)_2$ for the chromium and tungsten complexes respectively.
The photolysis of $W(CO)_5CNpy$ in toluene in the presence of excess ligand (0.01 M) with different broad-band irradiations and also with monochromatic light produced the cyano-bond complex $W(CO)_5$(cyano-CNpy) along with the tetracarbonyl complex. Photolysis of $Cr(CO)_5Acpy$ at different wavelengths resulted the formation of linkage isomer $Cr(CO)_5$(O-Acpy). Reformation of the N-bond complex occurred at room temperature upon leaving the solution in the dark.
The analysis of the laser flash photolysis data for these complexes reveals the presence of two transient species. The first transient species is assigned to ligand loss product to form the coordinatively unsaturated $M(CO)_5$ species, while the second resulted from the CO loss process forming $M(CO)_4L$. Matrix isolation studies on the complex $Cr(CO)_5Py$ and $Cr(CO)_5Acpy$ in an argon matrix indicated both the ligand loss and CO loss process.

Chapter 3 deals with the matrix isolation studies of $(\eta^6\text{-}C_6H_5\text{-}X)Cr(CO)_3$ complexes, (X = H, NH_2, OCH_3, CHO, or COOMe) in methane, dinitrogen, 2 %, 5%, or 10 % CO-methane matrixes. The nature of the substituent on the benzene ring has been shown to affect the photochemical properties of these complexes.

The studies were extended to the molybdenum complexes. Chapter 4 presents the matrix isolation experiments on complexes of the type $(\eta^6\text{-}C_6H_5\text{-}X)Mo(CO)_3$, X = CH_3, OCH_3, or $N(CH_3)_2$ in methane, dinitrogen, 2 %, or 5 % CO-methane mixtures at 12 K. The formation of molybdenum hexacarbonyl and $(\eta^1\text{-}C_6H_5\text{-}X)Mo(CO)_3(N_2)_2$ upon the photolysis of $(\eta^6\text{-}C_6H_5\text{-}X)Mo(CO)_3$ complexes in CO-methane matrix and N_2 matrix respectively provides good evidence of that haptotropic shift.

Chapter 5 deals with the theoretical studies on the complexes of the type $Cr(CO)_5L$, L = Py, Acpy or CNpy and the complexes of the type $(C_6H_5\text{-}X)Cr(CO)_3$ complexes, (X = H, NH_2, OCH_3, CHO, or COOMe). DFT calculations provides geometries, IR

Chapter 5 deals with the theoretical studies on the complexes of the type $Cr(CO)_5L$, L = Py, Acpy or CNpy and the complexes of the type $(C_6H_5\text{-}X)Cr(CO)_3$ complexes, (X = H, NH_2, OCH_3, CHO, or COOMe). DFT calculations provides geometries, IR frequencies, and the molecular orbitals of these complexes which compared with the experimental data available.

TD DFT calculations for the first three low lying excited states of this set of complexes generally reveals that these excitation involve transition of electron from the highest occupied molecular orbital (HOMO) which carry c.a. 60 % Cr-d character to the lowest unoccupied molecular orbitals (LUMO) which are principally located on the pyridine or CO ligands. So the low lying excited state for pyridine complex is similar to that of acetyl- or cyano-pyridine complexes, and carries mainly a Cr-Py CT or Cr-CO CT character.

The electronic structure and the orbital composition for each these complexes were calculated. Many of the molecular orbitals of the benzene complex are degenerate. The degeneracy is lost upon substitution of the arene ligand. Electron-donor substituents on the arene ligand destabilise the molecular orbitals. While electron-drawing substituents stabilise the molecular orbitals. Complexes with donor substituents tend to stabilise the d_{xz} orbital and destabilize the d_{yz} orbital. The reverse occurs with electron withdrawing substituents. This was explained by considering geometry and substituent effects.
TDDFT calculations on the three lowest excited states of these complexes reveal that the transitions occur from the highest occupied molecular orbitals (HOMO), which are natively localised on chromium d-orbitals to the lowest unoccupied molecular orbitals, which are localised on the arene or CO ligands. The excitations are a mixture of mainly Cr-arene CT, Cr-CO CT and to smaller extent LF (Cr d-d) transition).

Outlined in chapter 6 are the experimental details and suggestions for future work.

TABLE OF CONTENTS

Chapter 1

Introduction

Chapter 1

Introduction

Transition metals have by definition partially filled d orbitals in at least one of their oxidation states. In low oxidation states they have the ability to form complexes with variety of neutral molecules such as carbonmonoxide, substituted phosphines, arsines, stibines, sulfides, nitric oxide and molecules with delocalised π-orbitals such as pyridine, 2,2\-bipyridine, and 1,10-phenanthrolene. Carbon monoxide (CO) is a common π-acid ligand in organometallic chemistry and the primary mode of attachment of CO to the metal atom is through the C atom.[1, 2]

The interaction of small molecules like CO, NO, N_2, H_2 and olefins to form different complexes have been extensively investigated owing not just to their structural properties but also to the important roles they play in synthesis, biological, and environmental chemistry.[3, 4]

In the following sections we will discuss complexes containing carbon monoxide, pyridine and arenes with a transition metal atom.

1.1 Some bonding considerations of carbonyl, pyridine and arene ligands: -

1.1.1 Molecular orbitals of CO: -

Fig 1.1 contains a diagram, which represent the mixing of the atomic orbitals on carbon and oxygen (with the suitable symmetry) to produce the molecular orbitals of CO. The Highest Occupied Molecular Orbital (HOMO) has mainly carbon character and points away from the C atom (σ-antibonding).

1.1.2 Bonding in Group VI metal carbonyl complexes $M(CO)_6$: -

In octahedral complexes, such as $M(CO)_6$ (M = Cr, Mo, or W) CO acts as weak donor ligand to the metal atom through a covalent bond overlap of the CO HOMO with empty e_g orbital set on the metal. In addition the Lowest Unoccupied Molecular Orbital (LUMO) on CO plays an additional role in the bonding as it overlaps with the metal orbitals of t_{2g} symmetry, Fig 1.2.

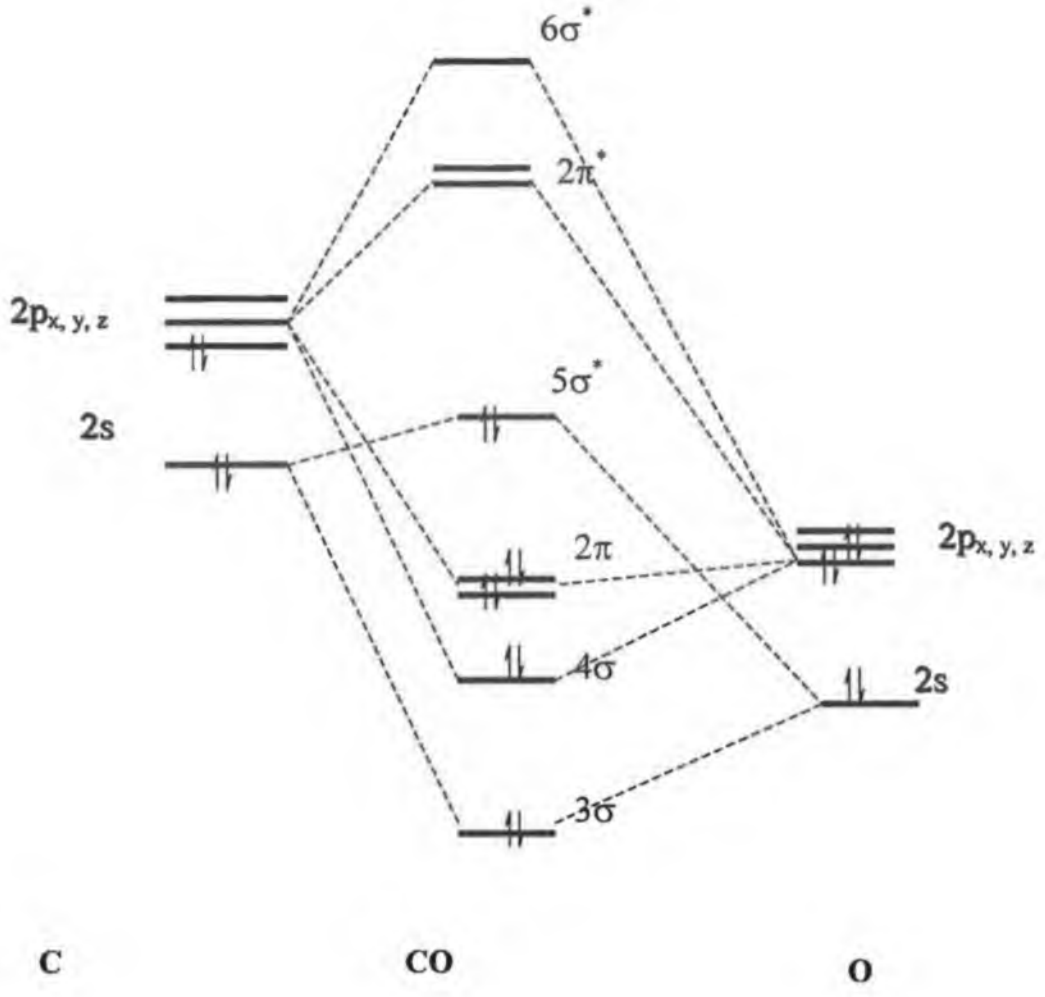

Fig. 1.1 The energy level diagram for carbonmonoxide

(a)

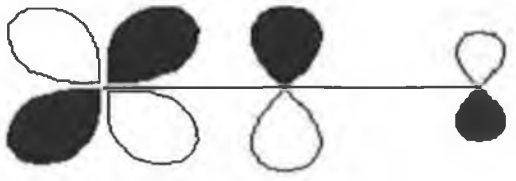

(b)

M C O

Fig 1.2 the coordination of a CO molecule to the metal atom. a) M(σ) ← CO(5σ), σ-donor interaction; b) M(π)→ CO, π-acceptor interaction, i.e. backbonding.

The effect of this π-bonding between the metal and CO ligand gives the $2t_{2g}$ molecular orbitals some bonding character and increases the M—CO bond strength. The energy splitting between the HOMO ($2t_{2g}$) and LUMO ($9t_{1u}$) is also increased leading to a blue shift of the lowest energy absorptions, and subsequently $M(CO)_6$ complexes are colourless.

All of the d-orbitals of the metal take part in the coordination with the CO ligands. Both σ and π bonding interactions result, with the e_g orbitals (d_z^2, $d_{x^2-y^2}$) directed toward the ligands providing positive overlap to form σ-bonding, and the other three d-orbitals with t_{2g} symmetry (d_{xy}, d_{xz}, d_{yz}) directed between the ligands to form π -backbonding with π^* of the six CO ligands.

The π-backbonding causes a drift of π -electron density from the metal centre and enhances the σ -donating ability of the carbonyl ligand. This is known as the synergetic effect[1].

The electronic spectra of all group 6B metal carbonyls $M(CO)_6$ (M = Cr, Mo, or W) are similar. Two intense absorption bands are observed at approximately 285 nm and about 232 nm with low-energy shoulder at ca. 310 nm. Gray and Beach[5] assigned this shoulder to vibrational components of the Ligand Field (LF) transition in the $^1T_{1g}$ excited state, which has to the $t_{2g}^5e_g^1$ configuration, Fig 1.3. The higher energy shoulders at 4.83, 4.66, and 4.54 eV in $Cr(CO)_6$, $Mo(CO)_6$, and $W(CO)_6$, respectively were assigned to the $^1T_{2g}(t_{2g}^5\, eg^1)$ LF state. These transitions involve depopulation of a metal ligand bonding orbital (i.e. t_{2g} orbital) and a population of an orbital that is strongly antibonding (i.e. e_g orbital) between the metal and the ligand. It is more likely this assignment appeared to be confirmed by the original extended Hückel [6] as well as semi-empirical INDO/S CI [7] and ab intio RHF [8] calculations.

Recent theoretical studies by Pollak and co-workers[9] using density functional calculations on the excited states of $Cr(CO)_6$ reveals that the symmetry forbidden low-energy shoulder of the first charge transfer band originates charge transfer transitions (CT) and not from LF transitions. Since the electronic spectra of $M(CO)_6$ series are very similar it is unlikely that LF states lie at lower energy in $Mo(CO)_6$ and $W(CO)_6$ than in $Cr(CO)_6$ [5, 10].

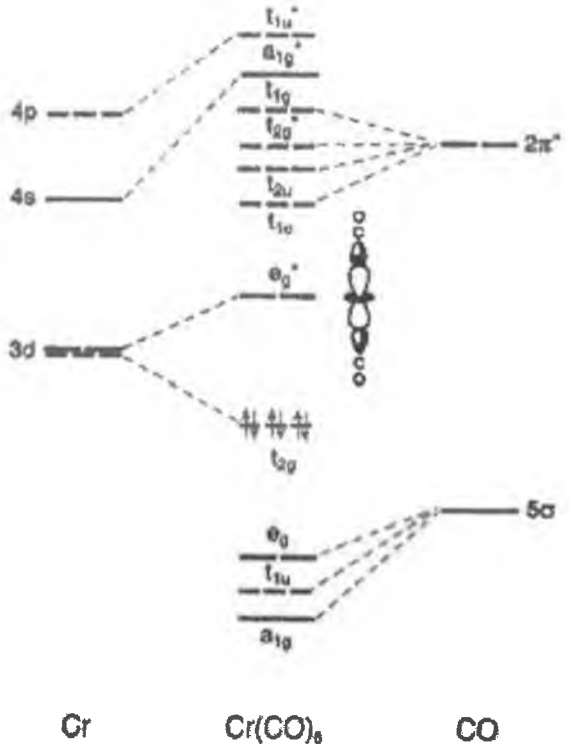

Fig. 1.3 Typical qualitative MO level diagram for a d^6 metal carbonyl, according to the LF splitting and rationalize the low-energy LF excitation and photoreactivity upon low-energy absorption. Such diagrams can provide a simple explanation for the high efficiency of CO loss following excitation. The lowest energy transition is involving the HOMO and LUMO orbitals would reduce the electrondensity in M – CO bonding orbitals, which popularity the σ^* orbitals. This would then result in a significant lablisation of M – CO interaction.[10]

The modern energy level scheme for the three group 6 metal hexacarbonyl compounds can be shown in Fig. 1.4.

Although ab intio calculations suggest that the lowest excitation state of $Cr(CO)_6$ is of CT character at equilibrium geometry, which is dissociative with respect to a CO ligand, CO dissociation is still dominated by a higher lying strongly-dissociative LF state. This can be explained by looking at the change in molecular orbitals of the $M(CO)_6$ system as one of the CO ligands is removed Fig.1.5.

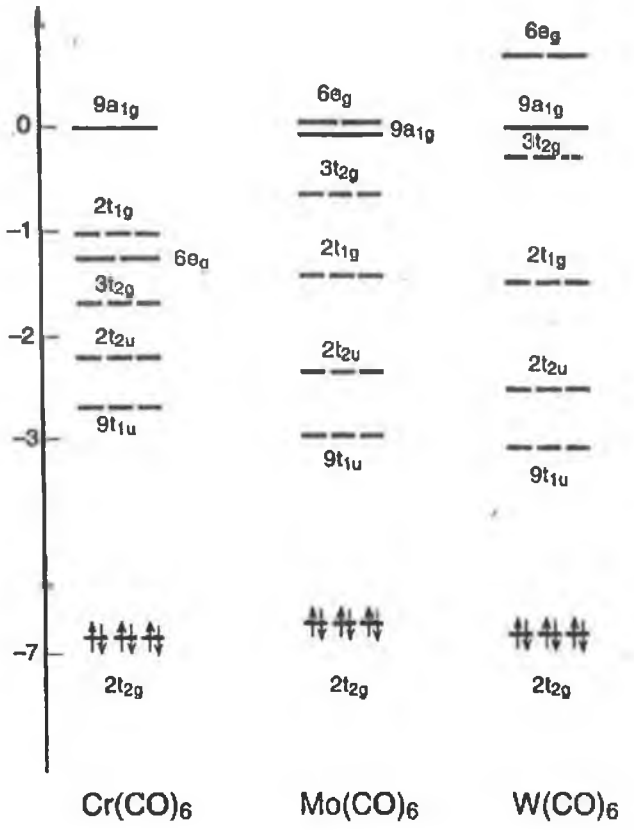

Fig. 1.4 The molecular orbital scheme of $M(CO)_6$; M = Cr, Mo, or W

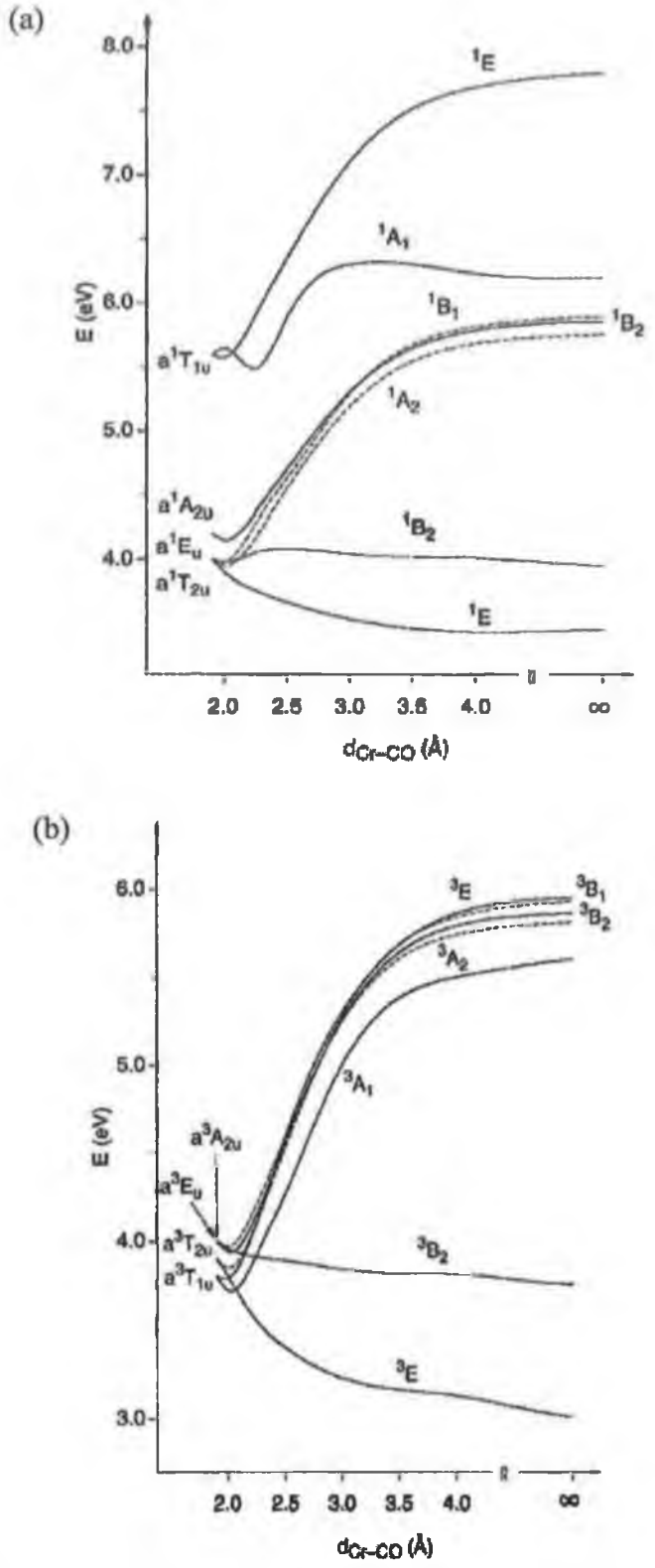

Fig. 1.5 (a) Potential energy curves (PECs) along the Cr-CO dissociation coordinate for the singlet states (in C_{4v} symmetry) arising from the lowest excited (charge-transfer) configuration, $(2t_{2g})^5(9t_{1u})^1$. (b) The same for the corresponding triplet state.[10]

1.1.3 The molecular orbitals of Pyridine and other Arenes: -

The π-molecular orbitals of benzene consist of four sets of occupied molecular orbitals, which are the singly degenerate a_{2u}, and the doubly degenerate orbitals e_{1g}, which are filled with the six π electrons. The low energy unoccupied orbitals are the doubly degenerate orbitals e_{2u} and the singly degenerate orbital b_{1g}, Fig 1.6.

Both the HOMO and LUMO energies in pyridine are lower than the corresponding orbitals in benzene[11]. Pyridine when a coordinate to the metal in (η^6) is therefore a poorer π -donor but better π - acceptor ligand than benzene.

The pyridine can be coordinated to the metal either through the nitrogen atom (η^1) or through the ring π-orbitals (η^6). When the nitrogen binds in a η^1 mode, the $\pi \rightarrow \pi^*$ transitions of the pyridine ring are not greatly affected because the bonding is directly through the lone pair on the nitrogen. The transition from the $n \rightarrow \pi^*$ level on the ring is significantly altered however and the $n \rightarrow \pi^*$ state becomes obscured by other energetically similar states.

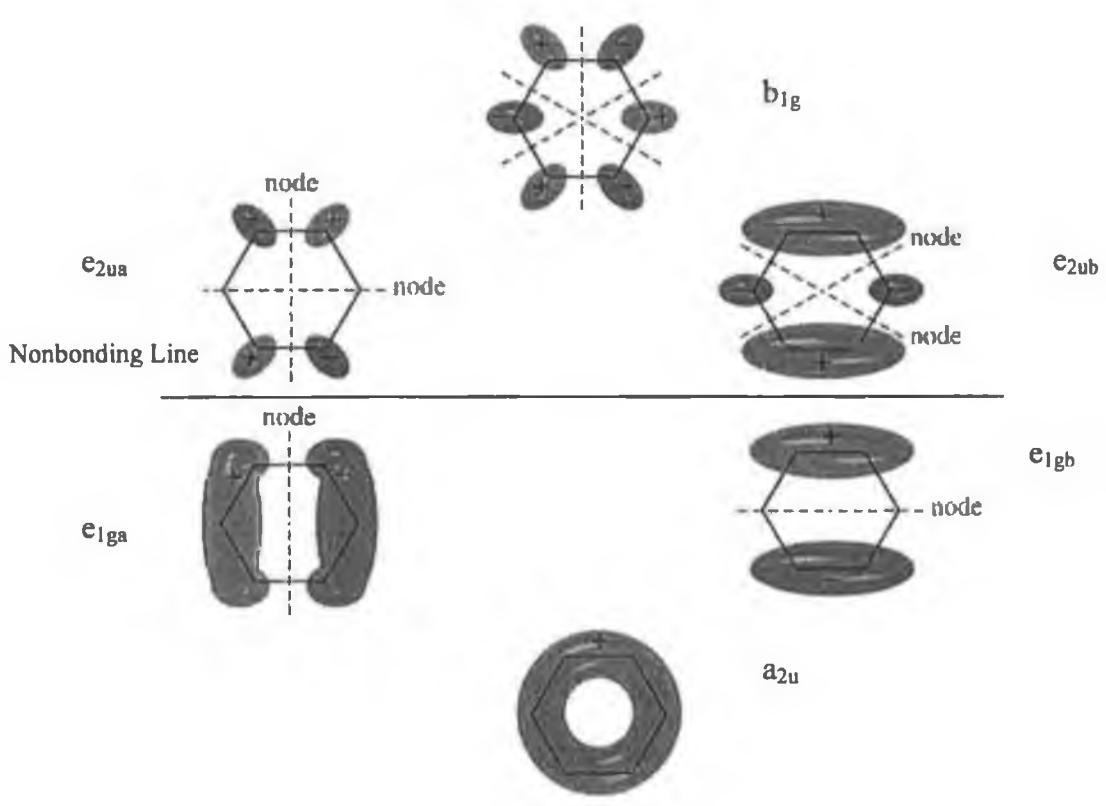

Fig.1.6 The π - molecular orbitals of benzene.

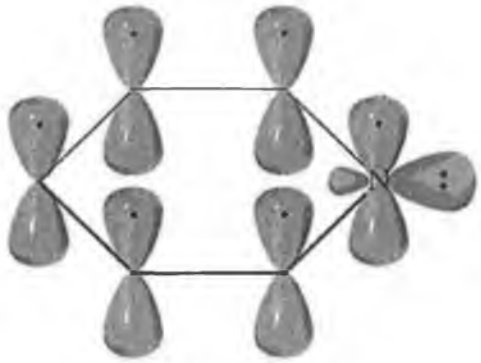

Fig.1.7 Orbital structure of pyridine. The lone pair on the nitrogen atom is perpendicular on the p_z orbitals of the carbon and nitrogen atoms so that it does not take part in the conjugation of the π bonds.

1.1.4 Metal-Arene bonding

In the case of $(\eta^6$-arene$)Cr(CO)_3$ complexes, the planar ligand lies above the metal, forming a perpendicular bond between the arene ring and the metal[12]. The π orbitals of benzene are shown below in Fig 1.8.

If the z-direction is assigned to the axis joining the metal atom nucleus and the arene ring centre, the d_z^2 orbital should have the correct symmetry to interact with the a_{2u} orbital, Fig 1.6. The interaction is inefficient as the d_z^2 orbital points at the centre of the benzene ring. The two degenerate orbitals the e_{1gb} and e_{1ga} on the benzene ring donate electrons to the d_{xz} and d_{yz} orbitals and in this instance the overlap is large. The e_{2u} set does not have the correct symmetry to interact with the metal orbitals except for weak interaction with the d_{xy} and $d_{x^2-y^2}$ orbitals, Fig 1.8. Thus benzene is a good electron donor, but a poor electron acceptor. However by introducing substituents on the arene ring electronic properties can be altered.

The vibrational studies of $(\eta^6$-arene$)M(CO)_3$[12 b] found that there is no synergistic transfer of electron density from the arene to the carbonyl ligands. Instead there are two processes donation or withdrawal to or from the metal. Both of the ligands donate electron density into the unoccupied metal d_{xz}, d_{yz} orbitals. For the arene, this is a π- interaction; for the carbonyl ligand, it is a σ-interaction. Similarly the arene accepts electron density from filled metal d_{xy}, $d_{x^2-y^2}$ orbitals in a δ-backbonding

interaction. The carbonyl ligand also withdraws electron density from these metal orbitals via a π-backbonding interaction. The vibrational analysis showed that both the π and δ interactions were important in the arene-metal bonding and suggested that σ bonding was relatively insignificant.

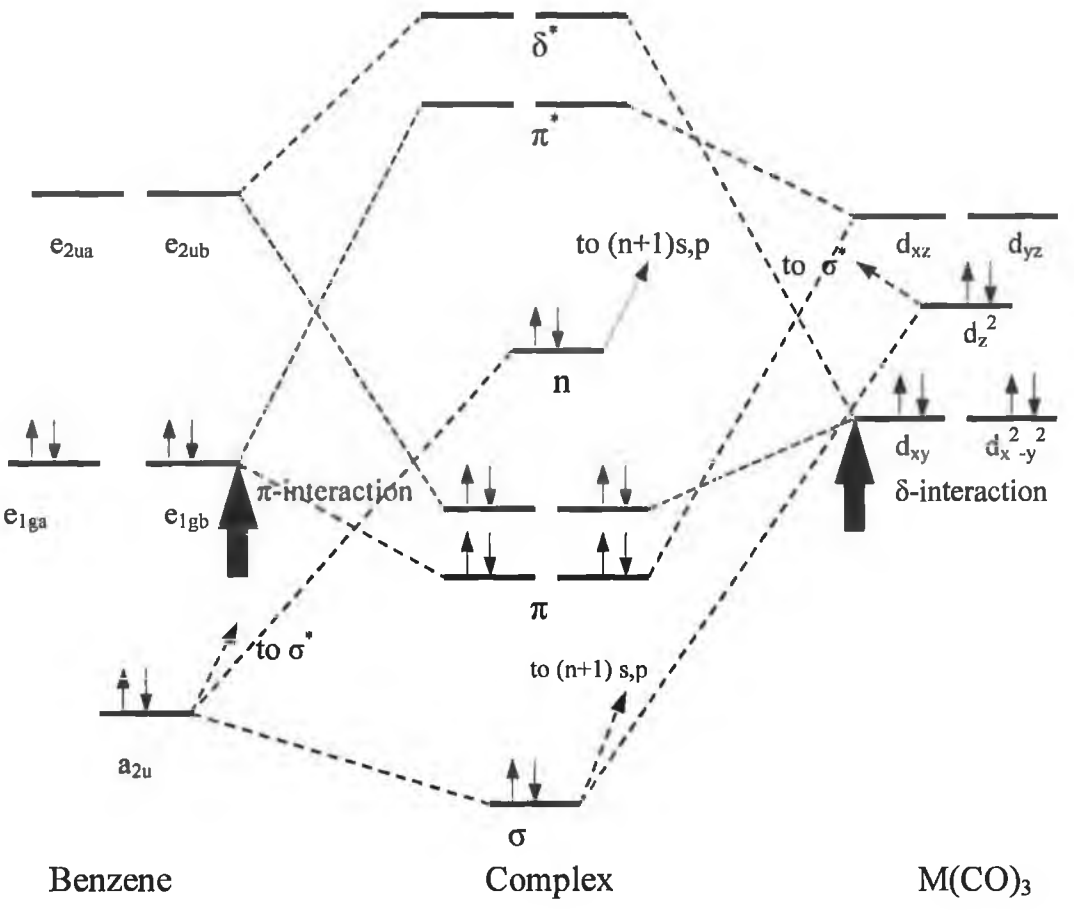

Fig 1.8 The orbital interaction diagram for the formation of (η^6-benzene)$M(CO)_3$ complexes.

1.2 The techniques are used in the study of organometallic photochemical intermediates: -

1.2.1 Time resolved techniques: -

Since many organometallic reactions are carried out at near room temperature, it is very important to observe these reaction intermediates in their natural lifetime by rapid detection techniques e.g. flash photolysis, time resolved infrared (TRIR), and time resolved resonance Raman spectroscopies (TR^3).

These fast techniques provide valuable kinetic and, in the case of TRIR, structural information, which is complementary to low temperature studies. Therefore, in many studies, structural information about reactive intermediates has been obtained by matrix isolation or liquid noble gas techniques, and the room temperature kinetics have been investigated by fast spectroscopy.[13]

1.2.1.1 Flash photolysis

This technique, pioneered by was developed in the 1950s by Norrish and Porter[14] for which they later won Nobel Prize in 1967. It involves the generation of intermediates using a short pulse of irradiation, originally form a UV flash lamp but later by a pulsed laser.[15] The transient species produced and their subsequent thermal reactions are studied by UV/vis absorption spectroscopy. Since organometallic compounds tend to have high extinction coefficients in this spectral region, detector sensitivity is not usually a problem and current technology allows femtosecound time resolution. The advantages of lasers consist of the monochromatic nature of the beam, its high intensity and short pulse duration.

The principle of this technique consists of exposing a sample to a high intensity pulse of light (e.g. laser or discharge lamp), which generates a relatively high concentration of transient species, radicals or excited molecules. By monitoring the reaction using UV/vis it is possible to determine the reactivity of the intermediates involved in the process. Unfortunately, whilst flash photolysis is able to provide kinetic data, the broad and featureless absorption bands supply little structural information.

1.2.1.2 Time resolved infrared spectroscopy (TRIR)

The initial TRIR experiments were performed by Pimentel, producing transient gas phase molecules, which were detected using a modified depressive IR spectrometer with a rapidly scanning prism, which allowed sub-millisecond time resolution[16].

Modern methods employ a point-by-point approach, which gives a resolution limited only by detector technology. The IR source is tuned to a particular frequency, and the reaction is initiated with a UV flash from a laser. The IR absorption changes are monitored with time. The process is repeated at different wavelengths until the required spectral region has been covered. In the study of transition metal carbonyls, the use of a line tuneable CO laser as the IR source has given good results. However, the spectroscopic resolution is limited to 4 cm^{-1} and the region covered is approximately 2010-1650 cm^{-1}. The use of tuneable IR diode lasers has improved the resolution (to 1 cm^{-1}), and a tuning range of 2150-1735 cm^{-1} can be achieved.

1.2.1.3 Time-resolved resonance Raman spectroscopy (TR^3)

The development of time-resolved vibrational spectroscopy has followed advances in laser and detector technology. Many advances in technology have been made since the initial TR^3 experiments[17].

The development of optical multichannel analyser (OMAs) and charge-coupled devices (CCDs) has provided the ability to measure a complete Raman spectrum for each laser pulse when the appropriate OMAs and CCDs are coupled to a single spectrograph.

Techniques have been developed to produce picosecond and femtosecound pulses for the applications in the spectroscopy.[18] Transient picosecond Raman spectroscopy has recently become an area of active research. Advances in laser technology (generation of ultrafast pulses with a stable, high repetition rate) and detection systems (such as CCDs) have helped to advance developments in this experimentally challenging area. The first experiments in this area used a single laser pulse, and the transient species was identified by subtracting a lower-power, nonphotolyzed spectrum from the higher-power spectrum.[19]

1.2.2 Matrix isolation

In matrix isolation spectroscopy, individual molecules of a chemical compound are trapped and isolated from one another in a solid, inert matrix at low temperature while their spectrum is measured. Under these conditions, the molecules cannot interact with each other and interact only weakly with the surrounding inert matrix, thereby simulating the gas phase. A prepared sample thus can be preserved as long as the matrix is maintained. However experimental difficulties usually limit the length of time available to any sample, thus, the matrix isolation technique is particularly

well suited to the study of highly reactive chemical species such as free radicals. Reactive species such as these are typically generated either in the gas phase prior to deposition in the matrix, or after deposition by *in-situ* photolysis of an appropriate matrix-isolated precursor.[20]

Matrix isolation spectroscopy is applied to reactive organometallic intermediates and processes of interest in atmospheric chemistry in order to obtain vibrational spectra of unstable reactive molecules, such as molecular metal oxides, silicon compounds, metal carbonyls and weak molecular adducts, in low-temperature matrix.

Pimentel[21] was the first to carry out matrix isolation experiments in solidified noble gases, superseding the earlier method of Lewis and co-workers[22] in the 1930's of using low temperature organic glasses. These glasses were made up of a mixture ethanol, ether and iso-pentane and formed glasses at 77 K using liquid nitrogen. The glasses formed were transparent throughout the ultraviolet/visible region. Unfortunately the organic glasses are not chemically inert to reactive species such as metal atoms and they also absorb over much of the infrared region. The technique of matrix isolation has evolved into an analytical tool suited to a vast expanse of applications, depending on detection mode employed.

The matrix isolation experiment can take a number of forms [23]: -

i) Mixing the organometallic compound with relatively inert gas especially Ar, Ne, Xe, or methane and depositing them under cryogenic conditions. Irradiation of the organometallic compound, under these conditions yields highly reactive intermediate species, which are sufficiently long lived to allow their detection at leisure by conventional spectroscopic techniques such as UV/visible, IR, or EPR spectroscopy.

ii) Hydrocarbon/polymers as matrixes: conventional frozen gas matrix experiments requires that the only the volatile and stable organometallic complex in the gaseous state. Not all organometallic compounds are volatile however. A new technique has been developed in which the organometallic complex is introduced into the hydrocarbon or polymer matrix material.

Most polymers are transparent in the frequency region between 2200 and 1600 cm^{-1}. The use of polymers at ambient temperature also permits a higher mobility of molecules within the bulk, reducing the need for high reagent concentrations, which would be required to study bimolecular processes when using frozen gases.[24]

As polyethylene (PE) does not absorb strongly in the near UV it provides a suitable medium to carry out photochemical and photophysical studies.

In the field of organometallic chemistry, polymers have been used as low temperature matrixes and for studying reactions under ambient conditions. Also, PE is stable as a solid over a much wider temperature range than gas matrixes, allowing thermodynamic and kinetic studies of thermal reactions.

Polymer matrixes have proved to be useful and versatile media, and furthermore, can overcome many of the problems inherent in gas matrix isolation.[25]

1.3 Theoretical calculations

In 1956 Orgel *et. al* [26] highlighted the potential of the molecular orbital method as a predictive tool in organometallic chemistry. Indeed he predicted the existence of iron-cyclobutadiene complexes some two years before it was actually synthesised. At that time high-speed computers were not available and this type of molecular analysis depended heavily on symmetry arguments, leading to some simplifications. During the last twenty years, the general availability of high-speed computers has led to major developments in theoretical organometallic chemistry and molecular orbital calculations have been reported at various levels of accuracy and development e.g. ab intio and density functional calculations.

1.3.1 Density Functional Theory (DFT)

Density Functional Theory (DFT) is a powerful and elegant method for evaluation a variety of ground-state properties of a system of interacting electrons with accuracy close to that of post-HF methods.[27, 28] The system can be a single atom, gas molecules, together, or adsorbed or reacted atoms of the solid surface. For systems involving *d*-block metals, DFT results are frequently in closer agreement to experimental results than are the results of HF calculations. The high accuracy of the DFT in the calculation of molecular properties such as ground state geometries, force constants, molecular energies and electronic transitions makes this method to become a popular alternative to traditional ab intio electronic structure methods.

The advances of two theoretical arguments resulted the growth of DFT methods. The first is the time-independent Schrödinger equation (Equation 1.1). Solution to Schrödinger equation determines the energy and structure of a molecule. Practically

it is not feasible to do so for any systems other than hydrogen atom due to the so-called many body problems.

$$H\Psi = E\Psi \qquad 1.1$$

The second achievement by Fermi and Thomas[29], who expressed the total energy of the system as a function of the total electron density (this provided an alternative to solving the many-electron Schrödinger equation). However it wasn't until the 1960s that Hohenberg and Kohn[28] formulated the theorems, which underpin DFT, and later Kohn and Sham developed the practical computational scheme, which is now used for DFT.

1.3.1.1 Basic concepts for DFT calculations

DFT calculations start with the electron probability density thus for a system with n-number of electrons, there are 4n coordinates (x, y, z and a spin term), however the electron density is equal to the product of the wavefunction with its complex conjugate, integrated over (n-1) electron coordinates which is dependent only on three coordinates and is independent of the number of electrons. The Hohenberg-Kohn theorem states that the ground state energy E is uniquely determined by the corresponding electron density ρ(r) (Equation 1.2).

$$E = E[\rho(r)] \qquad 1.2$$

This provides the ability to approximate all chemical properties (e.g. the exchange-correlation energy) based on ρ (density functional theory). The result is a surprising success of the DFT to describe the energetics of materials. The total energy has three terms, a kinetic energy, a Columbic energy due to electrostatic forces between the charged particles in the system and the exchange correlation function, which deals with the many-body interactions. Kohn-Sham showed that the exact ground state electronic energy is represented by:

$$E_{KS} = V + \langle hP \rangle + 1/2\langle PJ(P) \rangle + E_X[P] + E_C[P] \qquad 1.3$$

$E_X[P]$ is the exchange functional

$E_C[P]$ is the correlation functional.

V The nuclear repulsion energy.

P The density matrix.

<hP> The one-electron (kinetic plus potential) energy

1/2<PJ(P)> The classical coulomb repulsion of the electrons.

Hartree-Fock theory can be considered as a special case of density functional theory, with $E_X[P]$ given by the exchange integral -1/2<PK(P)> and E_C=0. The functionals normally used in density functional theory are integrals of some function of the density and possibly the density gradient:

$$E_X[P] = \int f(\rho_\alpha(r),\rho_\beta(r), \nabla\rho_\alpha(r), \nabla\rho_\beta(r))dr \qquad 1.4$$

Where the methods differ in which function f is used for E_X and which (if any) f is used for E_C. In addition to pure DFT methods, the gaussian suite of programmes used in this study support hybrid methods in which the exchange functional is a linear combination of the Hartree-Fock exchange and a functional integral of the above form. Proposed functionals lead to integrals, which cannot be evaluated in closed form and are solved by numerical quadrature.

The exact ground state electronic energy of an n-electron system is represented by: -

$$E(\rho)=-\frac{\hbar^2}{2me}\sum_{i=1}^{n}\int\psi_i^*(r_1)\nabla_1^2\psi_i dr-\sum_{I=1}^{N}\int\frac{Z_1e^2}{4\pi\varepsilon_{01}r_{I1}}\rho(r_1)dr_1+\frac{1}{2}\int\frac{\rho(r_1)\rho(r_2)e^2}{4\pi\varepsilon_0 r_{12}}dr_1dr_2+E_{xc}[\rho]$$

Where ψ are the Kohn-Sham orbitals (these can be found by solving the Kohn-Sham equation). These must first be calculated to obtain the electron density before solving the equation above.

A number of DFT functionals (or methodologies) have been developed in the field of computational chemistry. In this thesis, a hybrid of the Becke-style 3 parameter functional [30] (which includes a mixture of a Hartree-Fock and DFT exchange functionals) and the Lee, Yang, and Parr[31] gradient corrected correlation energy functional (which is parameterised by fitting to empirical data for the He atom), known as B3LYP.

1.3.1.2 The computational procedure of solving Kohn Sham equation: -

The flow chart for the computational procedure for KS SCF coverage is shown in Fig 1.9.[32] The first step is choosing of the basis set among wide range of basis sets can be used in the DFT calculations. Continuing with the choosing of the molecular

geometry of the molecule. Then the overlap integrals and the kinetic energy and nuclear-attraction integrals are computed. New orbitals are determined from the solution of the secular equation, the density is determined from those orbitals, and it is compared to the density from the preceding iteration. Once the SCF is achieved, the energy is computed. At this point either the calculations finished or if the geometry optimisation is the goal, a determination of whether the structure corresponds to stationary point is made.

1.3.1.3 Excited states

The calculation of excited-state properties typically requires significantly more computational effort than is needed for the ground states.[32]

Exploring the energetically lowest lying state of each spatial or spin irreducible representation of the system is possible with density functional techniques.[34] As these techniques represent the ground state in that particular symmetry as shown by Gunnarsson and Lundqvist.[35]

It is quite difficult to calculate the properties of molecules in their electronic excited states, especially for relatively large molecular systems. Compared to the ground state studies, few calculations have been published for excited states, and even fewer considered changes in the molecular structure upon excitation. However many photochemical processes require excited state geometry optimisations as significant conformational relaxations take place after photoexcitation.

Time-dependent density-functional theory (TDDFT) is an extension of density-functional theory to time-dependent problems, and can be viewed as an alternative formulation of time-dependent quantum mechanics.

TDDFT is usually most successful for low-energy excitations, because the KS orbitals energies for orbitals that are high up in the virtual manifold are typically quite poor[32]. Casida, Casida, and Salahub[36] have suggested that TDDFT results are most reliable if the following two criteria are met:

(i) The excitation energy should be significantly smaller than the molecular ionisation potential (note that excitations from occupied orbitals below the HOMO are allowed)

(ii) Promotions should not take place into orbitals having positive KS eignvalues.

Efforts to improve TDDFT for higher excitations have shown some early success. Tozer and Handy[37] have proposed a correction procedure to deliver

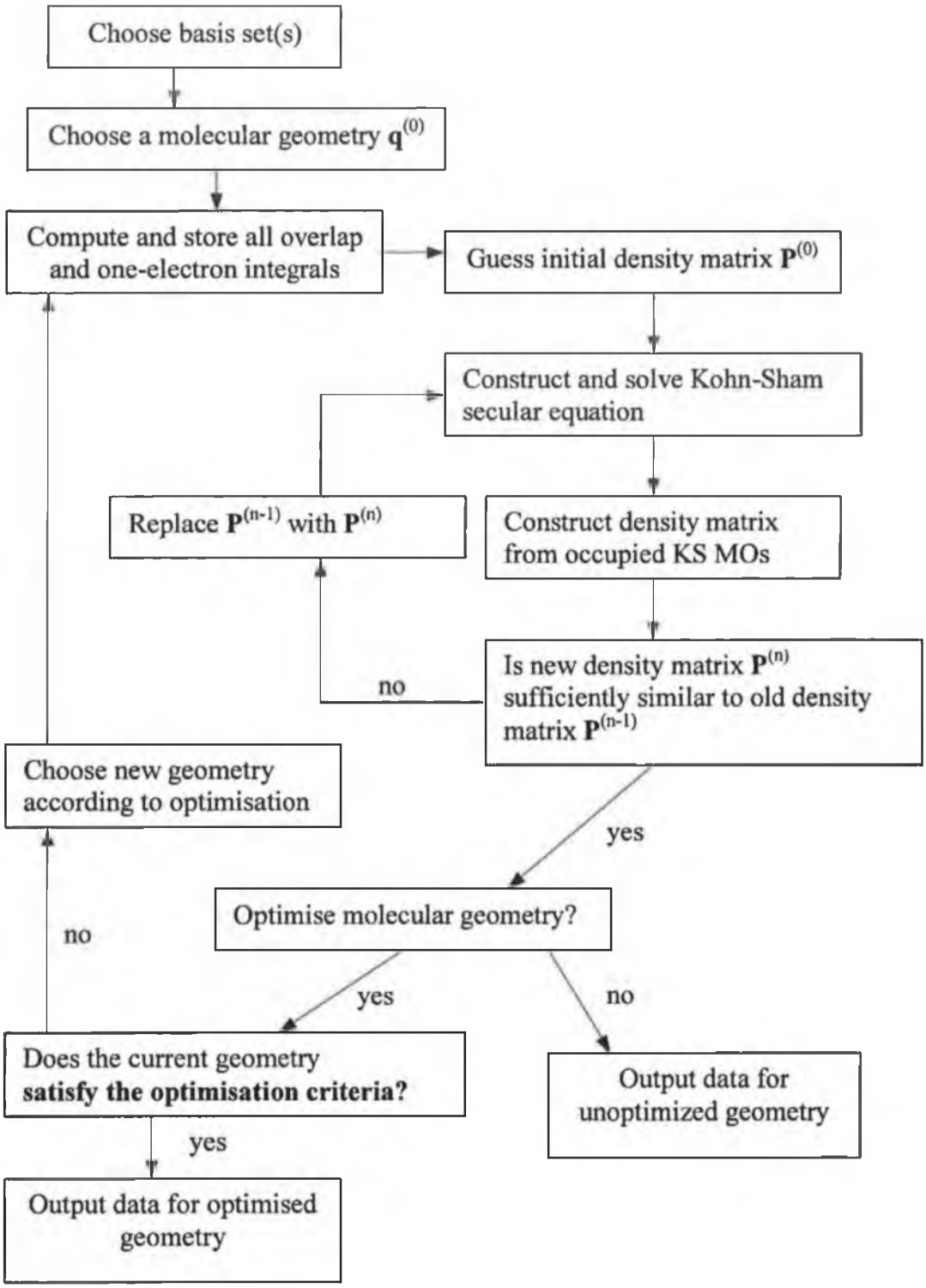

Fig 1.9 Flow chart of the Kohn-Sham SCF procedure.[32]

functionals having asymptotically correct potentials, and Adamo and Barone[38] have demonstrated that the hybrid PBE1PBE functional, for reasons that are not entirely clear, seems to be significantly less affected by high energy errors than other hybrid functionals. Further developments aimed at

correcting systematic errors in TDDFT offer great promise for future applications.

1.4 References: -

1) Cotton, F.A.; Wilkinson, G., *Advanced Inorganic Chemistry, A comprehensive Text*, Fifth edition, John Wiley, 1987.

2) Green Wood, N.N.; Earnshaw, A., *Chemistry of the elements*, First edition, Pregamon press, 1986.

3) Kawaguchi, S., *Inorganic Chemistry Concepts*, Vol. II, Springer-Vilag, 1988.

4). Hughes, M. N, *The inorganic Chemistry of Biological Processes*, second edition, Wiley, 1988.

5) Gray, H. B., Beach, N., *J. Am. Chem. Soc.,* 1963, 85, 2922.

6) Beach, N., Gray, H. B., *J. Am. Chem. Soc.,* 1968, 90, 5721.

7) Kottzian, M.; Rösch, N.; Schröder, H.; Zerner, M.C., *J. Am. Chem. Soc.*, 1989, 111, 7687.

8) Pierloot, K.; Verbeke, J.; Vanquickenborne, L.G.; *Inorg. Chem.,* 1989, 28, 3059.

9) Pollak, C.; Rose, A.; E.J., *J. Am. Chem. Soc.*, 1997, 119, 7324.

10) a) Baerends, E. J.; Rosa, A., *Coord. Chem. Rev.*, 1998, 177, 97. b) Rosa, A.; Baerends, E. J.; Gisbergen, S. J. A. van; Lenthe, E. van; Groeneveld, J. A.; Snijders, J. G.; *J. Am. Chem. Soc.,* 1999, 121, 10356.

11) L Jorgenson, W.; Salem, L., *The organic Chemists Book of Orbitals*; Academic Press; New York, 1973.

12) a) Ellian, M.; Chen, M.M.I.; Mingos, D.M.P.; Hoffiman, R., *Inorg. Chem.* 1976, 15, 149. b) Barnes, C.M.; Kennedy, B. J., *J. Mol. Struc.*, 1995, 344, 233. c) Armstrong, R.S.; Aroney, M.J.; Barnes, C.M.; Nugent, K.W., *J. Mol. Sturc.*, 1994, 323, 15. d) Armstrong, R.S.; Aroney, M.J.; Barnes, C.M.; Nugent, K.W., *J. Organomet. Chem.,* 1990,4, 569.

13) a) Creaven; B. S.; Dixon, A. J.; Kelly, J. M.; Long, C.; Poliakoff, M., *Organometallics*, 1987, 6, 2600. b) Hodges, P.M.; Jackson, S.A.; Jacke, J.; Poliakoff, M.; Turner, J.J.; Grevels, F.W., *J. Am. Chem. Soc.,* 1990, 112, 1234. c) Jackson,

S.A.; Hodges, P.M.; Poliakoff, M.; Turner, J.J.; Grevels, F.W.; *J. Am. Chem. Soc.*, 1990, 112, 1221.

14) Norrish, R.G.; Porter, G., *Nature*, 1949, 164, 658.

15) Shank, C.V., *Science*, 1983, 219, 1027.

16) Pimentel, G.C.; Tan, L.Y.; Winer, A.M., *J. Chem. Phys.*, 1972, 57, 4028.

17) a) Wilbrandt, R., *Biospectroscopy*, 1996, 2, 263. b) Wilbrandt, R.; Jenson, N.H.; Pagsberg, P.; Sillesen, A. H.; Hanson, K. B.; *Nature*, 1978, 276, 167. c) Dallinger, R. F.; Woodruff, W. H., *J. Am. Chem. Soc.*, 1979, 101, 4391.

18) a) *Ultra fast phenomena IX*; Barbara, P. F., Ed; Springer-Verlag, Berlin, 1994; p 1976. (b) Simon, J. D., *Rev. Sci. Instrum.*, 1989, 60, 3597. (c) Squir, J.; Mourou, G., *Laser Focus World*, 1992, 28, 51.

19) Delhay, M., *Lasers in physical chemistry and biophysics;* Elsevier: Amsterdam, 1975; p213.) ((a) Gustafson, T. L.; Roberts, D. M.; Chernoff, D. A., *J. Chem. Phys.* 1983, 79, 1559. (b) Hopkins, J. B.; Renzepis, P. M. *Chem. Phys. Lett.* 1986, 124, 79. (c) Atkinson, G. H.; Brack, T. L.; Blanchard, D.; Rumbles, G. *Chem. Phys.* 1989, 131, 1. (d) Reid, P. J.; Doig, S. J.; Mathies, R. A. *Chem. Phys. Lett.* 1989, 156, 163. (e) Iwata, K.; Hamaguchi, H. *Chem. Phys. Lett.* 1992, 196, 462.).

20) Almond, M. J. *Short-Lived Molecules,* Ellis Horwood, Chichester, England, 1990.

21) Whittle, E.; Dows, D. A; Pimentel, G.C., *J. Chem. Phys.*, 1954, 22, 1943.

22) Lewis, G. N.; Lipkin, D., *J. Am. Chem. Soc.*, 1942, 64, 2801.

23) Dunkin, I. R., *Matrix-Isolation Techniques, A practical Approach*, Oxford University Press, Oxford, 1998.

24) De Paoli, M. A.; De Oliveira, S. M.; Galembeck, F., *J. Organomet. Chem.*, 1980, 193, 105.

25) Baldenius, K.U.; campen, A.K.; Höhnk, H.D.; Rest, A.J.; *J. Mol. Struct.*1987, 157, 295.; Campen, A.K.; Rest, A.J.; Ollino, M.A., *Inorg. Chim. Acta.*, 1991, 180, 133. Campen, A.K.; Rest, A.J.; Yoshihara, K., *J. Photochem. Photobiol. A: Chem.*, 1991, 55, 301.; Rest, A.J., *J. Mol. Struct.*1990, 222, 87; Cooper, A.I., *PhD thesis*, University of Nottingham, 1994.

26) Orgel, L.E., *Introduction to transition-metal chemistry*, Methuen, London, 1960.

27) Kohn, W.; Sham, L.J., *Phys. Rev.*, 1965, 140, A1133.

28) Hohenberg, P., Kohn, W. *Phys. Rev.*, 1964, 136, B864.

29) Bickelhaupt, F. M.; Baernds, E. J., *Rev. Comput. Chem.*, 2000, 15, 1.

30) Becke, A. D., *Phys. Rev. B,* 1988, 38, 3098.

31) Lee, C.; Yang, W.; Parr, R.G., *Phys. Rev. B,* 1988, 37, 785.

32) Cramer, C. J., *Essentials of the computational chemistry, Theories and Models*, Wiley, West Sussex, 2004.

33) Yang, L.; Ren, A.M.; Feng, J.K.; Liu, X.D.; Ma, Y.G.; Zhang, H.X., *Inorg. Chem.*, 2004, 43, 19, 5961.

34) Koch, W.; Holthausen, M.C.A., *Chemist's Guide to density Functional Theory*; Wiley-VCH, Weinheim, Germany, 2000.

35) Gunnarsson, O.; Hjeimberg, H.; Lundqvist, B. I., *Surf. Sci.*, 1977, 63, 348.

36) Casida, M. E., Casida, K.C., Salahub, D.R., *Int. J. Quantum Chem.*, 1998, 70, 933.

37) Tozer, D.J.; Handy, N. C., *J. Chem. Phys.,* 1998, 109, 10180.

38) Adamo, C.; Barone, V., *Chem. Phys. Lett.,* 1999, 314, 152.

Chapter 2

The Photochemical Substitution Reactions of Group 6 Metal Carbonyl Compounds $M(CO)_5L$, M = Cr, Mo, or W; L = pyridine, pyridine derivatives, or phosphines

Chapter 2

The Photochemical substitution reactions of group 6 Metal carbonyl compounds $M(CO)_5L$

2.1) Literature survey: -

During the last four decades, extensive photochemical investigations on the group 6 metal carbonyl compounds have been reported. The photochemical substitution reaction of carbonyl ligands in group 6 metal carbonyls $M(CO)_6$, M = Cr, Mo, or W yields the coordinatively unsaturated species $M(CO)_5$ which reacts with the ligand L to give the complex $M(CO)_5L$, reactions 2.1, 2.2.

$$M(CO)_6 \xrightarrow{h\upsilon} M(CO)_5 + CO \qquad 2.1$$

$$M(CO)_5 + L \xrightarrow{\Delta} M(CO)_5L \qquad 2.2$$

Strohmeier[1] determined that the quantum yield ϕ of the primary photochemical step (Reaction 2.1) was independent of the central atom M and the donor ligand L at least for the excitation wavelengths λ = 366 or 436 nm.

The thermal reaction of L with $M(CO)_5$ (reaction 2.2) is dependent on the nature of L, and M. In addition some of the librated CO gas remains dissolved in the solvent and takes part in the reverse reaction.

Selective formation of $M(CO)_5L$ derivatives can be aided by allowing only a small conversion to prevent competitive absorption of light by the product, or by first forming a photostable $M(CO)_5L`$ complex followed by thermal exchange of L` by L. THF can be used as L` in the synthesis of $M(CO)_5L$ where L itself is photosensitive.[1]

There have been many investigations of the photochemistry of $M(CO)_5L$ complexes. In many instances the photolysis of $M(CO)_5L$ leads to loss of the ligand L, while there are some reports of the photochemical loss of CO, reactions 2.3, and 2.4: -

$$M(CO)_5L \xrightarrow{h\nu} M(CO)_5 + L \qquad 2.3$$

$$M(CO)_5L \xrightarrow{h\nu} M(CO)_4L + CO \qquad 2.4$$

In the presence of the excess ligand, the first reaction (i.e. Reaction 2.3) leads simply to ligand exchange with the other ligand present in the solution while the second reaction leads to two geometrical isomers cis and trans $M(CO)_4L_2$. The relative

efficiencies of the two processes were found to be very sensitive to the nature of the ligand L.

Reactions 2.3 and 2.4 exhibit wavelength dependent photochemistry resulting in varieties in the quantum efficiencies for different excitation wavelengths as presented in Table 2.1 (M = W; L = Pyridine).

$\lambda_{exc.}$, nm	Φ_{CO}	Φ_L
436	0.00	0.63
366	0.01	0.50
313	0.03	0.38
254	0.04	0.34

Table 2-1 The quantum efficiencies for the loss of unique ligand L (Φ_L) or CO (Φ_{CO}) from $W(CO)_5Py$ at various excitation wavelengths.[2]

L	Φ_L		Nature of Lowest Energy Excited State
	436 nm	514 nm	
3,4-Dimetylpyridine	0.53		LF
4-Methylpyridine	0.55		LF
Pyridine	0.62		LF
3-Bromopyridine	0.66		LF
3-Acetylpyridine	0.75		LF
3-Benzoylpyridine	0.73		LF
3,5-Dibromopyridine	0.82		LF
4-Benzoylpyridine	0.12	0.02	W→L CT
4-Cyanopyridine	0.12	0.02	W→L CT
4-Acetylpyridine	0.15	0.02	W→L CT
4-Formylpyridine	0.05	0.002	W→L CT
Piperidine	0.58		LF

Table 2.2 Photosubstitution of L in $W(CO)_5L$ by 1-pentene in isooctane as solvent.[3]

Wrighton *et al.* [2] published a series of papers on the investigation of the photosubstitution reactivity of $W(CO)_5L$ complexes (L = substituted pyridine). In all

cases they observed photosubstitution of L upon irradiation into the lowest-energy absorption band.

From Table 2.2 we can see that the quantum efficiency for the unique ligand substitution for compounds containing electron-withdrawing constituents on the 4-postion on the pyridine ligand is lower than the unsubstituted pyridine. As an explanation for these results, Wrighton suggested that the W → LCT transition has lower energy than LF transition and the latter is responsible for the unique ligand substitution. In the pyridine complex however the W → LCT transition is higher in energy than LF transition.

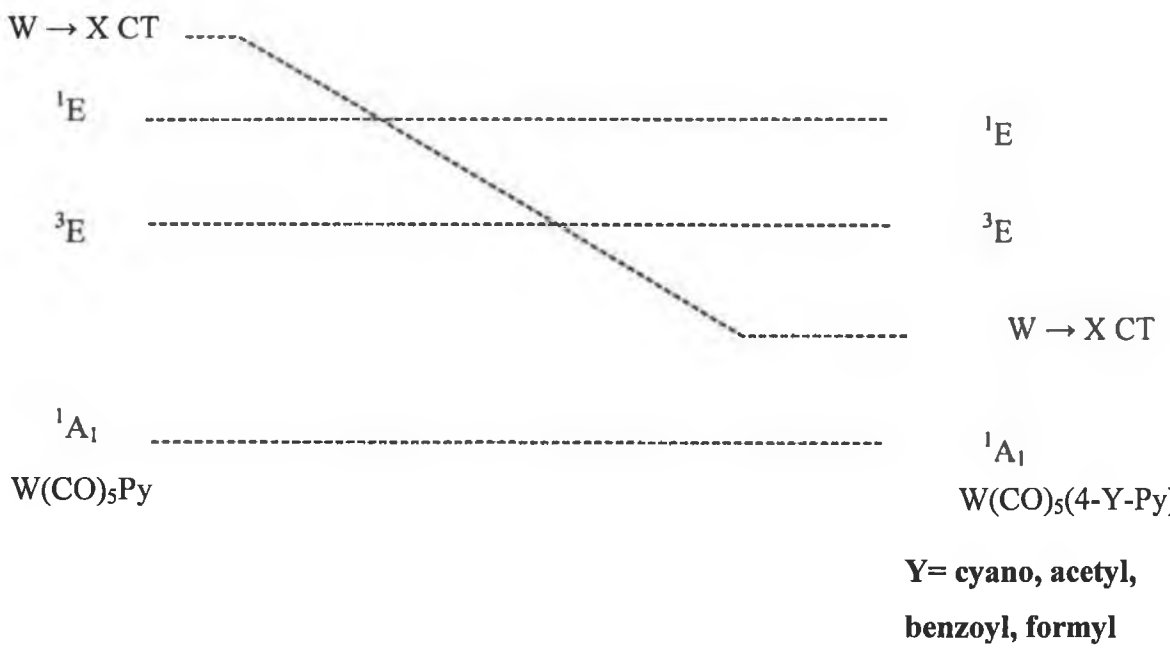

Fig.2.1 Correlation of lowest excited state and substitution efficiencies as suggested by Wrighton [2]

Both the spectral and photochemical data indicate that these complexes fall into two distinct classes[4]: -

1) Those bands which traditionally assigned as lowest energy LF absorption bands, emission lifetime close to 1 μ sec and high Φ_L values (0.5-0.8) and

2) Those with lowest energy MLCT absorption, emission lifetimes in the range 15-40 μ sec. and much smaller; λ irr dependent Φ_L values.

Since the properties of the first group are closely analogous to those of the piperidine complex which does not possess low lying π^* orbitals it was concluded

that these complexes have lowest energy LF states, and the second class of complexes have lowest energy MLCT states.

A higher quantum yield of CO ejection was found after short wavelength irradiation and/or in going from M = W to Mo or Cr. A reduction of the quantum efficiency is found when a MLCT state is the lowest in energy for ligands having low-lying π orbitals. For the two photochemical processes (i.e. pyridine ligand loss and CO loss) the total reaction quantum yield was less than unity, showing that radiative and non-radiative deactivation processes must be involved.[2]

Very weak emissions with decays in fluid solution have been observed for complexes of the type $W(CO)_5L$, where L = pyridine, piperidine, diethyl methylamine, triethylamine, 2,4,6-trimethylpyridine, 2-acetylpyridine, 2-benzoylpyridine.[3] The more electron withdrawing subsistents give rise to lower energy MLCT excited states, when the ligand subsistent is the acetyl, benzoyl, cyano, or formyl groups in the 4- position on the pyridine ring. Thus for these systems, the MLCT excited state moves below the LF excited state. The $W(CO)_5L$ complexes which have MLCT excited state as the lowest-energy absorption features exhibit measurable luminescence and relatively long radiative decays in fluid solution. These observation support those made previously for $W(CO)_5L$ complexes in EPA glasses.

Kolodziej and Lees[4] studied the quantum yields of $Mo(CO)_5L$ complexes (L = 3-cyanopyridine, and 4-cyanopyridine) with triphenylphosphine in benzene using different irradiation wavelengths. From these results they noted that the complexes with low lying LF excited state have significantly more photoactive than complexes in which the MLCT state is lowest lying. Furthermore the quantum yields for each of these complexes decrease as the irradiation wavelength was increased.

When studying the photolysis of $W(CO)_5$(4-cyanopyridine) in methylcyclohexane, Lees and Adamson observed loss of the isosbestic point.[5] They assigned this to secondary reactions forming binuclear products. However in the presence of 0.1 M ethanol the substitution product was $W(CO)_5(C_2H_5OH)$ and the reaction appears to be uncomplicated by side or subsequent reactions. The quantum yield is 0.021± 10%. Photosubstitution quantum yields for CO vs. amine dissociation for complexes of the type $M(CO)_5$ (amine) (M = Cr, Mo, or W; amine = piperidine, or pyridine) in the presence of ^{13}C-labled carbonmonoxide as entering ligand were found to be highly dependent on the metal centre.[6] The chromium complexes exhibiting greater propensity for CO dissociation as opposed to amine loss, while the molybdenum and

tungsten compounds were shown to undergo amine dissociation with a greater quantum efficiency than CO loss.

The stereochemical position of an incoming ^{13}CO ligand showed that CO dissociation is exclusively cis to the amine ligand. This means that the only stable form of the [$M(CO)_4$amine] intermediate is the Cs isomer and also that this intermediate does not scramble CO groups during its life time in solution.

The photosubstitution chemistry of the compounds $W(CO)_5L$ (L = NH_3 , pyridine , piperidine, PPh_3 , PBr_3 , PCl_3 , PH_3 , $P(n\text{-}Bu)_3$ have been studied by Dahlgren and Zink [8].They found that for L = NH_3, piperidine, and pyridine $\Phi_1 \approx 0.5$; $\Phi_2 \leq 10^{-2}$ (Φ_1, and Φ_2 are the quantum efficiencies of the substitution of L and CO respectively) while for L = PPh_3, PBr_3, PCl_3, PH_3, or $P(n\text{-}Bu)_3$), $\Phi_1 \cong \Phi_2 \cong 0.3$.

The ligand photosubstitution chemistry of $Mo(CO)_5PPh_3$ has been demonstrated by Darensbourg and Murphy [7] to proceed with a high quantum efficiency for CO loss ($\lambda_{366} = 0.58$). When this reaction was carried out in the presence of either PPh_3 or ^{13}CO both cis and trans primary photoproducts were observed. Presumably this results from the incoming ligand trapping the $Mo(CO)_4PPh_3$ intermediate in its C_s or C_{4v} isomeric forms respectively. On the other hand, the quantum efficiency for unique the loss of PPh_3 was only 0.11 at 366 nm. The trans-$Mo(CO)_4(PPh_3)_2$ complex was found to undergo photoisomerisation to the cis-$Mo(CO)_4(PPh_3)_2$ isomer via loss of PPh_3 followed by subsequent rearrangement of $Mo(CO)_4PPh_3$ C_{4v} intermediate to the C_s analogue prior to recapture of PPh_3.

Lees *et al.*[9] found that the reaction of $W(CO)_5$(THF) with 4-cyanopyridine (4-CNpy) leads to two linkage isomers of $W(CO)_5$(4-CNpy), in which one is bound through the ring nitrogen and the other through cyano nitrogen. The later is thermally unstable in solution and converts to the pyridine-bound species by a first-order process. A kinetic analysis revealed that this thermal reaction takes place via an interamolecular mechanism.

2.1.1 Flash photolysis studies of group 6 hexacarbonyl complexes and their monosubstituted amine and phosphines derivatives

Dougherty and Heilweil[10] used Femtosecound transient absorption studies to monitor the formation of $M(CO)_5$(n-hexane) after UV excitation of $M(CO)_6$ complexes, M = Cr, Mo, or W complex in hexane solution.

Moralejo and Langford[11] using picosecond time relaxation the photolysis of $W(CO)_6$ and $W(CO)_5L$ in cyclohexane where is L = Py, Pip, presented evidence for the

formation of the solvated species $W(CO)_5S$ which forms in less than 20 ps. They also considered the evidence from picosecond spectra for competition between different trapping pathways. Fig 2.2 shows the transient absorption on the pico second time scale following photolysis of $W(CO)_6$, $W(CO)_5$ Py, $W(CO)_5$(piperidine)

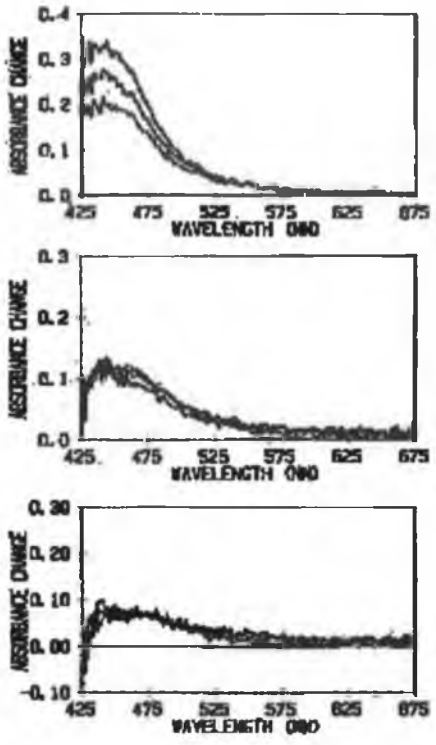

Fig. 2.2 Transient absorption spectra of $W(CO)_5$ in cyclohexane between 0 and 50 ps, which were formed during the picosecond flash photolysis of (a)$W(CO)_6$, (b)$W(CO)_5$Py, and (c)$W(CO)_5$Pip respectively.[10]

Johnson and co-workers[12] studied the structure of $W(CO)_5L$ (L = Py or piperidine) in low temperature glasses by fast time-resolved IR spectroscopy and found after irradiation with 354.7 nm (the lowest ligand field excited state (LF)) that ν_{CO} vibrational frequencies and C-O force constants decrease on promotion into the lowest energy excited state. In addition the C-O bond lengths all increase, and the change in the force constants between the excited and ground state is considerably greater for the equatorial than for the axial CO groups.

Because $W(CO)_5$Acpy is soluble in both polar and non-polar solvents, Clark and co-workers[13] used time resolved infrared spectroscopy to study the υ_{CO} bandwidths of the MLCT excited state bands of this complex. Considerably broader excited state

bands were observed in polar solvents (such as CH_2Cl_2) indicating that the broadening of the υ_{CO} bands is a consequence of solvent-solute interactions.

Excited states, with no charge transfer character, exhibit no such broadening of υ_{CO} bands upon excitation and consequently it was concluded that the υ_{CO} bands in the excited state of CO-containing transition metal species can be used a probe of the nature of the excited state.

In order to understand the early excited state dynamics of $W(CO)_5$(4-CNpy) and $W(CO)_5$(4-formylpyridine), Lindsay et al. ,[14] studied the picosecond time-resolved absorption spectra of these complexes following excitation into the ligand field transition (354.7 nm) and for the later complex also into MLCT (532 nm) absorption bands. They concluded that the temporal changes observed are due to the kinetics of the formation of vibrationally cold ^{3}MLCT state by a ^{1}MLCT$\rightarrow^3$MLCT or ^{1}LF $\rightarrow^3$MLCT intersystems crossing (ISC).

Turner et al., used time resolved infrared spectroscopy to study the photochemistry of $W(CO)_5$(4-CNpy)[15] and $W(CO)_5$(4-Acpy)[16] following population of the metal to 4-CNpy or to 4-Acpy charge transfer states ($\lambda_{exc.}$ = 510 nm) in either methylcyclohexane or heptane. Here the CO stretching vibration shifts to higher energy upon excitation, confirming that in the excited state the metal centre is oxidized. The excited state decays to the ground state and via the LF excited state, which decomposes to $W(CO)_5$ and 4-CNpy or 4-Acpy. The rate constants for these processes are $4x10^{-6}$ s^{-1} for 4-CNpy complex and 2.6 x $10^{-6}s^{-1}$ for 4-Acpy complex suggesting that there is a rapid equilibrium between the MLCT and LF states.

2.1.2 Matrix isolation studies of $M(CO)_6$ and $M(CO)_5L$ complexes, M = Cr, Mo, or W; L = pyridine, pyridine derivatives, or phosphines: -

In early 1960's Sheline and co-workers[17] obtained IR spectra for $M(CO)_5$ intermediates after photolysis of $M(CO)_6$ at 77 K in methylcyclohexane glasses. The IR spectra suggested that $M(CO)_5$ had C_{4v} symmetry

In 1971 Turner and Poliakoff, [18] obtained 16-electron $M(CO)_5$ species upon photolysis of $M(CO)_6$ (M = Cr , Mo, or W) in argon or methane matrixes at 20 K. In addition to the matrix splitting effects they observed four bands upon photolysis, one of these at 2140 cm^{-1} which indicated the presence of uncoordinated CO, a further three bands were assigned to $Cr(CO)_5$ fragment with C_{4v} symmetry

The reaction of Cr atoms with CO at 4.2-10 K was investigated by Kündig and Özen,[19] who observed the formation of $Cr(CO)_5$ with D_{3h} symmetry.

Turner *et al.* [20] carried out an in depth study of the group 6 metalhexacarbonyl complexes in a variety of matrixes, employing both UV/visible and infrared detection. When $Cr(CO)_6$ was photolysed in a methane matrix new IR spectrum was produced, which was indicative of a $Cr(CO)_5$ species with C_{4V} symmetry. A visible band was observed that grew in the same rate, clearly this band could also be assigned to the C_{4v} $Cr(CO)_5$ species. With all hexacarbonyl complexes and in a variety of matrixes, it was possible to regenerate the parent $M(CO)_6$ by long wavelength photolysis into the visible band. The visible band position was extremely sensitive to the matrix, varying from 624 nm in Ne to 489 nm in methane, Table 2.3. This sensitivity to the matrix environment was not observed in the IR spectrum, where variations in the ν_{CO} bands with matrix were not significant. It was necessary to determine if this variation was the result of interaction between $Cr(CO)_5$ and the matrix or alternatively a general solvent effect. The calculation carried out demonstrated the change in the intensity of the high frequency A_1 band from $Cr(CO)_5$-Ar to $Cr(CO)_5$-Xe was caused by a decrease in the axial-radial bond angle of about 4°. Any change in this angle has dramatic affect on the energies of the molecular orbitals.

Matrix	nm	cm^{-1}
Ne	624	16 000
SF_4	560	17 900
CF4	547	18,300
Ar	533	18 800
Kr	518	19 300
Xe	492	20 300
CH_4	489	20 400

Table 2.3 Comparison of the visible bands of $Cr(CO)_5$ in matrix experiments [20]

Rest *et al* [21], reported the matrix isolation of $W(CO)_5L$, where L = pyridine, 3-bromopyridine, or H_2S in an argon or CH_4 matrixes at 12 K. Upon the photolysis with broad band ($320 < \lambda < 390$nm), new IR bands at 1962.5 and 1930.7 cm^{-1} were produced in all cases. No absorption band at 2138 cm^{-1}, the region associated with

the production of CO in a matrix was observed, therefore they assigned these bands (i.e. the bands at 1962.5 and 1930.7 cm^{-1}) to $W(CO)_5$ species. The reaction shown to be photochromic since subsequent uv irradiation with visible light regenerates $W(CO)_5L$. They also provided further evidence for the formation of $W(CO)_5$, by conducting the experiment in CO or nitrogen matrixes. Photolysis produced $W(CO)_6$ and $W(CO)_5N_2$ respectively.

Balk *et al.* [22] reported the matrix isolation of $[Cr(CO)_5(pydz)]$ (pydz=pyridazine) in argon or methane matrixes at 10 K. These compounds were chosen because they exhibit MLCT absorption bands at low energy compared is the ligand-field band. The photolysis in both matrixes with short wavelength radiation (λ =254 nm) resulted primarily in the formation of $Cr(CO)_4(pydz)$ with Cs symmetry and free CO. Photolysis with longer wavelengths (i.e. λ=366 or 436 nm) resulted the formation of both $Cr(CO)_5$ and cis-$Cr(CO)_4(pydz)$. The yield of the second species was high compared to other $[Cr(CO)_5(N\text{-donor})]$ complexes.

Boxhoorn *et al* [23]provided good evidence for the formation of cis-$W(CO)_4Py$ upon short wavelength photolysis (λ = 229 and 254 nm). This species has four CO stretching bands at 2033.1, 1912.9, 1906.2, and 1879.6 cm^{-1}. In contrast to the results obtained with the $Cr(CO)_5Py$ complex, almost the same quantum yield was found for the formation of $W(CO)_5$ after short wavelength photolysis.

Black *et al* [24] studied the photolysis of $Mo(CO)_5PCx_3$ (Cx = Cyclohexyl) in hydrocarbon glasses and found the generation of $Mo(CO)_4PCx_3$ which has two isomers (i.e. cis and trans isomers). Similar results were obtained by Poliakoff [25] using matrix isolation techniques on complexes of the type $M(CO)_5CS$. The formation of both cis and trans isomers of $M(CO)_4CS$ was observed with no evidence for the formation of either $M(CO)_5$ or free CS.

Dobson *et al* [26] reported the characterisation of cis and trans isomers of $W(CO)_4PPh_3$, upon photolysis of $W(CO)_5PPh_3$ in argon matrix at 20 K and that the two isomers could be photchemically inter-converted.

Goff *et al* [27] reported, the photolysis of $W(CO)_5CS$ in polyethylene matrix under N_2 and H_2 atmospheres at 190 K. The photolysis gave five and three product bands under N_2 and H_2 respectively along with one ν(N-N) band. These bands were assigned to $W(CO)_4CS(L)$, (L = N_2 or H_2). Visible photolysis with (λ_{exc}>400 nm) of cis- $W(CO)_4CS(L)$ provided evidence of cis → trans photoisomerisation.

Broadband UV photolysis (300< λ <400 nm) favours formation of the cis-compounds, possibly due to photoisomerisation of the trans-isomer at these wavelengths. Both $W(CO)_4CS(N_2)$ and $W(CO)_4CS(H_2)$ react with CO above 190 K to re-form $W(CO)_5CS$.

Boxhoorn *et al.*[28] studied the photochemistry of $Cr(CO)_5PCl_3$, $Cr(CO)_5Py$ and $Cr(CO)_5$Pyrazine in argon matrixes at 10 K and found that upon photolysis of $Cr(CO)_5PCl_3$ with different wavelengths (λ = 229, 254, 280, 313 or 366 nm) formation of $Cr(CO)_5$ resulted while the photolysis of $Cr(CO)_5Py$ or $Cr(CO)_5$Pyrazine generated CO or the unique ligand loss depending on the excitation wavelength. The irradiation with longer wavelengths (such as λ = 405 or 436 nm) produced $Cr(CO)_5$, while the irradiation with shorter wavelengths (229, 254, 280, or 313 nm) the main product was cis-$Cr(CO)_4L$, (L = Py or Pyrazine).

Pope and Wrighton.[29] studied the wavelength dependence of light induced loss of either CO or alkene from $W(CO)_5$(alkene), where alkene = C_2H_4, C_3H_6, 1-C_5H_{10} in methyl cyclohexane at 77 K. The loss of CO is more efficient following shorter wavelength photolysis for the smaller alkenes.

The photolysis of $W(CO)_5PCl_3$ in argon matrix at 10 K with short wavelengths light (λ = 229, 254, 280, 313, or 366 nm) has also been studied[30] and resulted to the loss of PCl_3. No evidence for the formation of $W(CO)_4PCl_3$ was obtained in these studies.

2.1.3 The role of MLCT or LF excited states in the photochemistry of $M(CO)_5L$ complexes

As mentioned in Chapter 1, The understanding to the contribution of ligand field states to the photochemical dissociation of metal-ligand bonds have changed in recent years.

The traditional picture of photoinduced ligand loss, assigned the main role to LF and not to MLCT states. This provided an explanation for the efficient loss of pyridine ligand upon photolysis of $W(CO)_5Py$ while the loss of Acpy was less efficient. Wrighton suggested that the MLCT band in pyridine complex lies at higher energy than the LF while the reverse is true for Acpy and CNpy systems.

Modern theoretical calculations using TDDFT and other ab intio calculations highlighted the important role of the MLCT state in the photochemistry, and

photophysics of systems like $[M(CO)_5L]$ M= Cr, or W; L = pyridine; and $M(CO)_4(L_2)$ where; L_2 = Bidentate diammine ligand.

Goumans *et. al.*[31] used time-dependent DFT theory to explore the photochemistry of the phosphine-substituted transition metal carbonyl complexes $Cr(CO)_5PH_3$. The lowest excited states of $Cr(CO)_5PH_3$ are metal-to-ligand (CO) charge transfer (MLCT(CO)) states, of which the first three are repulsive for PH_3 but modestly bonding for the axial and equatorial CO ligands. The repulsive nature is due to mixing of the initial MLCT state with a ligand field (LF) state. A barrier is encountered along the dissociation coordinate if the avoided crossing between these states occurs beyond the equilibrium distance. This is the case for the expulsion of CO but for the PH_3 group, as the avoided state crossing occurs within the equilibrium Cr-P distance. The nature of the phosphorus ligand in this Cr complex is only of modest importance. Complexes containing the three-membered phosphirane or unsaturated phosphirene rings have dissociation curves for their lowest excited states that are similar to those having a PH_3 ligand. Analysis of their ground state Cr–P bond properties in conjunction with frontier orbital arguments indicate these small heterocyclic groups differ from the PH_3 group mainly by their enhanced σ-donating ability. All calculations indicate that the excited $Cr(CO)_5L$ molecules (L = PH_3, $P(C_2H_5)_3$ or $P(C_2H_3)_3$) prefer dissociation of their phosphorus ligand over that of a CO ligand.

The recent study of Záliš *et al* [32] who used a combination of picosecond time-resolved IR and resonance Raman spectroscopy and TD-DFT calculations to investigate the roles of the W→L and W→CO MLCT and LF excited states for $W(CO)_5$(Pip) and $W(CO)_5$(CNpy). They found that the molecular orbitals are largely delocalised and the distribution of d-character is over more molecular orbitals than predicated by simple LF arguments. When L is a strong π-acceptor (e.g. L = CNpy, Py), complexes will have a predominantly π^*(L) LUMO. It is closely followed in energy by a set of low-lying cis CO π^* orbitals. When L is ligand has no π-system (Pip) the complex has a predominantly cis CO π^*-based LUMO, followed by molecular orbitals of the same cis π^*(CO) character. Orbitals with significant d (σ^*) contribution are also rather delocalised. So the low lying electronic transitions and excited states of $[W(CO)_5L]$ and related complexes are of a W→L and W→CO MLCT character. No LF transitions were found to occur in a spectroscopically relevant energy range up to 6-7 eV. The lowest excited states have MLCT (CO) character for weakly electron-accepting or saturated ligands L (Pip, Py) and MLCT

(L) character for strongly accepting L (PyCN). Spectroscopy, photophysics, and photochemistry of $[W(CO)_5L]$ and related complexes are described by the MLCT(L)/(CO) model in which the absorption, emission, and W-N bond dissociation are determined by closely lying MLCT(L) and MLCT(CO) excited states while the high-lying LF states play only an indirect photochemical role by modifying potential energy curves of MLCT(CO) states, making them dissociative.

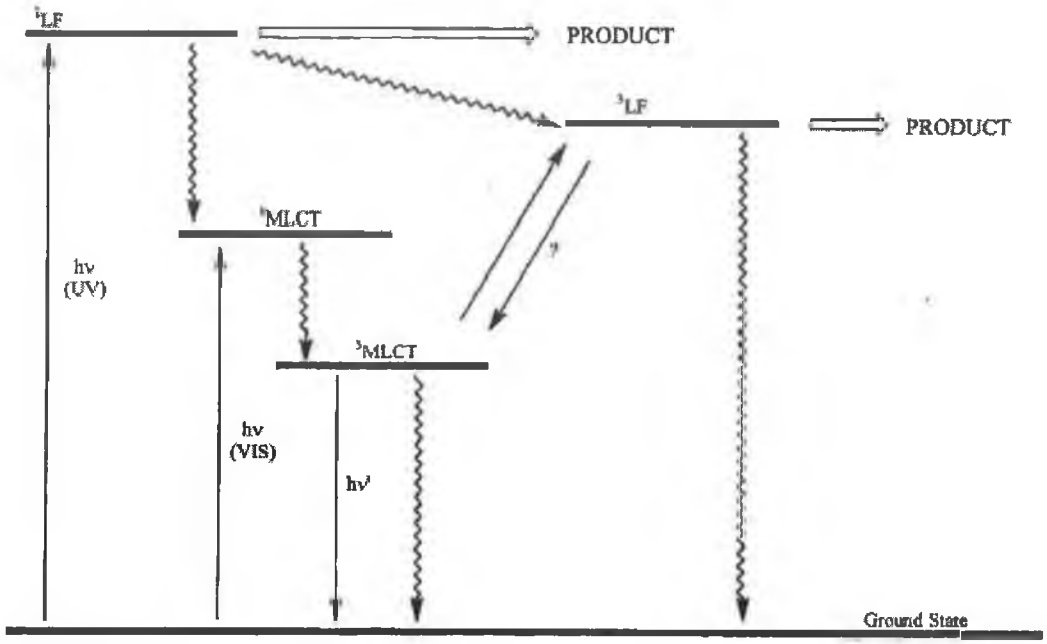

Fig 2.3 Jablonski diagram describing the delayed ligand photosubstitution of $W(CO)_5$(py-X) and related complexes. Visible irradiation excites the GS→^{1}MLCT transition. The ^{1}MLCT state relaxes to long-lived ^{3}MLCT state, from which the reactive ^{3}LF state is populated thermally. UV irradiation excites the GS→^{1}LF transition. The ^{1}LF state undergoes ligand dissociation and/or it relaxes to the reactive ^{3}LF state.[32]

2.2 Results

Three techniques have been used to investigate the photochemistry of complexes of the type $M(CO)_5L$, M = Cr, or W; L= pyridine, 4-acetylpyridine, 4-cyanopyridine, or triphenylphosphine. These techniques are: -

- Steady state photolysis: - to monitor the photochemical reactions at room temperature using UV/vis., IR, and occasionally NMR spectroscopy.
- Laser Flash Photolysis: - to obtain kinetic data (life time of the transient species and rate constants) for their reactions using UV/vis.
- Matrix Isolation: - to identify reactive intermediates, two complexes have been studied in this study, $Cr(CO)_5Py$, and $Cr(CO)_5Acpy$ in argon matrixes at 12 K.

2.2.1 Steady state photolysis of the complexes of the type $M(CO)_5L$, M = Cr, or W; L= pyridine, 4-acetylpyridine, 4-cyanopyridine, or triphenylphosphine

2.2.1.1 Steady state photolysis of $Cr(CO)_5Py$ complex: -

The steady state photolysis of $Cr(CO)_5Py$ (Py = Pyridine) in cyclohexane in the presence of excess pyridine ligand (0.01 M pyridine) was undertaken using various broad band irradiations (i.e. filters >410nm, >340nm). In these experiments a significant change in the UV/vis. absorption spectra was only observed using wavelengths greater than 340nm were used, Fig 2.4. Similar changes were also observed following photolysis using monochromatic light $\lambda_{exc.}$ 354.7 nm. Two new bands centred at 450 and 340 nm were formed which are assigned to the formation of the tetracarbonyl complex cis-$Cr(CO)_4Py_2$[7].

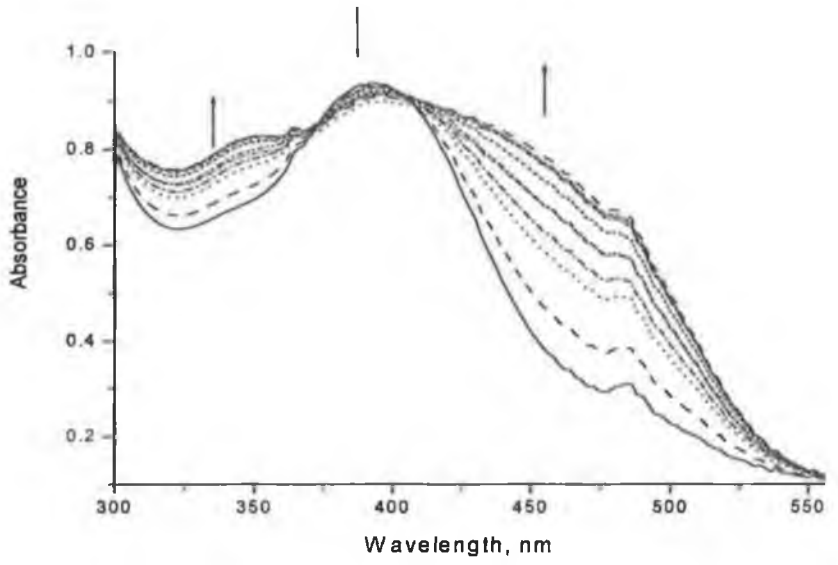

Fig 2.4 UV/vis spectra recorded during steady state photolysis of $Cr(CO)_5PY$ in cyclohexane ($\lambda_{exc.}$ >340 nm) under one atmosphere of argon in presence of excess pyridine (0.01 M), showing the growth of the bands at ~ 450 nm and 350 nm.

2.2.1.2 Steady state photolysis of $Cr(CO)_5Acpy$: -

The steady state photolysis of $Cr(CO)_5Acpy$ (Acpy = acetylpyridine) in cyclohexane in the presence of excess acetylpyridine (0.01 M) using different broad band irradiations (i.e. > 520nm, > 410nm, > 400nm, > 340nm, > 320nm, > 300nm)resulted in a rapid change in the UV/vis. absorption spectrum with the appearance of a new absorption band at 548 nm, Fig 2.5. The colour of the solution changed from bright orange to purple (with the formation of purple precipitate in concentrated solutions). The solution returned to its original colour when left in the dark overnight. This result was also observed following irradiation with λ_{exc} > 400 nm but was not fully reversible following irradiation with λ > 300 nm or monochromatic irradiation at 354.7 nm, Fig. 2.6.

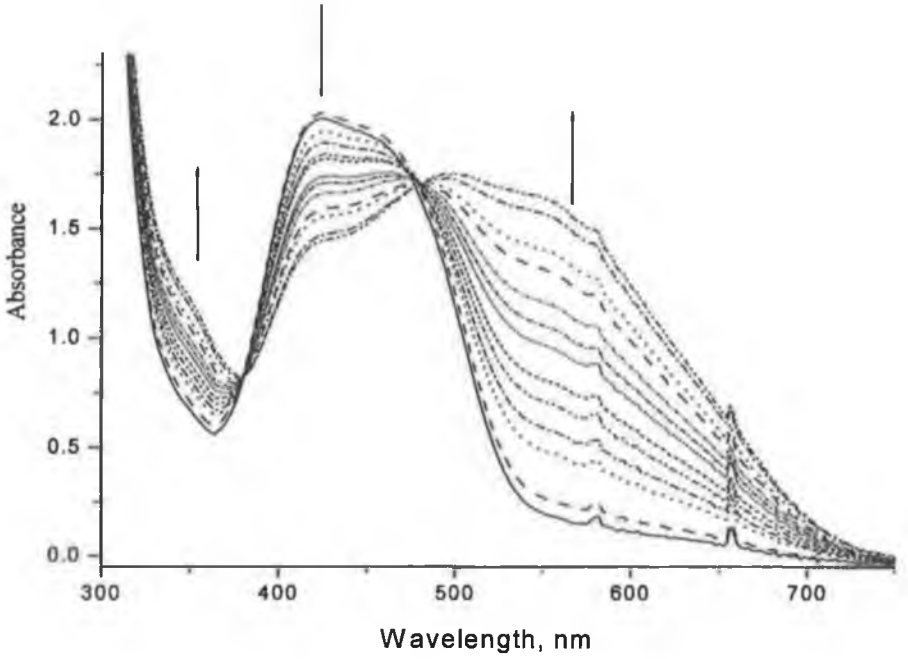

Fig 2.5 Steady state photolysis of $Cr(CO)_5Acpy$ plus 0.01 M Acpy in cyclohexane using broad band λ_{exc} >520 nm.

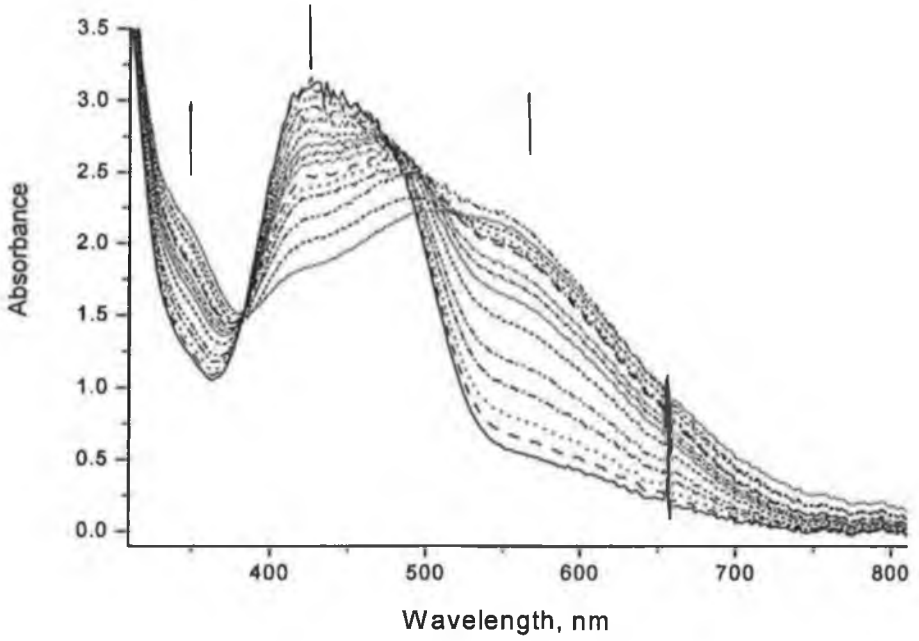

Fig 2.6 Monochromatic irradiation ($\lambda_{exc.}$ = 354.7 nm) of $Cr(CO)_5Acpy$ in the presence of 0.01 M Acpy in cyclohexane following exposure to an increasing number of laser pulses.

The infrared spectrum of the solution obtained after photolysis showed the formation of a new ν_{CO} stretching band at 1987 cm^{-1}, Fig. 2.7, This band has been assigned to $Cr(CO)_5$(O-Acpy) in which the acetylpyridine ligand coordinates through O-atom of acetyl group and not through the pyridine nitrogen[32]. The O-bound linkage isomer is thermally unstable and reverts to the N-linkage isomer over time. The second ν_{CO} stretching band at 1924 cm^{-1}, was assigned band to the trans–$Cr(CO)_4(Acpy)_2$ in which the coordination of acetylpyridine ligands is through oxygen. Further evidence for this assignment comes by the change in the uv spectra of the solution following irradiation with 354.7 nm or >300 nm, in which an isosbestic point was not maintained. As the product of isomerisation begins to absorb strongly and the CO loss become more important than the ligand loss, the reaction becomes more complicated.

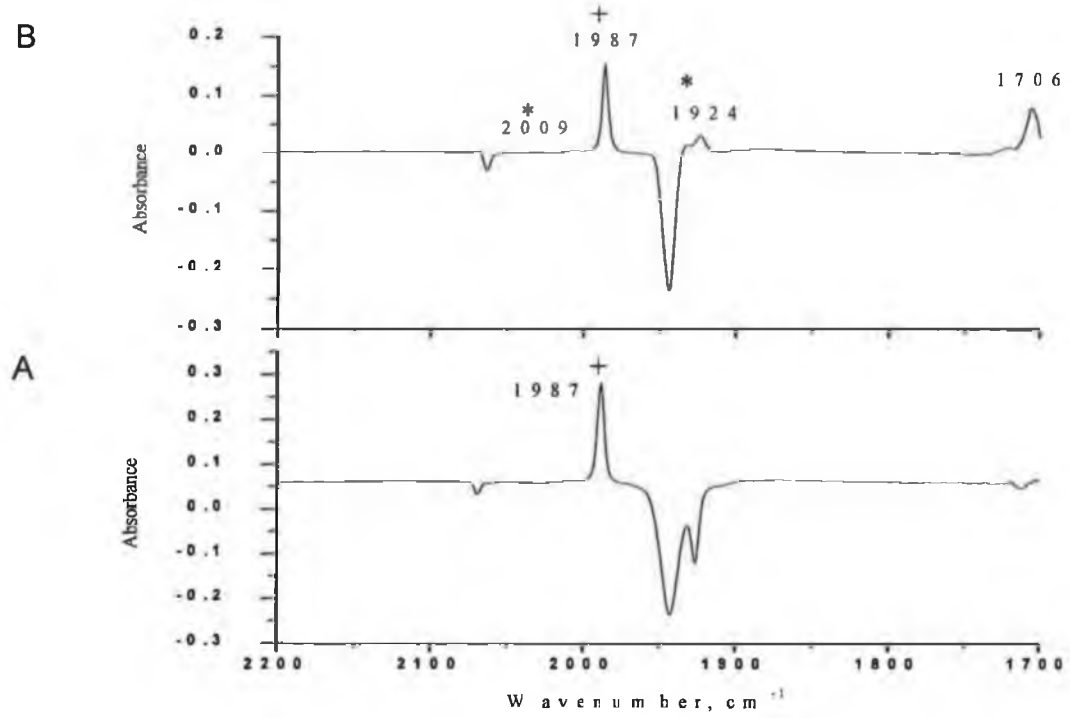

Fig 2.7 A difference IR spectrum obtained following irradiation of $Cr(CO)_5$Acpy plus 0.01 M Acpy, (A) in pentane with visible light $\lambda_{exc.}$ > 410 nm, (B) in cyclohexane $\lambda_{exc.}$ = 354.7 nm.

The reaction was also investigated using ^{1}H-NMR spectroscopy in deutrated cyclohexane in the presence of excess of ligand (0.01 M Acpy) under an argon atmosphere. Photolysis of this solution with $\lambda_{exc.}$ >410 nm reveals the disappearance of the protons signals of the N-coordinated ligand with an increase of the bands for

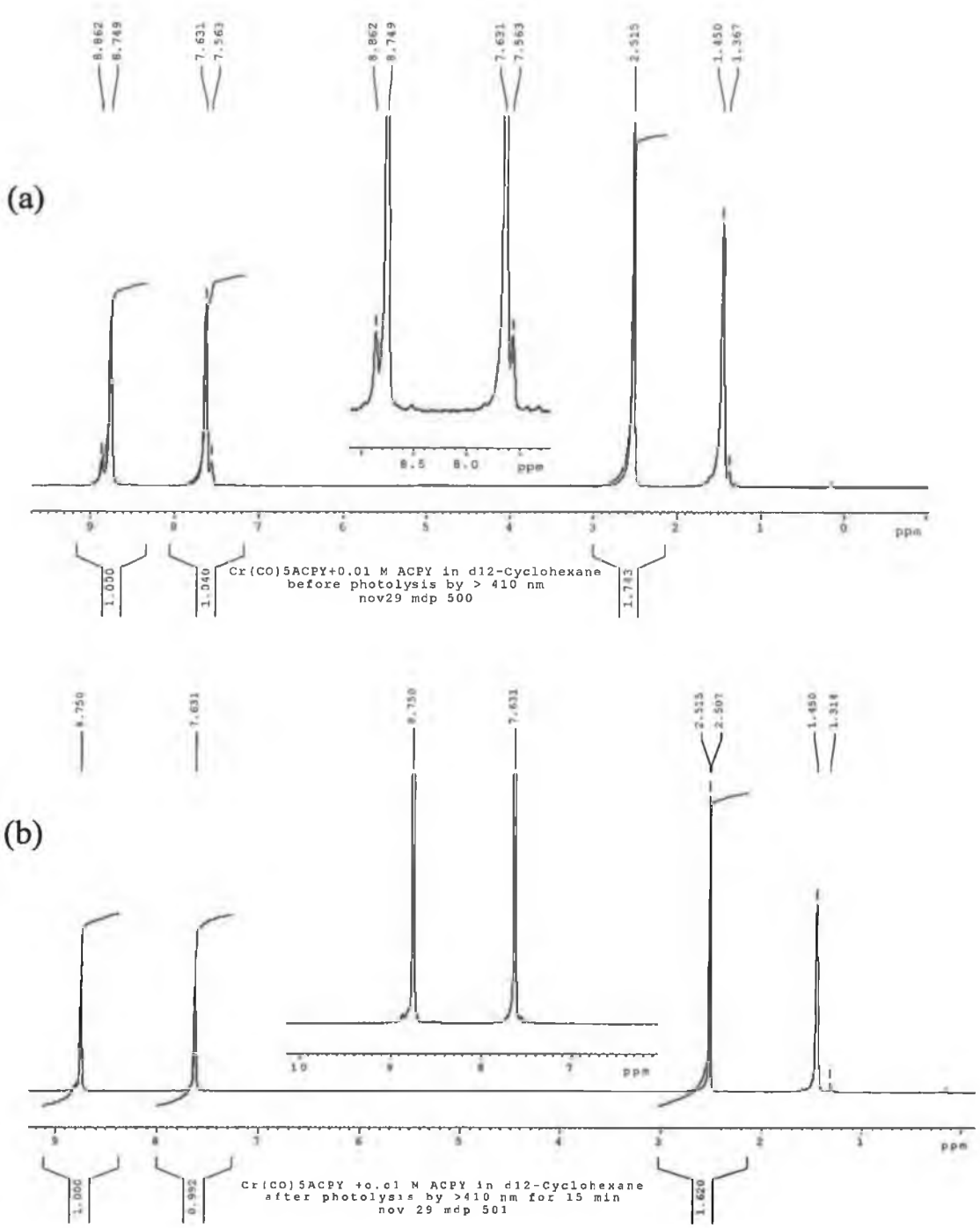

Fig. 2.8 ^{1}H-NMR spectrum of the solution of $Cr(CO)_5$Acpy plus 0.01 M Acpy in ^{12}D-cyclohexane, (a) before photolysis, (b) after photolysis with > 410 nm for 15 min..

the free ligand, which clearly indicates that the ligand coordinates through the acetyl oxygen, which does not affect the ring proton shifts to any great extent, Fig. 2.8. DFT calculations on the proposed complex $Cr(CO)_5$(O-Acpy) (table 2.4 gives the

bond lengths and bond angle for the optimised structure) shows that this complex has the structure shown in Fig 2.9 with local C_{4v} symmetry of the $Cr(CO)_5$. The IR spectrum of this complex has five ν_{CO} bands (Table 2.5) in consistent with this point group.

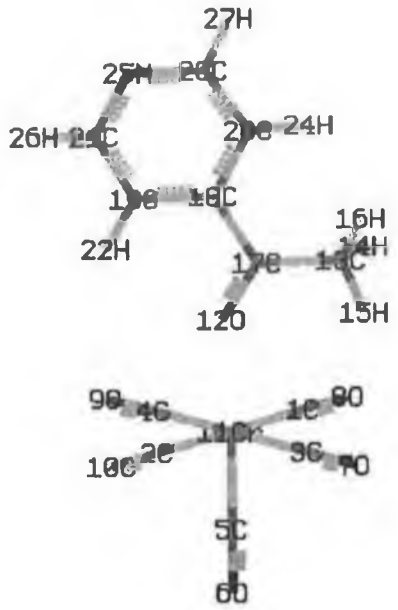

Fig. 2.9 The optimised structure of the proposed complex $Cr(CO)_5$(O-Acpy) using B3LYP/LANL2DZ level of theory.

	B3LYP/ LANL2DZ
Bond lengths: -	
Cr11-O12	2.14705
Cr11-C1	1.89309
Cr11-C2	1.90358
Cr11-C5	1.85005
C1-O8	1.17956
C2-O10	1.17662
C17-O12	1.26293
Bond angles: -	
O12Cr11C1	92.83604
O12Cr11C2	86.53343
O12Cr11C5	175.82619
O12Cr11C17	145.05440
C1Cr11C2	179.16069
C3Cr11C4	179.15431
C2Cr11C5	90.50727
C2Cr11C5	90.09382

Table 2.4 The calculated bond lengths and bond angles of the proposed complex $Cr(CO)_5$(O-Acpy) using B3LYP/ LANL2DZ level of theory.

	υ_{CO} band, cm^{-1}	assignment
Calculated*	2068(w)	Symmetric ν_{CO}
	1989(w)	Asymmetric ν_{CO}
	1961(s)	Asymmetric ν_{CO}
	1957(s)	Asymmetric ν_{CO}
	1951(s)	Asymmetric ν_{CO}
	1663(w), for ketone CO group	ν_{CO} of ketone
Experimentally	1987(s)	

* The calculated frequencies have been corrected by factor 1.02021

Table 2.5 The calculated υ_{CO} frequencies of the proposed complex $Cr(CO)_5$(O-Acpy) in comparison with that observed experimentally.

2.2.1.3 Steady state photolysis of $Cr(CO)_5$CNpy: -

Degassing a solution of $Cr(CO)_5$CNpy in toluene in the presence of excess of the CNpy ligand (0.01 M) resulted in significant change to the UV-vis. spectrum of the solution. It is thought that this change is related to the thermal isomerisation of the cyanopyridine ligand from pyridine N-linkage to cyano N-linkage isomer. Using different broadband irradiations (i.e. > 410nm, > 340nm, > 320nm, > 300nm and monochromatic laser ($\lambda_{exc.}$ = 354.7 nm) irradiation of this solution resulted in significant changes in the uv-visible absorption spectrum, Fig. 2.10, and the appearance of a new absorption band at 548 nm. The solution changed colour from bright orange to purple. Upon standing for several days in the dark, the solution reverted to its original colour.

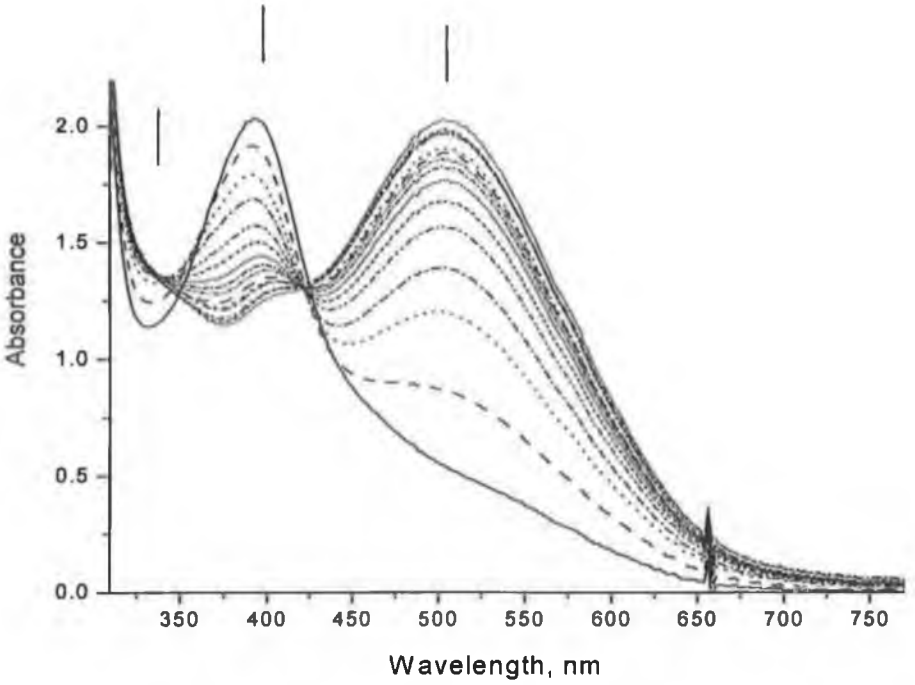

Fig 2.10 Steady state photolysis of $Cr(CO)_5CNpy$ plus 0.01 M CNpy in toluene using broad band irradiations $\lambda_{exc.} > 340nm$ for 0, 1, 2, 3, 4, 5, 6, 7, 8, 9, 10, 12, 15, 20, and 30 min..

After photolysis the solvent was removed under reduced pressure and the solid was dissolved in CH_2Cl_2. The colour of this solution rapidly changed from purple to orange. The IR spectrum was taken as soon as the solid had dissolved. The IR spectra after and before photolysis are shown in Fig 2.11.

The new peaks at 2011, 1852 cm^{-1} are assigned to the formation of tetracarbonyl complex cis-$Cr(CO)_4(CNpy)_2$.

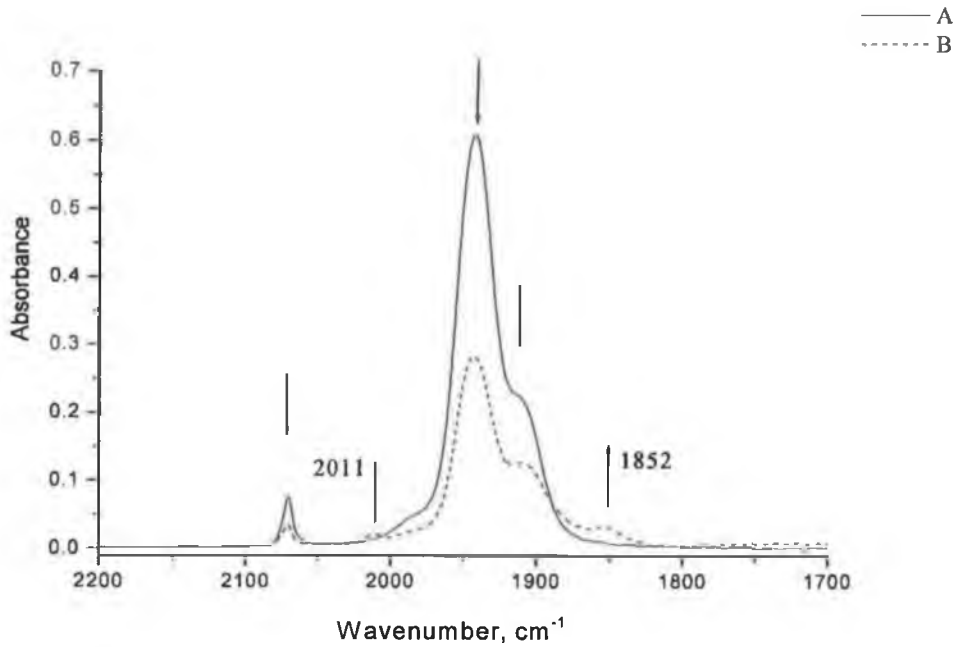

Fig. 2.11 IR spectrum for $Cr(CO)_5CNpy$ plus 0.01 M CNpy obtained in CH_2Cl_2 (A) before and (B) after steady state photolysis by broad band $\lambda_{exc.} > 340nm$ in toluene solution.

2.2.1.4 Steady state photolysis of $Cr(CO)_5PPh_3$: -

The steady state photolysis of $Cr(CO)_5PPh_3$ (PPh_3 = triphenylphosphine) in cyclohexane was studied under two conditions :- a) in the presence of additional PPh_3 and b) in the presence of CO.

a) in the presence of additional PPh_3: The steady state photolysis of $Cr(CO)_5PPh_3$ in cyclohexane solution with excess of PPh_3 using various broad band irradiations (i.e. $\lambda_{exc.}$ >410nm, >340nm) reveals a change in the UV spectrum of the solution with a red shift of the lowest energy absorbance. This effect was also observed following monochromatic irradiation ($\lambda_{exc.}$ = 354.7 nm), Fig. 2.12.

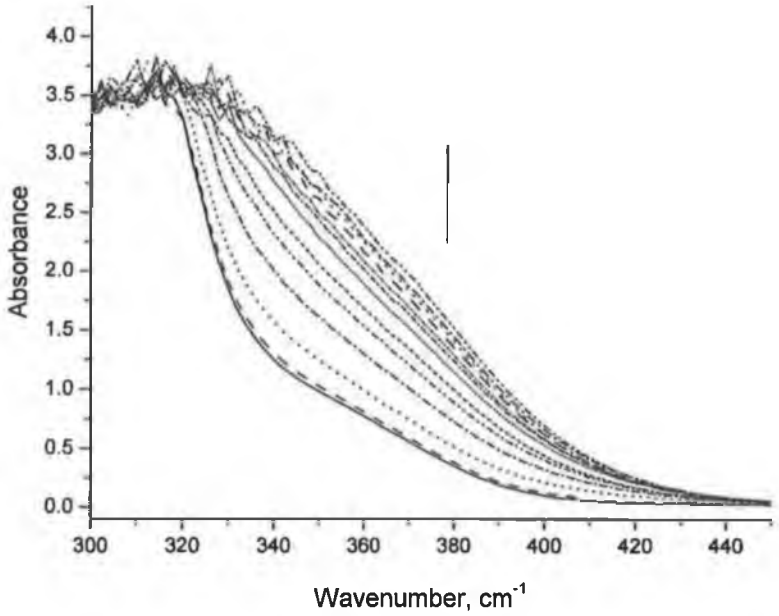

Fig 2.12 Monochromatic irradiation (λ_{exc} = 354.7 nm) of $Cr(CO)_5PPh_3$ plus 0.01 M PPh_3 in cyclohexane following increasing number of laser pulses.

The IR spectrum after photolysis reveals the formation of trans-$Cr(CO)_4(PPh_3)_2$, Fig. 2.13 in which has two ν_{CO} stretching vibrations at 1895 cm^{-1}.[33]

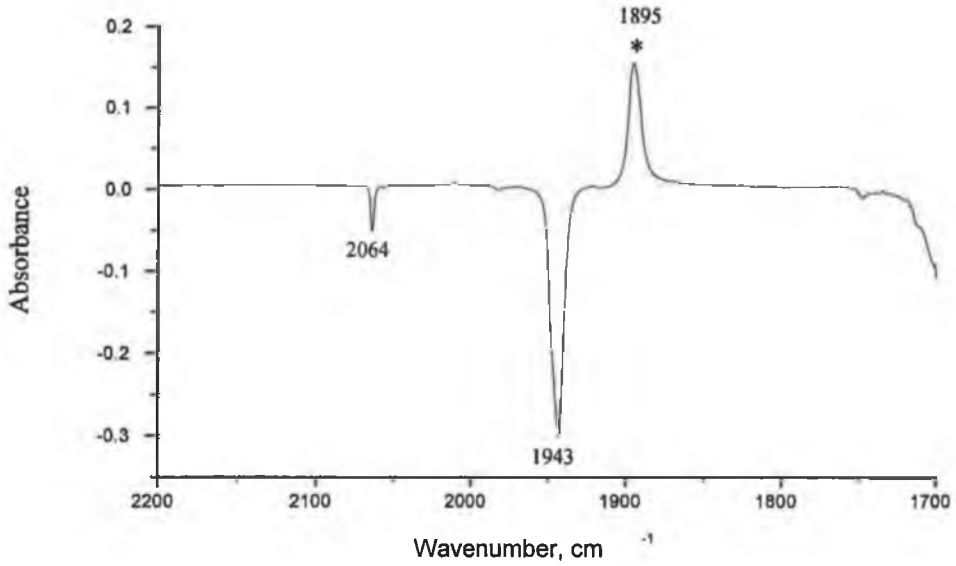

Fig 2.13 The difference in the IR spectrum of $Cr(CO)_5PPh_3$ plus 0.01 M PPh_3 in cyclohexane before and after laser irradiation at 354.7 nm.

b) In the presence of CO: - The steady state photolysis of $Cr(CO)_5PPh_3$ in the presence of CO (1 atm CO (0.009 M)) results in significant change in the UV spectrum of the solution, Fig. 2.14, the band shifting toward shorter wavelength (blue shift). The IR spectrum indicated the formation of $Cr(CO)_6$ which has ν_{CO} band at 1986 cm^{-1}, Fig. 2.15.

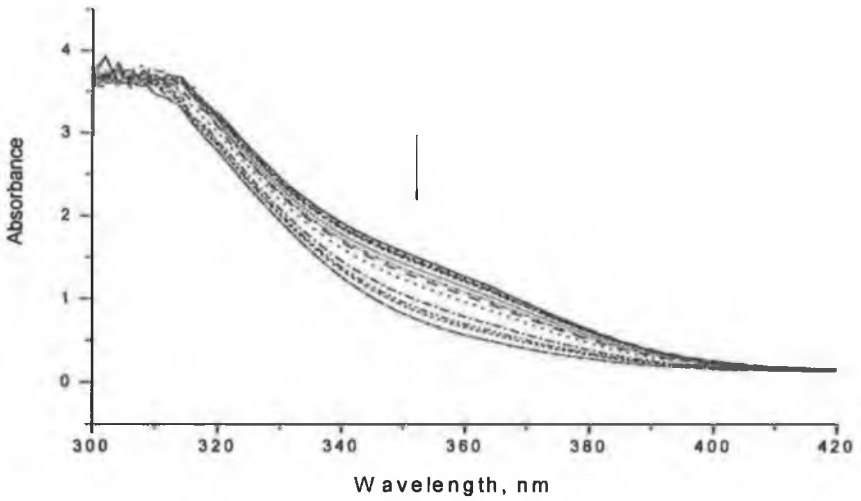

Fig 2.14 Steady state photolysis of $Cr(CO)_5PPh_3$ under one atmosphere of CO (0.009 M) in cyclohexane ($\lambda_{exc.}$ >340 nm) for various times up to 120 min..

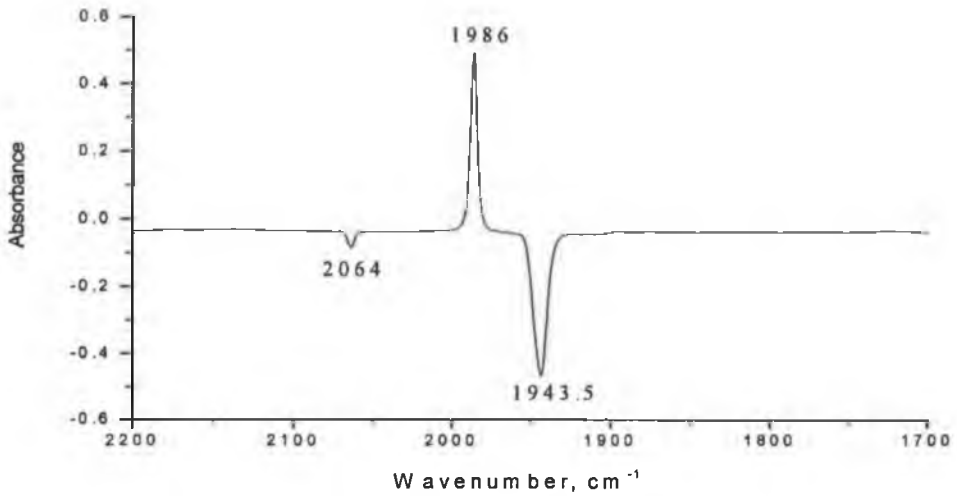

Fig. 2.15 The difference in the IR spectrum of $Cr(CO)_5PPh_3$ under 1 atm CO (0.009 M) before and after steady state photolysis ($\lambda_{exc.}$ >340 nm).

2.2.1.5 Steady state photolysis of $W(CO)_5Py$: -

Steady state photolysis of $W(CO)_5Py$ in cyclohexane in the presence of excess pyridine (0.01M) using λ_{exc} >390, >340, >320, or >300 nm did not result in any change to the UV/vis spectrum of the solution, Fig 2.16. However using monochromatic irradiation λ_{exc}=354.7 nm, Fig 2.17. a significant change was observed in the UV/vis spectrum with the formation of new band in the region (440-500 nm) which is assigned to cis-$W(CO)_4Py_2$.[34]

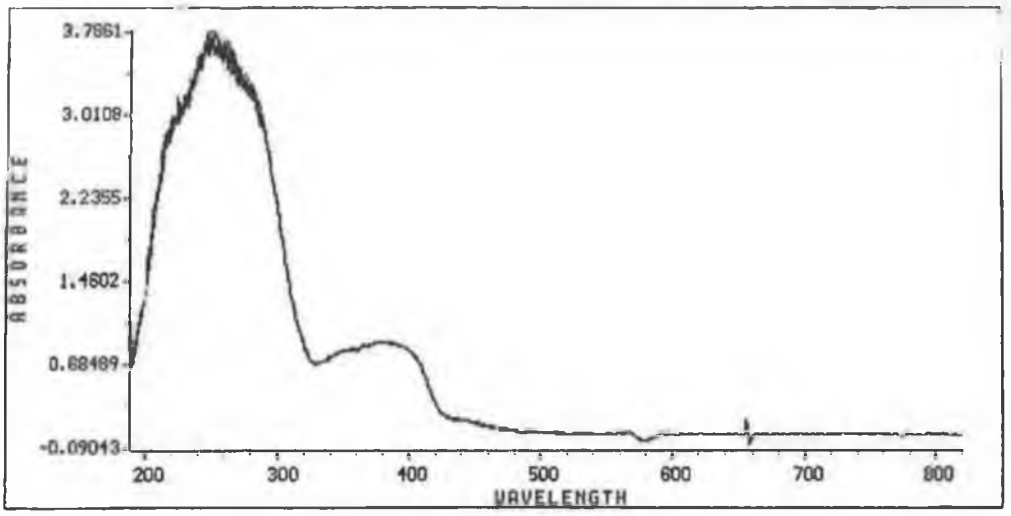

Fig 2.16 UV/vis absorption spectra recorded during photolysis (λ_{exc} >300 nm) of $W(CO)_5Py$ plus 0.001 M Py in cyclohexane.

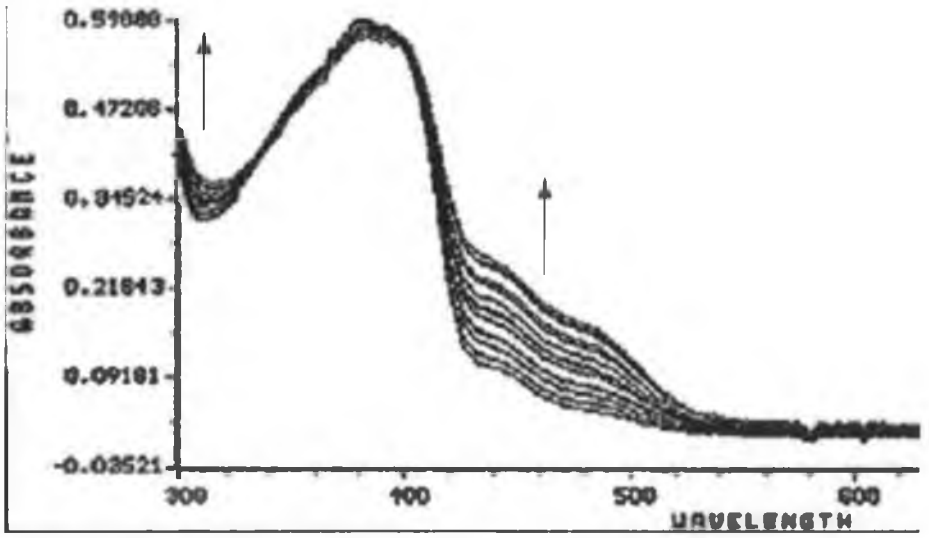

Fig. 2.17 UV/vis absorption spectra recorded during monochromatic photolysis (λ_{exc} = 354.7 nm) of $W(CO)_5Py$ plus 0.01 M Py in cyclohexane.

The IR spectrum of the solution after photolysis reveals the formation of new bands at 2007, 1887, 1828 cm^{-1}, we assigned to the formation of cis-$W(CO)_4Py_2$ which are close to those bands observed for this complex in C_6H_6 in the literature (2006, 1879, 1869, 1844 cm^{-1})[34], Fig. 2.18.

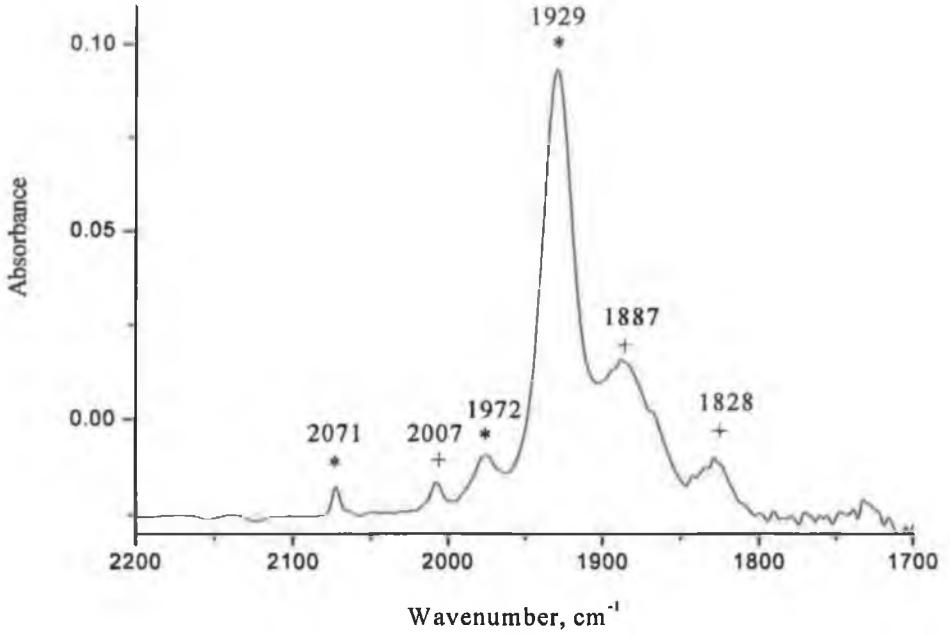

Fig 2.18 The IR spectrum of $W(CO)_5Py$ plus 0.01 M Py obtained following excitation at λ_{exc} = 354.7 nm indicating the formation of cis-$W(CO)_4Py_2$, The bands labelled with * are for the parent pentacarbonyl complex, while the bands labelled with + are for the tetracarbonyl species (i.e. cis-$W(CO)_4Py_2$).

2.2.1.6 Steady state photolysis of $W(CO)_5$Acpy: -

Steady state photolysis of $W(CO)_5$Acpy in cyclohexane in presence of excess ligand (0.01M Acpy) using broadband irradiation failed to produce any change to the uv-visible spectrum of the solution. Again using monochromatic excitation (354.7 nm), Fig 2.19 a significant change to the UV/vis. spectrum was observed, accompanied by the formation of a maroon precipitate. This precipitate was identified by IR spectroscopy to be the tetracarbonyl complex cis-$W(CO)_4(Acpy)_2$. The spectroscopic properties were compared to those of an authentic sample of cis-$W(CO)_4(Acpy)_2$ prepared by literature procedure[35] and were found to be identical, Fig 2.20.

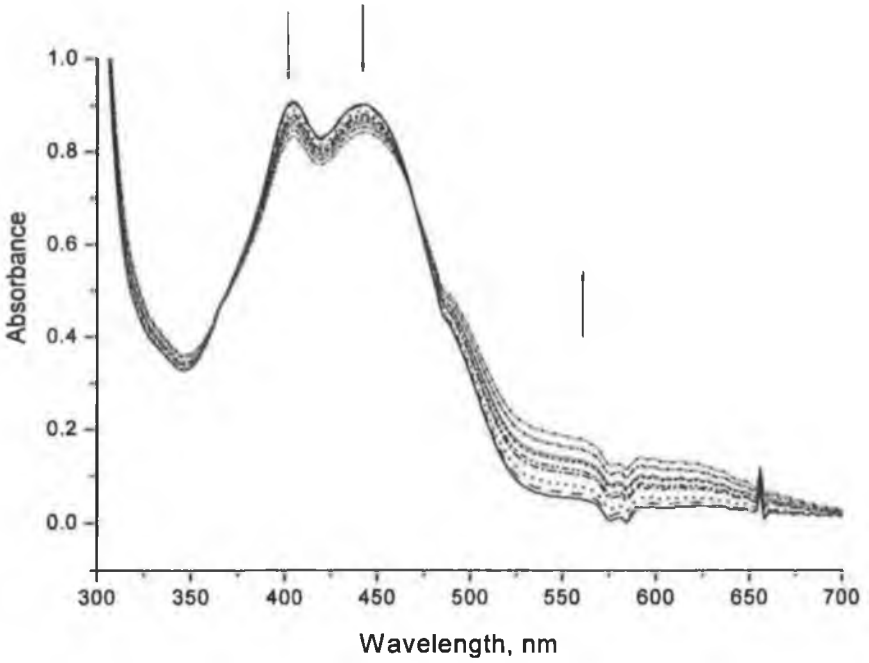

Fig 2.19 UV/vis absorption spectra recorded during photolysis $W(CO)_5$Acpy plus 0.01M Acpy in cyclohexane under 1 atmosphere of argon (λ_{exc} = 354.7 nm) showing a decrease in intensity of the two bands at 400 and 450 nm and increase in intensity of the shoulder at > 520 nm.

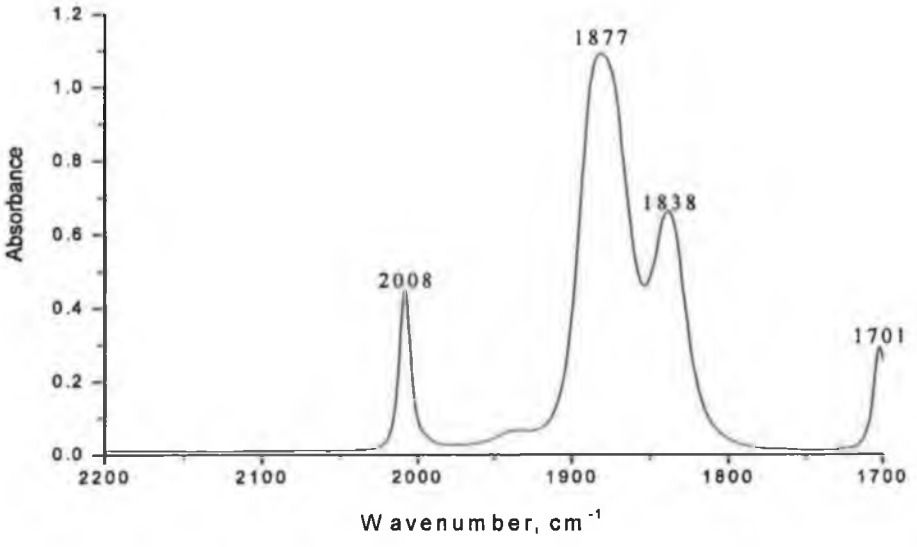

Fig 2.20 The IR spectrum of cis-$W(CO)_4(Acpy)_2$ in CH_2Cl_2, prepared by literature procedure.[35]

2.2.1.7 Steady state photolysis of $W(CO)_5CNpy$: -

Because $W(CO)_5CNpy$ and also the CNpy ligand were insoluble in cyclohexane toluene was used as a solvent in this experiment.

Upon irradiation with broadband light using $\lambda_{exc} > 410$ nm the observed UV/vis spectrum exhibited a shift of λ_{max} to longer wavelength, Fig. 2.21. This change is assigned to a linkage isomerism from pyridine N-bound species to cyano N-bound isomer. Lees, and co-workers[9] were not able to induce photoisomerization of the pyridine -bound species to the cyano-bound analogue in benzene and in presence of 0.1 M of the free ligand. The UV/vis spectrum suggests that there is no formation of the metal tetracarbonyl complex under these conditions.

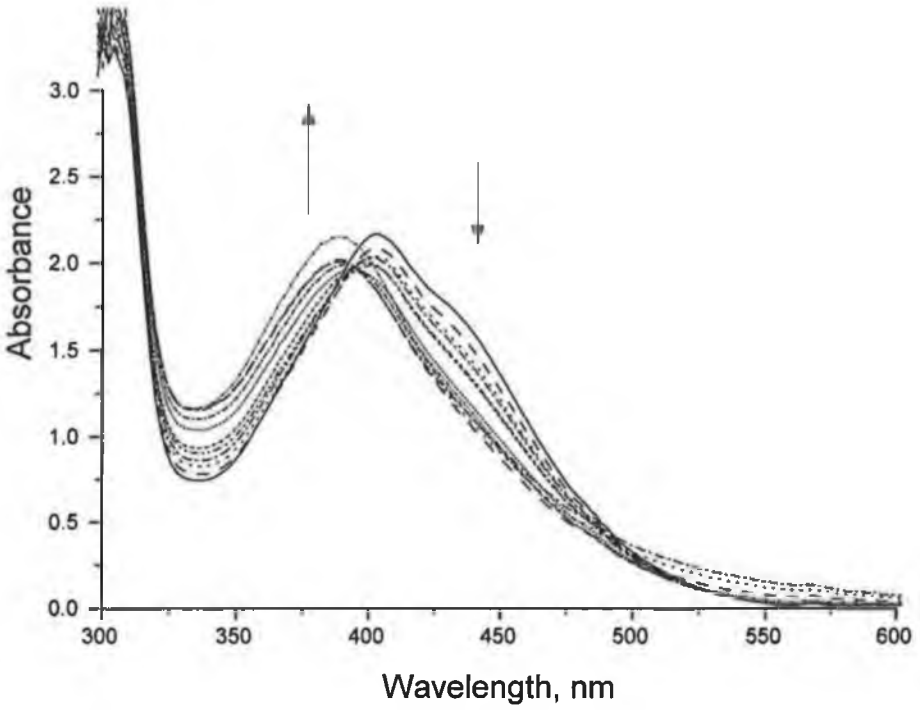

Fig.2.21 UV/vis absorption spectra recorded during photolysis (λ_{exc} >410 nm) of $W(CO)_5CNpy$ under one atmosphere of argon in presence of 0.01 M CNpy in toluene.

Upon irradiation of $W(CO)_5CNpy$ with an excess of the ligand 0.01M CNpy using different broad-band filters (λ_{exc} >400, >340, or >300) (Fig 2.22) and initial blue shift of the of the uv band were observed in the first 15 min.. Following this change, the intensity of the band then reduces and shifts to longer wavelength with the creation of new band at about 500 nm, which is related to the metal tetracarbonyl complex.[34]

The first shift is assigned to the linkage isomerism of the ligand from N-pyridine ring linkage to N-cyano linkage.[9]

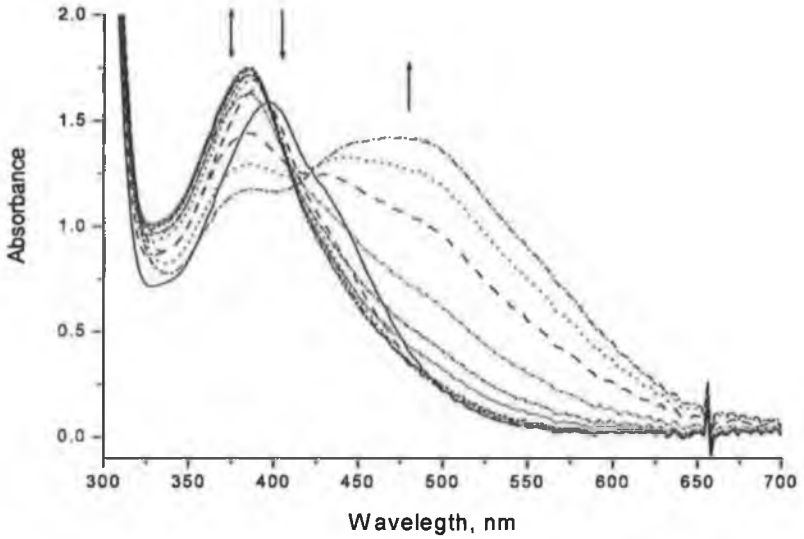

Fig 2.22 UV/vis absorption spectra recorded during steady state photolysis of $W(CO)_5CNpy$ plus 0.01 M CNpy in toluene at λ_{exc} >400 nm under one atmosphere of argon in presence of 0.01 M CNpy

This process was not observed following monochromatic irradiation λ_{exc} = 354.7 nm, Fig 2.23. Following photolysis the solvent was removed under reduced pressure at room temperature and the solid was dissolved in CH_2Cl_2. The IR spectrum of this solution was obtained which indicated the formation of the metal tetracarbonyl compound (ν_{CO} 2010 m, 1891 sbr., 1846 cm^{-1} sbr.) Fig 2.24.[34]

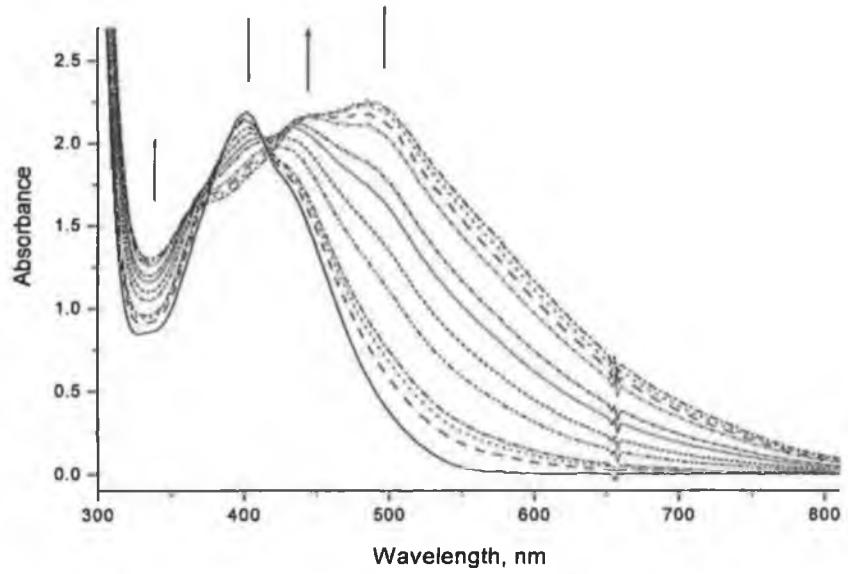

Fig 2.23 Monochromatic irradiation ($\lambda_{exc.}$ = 354.7 nm) of $W(CO)_5CNpy$ plus 0.01 M CNpy in toluene for increasing number of laser pulses. The band at ~ 500 nm is assigned to the formation of metal tetracarbonyl complex.

The IR spectrum of the product after removal the solvent and dissolving the resulting solid in CH_2Cl_2 reveals the formation of the metal tetracarbonyl complex as indicated in Fig 2.24.

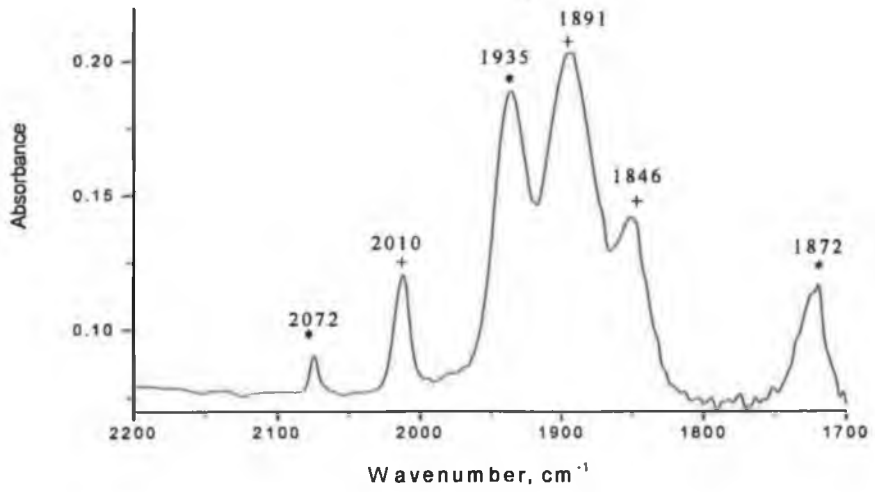

Fig 2.24 The IR spectrum of $W(CO)_5CNpy$ plus 0.01 M CNpy in CH_2Cl_2 after monochromatic irradiations $\lambda_{exc.}$ = 354.7 nm. The bands labelled with *, + are for $W(CO)_5CNpy$, and cis-$W(CO)_4(CNpy)_2$ complexes.

by the υ_{CO} bands at 2010, 1891, 1846 cm^{-1} which are close to the published for cis-$W(CO)_4(CNpy)_2$ in benzene (2006, 1890, 1878, 1860)[34].

2.2.1.8 Steady state photolysis of $W(CO)_5PPh_3$: -

The steady state photolysis of $W(CO)_5PPh_3$ in cyclohexane was studied under two conditions: -a) in the presence of additional of PPh_3, b) in the presence of CO.

a) In the presence of additional PPh_3 ligand (0.01M): -The steady state photolysis of this solution used different broadband irradiations (i.e. filters >340nm, >320 nm, >300nm) and also monochromatic excitation λ_{exc} = 354.7 nm, Fig 2.25

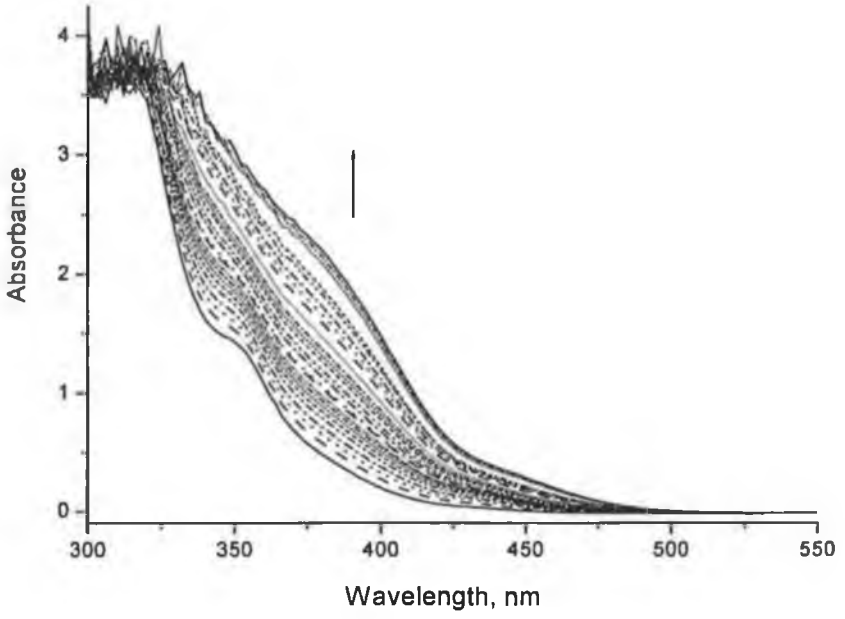

Fig 2.25 UV/vis absorption spectra recorded during laser photolysis of $W(CO)_5PPh_3$ in cyclohexane in the presence of 0.01 M PPh_3 ($\lambda_{exc.}$ = 354.7 nm) under one atmosphere of argon.

At the end of the experiment the solvent was removed under reduced pressure at room temperature and the resulting solid was dissolved in CH_2Cl_2. IR spectrum of this solution revealed peaks at 2018,1936.5,1892, 1842 cm^{-1} which were assigned to cis–$W(CO)_4(PPh_3)_2$[26], Fig 2.26.

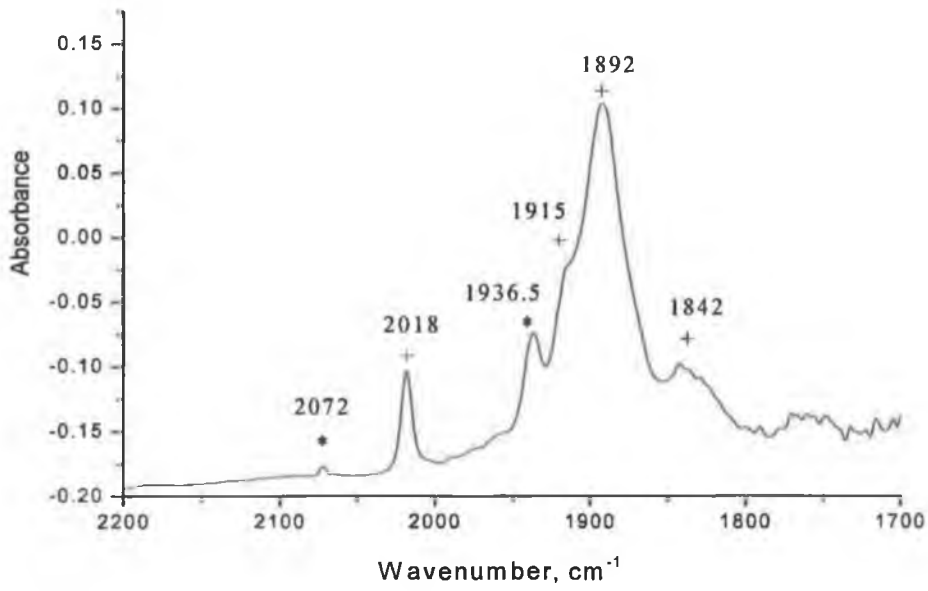

Fig 2.26 The IR spectrum of $W(CO)_5PPh_3$ plus 0.01 M PPh_3 in CH_2Cl_2 following photolysis with λ_{exc} >300 nm in cyclohexane.

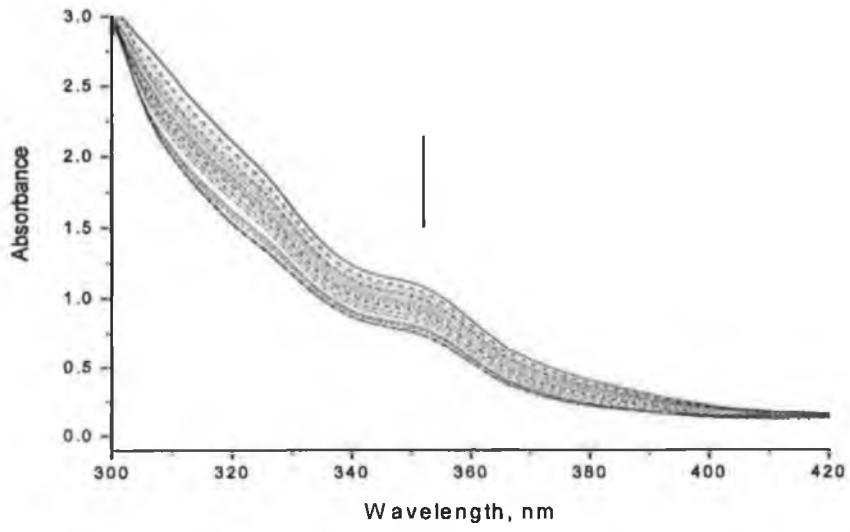

Fig 2.27 UV/vis absorption spectra recorded during monochromatic photolysis of $W(CO)_5PPh_3$ in cyclohexane with λ_{exc}= 354.7 nm under one atmosphere of carbonmonoxide (i.e. 0.009 M CO)

b) In the presence of CO atmosphere: - The steady state photolysis of this solution under 1 atm (~0. 009M CO) using different broad band irradiations (i.e. λ_{exc} > 340nm, > 320nm, or > 300nm) and monochromatic irradiation λ_{exc} = 354.7 nm resulted in significant changes to the UV/vis spectrum, Fig. 2.27.

The IR spectrum of the solution revealed a υ_{CO} stretching band at 1982 cm^{-1}, which is assigned to tungsten hexacarbonyl Fig 2.28.

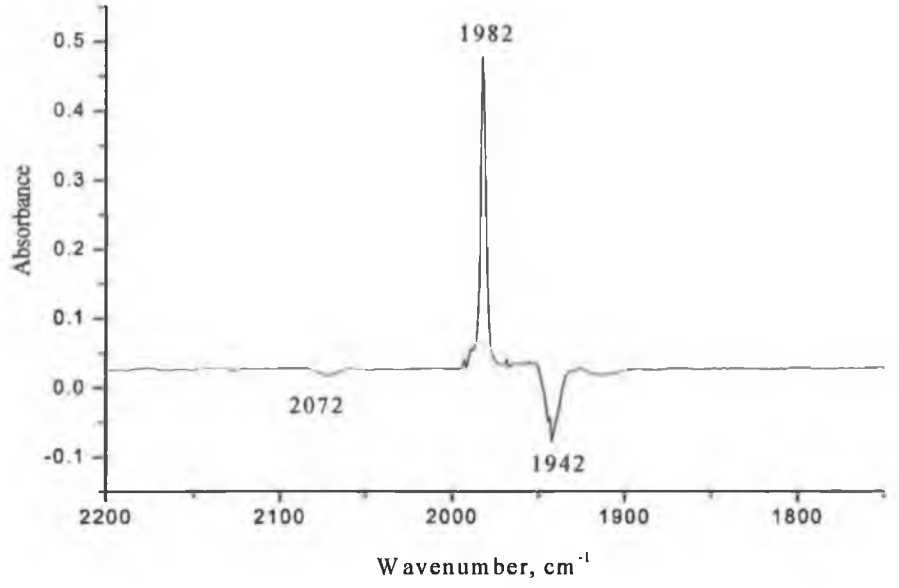

Fig 2.28 The difference in IR spectra of $W(CO)_5PPh_3$ following steady state photolysis with $\lambda_{exc.}$ =354.7 nm in cyclohexane under one atmosphere of carbonmonoxide (i.e. 0.009 M CO).

2.2.2 Laser flash photolysis of the complexes of the type $M(CO)_5L$, M = Cr, or W ; L=Py, Acpy, CNpy, or PPh_3

The laser flash photolysis experiments on the complexes of the type $M(CO)_5L$, (M = Cr or W; L = pyridine, 4-acetylpyridine, 4-cyanopyridine, or triphenylphosphine) were conducted in the presence of excess ligand. In addition, for the PPh_3 complexes, experiments were also carried out in the presence of 1 atm of CO gas.

Cyclohexane was chosen as a solvent in this study because it is a weakly coordinating solvent. The second benefit of choosing cyclohexane as a solvent is that the absorbance of this solvent in the UV/vis region is low so it will not interfere the transient absorption measurements. However, in the case of cyanopyridine complexes both the complex and the free ligand were insoluble in cyclohexane so toluene was used. Toluene is more coordinating solvent than cyclohexane because of the presence of π-delocalised electrons which can coordinate to the metal, thus

toluene is a bad leaving ligand and toluene adduct species have significantly longer lifetimes than the cyclohexane analogues.[32b]

Complex	Conditions	UV/vis. bands, nm	The final photoproduct(s)
$Cr(CO)_5Py$	0.01 M Py, under argon	486, 394	cis-$Cr(CO)_4Py_2$
$Cr(CO)_5Acpy$	0.01M Acpy, under argon	424, 465	$Cr(CO)_5$(O-Acpy) + cis-$Cr(CO)_4(Acpy)_2$
$Cr(CO)_5CNpy$	0.01M CNpy, under argon	416→ 396 (after degassing)	$Cr(CO)_5$(cyano-CNpy) + cis-$Cr(CO)_4(CNpy)_2$
$Cr(CO)_5PPh_3$	0.01 M PPh_3, under argon	Ca. 360	cis-$Cr(CO)_4(PPh_3)_2$
$Cr(CO)_5PPh_3$	Under 1 atm CO	Ca. 360	$Cr(CO)_6$
$W(CO)_5Py$	0.001 M Py, under argon	390, 442	cis-$W(CO)_4(Py)_2$
$W(CO)_5Acpy$	0.001 M Acpy, under argon	402, 440	cis-$W(CO)_4(Acpy)_2$
$W(CO)_5CNpy$	0.01 M CNpy, under argon	404, 442	$W(CO)_5$(cyano-CNpy) + cis-$W(CO)_4(CNpy)_2$
$W(CO)_5PPh_3$	0.001 M PPh_3, under argon	ca. 350 nm	cis-$W(CO)_4(PPh_3)_2$
$W(CO)_5PPh_3$	Under 1 atm CO	ca. 350 nm	$W(CO)_6$

Table 2.5 The $M(CO)_5L$ complexes studied in the laser flash photolysis experiments upon analysis of the transient signals of $Cr(CO)_6$ in cyclohexane under 1 atm of argon at different wavelengths

Transient absorption measurements at room temperature for the complex $M(CO)_5L$, (M = Cr or W; L = Py, Acpy, or PPh_3, [L] = 0.01-0.001 M, $\lambda_{exc.}$ = 354.7 nm) under one atmosphere of argon gave rise to rapid increase in the absorbance within the laser pulse (~10 ns). The absorbance difference spectrum, plotted at increasing time

delays after the laser pulse, is shown in Fig. 2.29. The grow-in of a new species is observed in the range 420-630 nm and 330-370 nm. A depletion of the parent compound was also observed in the range 370-410 nm. The electronic absorption spectrum changed throughout the experiment indicating the formation of cis-$M(CO)_4L_2$, or $M(CO)_6$ for reactions with ligand L or CO respectively. This was confirmed by IR spectroscopy of the solution upon completion.

The kinetic analysis of the transient signals monitored at different wavelengths has different values for the second order rate constant Table 2.6. This clearly shows the presence of two transient species. Tables 2.8-13 for the analysis of typical transient signals obtained in these experiments and the transient absorption spectra.

λ, nm	k_2 (S^{-1}. $Mol.^{-1}$ L)
530	7.0×10^{08}
510	3.5×10^{09}
490	4.7×10^{09}
470	3.3×10^{09}
430	1.7×10^{09}
410	1.6×10^{09}

Table 2.6 Kinetic data obtained upon analysis of the transient pulsed photolysis of $Cr(CO)_5Py$ plus 0.01 M Py in cyclohexane at various wavelengths.

λ, nm	$k_{obs.}$ (S^{-1})
560	3.0×10^4
540	3.2×10^4
520	3.0×10^4
450	3.2×10^4

Table 2.7 Kinetic data obtained from the transient signals following photolysis of $Cr(CO)_6$ in cyclohexane under 1 atm of argon at different wavelengths.

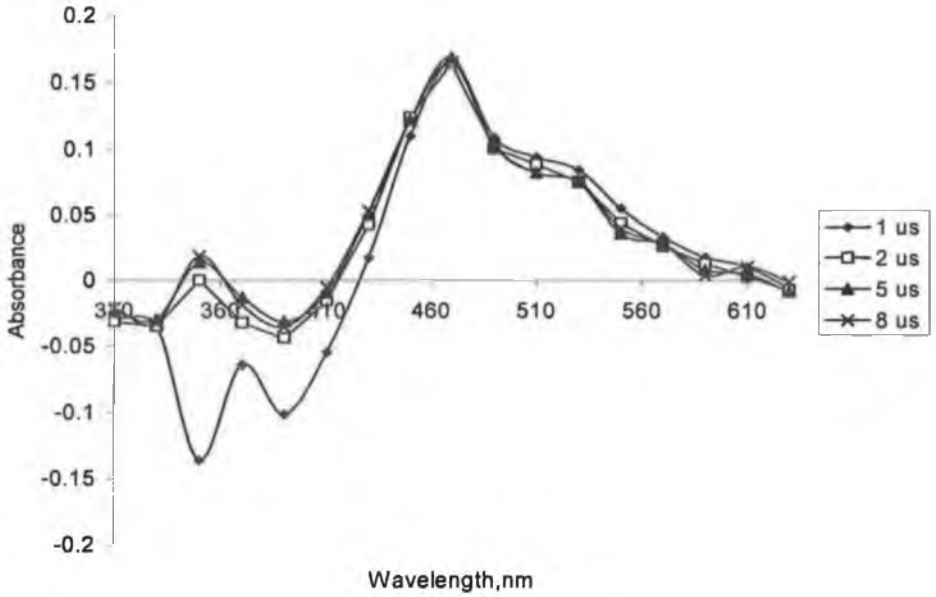

Fig. 2.29 The laser flash photolysis of the complex $Cr(CO)_5Py$ plus 0.01M Py in cyclohexane by 354.7 nm .This spectrum was obtained by monitoring the transient signals at 20 nm intervals.

λ, nm	k_2, (S^{-1}. $Mol.^{-1}$ L)
630	9.4×10^4
620	$7. \times 10^4$
600	6.4×10^4
580	7.2×10^4
560	7.2×10^4

Table 2.8 Kinetic data obtained upon analysis of the transient of $Cr(CO)_5Acpy$ plus 0.01 M Acpy in cyclohexane at different wavelengths

λ, nm	k_2 (S^{-1}. $Mol.^{-1}$ L)
570	2.3×10^8
550	2.4×10^8
530	1.7×10^8
510	1.1×10^8
490	4.9×10^7
470	4.2×10^7

Table 2.9 Kinetic data obtained upon analysis of the transient of $Cr(CO)_5CNpy$ plus 0.01 M CNpy in toluene at different wavelengths.

λ, nm	k_2, (S^{-1}. $Mol.^{-1}$ L)
560	2.1×10^5
540	2.2×10^5
520	3.1×10^5
500	2.4×10^5
480	2.9×10^5
460	2.1×10^5
450	1.4×10^5

Table 2.10 Kinetic data obtained upon analysis of the transient of $Cr(CO)_5PPh_3$ plus 0.01 M PPh_3 in cyclohexane at different wavelengths

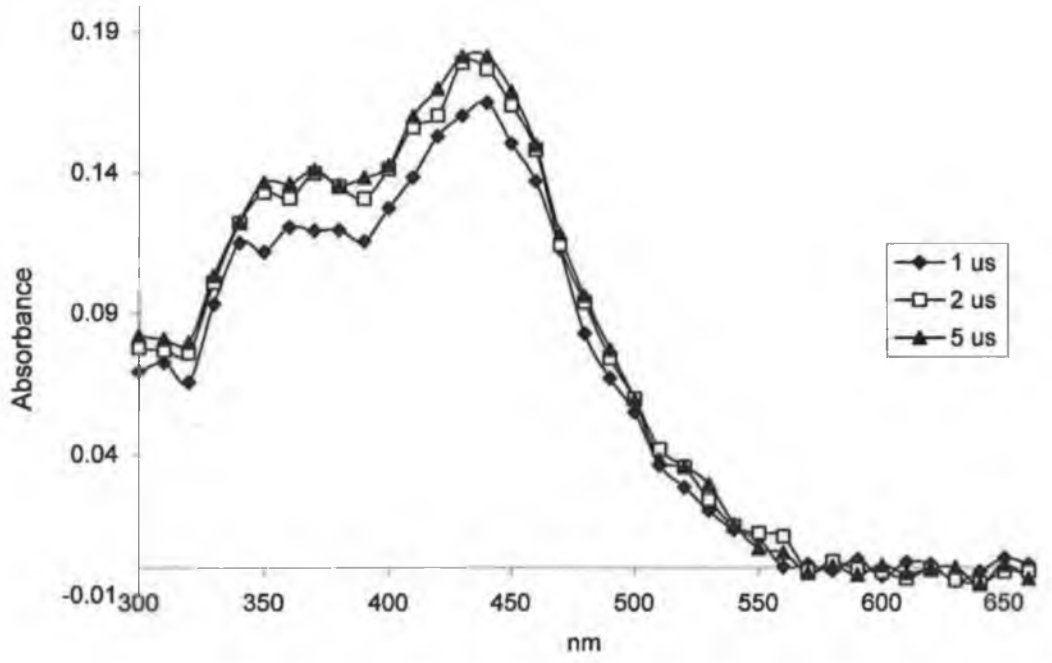

Fig 2.30 Transient absorption spectrum of the complex $Cr(CO)_5PPh_3$ under 1 atm CO (0.009 M).

λ, nm	k_2, (S^{-1}. $Mol.^{-1}$ L)
500	2.7×10^8
480	1.7×10^8
460	2.7×10^8
440	2.7×10^8
420	3.3×10^8
400	1.9×10^8
380	1.8×10^8

Table 2.11 Kinetic data for the analysis of the transient for $Cr(CO)_5PPh_3$ in cyclohexane under 1 atm CO at different wavelengths.

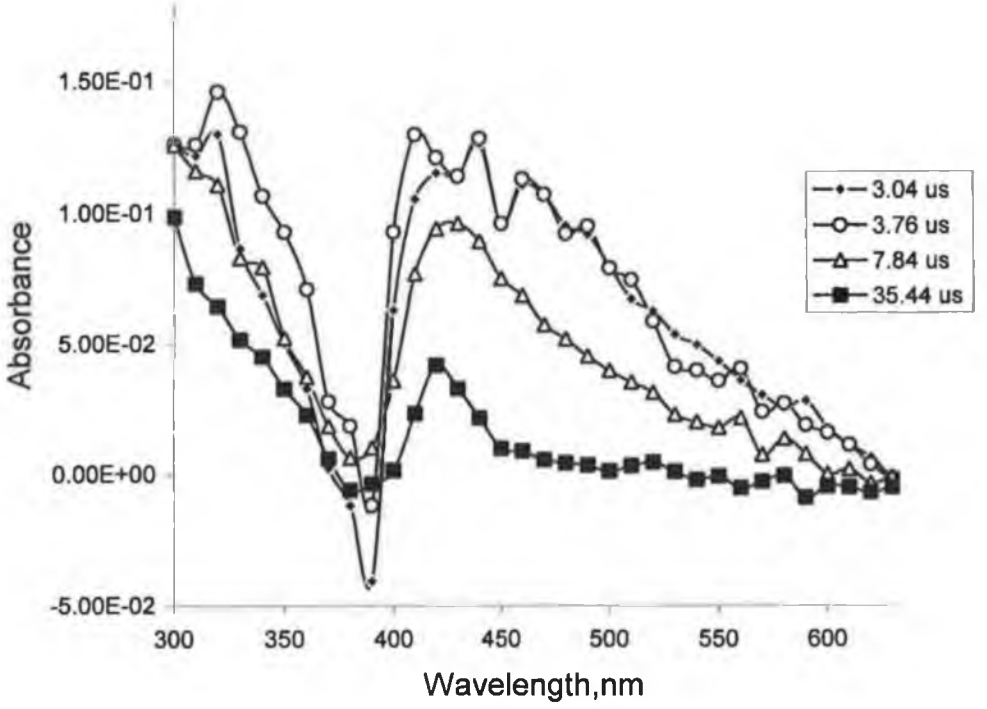

Fig 2.31 Transient absorption spectra obtained following photolysis of $W(CO)_5Py$ in cyclohexane in the presence of Py (0.001 M), $\lambda_{exc.}$ = 354.7 nm.

A typical transient signal at λ_{max} =420 nm of $W(CO)_5Py$ plus 0.001M Py was shown in Fig 2.32.

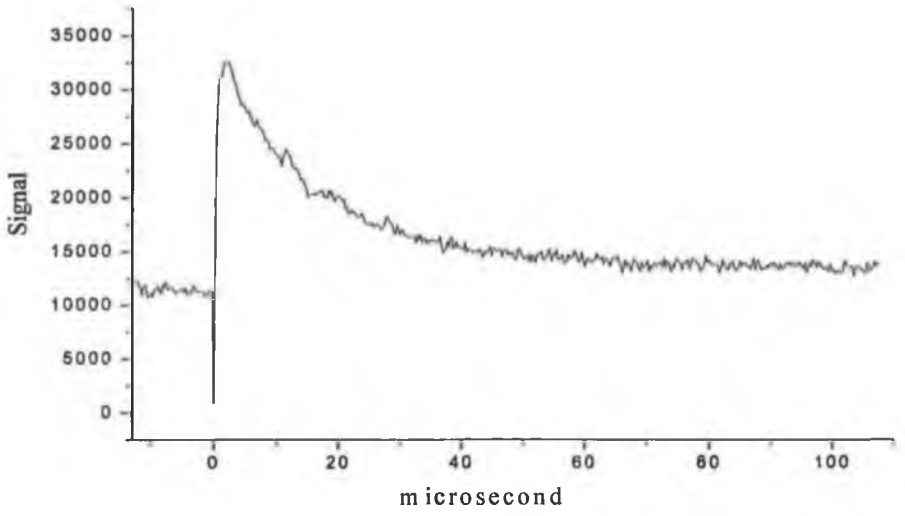

Fig 2.32 Typical transient monitored at the λ_{max} =420 nm of $W(CO)_5Py$ plus 0.001M Py

There is significant difference between the values of the observed rate constants for the transients signals obtained at different wavelengths as shown in Table 2.7.

λ, nm	k_2, (S^{-1}. $Mol.^{-1}$ L)
330	2.3×10^7
410	3.4×10^7
420	3.7×10^7
460	4.4×10^7
500	5.1×10^7
520	5.7×10^7

Table 2.12 The kinetic analysis of the transient obtained at different wavelengths for flash photolysis of $W(CO)_5Py$ plus 0.001 M Py

The kinetic analysis of the transient signals monitored at different wavelengths has different values for the rate constant Table 2.8. This clearly reveals we have two transient species.

λ, nm	k_2, (S^{-1}. $Mol.^{-1}$ L)
430	3.9×10^6
410	3.7×10^6
390	4.9×10^6

Table 2.13 Kinetic data obtained upon analysis of the transient of $W(CO)_5$Acpy plus 0.01 M Acpy in cyclohexane at various measuring wavelengths.

λ, nm	k_2, (S^{-1}. $Mol.^{-1}$ L)
460	6.8×10^7
440	6.4×10^7
420	7.3×10^7
400	9.1×10^7
360	4.4×10^8

Table 2.9 Kinetic data for the analysis of the transient species following photolysis of $W(CO)_5PPh_3$ in cyclohexane under 1 atm CO at different wavelengths.

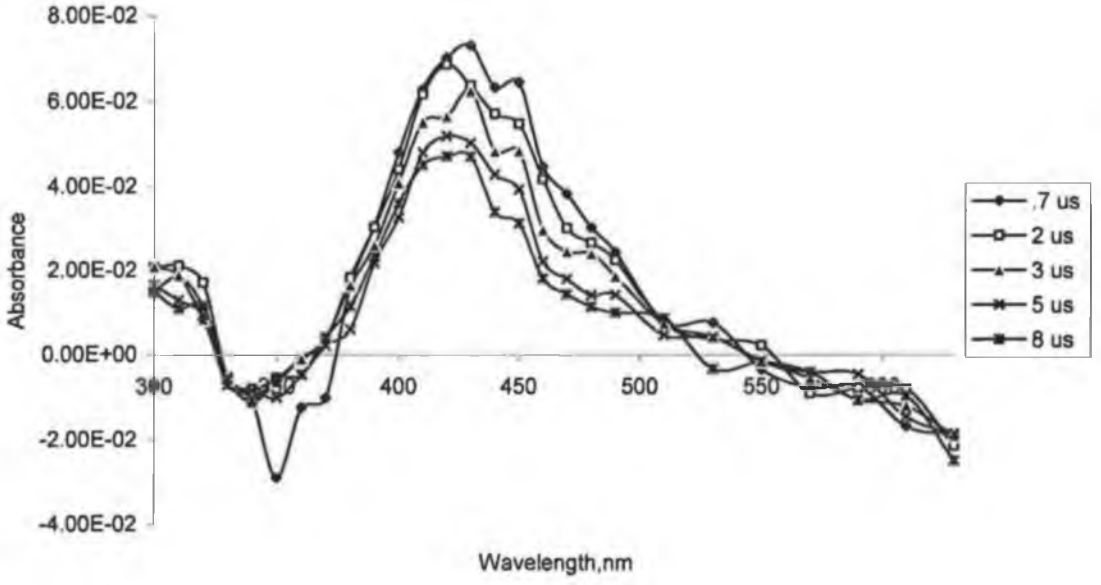

Fig 2.33 Transient absorption spectrum of $W(CO)_5PPh_3$ plus 1atm CO(0.009 M CO).

2.2.3 Matrix isolation photochemistry of $Cr(CO)_5L$, L = pyridine and 4-acetylpyridine in Argon matrix

The matrix isolation of these complexes reveals highly efficient ejection of the unique ligand to form $Cr(CO)_5Ar$ especially with long wavelength irradiation, while shorter wavelength irradiation induced CO loss but with lower quantum efficiency.

In some cases the irradiation with long wavelength induces the formation of $Cr(CO)_5L$, L = Py or Acpy in which the ligand coordinates through the aromatic C-H or π-electrons of pyridine ring.

Linkage isomerisation of acetylpyridine was also induced with longer wavelengths as observed in the steady state photolysis experiments (Section 2.1).

A further isomerisation occurs in two cases, those in which the cis-$Cr(CO)_4L$ isomerises to trans-isomer upon irradiation with 546 nm after first being produced with shorter wavelength irradiation.

Prolonging the photolysis with short wavelength radiation also induced the formation of the *fac*-$Cr(CO)_3L$ species in which the two argon molecules fill the vacant coordination sites on the metal centre.

2.2.3.1 Matrix isolation of $Cr(CO)_5Py$

Photolysis of $Cr(CO)_5Py$ in argon matrix at 12 K by 436 nm resulted in a change in the electronic absorption spectrum of the matrix, Fig. 2.34 with the production of a new band at 538 nm which is close to that observed for $Cr(CO)_5$ in pure argon matrix,[20] thus it appears that during this photolysis the cleavage of Cr—pyridine bond is an efficient process.

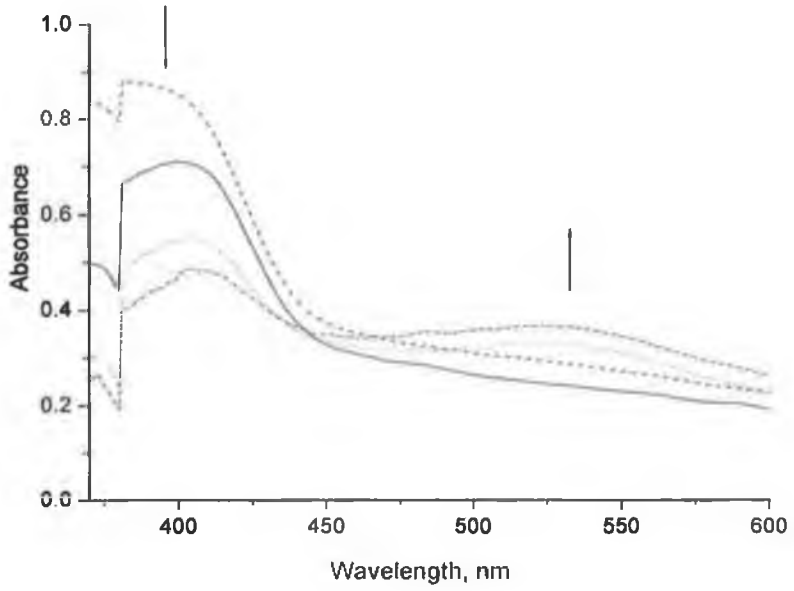

Fig. 2.34 UV/vis absorption spectra of $Cr(CO)_5$ Py in Argon matrix at 12 K during photolysis by 436 nm for 0, 5, 30, and 45 min..

IR spectroscopy was also used to monitor the process The difference in the IR spectra reveals clearly the formation of new species with bands at 2093, 1963 cm^{-1} which are assigned also by Boxhoorn *et al.*[28], to $Cr(CO)_5Ar$. We assigned the band at 2006 cm^{-1} to the formation of small amount of cis-$Cr(CO)_4Py$ although this band has not observed in previous studies. Fig 2.35 shows the IR spectra of the sample before and after photolysis with 436 nm.

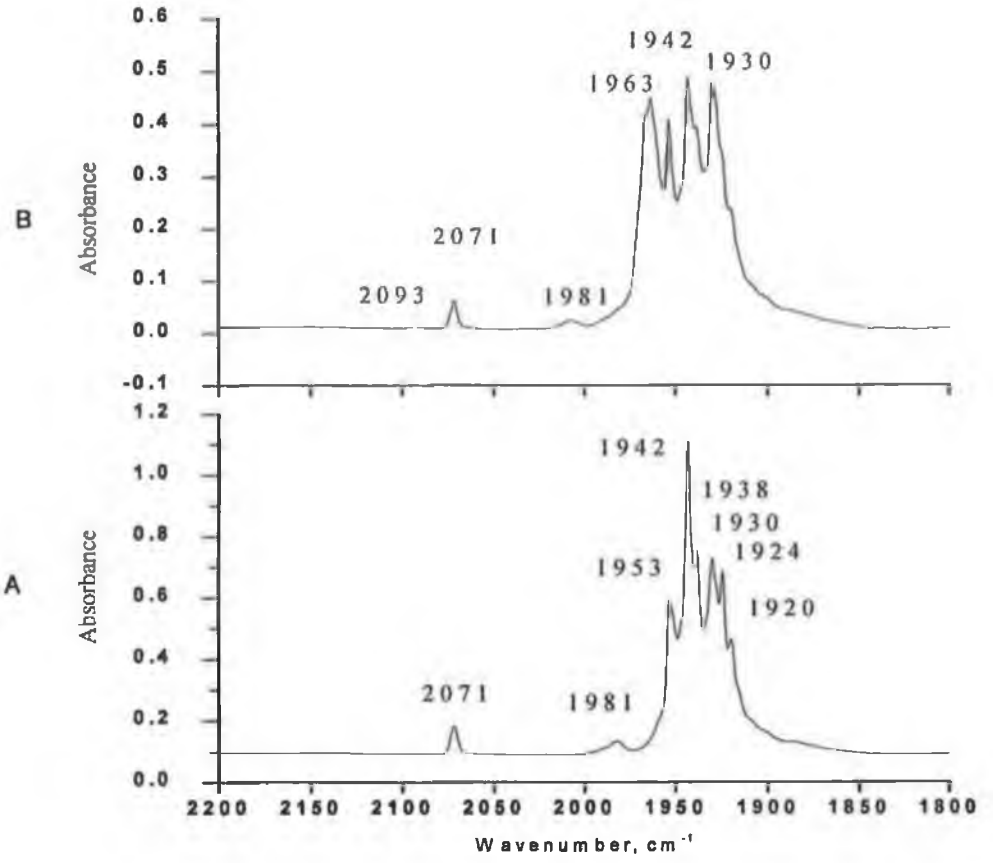

Fig 2.35 A) IR spectrum of $Cr(CO)_5Py$ in argon matrix at 12 K showed the matrix splitting of the υ_{CO} bands. B) The sample in A after photolysis with 436 nm for 45 min..

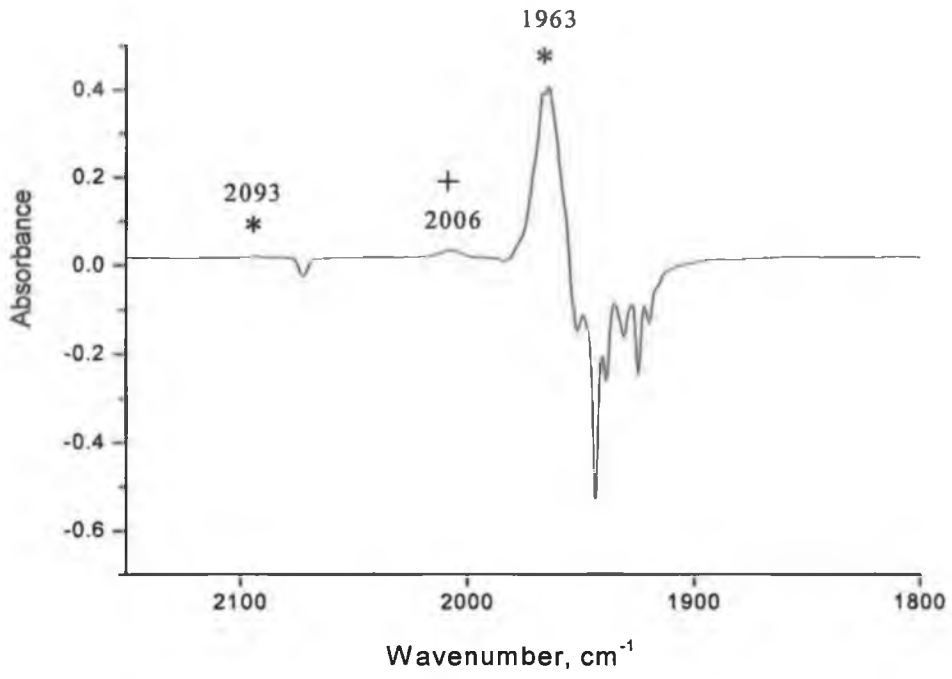

Fig 2.36 A difference IR spectrum following photolysis of $Cr(CO)_5Py$ in argon matrix at 12 K with 436 nm, negative bands indicate depletion.

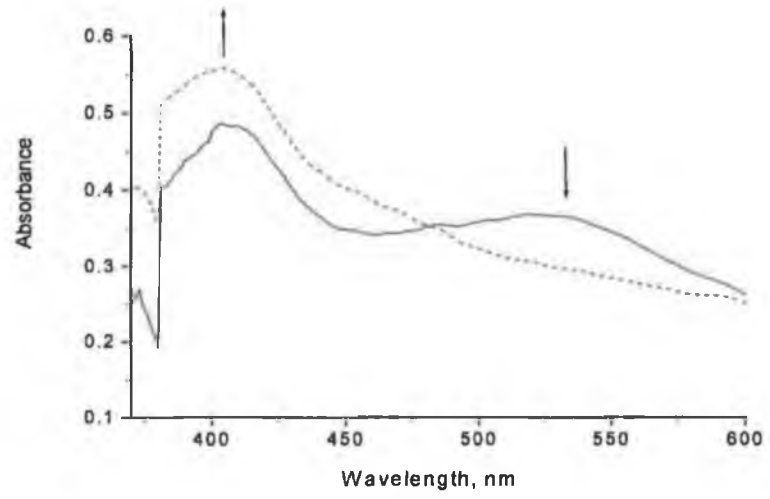

Fig. 2.37 UV/vis absorption spectra of $Cr(CO)_5Py$ in argon matrix at 12 K after photolysis by 436 nm 45 min. and by 546 nm for 60 min..

Photolysis of this matrix with longer wavelength (i.e. λ = 546 nm), resulted in regeneration of the parent compound as indicated by the depletion of the band at 538 nm in the electronic absorption spectra, Fig 2.37 and regeneration of the original band. This was confirmed by the IR spectra of the matrix, Fig 2.38. The regeneration process of the parent species after long wavelength photolysis is well known in the

literature for this type of complex and for the related metal hexacarbonyl systems.[20, 28]

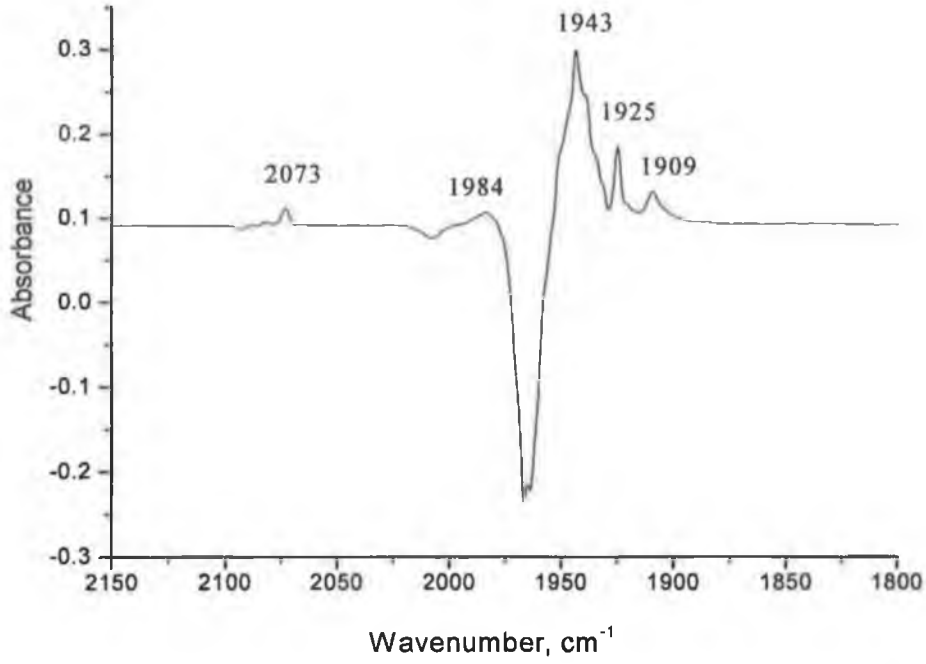

Fig 2.38 A difference IR spectrum of $Cr(CO)_5Py$ in argon matrix at 12 K following photolysis with 546 nm.

Following photolysis of this matrix with a broad band source ($\lambda > 400$ nm) a small blue shift of the λ_{max} by 4 nm was observed, Fig 2.39. The IR spectrum revealed the formation of new bands at 2088, 1977, 1970, 2023, 2006, and a band for free CO 2138 cm^{-1}. The first three bands are at lower wavenumber than those observed for $Cr(CO)_5Ar$ (2093, 1963, 1966 cm^{-1}), Fig 2.40. A possible explanation for this difference could be the coordination of the pyridine ring through a η^2-π of the ring interaction. This type of coordination of the arene ring was observed in the laser flash photolysis of $Cr(CO)_6$ at different arene solutions by Dobson *et al.*.[36]

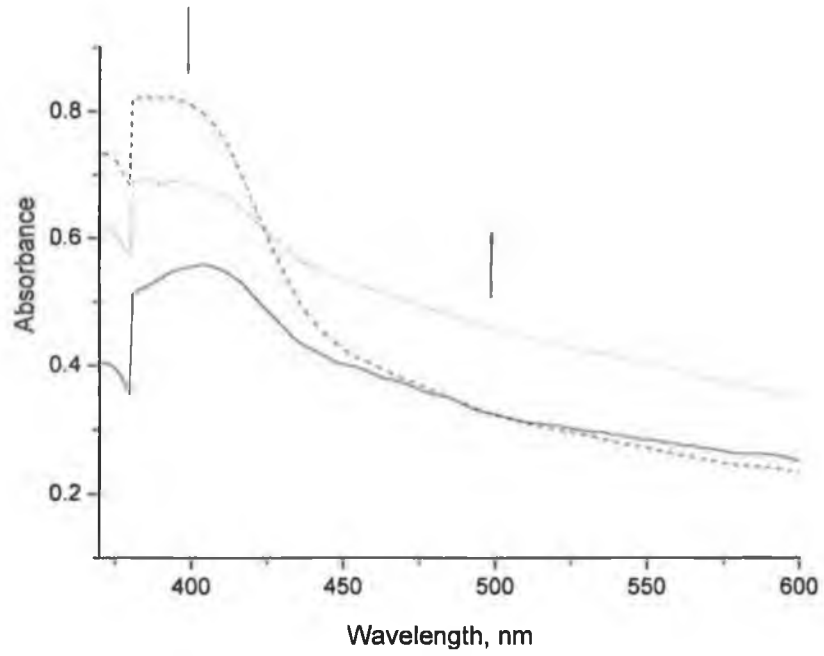

Fig 2.39 UV/vis absorption spectra of $Cr(CO)_5Py$ in argon matrix at 12 K during photolysis at 436 nm for 45 min., at 546 nm for 60 min. and by $\lambda > 400$ nm for 3 and 30 min..

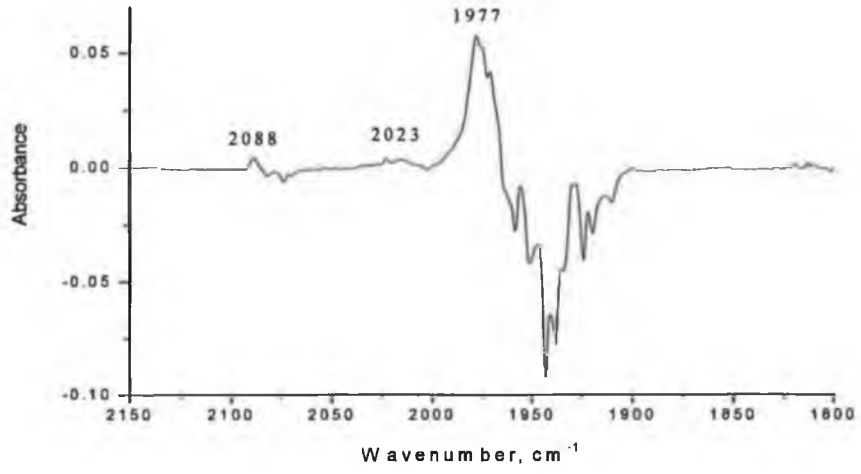

Fig 2.40 A difference IR spectrum of $Cr(CO)_5Py$ in argon matrix at 12 K following the photolysis with >400 nm for 30 min..

The band at 2023 cm^{-1} is relatively close to that observed for cis-$Cr(CO)_4Py$ in argon matrix 2032 cm^{-1} so this band is assigned to the complex cis-$Cr(CO)_4Py$ in which pyridine is coordinated through η^2-π system of the ring or alternatively a C—H bond of the pyridine ligand.

Photolysis of this matrix at 405 nm induced the cleavage of Cr—Py bond and also the formation of cis-$Cr(CO)_4Py$ as shown by the band at 2006 cm^{-1}, Fig 2.41.

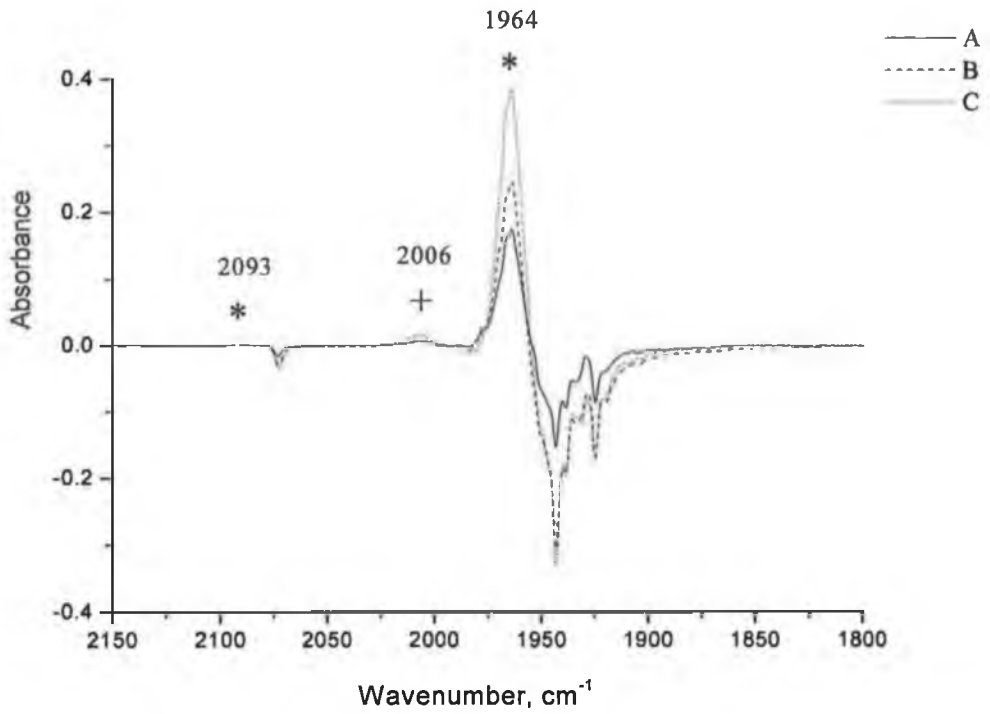

Fig 2.41 A difference IR spectrum of $Cr(CO)_5Py$ in argon matrix at 12 K following photolysis with 405 nm for (A) 10 min, (B) 30 min, (C) 60 min.

Photolysis 546 nm regenerates the parent complex with the additional appearance of band at 1909 cm^{-1} which is close to that observed by Boxhoorn *et al.*[28], 1907.8 cm^{-1} which they assigned to the trans-isomer of $Cr(CO)_4Py$ and they suggest that photolysis with this wavelength induced the cis-trans isomerisation of $Cr(CO)_4Py$, Fig 2.42.

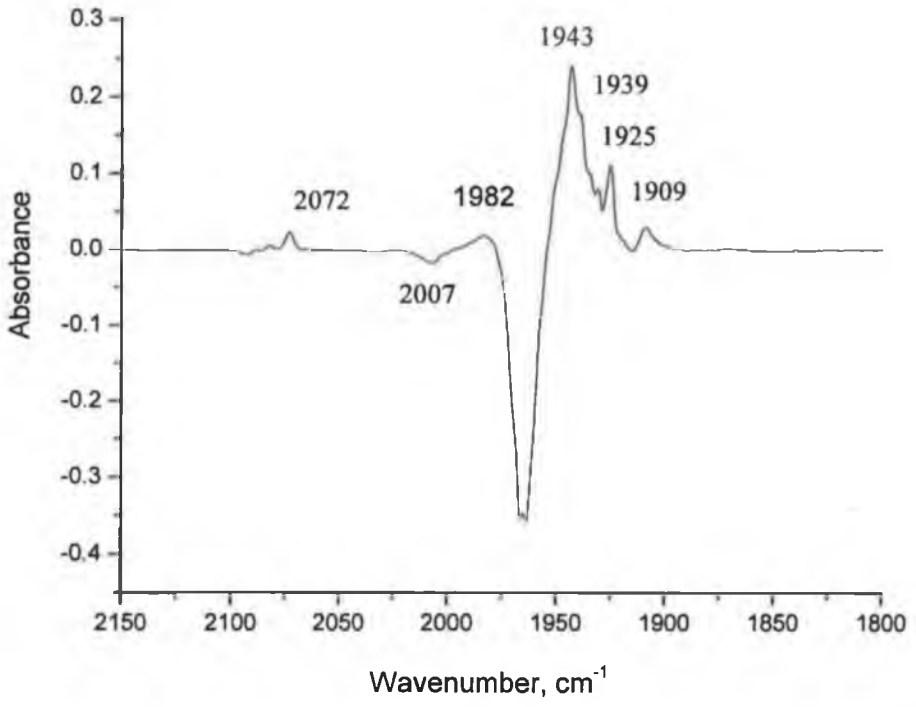

Fig 2.42 A difference IR spectrum of $Cr(CO)_5Py$ in argon matrix at 12 K following photolysis with 546 nm.

2.2.3.2 Matrix isolation of $Cr(CO)_5Acpy$

Consecutive irradiations of this complex have been undertaken in an argon matrix at 12 K and the results are as follows.

Photolysis with 436 nm produced a significant change in the electronic absorption spectrum of the sample Fig. 2.43 with the creation of a new band at 538 nm which is close to the wavelength observed for $Cr(CO)_5$ in pure argon matrix. Thus it would appear that during this photolysis the cleavage of Cr—acetylpyridine bond is a highly efficient process as photolysis times for this process are short.

This conclusion was confirmed by the IR spectrum of the matrix after photolysis Fig 2.44. The difference in the IR spectra reveals clearly the formation of new species with bands at 2092, 1964 cm^{-1}, which were assigned by Boxhoorn *et al.*[28], to $Cr(CO)_5Ar$, see also Fig.2.44. We assigned the band at 2005, 1885 cm^{-1} to the formation of small amount of cis-$Cr(CO)_4(Ar)(Acpy)$ confirmed by the formation of free CO in the matrix which has band at 2138 cm^{-1}.

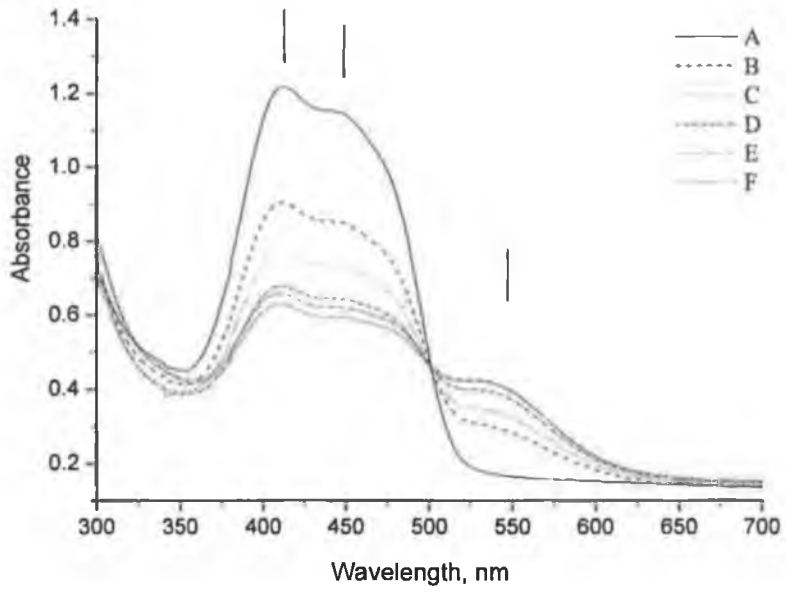

Fig. 2.43 UV/vis absorption spectra of $Cr(CO)_5Acpy$ at 12 K after photolysis with 436 nm for 0, 20, 40, 90, 130, and 145 min..

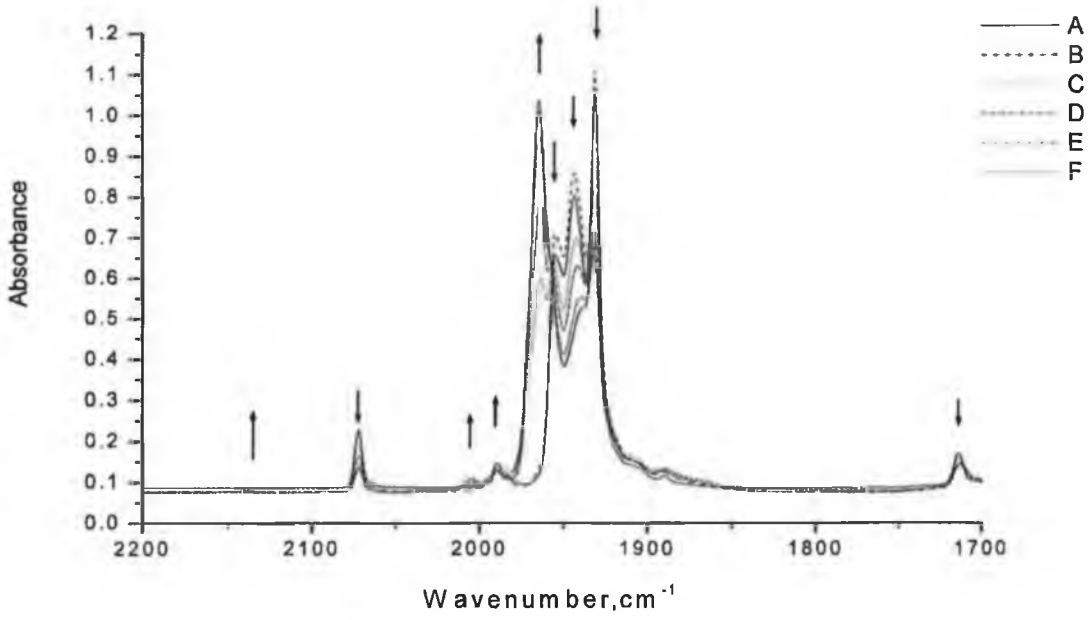

Fig. 2.44 IR spectrum of $Cr(CO)_5Acpy$ in an argon matrix at 12 K, and after photolysis with 436 nm for 0, 20, 40, 90, 130 and 145 min..

The isosbestic points in the UV and IR spectra confirm a clean conversion of $Cr(CO)_5Acpy$ to the $Cr(CO)_5$—argon complex and that the formation of tetracarbonyl species is at least only a minor product. The CO stretching band of the

ligand at 1708 cm^{-1}, Fig 2.45, also indicates the formation of free acetylpyridine ligand.

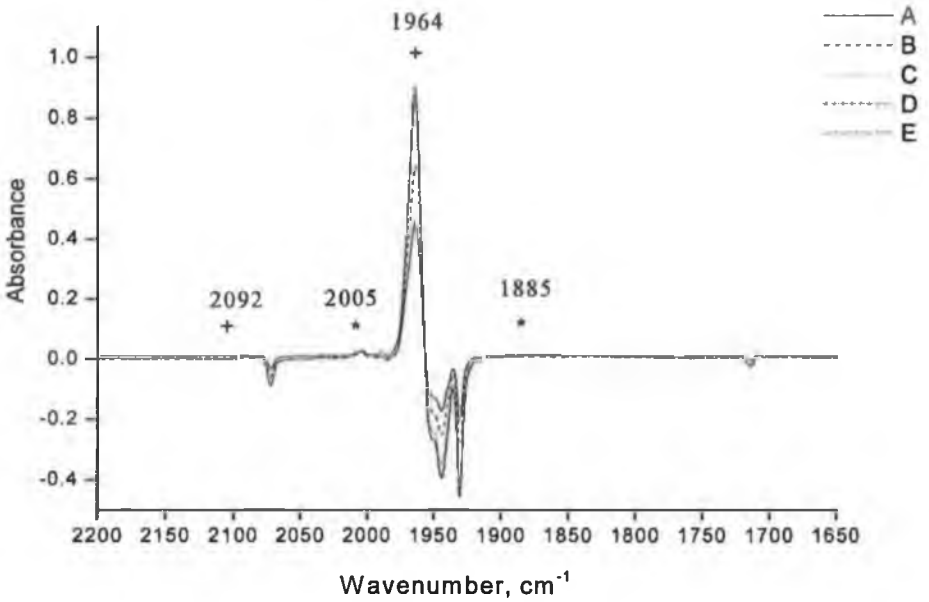

Fig. 2.45 A difference IR spectrum of $Cr(CO)_5Acpy$ in an argon matrix at 12 K after photolysis with 436 nm for (A) 20, (B) 40, (C) 90, (D) 130 and (E) 145 min..

Photolysis with 405 nm also produced the $Cr(CO)_5$—(Argon) complex as above, but the change here would appear to be more efficient than that at 436 nm Fig 2.46(a) and Fig 2.47. Some $Cr(CO)_4(Ar)(Acpy)$ is also formed as indicated by the band at 2005 cm^{-1} in the IR spectrum.

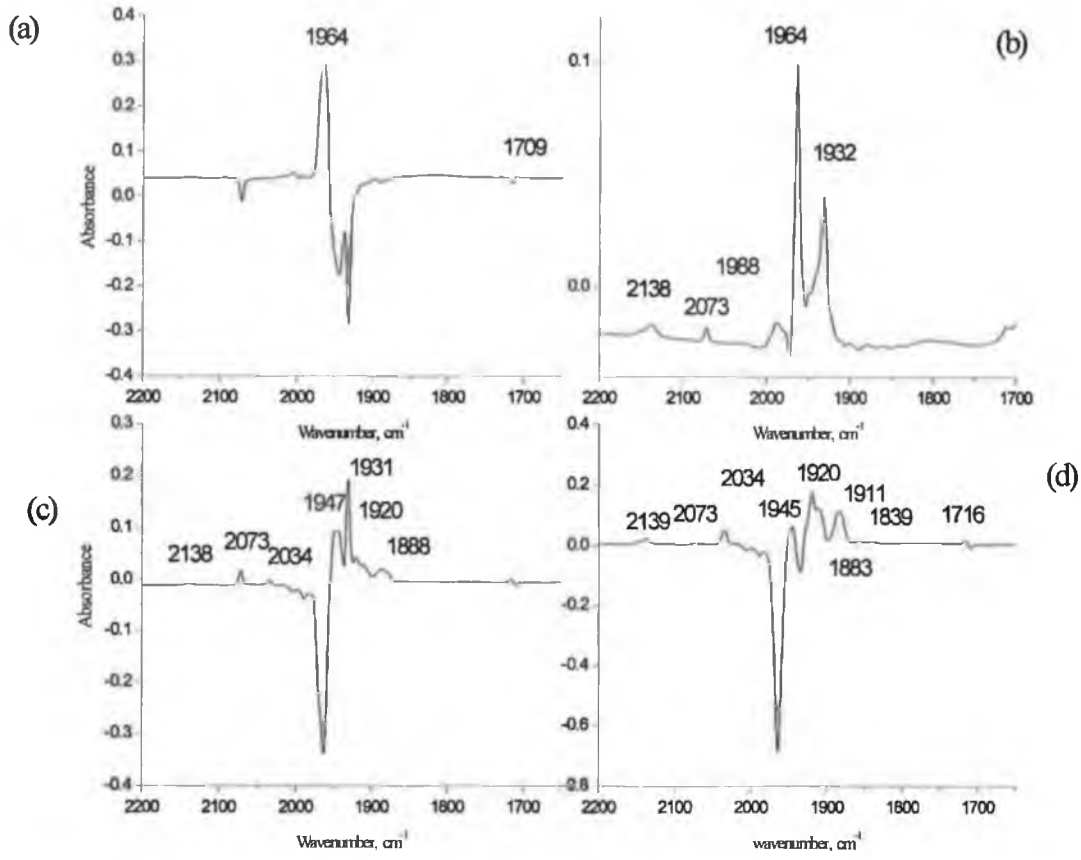

Fig. 2.46 A difference IR spectrum of $Cr(CO)_5Acpy$ in argon matrix at 12K (a) after photolysis with 405 nm for 80 min. (b) after a subsequent photolysis with 365 nm for 115 min. (c) after a subsequent photolysis with 334 nm (d) after a subsequent photolysis with λ_{exc} = 313 nm.

Subsequent photolysis with 365 nm produced a tetracarbonyl species as indicated by the stretching vibration peaks at 1899,1880 cm^{-1}. Fig 2.46(b), these were assigned to the cis and trans isomers of $Cr(CO)_4(Ar)_2$ in the argon matrix. Turner and co-workers observed the band at 1891 cm^{-1} and assigned that to cis-$Cr(CO)_4$[20] upon photolysis of $Cr(CO)_6$ in an argon matrix.

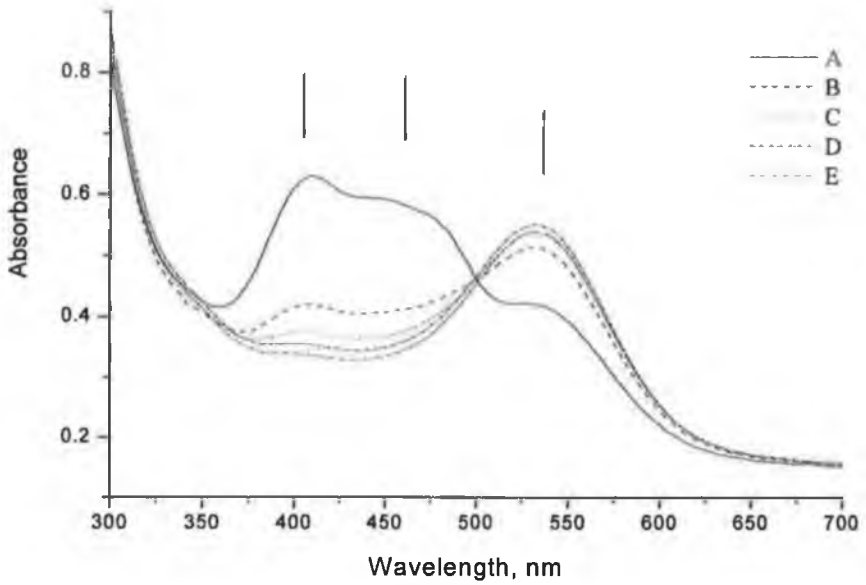

Fig. 2.47 UV/vis Absorption spectra of $Cr(CO)_5Acpy$ after photolysis by 436 nm for 145 min. and subsequent photolysis at 405 nm for 20, 40, 60, 80 min.

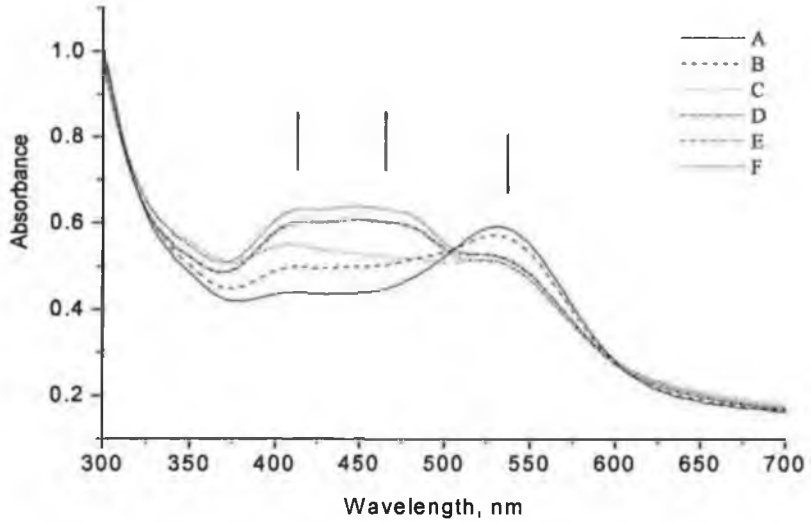

Fig 2.48 UV/vis absorption spectra of $Cr(CO)_5Acpy$ in an argon matrix at 12 K after photolysis with- 436 nm for 145 min., 405 nm for 80 min., 365 nm for 115 min. and with 334 nm for 0, 20, 70, 100, 130,and 150 min..

Subsequent photolysis of the matrix at 334 nm resulted in a significant regeneration of the parent compound $Cr(CO)_5Acpy$ as indicated by grow in of the bands at 2072, 1947, 1930 and 1715 cm^{-1} , Fig 2.46 (c). The recovery of the UV/vis band at 436 nm supported this assignment, Fig 2.48, The bands at 2034, 1919, 1887 cm^{-1} were

assigned to the formation of cis-$Cr(CO)_4Acpy(Ar)$. Boxhoorn *et al.*[28], assigned bands at 2037, 1927, 1915, and 1889 cm^{-1} to cis-$Cr(CO)_4Py$. The formation of cis-$Cr(CO)_4Acpy$ is also supported by the grow-in of the free CO band at 2138 cm^{-1}.

UV/vis absorption spectrum provides good evidence for the formation of these species as a broad band at 450 nm (which appears as of two overlapping bands) which are related to the products, and depletion of the band at 531 nm which related to $Cr(CO)_5Ar$ as shown in Fig 2.48.

Photolysis of the matrix with 313 nm radiation resulted in similar changes to those obtained with 334 nm radiation, but as the photolysis time was extended *fac*-$Cr(CO)_3(Ar)_2Acpy$ was produced with bands at 1857, and 1839 cm^{-1} which are close to that obtained by Boxhoorn *et al.*[28] for $Cr(CO)_3Pyrazine(Ar)_2$. Also the formation of the band at 2139 cm^{-1} indicates the formation of free CO.

The changes to UV/vis Fig. 2.49 following photolysis of $Cr(CO)_5Acpy$ produced a band at 460 nm which was assigned to cis-$Cr(CO)_4Acpy(Ar)$. This band suffered depletion upon prolonged photolysis.

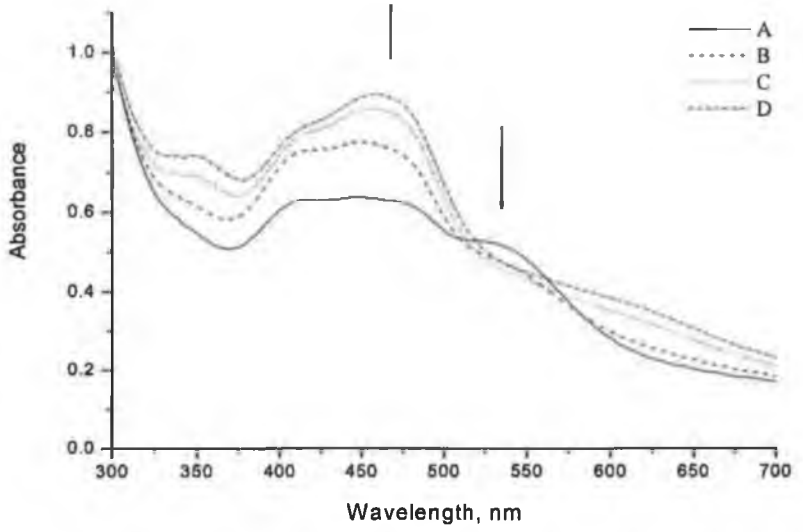

Fig 2.49 UV/vis of $Cr(CO)_5Acpy$ in argon matrix at 12 K after photolysis with 436 nm for 145 min., 405 nm for 80 min., 365 nm for 115 min., with 334 nm for 150 min., and with 313 nm for 0, 20, 75, and 100 min..

Subsequent photolysis of an argon matrix containing $Cr(CO)_5Acpy$ with 297 nm increased the intensities of the bands at 1919, 1909, 1882, 1856, 1839, 1718 cm^{-1},

Fig. 2.50, which means an increase in the formation of cis-$Cr(CO)_4$Acpy and *fac*-$Cr(CO)_3$Acpy, while the depletion of the bands at 1964, 1955, 1942, 1931 cm^{-1} indicates a decrease of the concentration of $Cr(CO)_5$Acpy and $Cr(CO)_5$Ar in the matrix. The changes here are small and this suggests that the yield of these species is low.

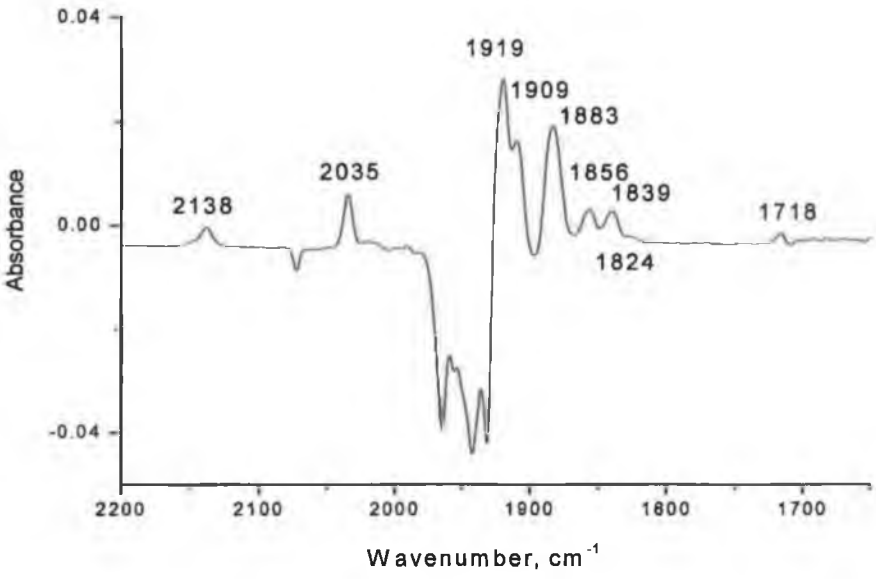

Fig 2.50 A difference IR spectrum of the $Cr(CO)_5$Acpy in an argon matrix following the photolysis with λ_{exc} = 297 nm.

Subsequent photolysis with broad band >520 nm radiation destroyed most of $Cr(CO)_5$, cis-$Cr(CO)_4$, and $Cr(CO)_3$ species while $Cr(CO)_5$Acpy regenerated as indicated by the growth of the bands at 2072, 1945, 1932, 1715cm^{-1}, Fig. 2.51.

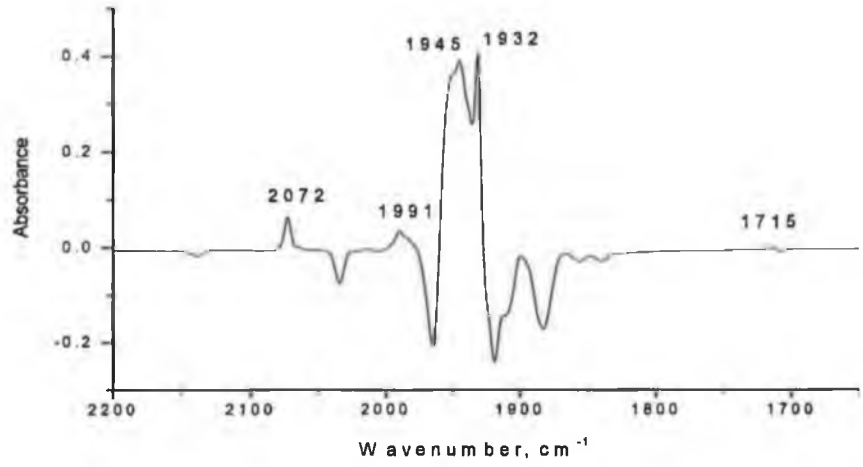

Fig 2.51 A difference IR spectrum of the $Cr(CO)_5$Acpy in an argon matrix following the photolysis with λ_{exc} >520 nm.

UV/vis spectrum also indicated the growth of the bands related to the parent complex $Cr(CO)_5Acpy$ as shown in Fig 2.52.

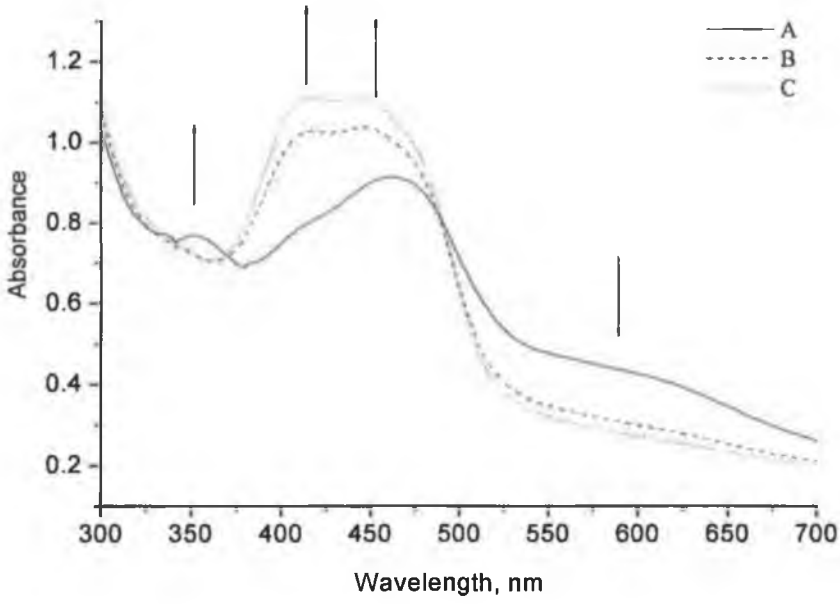

Fig. 2.52 UV/vis of $Cr(CO)_5Acpy$ in argon matrix at 12 K after photolysis with 436 nm for 145 min., 405 nm for 80 min., 365 nm for 115 min., with 334 nm for 150 min., with 313 nm for 100 min., with 297 nm for110 min., and with >520 nm for 0, 15, and 30 min..

Photolysis with λ_{exc} >400 nm induced the linkage isomerisation of Acpy ligand from coordination of nitrogen atom of pyridine ring to oxygen atom of acetyl group as shown by the formation of a band at 1988 cm^{-1}, previously observed in the steady state photolysis. The $Cr(CO)_5Ar$ species was also formed by (1966 cm^{-1}) while the band at 1908 cm^{-1} is close to that observed for trans-$Cr(CO)_4Py(Ar)$ 1907.9 cm^{-1} was assigned to trans-$Cr(CO)_4Py(Ar)$, Fig 2.53.

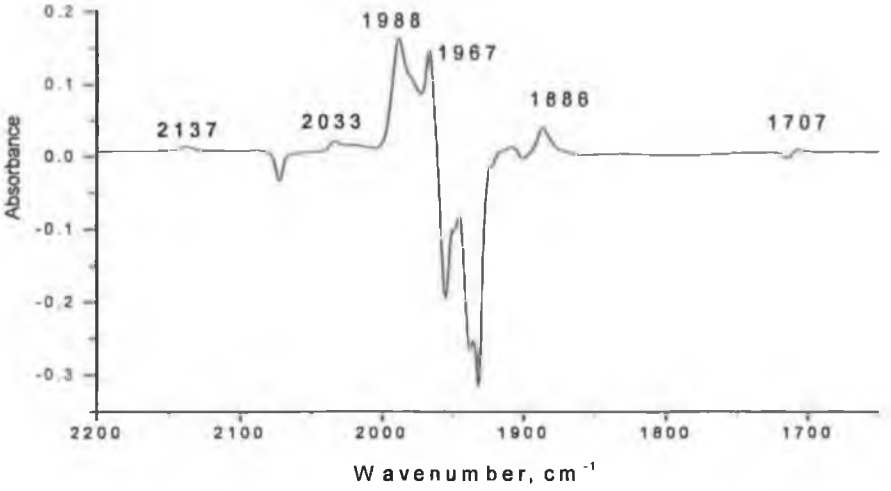

Fig. 2.53 A difference IR spectrum of the matrix before and after photolysis with λ_{exc} >400 nm

In these experiments the UV/vis spectrum shows a grow-in of the band at 532 nm and depletion of the band at 460 nm, Fig 2.54.

In a separate experiment $Cr(CO)_5Acpy$ in an argon matrix was photolysed with λ_{exc} >400 nm and new bands at 2088, 1977, cm^{-1} were observed as shown in Fig 2.55, these bands are assigned that to $Cr(CO)_5Acpy$ in which the aromatic C—H or the pyridine ring is coordinated to the metal centre through the π system. The bands at 2022, 1861 were assigned to the tetracarbonyl species $Cr(CO)_4(Acpy)(Ar)$.

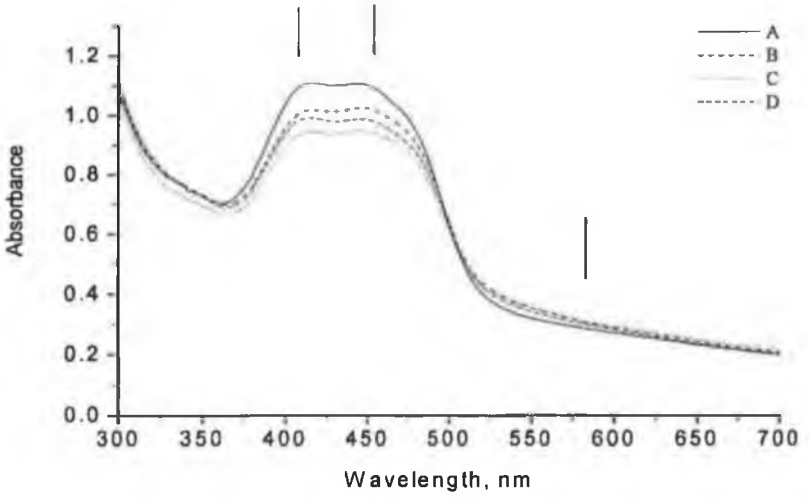

Fig. 2.54 UV/vis spectra of $Cr(CO)_5Acpy$ following photolysis of an argon matrix at 12 K with. 436nm for 145 min., 405 nm for 80 min., 365 nm for 115 min., with 334

nm for 150 min., with 313 nm for 100 min., with 297 nm for 110 min., with >520 nm 30 min and with >400nm for 0, 15, 60, and 80 min.

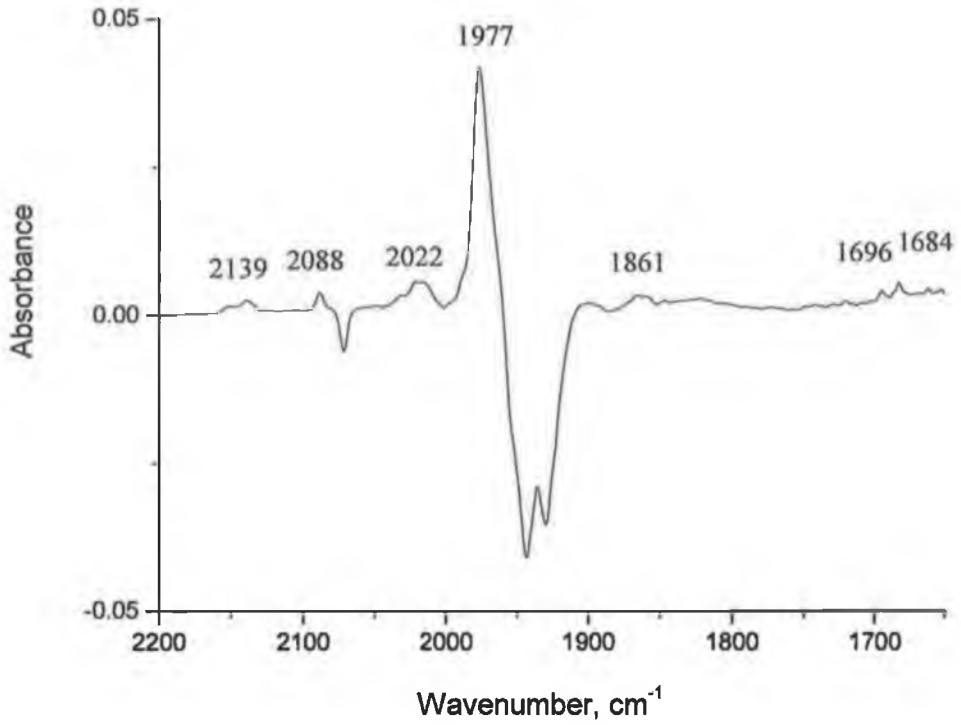

Fig. 2.55 A difference IR spectrum of the matrix of $Cr(CO)_5Acpy$ in argon matrix at 20 K following photolysis with λ_{exc} >400 nm for 15 min..

Photolysis of the matrix with broad band >300 nm produced $Cr(CO)_5Ar$, cis-and trans-$Cr(CO)_4Acpy(Ar)$, and *fac*-$Cr(CO)_3Acpy(Ar)_2$ as indicated by the vibrational spectra of the sample after photolysis, Fig 2.56.

Upon melting the matrix, the parent complex recovered, the linkage isomer and cis-, and trans-$Cr(CO)_4Acpy$ appear as shown in Fig 2.56 b.

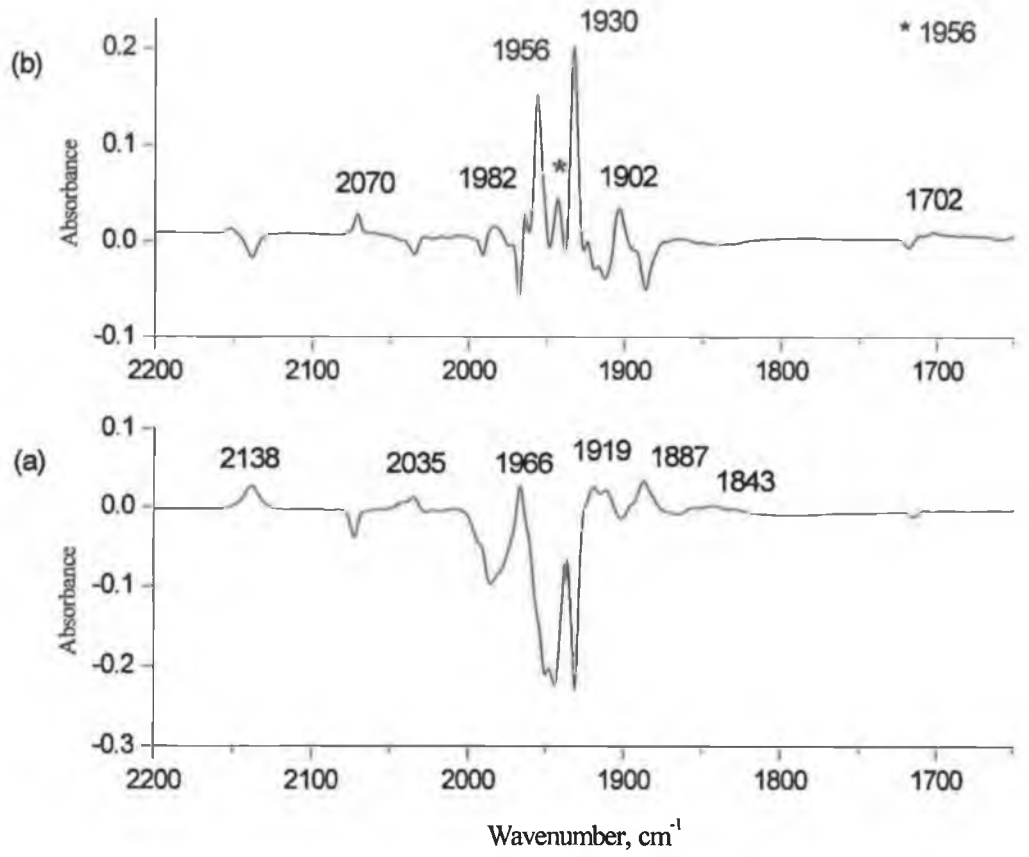

Fig 2.56 (a) The difference in the IR spectra of the sample which the irradiated matrix (which irradiated with > 400 nm only) following the photolysis with >300 nm. (b) A difference IR spectrum of the matrix following the promotion of the temperature to
40 K.

2.3 Discussion

2.3.1 Electronic spectra: - The assignments of the electronic absorption bands of the complexes under this study are depend on the traditional assignments of the electronic spectra which give the main role to LF as the low lying excited states in the electronic absorption of $W(CO)_5Py$.

The electronic spectrum of $W(CO)_5Py$ in cyclohexane exhibits a low-energy shoulder near 442 nm which has been previously assigned to a LF $^1A_1(e^4b_2^2)\rightarrow{}^3E$ $(e^3b^2a^1)$, while the band at 390 nm was assigned to LF $^1A_1(e^4b_2^2) \rightarrow{}^1E$ $(e^3b^2a_1^1)$ and the band at 355 nm was W→Py CT.

The electronic spectra of $W(CO)_5$Acpy and $W(CO)_5$CNpy are different to that of $W(CO)_5$Py. These spectra contain one band at 404 nm that assigned to LF $^1A_1(e^4b_2^2)$ $\rightarrow{}^1E$ $(e^3b_2^2a_1^1)$ transition. The band related to the LF transition $^1A_1(e^4b_2^2)$ $\rightarrow{}^3E$ $(e^3b^2a_1^1)$ was obscured by W$\rightarrow$ L CT absorption, which are represented by the absorption band at 440 and 455 nm for acetyl pyridine and cyanopyridine complex respectively.[3]

The intense absorption observed at 270 nm in all the absorption spectra which was also observed in the electronic spectrum of the tungsten hexacarbonyl was assigned to W$\rightarrow\pi$*CO CT transition. [3]

So the assignment of the LF and MLCT bands spectra in the case of the 4-acetyl- and 4-cyanopyridine complexes is different to that of $W(CO)_5$Py. W$\rightarrow$Py CT band in $W(CO)_5$Py is at higher energy than the LF, while the reverse is true for the other complexes.

The first low energy absorption band of $W(CO)_5PPh_3$, and $Cr(CO)_5PPh_3$ which appears as shoulder at ca. 350 nm has been assigned to the LF $^1A_1(e^4b_2^2)$ $\rightarrow{}^1E$ $(e^3b_2^2a_1^1)$ transition, where the higher frequency, more intense absorption at 315 nm is most likely W$\rightarrow\pi$*CO charge transfer.

The weak forbidden LF $^1A_1(e^4b_2^2)$ $\rightarrow{}^3E$ $(e^3b_2^2a_1^1)$ transition was not observed, however, this band has been noted in several analogues tungsten derivatives.[3]

Photolysis of the complexes of the type $M(CO)_5L$, where M = Cr, or W; L = Pyridine, 4-acetylpyridine, 4-cyanopyridine, or PPh_3 with broad band (i.e. >410, >400, >390, >340,>320, or >300nm) and monochromatic band (laser 354.7 nm) resulted loss of the unique ligand and/or loss of CO. Using the laser flash photolysis and low temperature matrix isolation experiments the two intermediate species (as a result of unique ligand loss or CO loss) were observed.

2.3.2 Steady state photolysis $M(CO)_5L$, M = Cr or W; L = Py, Acpy, CNpy, or PPh_3: -

Steady state photolysis of the complexes $Cr(CO)_5L$, L = Py, Acpy, or CNpy in the presence of excess ligand reveals dramatic change in the UV/vis spectra. For $Cr(CO)_5$Py the change is due to the loss of CO and formation of the tetracarbonyl

complex cis-$Cr(CO)_4Py_2$ especially with short wavelength irradiations. The band grow-in at 450 and 340 nm is assigned to cis-$Cr(CO)_4Py_2$.

The photochemical CO loss in chromium complexes is more efficient than tungsten analogues. It is more important than unique ligand loss especially following short wavelength irradiation thus the ratio of CO loss to the unique ligand loss is 1:1 upon irradiation with 366 nm, and jumps to 2:1 upon irradiation at 313 nm.[6]

In the presence of substituent on the pyridine ring (i.e for L = Acpy, or CNpy), the irradiation led to the linkage isomerism of the pyridine ligand especially with long wavelength irradiation. Wang and Lees [9] noticed that the pyridine-bound isomer is the thermodynamically preferred form but the cyano-bound isomer is the kinetically favored. This linkage isomer is thermally unstable and reverts to the original isomer in which coordination is through the ring nitrogen.

Degassing by freeze pump thaw procedure of the solution of $Cr(CO)_5CNpy$ in toluene in the presence of excess ligand (0.01 M) induced the linkage isomerism of the 4-cyanopyridine ligand.

Photolysis of $M(CO)_5PPh_3$, M = Cr, or W with 354.7 nm, >320 nm, or >340 nm was studied under two conditions: -

a) In cyclohexane under CO (1atm, 0.009 M). b) In the presence of 0.01 M PPh_3 under argon.

Two species formed upon photolysis one is $M(CO)_5$ which when trapped with PPh_3 forms the parent complex, while it forms the $M(CO)_6$ when trapped by CO. The last product identified by its specific ν_{CO} band at ca. 1986 cm^{-1}.

The second species formed is $M(CO)_4PPh_3$ which has C_s symmetry and is formed when the CO loss the parent complex when trapped by PPh_3, while it form $M(CO)_4(PPh_3)_2$ as cis isomer in the case of tungsten and trans product in the case of chromium. The formation of cis or trans isomers is dependant on the metal. The chromium system exhibits a larger steric effect between the two bulky triphenylphosphine ligands compared to the tungsten analogue, so the trans is more stable than the cis isomer for the chromium system. The other factors which affect the formation of cis or trans isomer is the life-time of C_s-$M(CO)_4PPh_3$ fragment in the solution relative to C_{4v}-isomer.

The complexes formed (i.e. trans-$Cr(CO)_4(PPh_3)_2$ and cis-$W(CO)_4(PPh_3)_2$ upon photolysis were characterised by their IR spectra and electronic spectra.

Steady state photolysis of $W(CO)_5Py$ or $W(CO)_5Acpy$ in the presence of excess ligand did not result in a significant changes to the UV/vis. spectrum. Although it is well known that the photolysis of these complexes with monochromatic light in the same range as the broadband irradiation used here, resulted in photochemical substitution reaction of the unique ligand or CO. No change in the UV/vis. spectrum upon irradiations with broadband light can be explained by two possibilities: -

1- Photolysis with broadband light does not induce any loss of the unique ligand or CO. This is in contrast with the fact that the irradiation with monochromatic light leads to ligand loss with quantum efficiencies dependant on the wavelength used.

2- The photolysis with broadband light induces the loss of the unique ligand and/or the loss of CO. At the same time the reverse reaction (i.e. the reaction of the photoproduct intermediates with the lost ligands to form the parent complex) is a highly efficient process. Consequently no change in the steady state UV/vis spectrum is observed.

In the literature it is well known that the photochemical reaction of pyridine or pyridine derivatives with tungsten hexacarbonyl using broad band irradiation is one route to the preparation of the disubstituted tetracarbonyl complexes $W(CO)_4L_2$ where L is pyridine or pyridine derivatives.

It is possible that the presence of $W(CO)_6$ in the solution may have a role as a catalyst for the reaction of $W(CO)_5L$ (which is formed as the first product of the photochemical reaction) with L to form $W(CO)_4L_2$.

The photochemically induced CO loss from $W(CO)_6$ is wavelength independent and highly efficient when compared to the unique ligand loss from $W(CO)_5L$ which is wavelength dependent and less efficient. So, the production of $W(CO)_5$ species from the hexacarbonyl is more efficient than from $W(CO)_5L$. The $W(CO)_5$ fragment may attack $W(CO)_5L$ molecule during life time in the solution to form the dinuclear species $(CO)_5W\text{-}OC\text{-}W(CO)_4L$ which dissociates to form the coordinatively unsaturated species $W(CO)_4L$ and the $W(CO)_6$. The former species reacts with a further ligand in the solution to form the cis-$W(CO)_4L_2$ complex. Formation of the dinuclear species was observed for systems like $Cr(CO)_6$, $(\eta^5\text{-}C_5H_5)Co(CO)_2$, $(\eta^6\text{-arene})Cr(CO)_3$, $(\eta^5\text{-}C_5H_5)Mn(CO)_3$ and $(\eta^5\text{-}C_5H_5)V(CO)_4$ upon photolysis.[37]

Steady state photolysis of $W(CO)_5CNpy$ using broadband irradiation ($\lambda_{exc.} > 410$ nm), produced a blue shift in the UV/vis. spectrum as a result of linkage isomerism of the cyanopyridine ligand from pyridine-bound species to cyano-bound isomer[9]. The later is photochemically stable but thermally unstable and tends to isomerise to pyridine bound isomer. No CO loss was observed upon photolysis under these conditions (i.e. > 410 nm). The reason for this may be that the photolysis in this range induces the reverse of the CO-loss process. So no cis-$W(CO)_4(4\text{-}CNpy)_2$ complex could be detected in the electronic spectrum.

Upon irradiation with λ_{exc} >400 nm, >340 nm, and >300 nm, isomerisation also occurred, comment to the loss of CO as indicated by the growth of the band around 500 nm which is assigned to the cis-$W(CO)_4(4\text{-}CNpy)_2$ complex. The irradiation with 354.7 nm induces the loss of CO to form the cis-$W(CO)_4(CNpy)_2$ complex but no isomerisation of $W(CO)_5CNpy$. This wavelength also induces the loss of CO to form the tetracarbonyl complex cis-$W(CO)_4(4\text{-}CNpy)_2$.

2.3.3 Laser flash photolysis: -

2.3.3.1 Spectroscopic characterisation and reactivity of the photoproducts of $M(CO)_5L$: - The main photoproducts obtained upon photolysis of $M(CO)_5L$ are $M(CO)_5$ and $M(CO)_4L$. It is likely that a molecule of solvent occupies the vacant coordination site of these intermediates. These transient signals (species) are extremely short lived, especially in the presence of excess ligand. Therefore these solvated species decay concurrent with the formation of ligated complexes $M(CO)_5L$ and $M(CO)_4L_2$. The quantum yield for the two photoproducts is highly dependant on the metal M, the type of the ligand L, and the wavelength of irradiation. The quantum yields for the production of $M(CO)_5$ follow the order M = W > Cr; L = Py >Acpy > CNpy > PPh_3.

Two transient species were expected in the laser flash photolysis experiments of these complexes. The contribution of these two transient species to the total transient absorption spectrum will depend on the concentrations, the extinction coefficients, and the life times of the transient species. So, the rate constants of the transient decay will change upon changing the monitoring wavelength.

The presence of two photoproducts from the photolysis can be detected by the comparison of the data of flash photolysis experiments for these complexes with

those of the parent metal hexacarbonyl complex under the same conditions. For the hexacarbonyl one value for the rate constant k_{obs} was obtained, which does not vary with changing monitoring wavelength. In these studies of the complexes different rate constants were obtained for different wavelengths. This gives good evidence that two transient species were formed. It should be noted that the flash photolysis apparatus uses UV/vis. detection and is insufficient to unambiguously identify the transient species. Formation of two transients signals following photolysis of one species is not uncommon and has been reported for $Cr(CO)_3$(arene) and P(O-i-pr)$_3$W(CO)$_5$.[36]

The electronic absorption spectra of the transient species formed upon laser flash photolysis of $Cr(CO)_5Py$, $W(CO)_5Py$ have λ_{max} at ca. 465, and 420 nm respectively. The transient signal in the $W(CO)_5Py$ system did not fully recover to preirradiated level. The first is $W(CO)_5$ which reform the parent complex upon reaction with pyridine. The second transient species is cis-$W(CO)_4Py$ which forms the tetracarbonyl complex cis-$W(CO)_4Py_2$ which has different absorption than the parent complex.

In the case of the $Cr(CO)_5Py$ system it appears that there is no recovery of the parent absorbance following photolysis as a result of highly efficient CO loss ($\lambda_{exc.}$ = 354.7 nm).

Further evidence for this assignment comes from the comparison of the rate constants of the transient signals when monitored at different wavelengths. This is also supported by monitoring the steady state electronic absorption of the solution after photolysis with laser beam. The new band at ca. 500 nm was assigned to the tetracarbonyl complex.

So the primary photoproducts formed upon photolysis of $Cr(CO)_5L$ in cyclohexane in the presence of L is $Cr(CO)_5$(cyclohexane) and $Cr(CO)_4L$(cyclohexane). From the previous studies the transient species $Cr(CO)_5$(cyclohexane) has an absorption maximum at ca. 500 nm[38] and is extremely short-lived, especially in the presence of excess ligand. Therefore this solvated species decays concurrent with the formation of ligated complex $Cr(CO)_5L$

The transient absorption spectra of the complexes $M(CO)_5L$, M = Cr, or W; L = 4-acetylpyridne, or 4-cyanopyridine have λ_{max} at ca. 520 nm which are related to transients as indicated by the kinetic data. The transient signals of Cr complex did

not recover fully to the parent absorption as a result of photoisomerisation and formation of the tetracarbonyl complex (i.e. $\lambda_{exc.}$ = 354.7 nm). Formation of maroon or purple precipitate indicates the formation of the tetracarbonyl complex.

The laser flash photolysis of $M(CO)_5PPh_3$, M = Cr, or W was undertaken in cyclohexane under two conditions (i) in the presence of CO gas (1 atm, 0.009 M) and (ii) in the presence of excess ligand 0.01 M PPh_3.

Upon comparison of the rate constants for the transient species formed for the same monitoring wavelength under the two conditions it is clear that the rate constants in presence of excess PPh_3 are higher than those in the presence of CO. This is because triphenylphosphine is a better σ-donor than CO so it is accelerate the reaction.

2.3.4 Matrix Isolation: - Matrix isolation of $Cr(CO)_5Py$ and $Cr(CO)_5Acpy$ in argon at 12 K was undertaken to study the effect of changing the excitation wavelength. The matrix isolation of the named complexes reveals efficient rupture of the M-L bond L = Py or Acpy especially with long wavelength irradiations (546 or 436 nm), while the photolysis with shorter wavelengths (365, 334, or 313 nm for Acpy complex) induces loss of CO. The coordinatively unsaturated species formed upon photolysis are $Cr(CO)_5$, $Cr(CO)_4L$, and $Cr(CO)_3L$. The last product formed upon extending the photolysis time with shorter wavelengths. The matrix gas molecules occupied the vacant sites of these species.

The coordinatively unsaturated species $Cr(CO)_5$ with C_{4v} symmetry is identified by its vibrational spectrum by appearance of ν_{CO} stretching vibration bands at ca. 2092, 1964 cm^{-1} which assigned to A_1 and E vibrations, while the band at 1932 cm^{-1} which observed by Tuner and Perutz[20] upon photolysis of $Cr(CO)_6$ and assigned to the second A_1 was not observed in these studies because it is obscured by the parent peaks. Further evidence of this assignment comes from the electronic spectrum, which has new band at 538 nm, which is close to the $\lambda_{max.}$ of $Cr(CO)_5$ in pure argon matrix.

The formation of small amounts of $Cr(CO)_4L$ was observed even upon photolysis with long wavelengths but the efficiency of the formation of this species with increasing excitation energy. This species has C_s point group, so 4 ν_{CO} stretching vibration bands should appear. However only two bands are observed at ca. 2090, and 1885 cm^{-1} which assigned to A', and A" bands while the other bands are obscured

by the parent peaks. These bands are close to those observed for $Cr(CO)_4$ L = Py, CS, or PCl_3 and $W(CO)_4Py$.[37] The $Cr(CO)_4L$ species with C_s point group can isomerise photochemically to $Cr(CO)_4L$ which has C_{4v} point group with ν_{CO} stretching vibration bands at ca. 1908 cm^{-1}.[28]

Prolonging the photolysis of the irradiated matrix with short wavelength radiation induced loss of CO from the $Cr(CO)_4L$ species, L = Py, or Acpy, forming a coordinatively 14 electron species *fac*-$Cr(CO)_3L$. The ν_{CO} stretching bands are at ca. 1857, and 1839 cm^{-1} which are close to those obtained by Boxhoorn *et al.*, for $Cr(CO)_3$Pyriazine.[28]

Further irradiation of the matrix with broadband (white light) reverses most of the photochemical processes and regenerates the parent complex. A cis to trans isomerisation of $Cr(CO)_4L$ also occurs.

In some cases the irradiation with long wavelengths or broad band light induces the formation of $Cr(CO)_5L$ in which the ligand coordinates through the aromatic C-H or π-electrons of pyridine ring. Also linkage isomerisation of acetylpyridine also occurs with longer wavelengths as we seen in the steady state photolysis (section 2.1). The coordination through the C-H or π-electrons of pyridine ring is thermodynamically unstable but kinetically more favourable than the coordination through pyridine nitrogen (The pyridine ligand has five C-H bonds, and three π-electron pairs can coordinate to the metal relative one lone pair on the nitrogen atom).

The metal tetracarbonyl complex may also be formed but as it absorbs strongly in this region (i.e. it may be subject to further photolysis, which induces the reaction of the tetracarbonyl with the librated CO. As the quantum efficiency of the formation of metal tetracarbonyl and the concentration of the metal pentacarbonyl

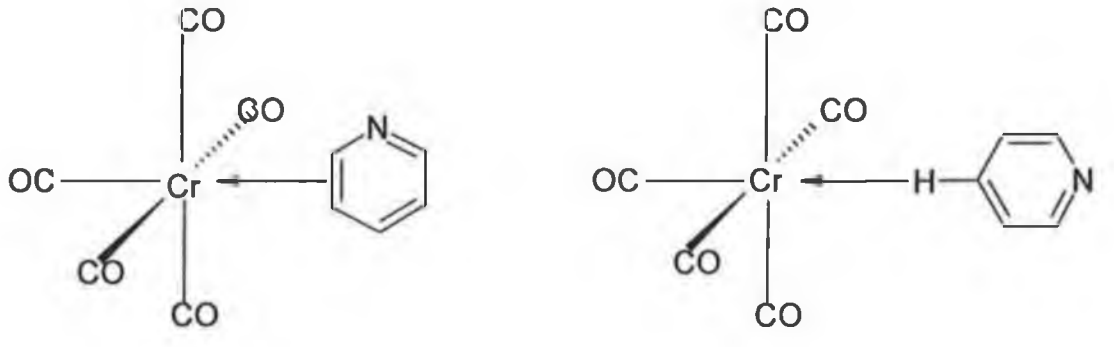

a b

Coordination of pyridine ligand through a) π-electrons b) C-H bond

Although it is well known that irradiation of $W(CO)_6$ in hydrocarbon solvent in the presence of excess of the pyridine ligand is one route for synthesis of the tetracarbonyl complexes cis-$W(CO)_4L_2$ [3], irradiation of $W(CO)_5L$, where L = Py, or Acpy failed is produce any change upon irradiation with broad band source. The presence of hexacarbonyl may have some role in the dissociation of the cis-CO group.

The laser flash photolysis studies give different values to the rate constant k at the monitoring wavelengths used. This suggests the presence of more than one transient signal. Irradiation at this wavelength (i.e. 354.7 nm) produces, in addition to the loss of unique ligand, loss of CO. For triphenylphosphine complexes the quantum efficiencies for loss of triphenylphosphine and the loss of CO are high and two transient species are produced in the flash photolysis experiments.[4]

The band at 1987 cm^{-1} in the infrared spectrum upon the photolysis of $Cr(CO)_5$Acpy although it should be observed three (2 A_1 + 1 E) IR active bands for this complex which expected to has locally C_{4v} point group. This assignment was supported by the ^{1}H-NMR study of this photolysis in deutrated cyclohexane. The DFT calculations reveal that this complex has C_{4v} geometry with ν_{CO} bands. No explanation about the difference in the number of ν_{CO} bands between the calculated and the observed IR spectrum but all the other spectral properties support this assignment. In addition to photoisomerisation process can be reversed when leaving the solution in the dark to form the parent complex and this support that this process is not the photodispropotionation which is known for the compound $W(CO)_5L$, L = Acpy, or CNpy to give $W(CO)_6$ and $W(CO)_4L_2$, which is irreversible.

2.4 Conclusion: -

This chapter describes the photochemistry of $M(CO)_5L$, M = Cr, or W; L = Pyridine, acetylpyridine, cyanopyridine, or triphenylphosphine. The steady state photolysis, laser flash photolysis and the matrix isolation studies on these complexes is presented. Generally, the steady state photolysis of most of these complexes resulted in ligand loss or CO loss photoproducts. In contrast with the literature no photochemical change upon the photolysis of $W(CO)_5$Py or $W(CO)_5$Acpy in the presence of excess of the ligand (0.01 M) with different broad band irradiations was observed. Monochromatic irradiations (354.7 nm) provided the tetracarbonyl complexes as precipitates from the cyclohexane solution. The photolysis of

$M(CO)_5PPh_3$; M = Cr, or W under CO atmosphere resulted the formation of the corresponding hexacarbonyl, while the photolysis in the presence of excess PPh_3 ligand resulted the tetracarbonyl photoproducts trans-$Cr(CO)_4(PPh_3)_2$ and cis-$W(CO)_4(PPh_3)_2$ for the chromium and tungsten complexes respectively.

The photolysis of $W(CO)_5CNpy$ in toluene in the presence of excess of the ligand (0.01 M) with different broad-band irradiation and with monochromatic irradiation gave the isomerised complex $W(CO)_5$(cyano-CNpy) and the tetracarbonyl complex. Photolysis of $Cr(CO)_5Acpy$ with different wavelengths resulted the formation of linkage isomer $Cr(CO)_5$(o-Acpy). The reverse of this reaction i.e. reformation of the parent complex occurred at room temperature upon leaving the solution in the dark.

The analysis of the laser flash photolysis kinetic data for these complexes reveals the presence of two primary transient species. The first species is the unique ligand loss species, while the second resulted from the CO loss.

Matrix isolation studies on the complex $Cr(CO)_5Py$ and $Cr(CO)_5Acpy$ in an argon matrix provided good indications of the ligand loss and CO loss. Wavelength dependence of the photoproducts formed was also observed. Clean formation of the coordinatively unsaturated photoproduct $Cr(CO)_5$ upon photolysis of these complexes with long wavelengths was observed. In addition to the formation of $Cr(CO)_5$ species the photolysis with shorter wavelengths resulted the formation of coordinatively unsaturated CO loss photoproduct cis-$Cr(CO)_4L$. Extending this photolysis resulted the formation of the coordinatively unsaturated tricarbonyl species *fac*- $Cr(CO)_3L$.

2.5 References: -

1) (a) Strohmeier, W;.Hobe, D. V., *Chem. Ber.*, 1961, 94, 2031.(b) Strohmeier, W.; Hobe, D. V. *Chem. Ber,* 1961, 94, 761,; *Z. physik. Chem. N. F.*, 1962,34, 393; (c) Strohmeier, W. *Aneg. Chem. Internat. Edit,* 1964, 3, 11, 730.

2) Wrighton, M. S. *Chem. Rev.,* 1974,74, 4, 401 and references therein.

3) Wrighton, M.S.; Abrahamson, H. B.; Morse, D. L. *J. Am. Chem. Soc*, 1978, 4105, 17, 1, 147.

4) Kolodziej, R. M.; Lees, A. J. *Organometallics*, 1986, 5, 450.

5) Lees, A. J.; Adamson, A. W. *J. Am. Chem. Soc.,* 1980, 102, 6874.

6) Darensbourg; D. J.; Murphy, M. A. *Inorg. Chem.*, 1978, 17, 4, 884.

7) Dahlgren, R. M.; Zink, J. L., *Inorg. Chem.,* 1977, 16, 12, 3154.

8) Darensbourg, D. J.; Murphy, M. A. *J. Am. Chem. Soc.*, 1978, 100, 2, 463.

9) Wang, Z.; Lees, A. J. *J. Organomet. Chem.*, 1989, 363, 335.

10) Dougherty, T. P.; Heilweil, E. J., *Opt. Lett.*, 1994, 19, 129.

11) Marlejo, C.; Langford, C. H. *J. Photochem. Photobiol. A: Chem.*, 1991, 59 285.

12) George, M. W.; Turner, J. J. *Coord. Chem. Rev.*, 1998,177, 201.

13) Clark, I. P.; George, M. W.; Turner, J. J. *J. Phys. Chem.* A, 1997, 101, 45, 8367.

14) Lindsay, E.; Vlček, A.; Langford, C. H. *Inorg. Chem.*, 1993, 32, 3822.

15) Johnson, F. P. A; George, M. W.; Turner, J. J., *Inorg. Chem.,* 1993, 32, 4226.

16) Johnson, F. P. A; George, M. W.; Morrison, S. L.; Turner, J. J., *J. Chem. Soc., Chem. Commun,* 1995, 391.

17) Stolz, I. W; Dobson, G. R.; Sheline, R. K, *J. Am. Chem. Soc.,* 1962, 84, 5589; *J.Am. Chem. Soc.*, 1963, 85, 1013.

18) Poliakoff, M.; Turner, J. J., *J. Chem. Soc. (A),* 1971, 654.

19) Kundig, E. P.; Özin, G. A. *J. Am. Chem. Soc.*, 1974, 96, 12, 3820.

20) Perutz, R. N.; Turner, J. J., *J. Am. Chem. Soc.*, 1975, 97, 17, 4791.

21) McHugh, T. M.; Rest, A. J, Sodeau, J. R., *J. Chem. Soc. Dalton Trans.*, 1979, 184.; Rest, A. J.,. Sodeau, J. R, *J. Chem. Soc., Chem. Commun.*, 1975, 696.

22) Balk, R. W; Boxhoorn, G.; Snoeck, T. L; Schoemaker, G. C.; Stufkens, D. J., Oskam, Ad, *J. Chem. Soc., Dalton Trans.,* 1981, 1524.

23) Boxhoorn, G.; Oskam, A, *Inorg. Chim. Acta,* 1980, 44, L1.

24) Black, J. D.; Braterman, P. S, *J. Organomett. Chem.*, 1973, 63, C19.

25) Poliakoff, M., *Inorg.Chem.*, 1976 15, 9, 2022.

26) Dobson, G. R.; Hodges, M.; Healy, M. A.; Poliakoff, M.; Turner, J. J.; Firth, S.; Asali, K. J.; *J. Am. Chem. Soc.,* 1987, 109, 4218.

27) Goff, S.E.J.; Nolan, T. F.; George, M.W.; Poliakoff, M., *Organometallics*, 1998, 17, 2730.

28) Boxhoorn, G.; Stufkens, J.; Oskam, A, *Inorg. Chim. Acta,* 1979, 33, 215.

29) Pope, K. R.; Wrighton, M. S., *Inorg. Chem.,* 1985, 24, 2792.

30) Boxhoorn, G.; Oskam, A., *Inorg. Chim. Acta,* 1978, 29, 243

31) Goumans, T.P.M.; Ehlers, A.W.; Van Hemert, M. C.; Rosa, A.; Baerends, E.J.; Lammertsma, K, *J. Am. Chem. Soc.*, 2003, 125, 354.7 8.

32) Záliš, S.; Busby, M.; Kotrba, T.; Matousek, P.; Towrie, M.; Vlček, A. J., *Inorg. Chem.*, 2004, 1723, 43, 5.

33) a) Dobson, G. R.; Spradling, M. D., *Inorg. Chem.*, 1990, 29, 880; b) Walsh, M. M., *Ph.D. Thesis*, Dublin City University, 1993.

34) Chatt, J.; Leigh, G.J.; Thankarajan, N., *J. Organomet. Chem.*, 1971, 29, 105.

35) Abrahamson, H. B.; Wrighton, M. S., *Inorg. Chem.*, 1978, 17, 12, 3385.

36) Kraihanzel, C. S.; Cotton, F. A., *Inorg. Chem.*, 1963, 2, 3, 533.

37) Ladogana, S.; Dobson, G. R.; Smit, J. P., *Inorg. Chim. Acta*, 1998, 278, 202; Ladogana, S.; Dobson, G. R.; Smit, J. P., *Inorg. Chim. Acta*, 1998, 271, 105.

38) Creaven, B., *Ph.D. Thesis*, 1989, Dublin City University; Asali, K.J.; Basson, S.S.; Tucker, J.S., Hester, B. C.; Cores, J. E.; Awad, H. H.; Dobson, G.R., *J. Am. Chem. Soc.*, 1987, 109, 5386.

39) a) Kelly, J. M.; Bent, D. V.; Hermann, H.; Schulte-Frohlinde, D.; Koerner von Gustorf, E.A., *J. Organomet. Chem.*, 1974, 69, 259. b) Bonneau, R.; Kelly, J. M., *J. Am. Chem. Soc.*, 1980, 102, 1220. c) Kelly, J. M.; Long, C.; Bonneau, R. *J. Phys. Chem.,* 1983, 87, 3344. d) Kelly, J.M.; Hermann, H.; Schulte-Frohlinde,D.; *.J .Chem. Soc., Chem. Commun.,* 1973, 105.

Chapter 3

Matrix Isolation Experiments on Complexes of the Type $(\eta^6\text{-arene})Cr(CO)_3$

Chapter 3

3.1 Literature Survey

3.1.1 Thermal chemistry of (η^6-arene)$Cr(CO)_3$ complexes

Although CO loss from the excited state of (η^6-arene)$Cr(CO)_3$ appears to be the most efficient process, arene exchange reactions dominate the ground state (i.e. thermal) reaction. Arene exchange between the free ligand and (η^6-arene)$Cr(CO)_3$ in a non coordinating solvent generally requires elevated temperatures. The following scheme for arene exchange was proposed, which involves the interaction of two molecules to give the final product, $Cr(CO)_3$, and the free arene, Scheme 3.1.[1]

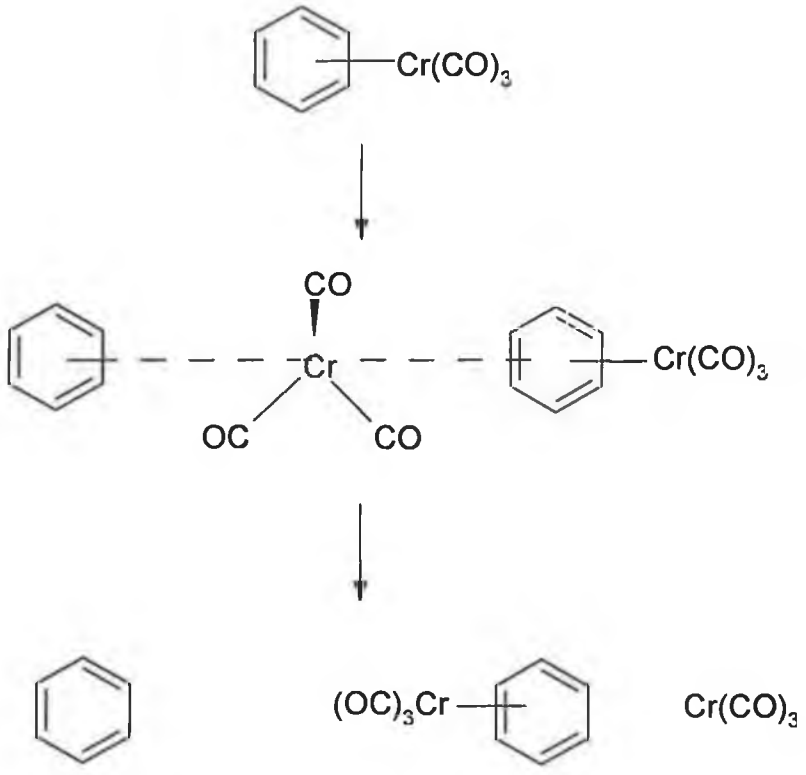

Scheme 3.1 The proposed mechanism of arene exchange in (η^6-arene)$Cr(CO)_3$ complexes.

Although this mechanism does not involve the solvent, donor solvents like THF, and acetonitrile catalyse the arene exchange as demonstrated by Mahaffy and Pausson.[2] They proposed that the solvents initiated partial arene displacement from the metal, Scheme 3.2. The presence of a donor solvent can stabilise the $Cr(CO)_3$ coordinatively unsaturated fragments.[3]

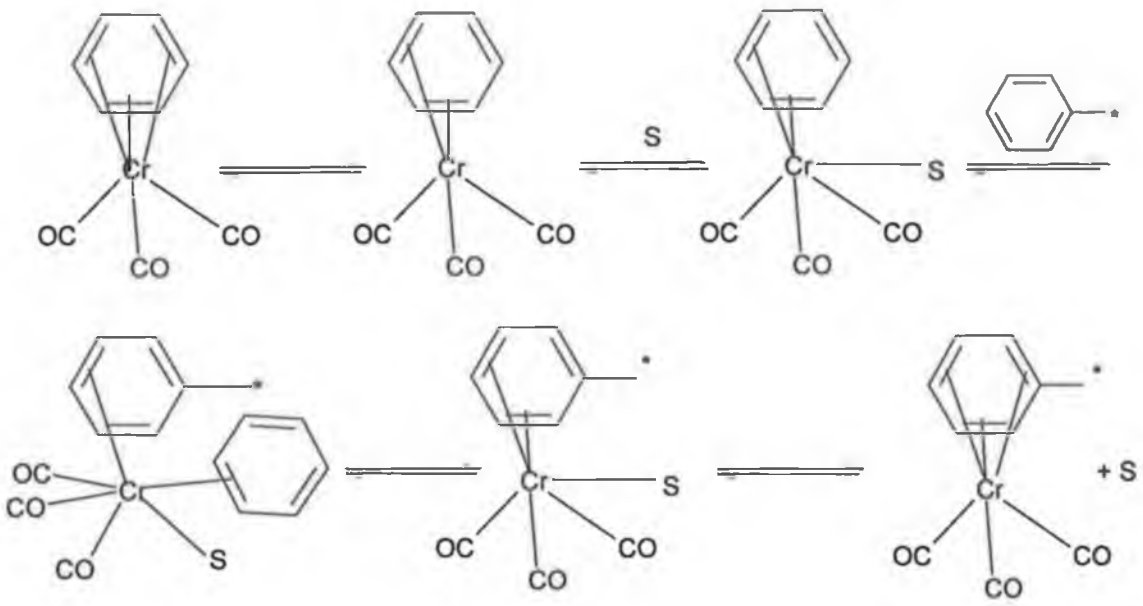

Scheme 3.2 Solvent initiated arene displacement

3.1.2 Photochemistry of (η^6-arene)Cr(CO)$_3$ complexes

The first report on the photochemistry of (η^6-arene)Cr(CO)$_3$ was published by Strohmeier *et al.* [1]. Two photoproducts were observed; the first being the CO-loss product formed with high quantum efficiency and the second the less efficient arene exchange photoproduct (Reactions 3.1 and 3.2).

$$(\eta^6\text{-arene})Cr(CO)_3 \xrightarrow[L]{h\nu,\ \Phi = 0.7} (\eta^6\text{-arene})Cr(CO)_2L + CO \qquad 3.1$$

$$(\eta^6\text{-arene})Cr(CO)_3 \xrightarrow[\text{arene}^*]{h\nu,\ \Phi = 0.12} (\eta^6\text{-arene}^*)Cr(CO)_3 + \text{arene} \qquad 3.2$$

Under inert atmosphere, the photoinduced arene exchange reaction takes place, but with low quantum yield (Φ = 0.12). The arene exchange may proceed through a ring slippage process. Extensive studies about the CO-loss from the (η^6-arene)Cr(CO)$_3$ have been presented.

Wrighton[4] has suggested that the primary photoprocess in the photochemical reactions of the isostructural series of (η^6-benzene)Cr(CO)$_3$, (η^5-C_5H_5)Mn(CO)$_3$, (η^4-C_4H_4)Fe(CO)$_3$ is dissociation of a CO ligand. The final photoproducts, upon photolysis of (η^6-arene)Cr(CO)$_3$ in cyclohexane solution are the arene ligand and

chromiumhexacarbonyl. Wrighton and Haverty [5] studied the photo-substitution of CO from (η^6-arene)$Cr(CO)_3$. The CO loss was identified as the primary photoprocess with a high quantum yield 0.72. The matrix isolation photochemistry of (η^6-benzene)$Cr(CO)_3$ in either inert (Ar or CH_4) or reactive (N_2) matrixes has been studied by Rest *et al.* [6], the only photoproduct observed in this study was the coordinatively unsaturated dicarbonyl species (η^6-benzene)$Cr(CO)_2$. This has C_{2v} symmetry and is characterised by two ν_{CO} bands at 1925, 1870 cm^{-1} in methane matrix. In a reactive matrix like N_2, the dinitrogen molecule occupies the vacant site to form (η^6-benzene)$Cr(CO)_2N_2$ which has two ν_{CO} bands at 1940, 1896 cm^{-1} with one ν_{N-N} band at 2148 cm^{-1}.

Bitterwolf *et al.* [7]studied the photolysis of (η^6 $-C_6H_6$)$Cr(CO)_3$, (η^5 $-C_5H_5$)$Mn(CO)_3$, (η^5 $-CH_3C_5H_4$)$Mn(CO)_3$, and (η^5 $-C_5H_5$)$Re(CO)_3$ as solution or Nujol mulls at 77 K. Products which closely parallel those observed when these material were photolysed in frozen gases at 12 K or in hydrocarbon glasses at 77 K, were observed. In all cases, the expected carbon monoxide loss fragments are observed. Long wavelength photolysis followed by annealing of the group 6 metal carbonyl complexes results in simple reversal of the carbonyl ejection process. For the arene and cyclopentadienyl metal tricarbonyl complexes, dinuclear products are formed in initial photolysis and subsequent annealing. These products probably result from reaction of dicarbonyl photoproducts with parent tricarbonyl compound.

A brief report on the photochemistry of (η^6-arene)$Cr(CO)_3$ in methyl-THF (mTHF) glasses at 77 K was reported by Black *et al.*[8] Photolysis gave rise to two pairs of bands, of which the higher frequency pair was less intense and disappeared on annealing. The bands were attributed to the creation by photolysis of two rotamers depending on the rearrangement of solvent molecules around the photolysed molecules. No evidence for the replacement of benzene by solvent was obtained.
Gilbert *et al.*[9] studied the flash photolysis of (η^6-benzene)$Cr(CO)_3$ in cyclohexane and assigned (η^6-benzene)$Cr(CO)_2$ as the sole transient species. McGrath[10] suggested that an additional photoproduct, possibly one involving a haptptropic or ring-slippage process may also be formed during photolysis of (η^6-C_6H_6)$Cr(CO)_3$

Creaven *et al.* [11] attempted to observe the ring slip reaction by laser flash photolysis. In addition to the known transient of CO loss (i.e. (η^6-benzene)$Cr(CO)_2$(alkane)) another transient signal was observed.

Upon studying the photochemistry of (η^6-arene)$Cr(CO)_3$ (arene = benzene, substituted benzene, or naphthalene), Pryce[12] observed a dependency of the rate constant of the reaction of the transient (η^6-arene)$Cr(CO)_2$(alkane) species with CO on both the solvent, and the nature and degree of the subsistents on the arene ligand. No detection of the ring slippage or ultimately formation of $Cr(CO)_6$ as final product was observed in the photolysis, which was carried out in alkane solvent under 1 atm of carbon monoxide.

Trembovler *et al.* [13] studied the visible light photolysis of (η^6-arene)$Cr(CO)_2L$ (arene = C_6H_6, $C_6H_5OCH_3$, $C_6H_5COCH_3$, $C_6H_5CO_2CH_3$, or 1,3,5- $C_6H_3(CH_3)_3$; L= PPh_3 or CO). The benzene complex undergoes photodecay to free benzene and $Cr(CO)_6$ as products. The electron donating substituents promote the decomposition of the complexes while electron-accepting substituents slightly retard it.

Using time-resolved IR spectroscopy the coordination of N_2 and H_2 with (η^6–C_6H_6)$Cr(CO)_x$ (x= 2, and 1) was studied in the gas phase by Zheng *et.al.*[14], who found that the addition of N_2 or H_2 to (η^6–C_6H_6)$Cr(CO)_2$ produces corresponding molecular nitrogen or hydrogen complexes with lifetimes longer than 1 ms under their experimental conditions. The positions of CO stretching bands of dinitrogen and dihydrogen complexes are very close, as was found in the condensed phase, indicating that the interaction between the metal centres and the ligand is similar for N_2 and H_2. However the shifts of the positions of CO stretching bands of (η^6–C_6H_6)$Cr(CO)_2$ are qualitatively different in the gas versus condensed phase. This implies that the contribution of coordinated solvent molecules to the positions of CO stretching bands of the formally unsaturated species must be considerable.

Time resolved infrared study of (η^6-benzene)$Cr(CO)_3$ in the gas phase was reported by Wang *et al.*[15] using $\lambda_{exc.}$ = 355 nm. Here photolysis produced (η^6-benzene)$Cr(CO)_2$ with ν_{CO} bands at 1917, and 1981 cm^{-1}.

3.1.2.1 Investigation of the mechanism of the haptotropic shift of (η^6-arene)$Cr(CO)_3$: -

Traylor *et al.* [16] suggested that the ring slippage process in the thermal arene exchange involves the gradual change in hapticity $\eta^6 \rightarrow \eta^4 \rightarrow \eta^2$ during the reaction. However no direct evidence for this process was provided. It is highly desirable to understand the nature of reduced hapticity complexes in the arene exchanges reaction, as well as their structure, relative stability, and interconversion, for (η^6-arene)$Cr(CO)_3$ type complexes, as they represent important reagents for aromatic ring functionalisation.

Cohen *et al.* [17] used DFT calculations to investigate the mechanism of formation and the interconversion of reduced hapticity (η^x-C_6H_6)$Cr(CO)_n$ complexes (n = 1-5, x = 1-6) on both singlet and triplet energy surfaces. Depending on the structures and energies of the intermediates and the transition states, they suggested a mechanism of the decomposition of the (η^6-C_6H_6)$Cr(CO)_3$ to $Cr(CO)_6$. This mechanism is closely related to the arene exchange reaction mechanism, involves the formation of (η^1-C_6H_6)$Cr(CO)_4$ and (η^2-C_6H_6)$Cr(CO)_5$ complexes as ring-slippage intermediates along pathway for the complete replacement of the benzene ring by carbonyl ligands.

There are several reports on the haptotropic rearrangement of $Cr(CO)_3$ moiety at different substituted naphthalenes. Jahr et al. 18 reported one of these studies in which one of the substituted the naphthohydoquinone complexes prepared could be used as a molecular switch. Depending on the reversible thermo- or photo-induced haptotropic shift of a $Cr(CO)_3$ fragment along a naphthohydoquinone skeleton, stereospecific molecular switches could be achieved Scheme 3.3.

They added CO to the solvent in order to limit the decomposition following CO-loss stabilise the dicarbonyl, which should be subsequently exchanged again with CO in the dark regenerating a tricarbonyl chromium complex. UV irradiation of the complexes (R)-1 or (S)-2 in the presence of an excess of cyclooctene afforded a brown-black dicarbonyl cyclooctene adduct, which changed slowly in the dark to the orange colour typical of the tricarbonyl chromium complexes.

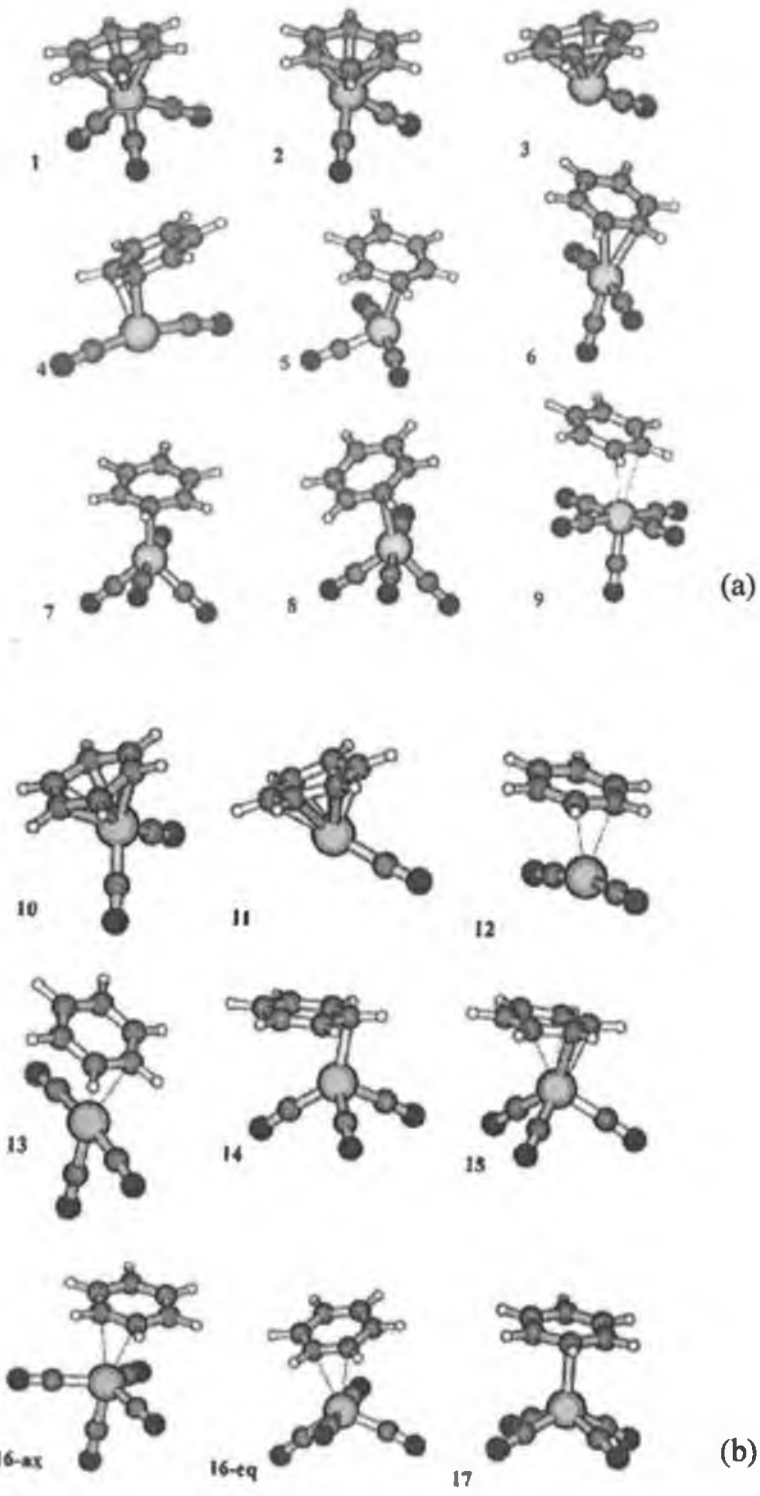

Fig 3.1 Structures of the complexes found under DFT calculations[17] for the decomposition of $(\eta^6\text{-}C_6H_6)Cr(CO)_3$ to $Cr(CO)_6$ (a) the singlet complexes, (b) the triplet complexes.

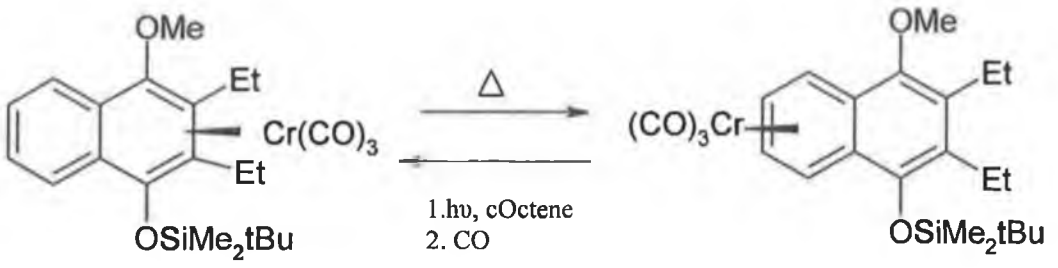

(R)-1 (S)-2

Scheme 3.3 Tricarbonyl naphthalene chromium complexes as an organometallic molecular switch., cOctene = cyclooctene.

Goff, *et al.* [19] studied, the UV irradiation of $(\eta^6\text{-}C_6H_3Me_3)M(CO)_3$ (M = Cr or Mo) in polyethylene matrix in the presence of N_2. Here both the mono-, bis -, and tris-N_2 complexes, $(\eta^6\text{-}C_6H_3Me_3)M(CO)_{3-x}(N_2)_x$ were observed at room temperature. By contrast, irradiation of $(\eta^6\text{-}C_6H_3Me_3)M(CO)_3$ in polyethylene in the presence of H_2 only generated the mono-H_2 complex $(\eta^6\text{-}C_6H_3Me_3)M(CO)_2(H_2)$.

Shaver *et al.* [20] studied the photochemistry of $(\eta^6\text{-arene})Cr(CO)_3$, where arene = C_6H_6, $C_6H_5NH_2$, ortho-$C_6H_4(NH_2)Me$ in various polymer matrixes. In contrast to the results of Rest *et al.*[6] the photolysis with > 310 nm of $(\eta^6\text{-}C_6H_6)Cr(CO)_3$ at room temperature in polystyrene or polymethylmethacrylate led to the formation of $Cr(CO)_6$. As the tricarbonyl species seems to be well isolated in the polymer films, they assumed that $Cr(CO)_6$ formed by the scavenging of CO molecules generated by the decomposition of the photogenerated $(\eta^6\text{-}C_6H_6)Cr(CO)_2$.

In the co-polymer polystyrene-polyacrylonitrile (PS-AN) the major product has two CO bands at 1891 and 1835 cm^{-1}, which is assigned to $(\eta^6\text{-}C_6H_6)Cr(CO)_2$(PS-AN). In addition, weak bands due to $Cr(CO)_5$(PS-AN) were observed.

Using arenes which contain substituents capable of acting as a trap for the ring slippage intermediates, Breheny *et al.* [21] detected the ring slippage of $(\eta^6\text{-}C_5H_5N)Cr(CO)_3$ and its 2,6 methyl and silyl disubstituted derivatives. Pyridine was chosen as the ligand as it has the ability to coordinate via the nitrogen atom or through the ring π system. These workers used matrix isolation, TRIR and UV/vis flash photolysis to detect haptotropic changes at the heteroarene. The solution photochemistry provided evidence for the formation of $(\eta^1\text{-}C_5H_5N)Cr(CO)_5$. Ultimately $Cr(CO)_6$ was observed along with formation of the solvated dicarbonyl.

Matrix isolation studies showed that long wavelength irradiation results in a haptotropic change of the pyridine ring coordination from η^6- η^1. Both the ring slip and CO loss products were observed in the matrix upon irradiation with short wavelengths.

As it is possible to trap the ring slipped intermediates in the photolysis of (η^6-C_5H_5N)$Cr(CO)_3$ by the pyridine ligand, it should be possible to use a substituted benzene containing a functional group capable of trapping the ring slip intermediates. Brennan [22] reported the solution photochemistry of (η^6-arene)$Cr(CO)_3$, where arene is C_6H_6, $C_6H_5NH_2$, $C_6H_5OCH_3$, $C_6H_5CO_2CH_3$, or C_6H_5COH. The addition of a functional group into the arene ligand in (η^6-arene)$Cr(CO)_3$ was found to affected the photochemistry. Although (η^6-benzene)$Cr(CO)_3$ was found to undergo only CO loss as a primary photoprocess the complexes of the type (η^6-arene)$Cr(CO)_3$, where arene is functionalised benzene ring containing strongly electron withdrawing/electron donating (-CHO/-NH_2) groups, also undergo photochemical displacement of arene ring.

McKenna [23], subsequently studied the matrix isolation photochemistry of (η^5-C_4H_4Se)$Cr(CO)_3$ in inert (Ar or CH_4) or reactive (CO and N_2) matrixes at 20 K. Upon photolysis, this complex undergoes stepwise haptotropic shift from $\eta^5 \rightarrow \eta^4 \rightarrow \eta^2$ for the photochemical removal of selenophene ring from the Cr metal centre. Extended photolysis in CO matrixes forms of $Cr(CO)_6$. In dinitrogen matrixes the initial photoproduct was (η^4-C_4H_4Se)$Cr(CO)_3N_2$ and with extended photolysis the dicarbonyl photoproduct (η^5-C_4H_4Se)$Cr(CO)_2N_2$. So the photochemical behaviour of (η^5-C_4H_4Se)$Cr(CO)_3$ appears to depend on the matrix conditions used.

3.2 Results: - Matrix Isolation studies on (η^6-C_6H_5-X)$Cr(CO)_3$ (X = H, NH_2, OCH_3, CHO, or $COOCH_3$)

The matrix isolation photochemistry of the (η^6-C_6H_5-X)$Cr(CO)_3$ complexes was studied in a variety of matrix environments including methane, 2%, 5%, or 10% CO-methane matrixes. In the case of the methylbenzoate complex a dinitrogen matrix was also used. Matrix isolation photochemistry of benzene complex was also undertaken in a 5% CO- methane matrix.

In addition DFT calculations, using B3LYP/LanL2DZ level of theory have been undertaken on some of the dinitrogen complexes proposed to form during matrix isolation photochemistry of the methylbenzoate complex. Scheme 3.4 summarizes the photoproducts that observed during the photolysis of the arene complexes under matrix isolation experiments.

3.2.1 The matrix isolation photochemistry of (η^6-benzene)$Cr(CO)_3$

The IR spectroscopic data for (η^6-benzene)$Cr(CO)_3$ in the ν_{CO} region and all photoproducts obtain during this matrix isolation experiment are given in Table 3.1.
A sample of this complex was deposited in 5% CO- methane matrix at 20 K. The metal carbonyl stretching frequencies of the parent complex occur at 1978 and 1906 cm^{-1}. The UV/vis and IR spectra of (η^6-benzene)$Cr(CO)_3$ are given in Fig.3.2 a and b respectively.

The photolysis of this sample with visible broad-band ($\lambda_{exc.}$ >400 nm) light results in the formation of a new bands at 1982 and 1911 cm^{-1}, with a concomitant reduction in the parent bands at 1978 and 1906 cm^{-1}. Small features at 1922 and 1867 cm^{-1} in the IR spectrum were also observed (Fig 3.3). The separation between the two bands at 1982 and 1911 cm^{-1} is similar to the separation between the peaks of the parent.

COMPLEX	ν_{CO} (cm^{-1})
Deposition bands:	
$(\eta^6\text{-}C_6H_6)Cr(CO)_3$	1978, 1906
Photoproduct bands:	
Rotamer $(\eta^6\text{-}C_6H_6)Cr(CO)_3$	1982, 1911
$(\eta^6\text{-}C_6H_6)Cr(CO)_2$	1922, 1867
$Cr(CO)_6$	1984

Table 3.1: Spectroscopic data for $(\eta^6\text{-}C_6H_6)Cr(CO)_3$ and all its photoproducts observed during matrix experiments.

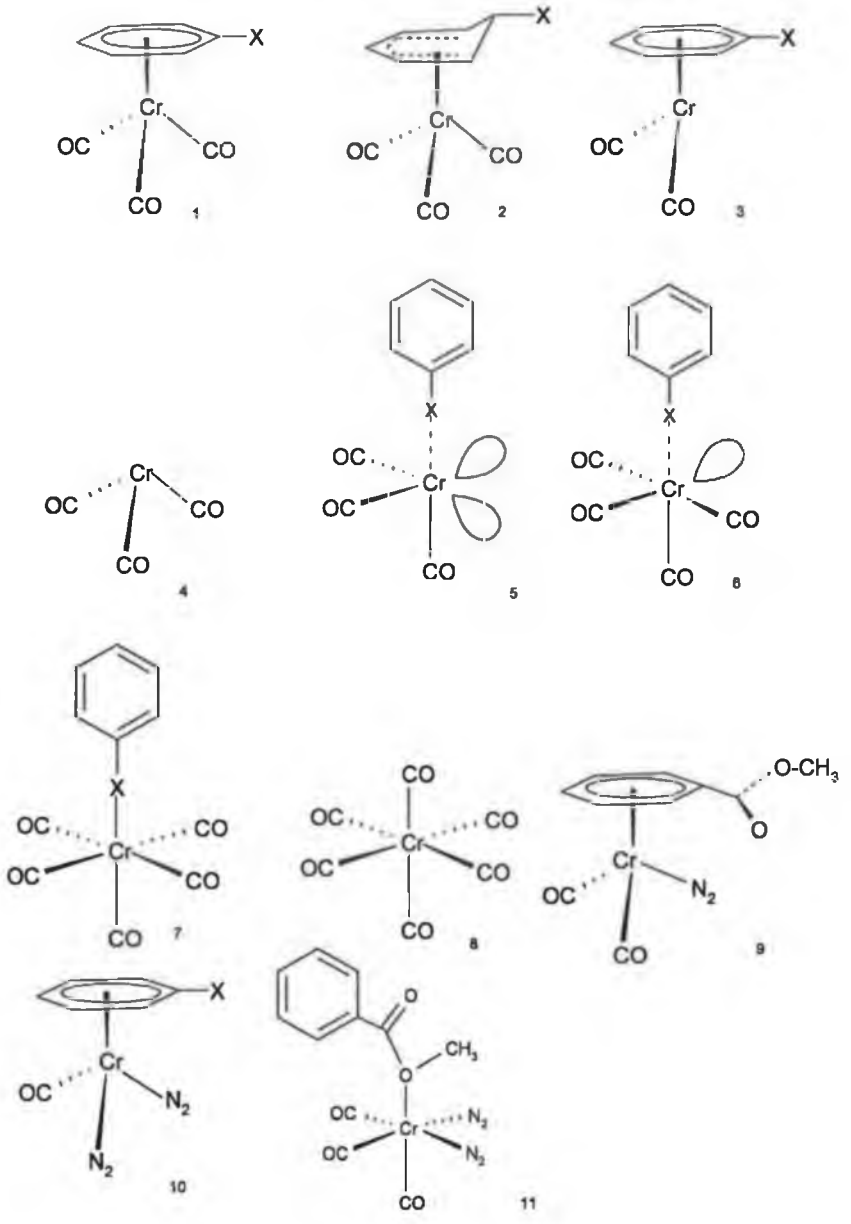

Scheme 3.4 Representation of structures of the parent tricarbonyl complex (1) and photoproducts (2-11) observed during these matrix isolation studies.

(a)

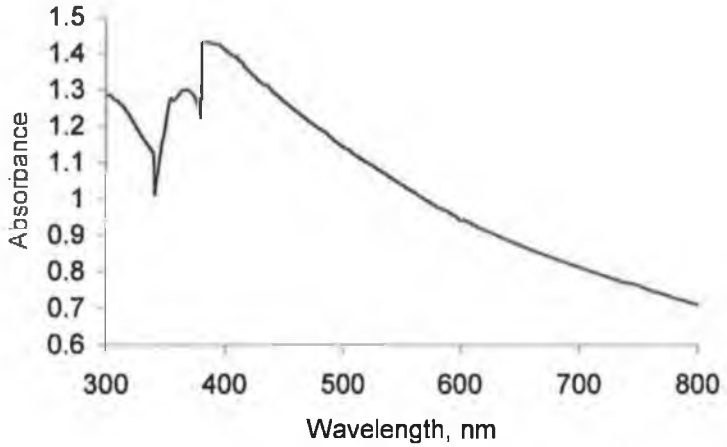

(b)

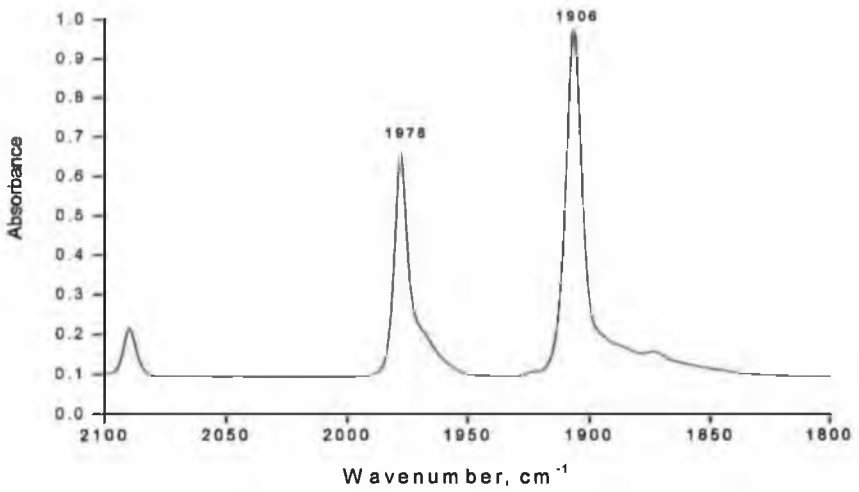

Fig 3.2 a) UV/vis spectrum of (η^6-benzene)$Cr(CO)_3$ in 5 % CO-CH_4 matrix at 12 K, b) FTIR spectrum recorded after deposition of (η^6-benzene)$Cr(CO)_3$ in 5 % CO-CH_4 matrix at 12 K.

compound bands at 1982 and 1911 cm^{-1} have been assigned to a rotamer of (η^6-benzene)$Cr(CO)_3$. The parent compound is thought to adopt a staggered conformation (I) at the matrix temperature, so upon the photolysis the benzene ring is rotated to give the eclipsed isomer (II). The bands at 1922 and 1867 cm^{-1} were assigned to the dicarbonyl species (η^6-C_6H_6)$Cr(CO)_2$.

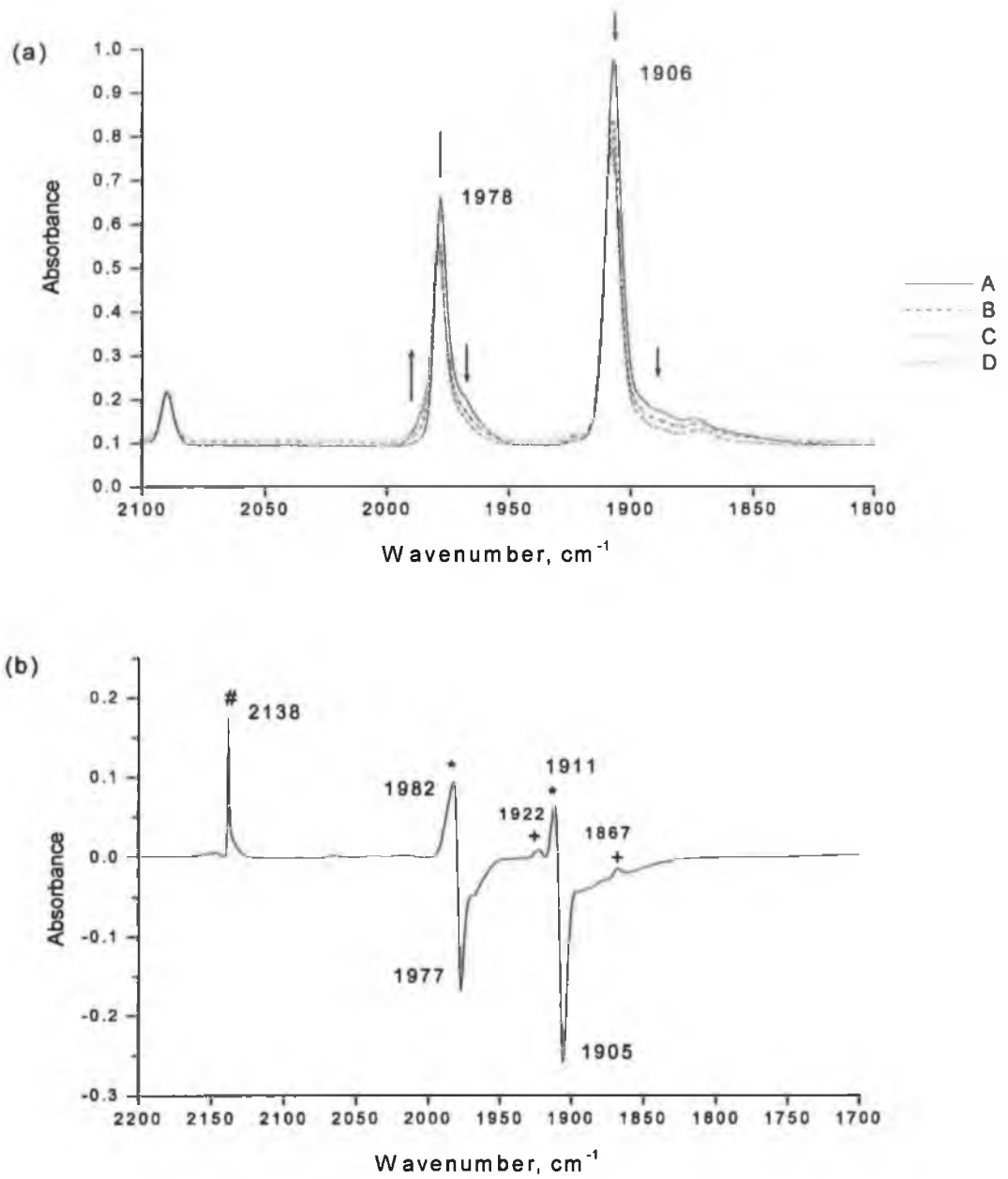

Fig 3.3 (a) FTIR spectrum of $(\eta^6\text{-}C_6H_6)Cr(CO)_3$ isolated in a 5% CO-CH_4 matrix, A before photolysis, B, C, D after visible photolysis with λ_{exc}>400 nm 130, 190, and 330 min. respectively, (b) Difference IR spectrum following visible photolysis of $(\eta^6\text{-}C_6H_6)Cr(CO)_3$ with λ_{exc} >400 nm for 330 min in 5 % CO-CH_4 matrix at 12 K. The bands labelled * to another rotamer, + to the dicarbonyl species.

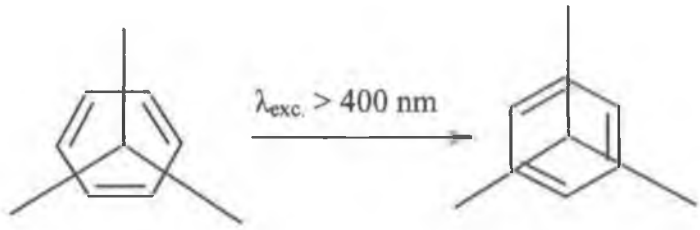

(I) (II)

When $(\eta^6\text{-}C_6H_6)Cr(CO)_3$ was photolysed in a 5 % CO-CH_4 matrix with UV broad band irradiation, $\lambda_{exc} > 300$ nm, a depletion in the parent bands at 1977 and 1907 cm^{-1} was observed. Two new carbonyl bands formed at 1922 and 1867 cm^{-1} Fig. 3.4. These bands are assigned to the CO-loss product, $(\eta^6\text{-}C_6H_6)Cr(CO)_2$, which has the similar spectral features to those obtained by Rest and co-workers[1]. In addition to the formation of the dicarbonyl species, this photolysis produced $Cr(CO)_6$ complex as assigned by the grow-in of the peak at 1984 cm^{-1}.

3.2.2 The matrix isolation photochemistry of $(\eta^6$-aniline$)Cr(CO)_3$:-

The parent ν_{CO} peaks for $(\eta^6$-aniline$)Cr(CO)_3$ in pure methane matrix are observed 1971, 1900, 1891 and 1862 cm^{-1}, Fig 3.5, The band at 1862 cm^{-1} appeared as very weak shoulder in the CO-methane matrixes (The appearance of four peaks is as a result of the matrix splitting). These peaks undergo small shifts upon changing the matrix gas. The IR spectroscopic data for $(\eta^6$-aniline$)Cr(CO)_3$ and all photoproducts obtain during this experiment is given in Table 3.2.

Photolysis of $(\eta^6$-aniline$)Cr(CO)_3$ in a methane matrix or methane-CO matrixes with 405 nm resulted very small change in the IR spectrum consistent with loss of CO to form $(\eta^6$-aniline$)Cr(CO)_2$. There was an apparent grow-in of new peaks at 1909, and 1848 $cm^{-1}$with depletion of the peaks related to the parent complex. The only change observed following photolysis in a 5% CO-methane matrix was depletion of the parent bands, while their intensity increased upon photolysis for a 10 % CO-methane matrix.

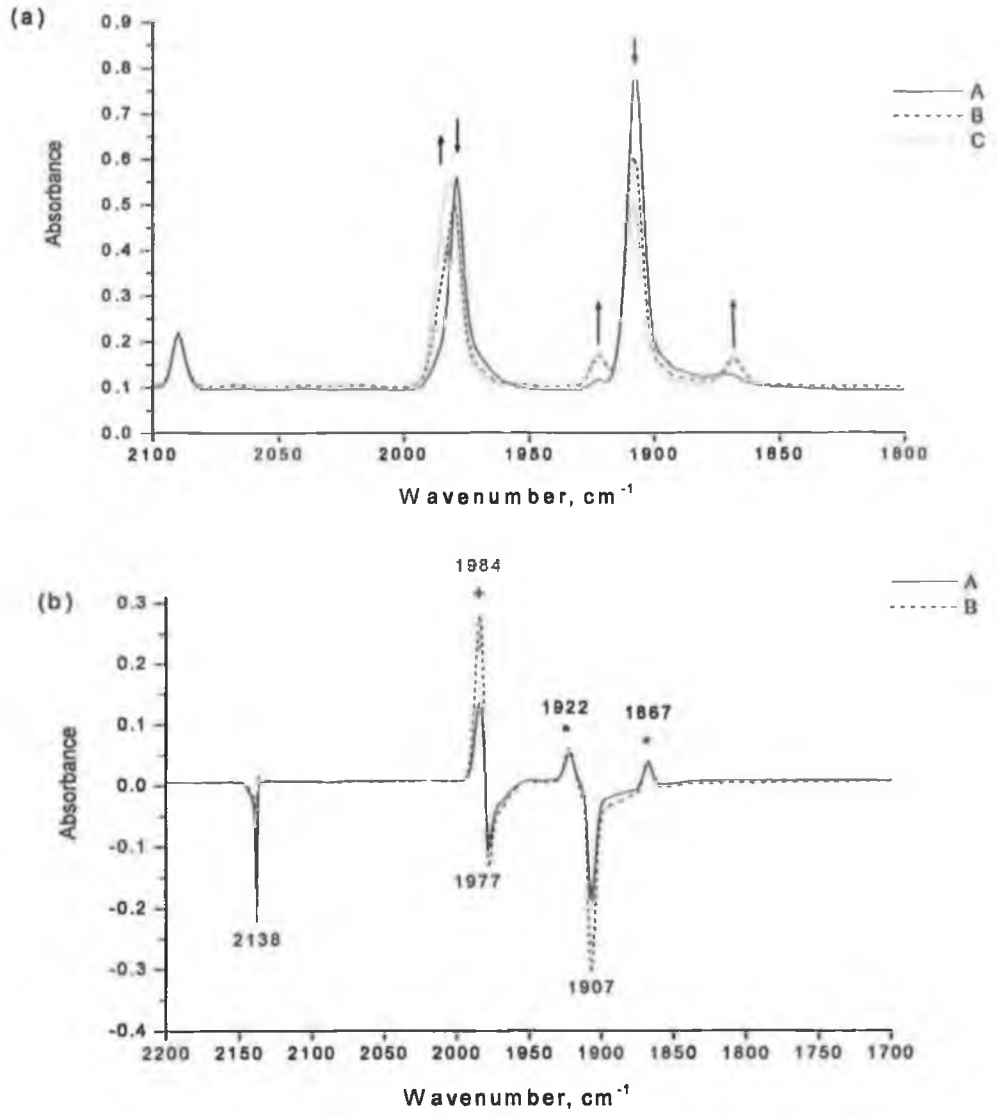

Fig 3.4 (a) FTIR spectrum of $(\eta^6\text{-}C_6H_6)Cr(CO)_3$ isolated in a 5% CO- CH_4 matrix A before photolysis, B, C after UV photolysis (λ_{exc}>300 nm) for 30, and 125 min respectively.(b) Difference IR spectrum following UV photolysis with λ_{exc} > 300 nm; 30, and 125 min of $(\eta^6\text{-benzene})Cr(CO)_3$ in 5 % CO-CH_4 matrix at 12 K The bands marked *,+ are due to $(\eta^6\text{-}C_6H_6)Cr(CO)_2$ and $Cr(CO)_6$ respectively.

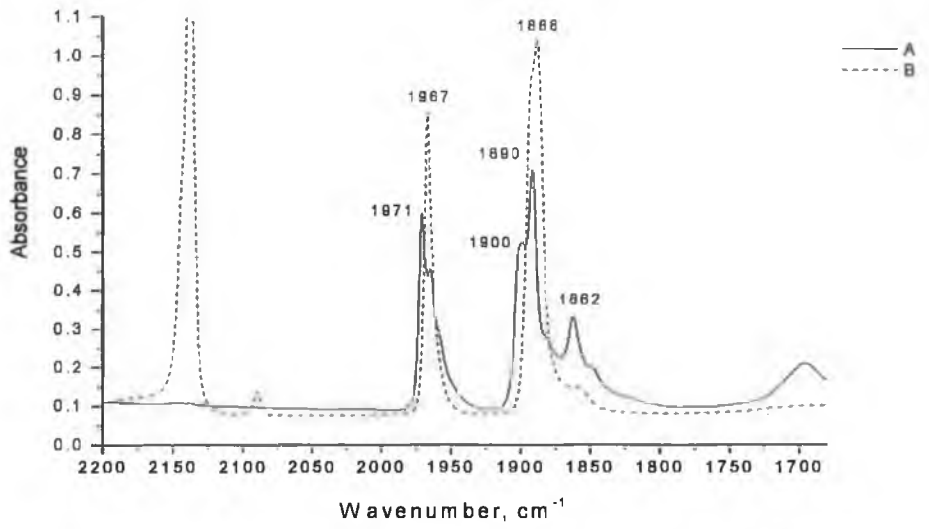

Fig. 3.5 FTIR spectra of (η^6-aniline)$Cr(CO)_3$ in (A) pure methane matrix (B) in 5% CO-CH_4 matrix.

COMPLEX	ν_{CO} (cm^{-1})	MATRIX
Deposition bands:		
(η^6-aniline)$Cr(CO)_3$	1971, 1900, 1891 1862 1967, 1888	CH_4 5 % CO/CH_4
Photoproduct bands:		
(η^6-aniline)$Cr(CO)_2$	1899, 1848	5 % CO/CH_4
(η^1-N-aniline)$Cr(CO)_5$	1970	5 % CO/CH_4
Cis-$Cr(CO)_4$(η^1-N-aniline)	2015	5 % CO/CH_4
$Cr(CO)_6$	1984	5 % CO/CH_4

Table 3.2: Spectroscopic data for (η^6-aniline)$Cr(CO)_3$ and all photoproducts obtained during matrix experiments.

In addition to the characteristic features of the dicarbonyl species, the photolysis with 365, 334, or 313 nm also leads to a grow-in of new peaks at 2014 and 1970 cm^{-1} in CO-methane matrix. These did not appear in a pure methane matrix. Comparing the band at 2014 cm^{-1} with those found for cis-$Cr(CO)_4L$,[24] we attribute this band to the sixteen electron species cis-$Cr(CO)_4$(η^1-N-aniline) We cautiously assign the peak at 1970 cm^{-1} to the pentacarbonyl species $Cr(CO)_5$(η^1-N-aniline) (IR bands for $Cr(CO)_5$(η^1-N-aniline) in KBr is 2060, 1990, 1960, 1900, 1860 cm^{-1} (3 ν_{CO} bands of this complex which should appear are subject to solid state splitting).[26]

Other weak bands were observed in the IR spectrum of the matrix at 1833, 1819 cm^{-1}, and these were assigned to the *fac*-$Cr(CO)_3$ moiety (literature at 1957,1841, 1833 cm^{-1})

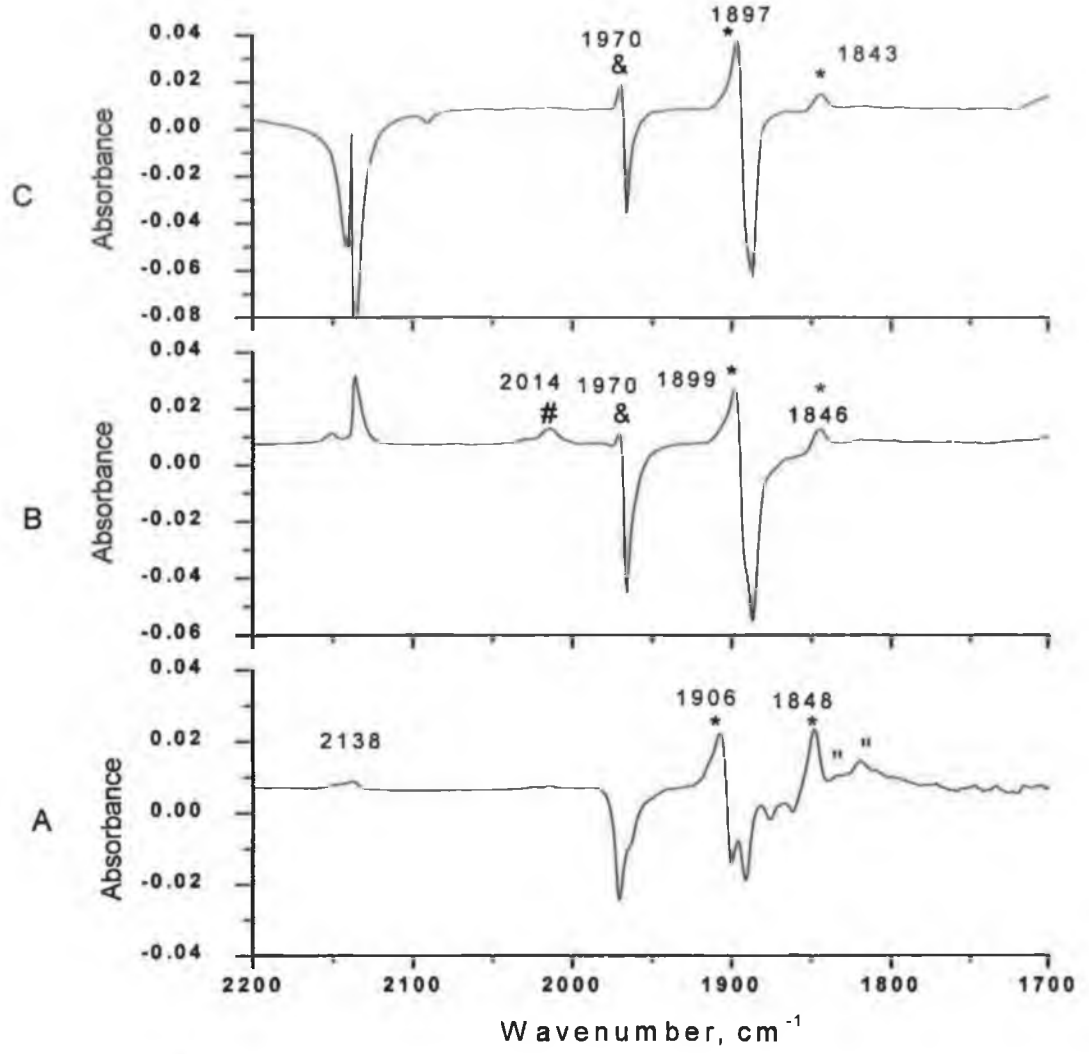

Fig. 3.6 The infrared difference spectrum recorded after irradiation (λ_{exc} = 365 nm) of (η^6-aniline)$Cr(CO)_3$ at 12 K. (A) in CH_4 matrix 65 min. B) for 75 min in 5% CO-CH_4 matrix C) for 60 min in 10% CO-CH_4 matrix. The bands labelled with *, #, & and " are related the complex (η^6-aniline)$Cr(CO)_2$, cis-(η^1-N-aniline)$Cr(CO)_4$, (η^1-N-aniline)$Cr(CO)_5$ and *fac*-$Cr(CO)_3$ respectively. The *fac*-$Cr(CO)_3$ are gradually disappeared upon increasing the percentage of CO in the matrix with the grow-in of the bands for cis-(η^1-N-aniline)$Cr(CO)_4$, and (η^1-N-aniline)$Cr(CO)_5$.

Photolysis with 297 nm resulted the recovery of the parent peaks and depletion of the dicarbonyl species in pure methane matrix. However in CO-methane matrixes all of the parent peaks were depleted without the appearance of any new ν_{CO} bands.

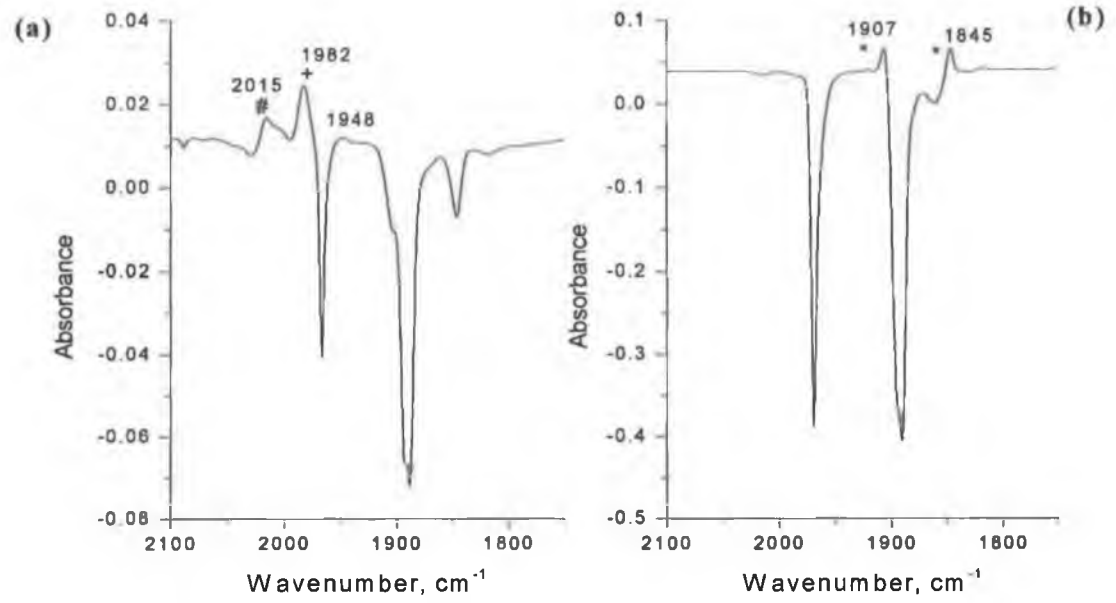

Fig. 3.7 Infrared difference spectrum recorded after visible broad band irradiation λ_{exc} >400 nm of (η^6-aniline)$Cr(CO)_3$ in 5% CO-CH_4 matrix at 12 K for (a) 45 min (b) 110 min in separate experiment immediately after deposition. The bands labelled with *, +, and # are related to (η^6-aniline)$Cr(CO)_2$, $Cr(CO)_6$, and cis-(η^1-N-aniline)$Cr(CO)_4$ respectively.

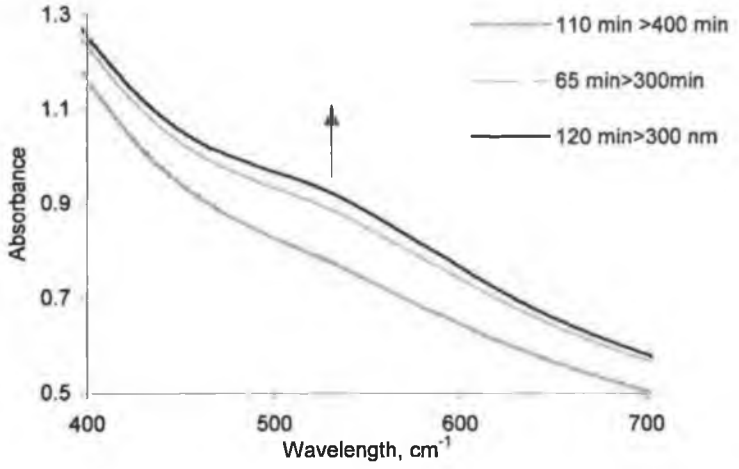

Fig 3.8 UV/visible spectra of (η^6-aniline)$Cr(CO)_3$ in 5% CO-CH_4 matrix at 12 K in separate experiment upon irradiation with $\lambda_{exc.}$ >300 nm. The direction of the arrow represents the growth of the band with increasing photolysis times.

Visible photolysis with broadband >400 nm resulted in depletion of the peaks of the tricarbonyl species, Fig 3.7, 3.8. In CO containing matrixes the formation of

chromium hexacarbonyl was indicated by the grow-in of the peak at 1982 cm^{-1}. The band at 2015 cm^{-1} can be assigned to cis-$Cr(CO)_4(\eta^1$-N-aniline) species.

Photolysis of (η^6-aniline)$Cr(CO)_3$ with broad band irradiation (λ_{exc}>300 nm) resulted in the formation of both the dicarbonyl species (η^6-aniline)$Cr(CO)_2$ and $Cr(CO)_6$ in CO containing matrixes. $Cr(CO)_6$ formation is indicated by the peak at 1984 cm^{-1} (Fig. 3.9). The hexacarbonyl complex was not observed in the photolysis of a freshly deposited sample however. Here the only product formed was the dicarbonyl species (Fig. 3.10). The dicarbonyl species was not observed in experiments conducted in a 10% CO-methane matrix.

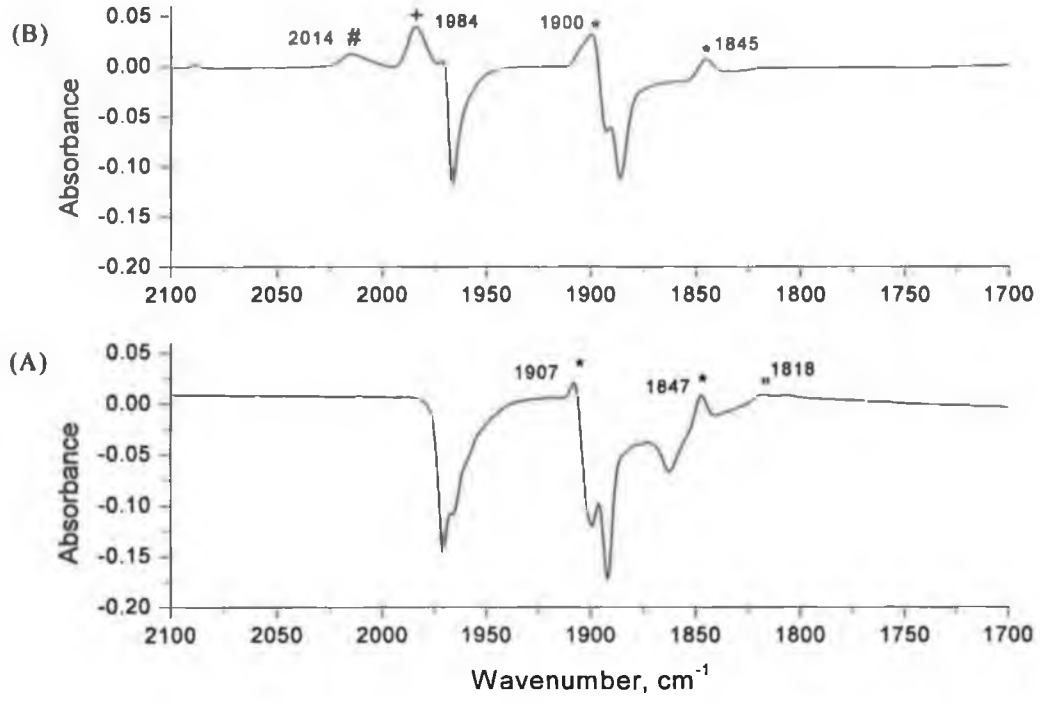

Fig. 3.9 The infrared difference spectrum recorded after UV broad band irradiation (λ_{exc} >300 nm) of (η^6-aniline)$Cr(CO)_3$ at 12 K A) 50 min in CH_4 matrix B) 40 min in 5% CO-CH_4 matrix. The bands labelled with *, +, #, and " are related to the complex (η^6-aniline)$Cr(CO)_2$, $Cr(CO)_6$, cis-(η^1-N-aniline)$Cr(CO)_4$, and *fac*-$Cr(CO)_3$ respectively.

Thus it would appear that in photolysis with ($\lambda_{exc.}$ >400 nm) and ($\lambda_{exc.}$ >300 nm), the formation of the tetracarbonyl and hexacarbonyl species as a result of photoreaction of *fac*-$Cr(CO)_3$ or *fac*-(η^1-N-aniline)$Cr(CO)_3$ with CO.

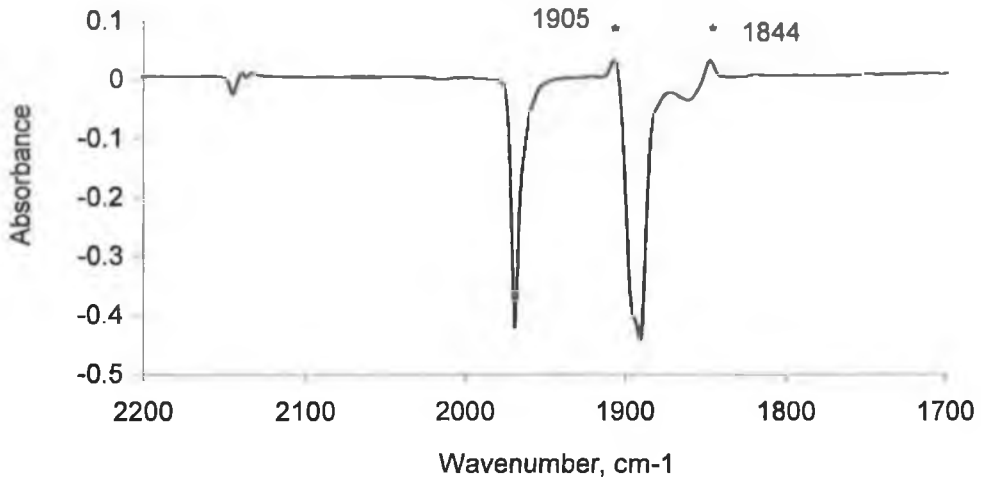

Fig. 3.10 Infrared difference spectrum recorded after UV broad band irradiation (λ_{exc} >300 nm; 40 min) of (η^6-aniline)$Cr(CO)_3$ in 5% CO-CH_4 matrix at 12 K. The labelled bands represent the dicarbonyl species.

3.2.3 The matrix isolation photochemistry of (η^6-anisole)$Cr(CO)_3$:-

The IR spectroscopic data in the ν_{CO} region for (η^6-anisole)$Cr(CO)_3$ and photoproducts obtained during this matrix isolation experiments are given in Table 3.3

The parent ν_{CO} peaks for (η^6-anisole)$Cr(CO)_3$ in pure methane matrix are at 1976, and 1904 cm^{-1}. The UV/vis spectrum of (η^6-anisole)$Cr(CO)_3$ is presented in Fig.3.11

Irradiation of (η^6-anisole)$Cr(CO)_3$ in either a methane matrix or CO-methane matrixes at 405 or 365 nm led to the loss of CO to form (η^6-anisole)$Cr(CO)_2$ as apparent from the grow-in of new peaks at 1917 and 1861 cm^{-1}. The separation between these two peaks is 56 cm^{-1} which is close to that found for (η^6-benzene)$Cr(CO)_2$ (= 54 cm^{-1}). The grow-in of a CO feature at 2137 cm^{-1} gave further evidence of the loss of CO.

COMPLEX	ν_{CO} (cm^{-1})	MATRIX
(η^6-anisole)$Cr(CO)_3$	1976, 1904, 1878	CH_4
Photoproduct bands :		
Rotamer (η^6-anisole)$Cr(CO)_3$	1895	CH_4
(η^6-anisole)$Cr(CO)_2$	1915, 1860	CH_4
$Cr(CO)_5(\eta^1$-O-anisole)	2067, 1907	5% CO/CH_4
cis-$Cr(CO)_4(\eta^1$-O-anisole)	2021	5% CO/CH_4
$Cr(CO)_6$	1985	5% CO/CH_4

Table 3.3: Spectroscopic data in ν_{CO} region for (η^6-anisole)$Cr(CO)_3$ and its photoproducts obtained during these matrix experiments.

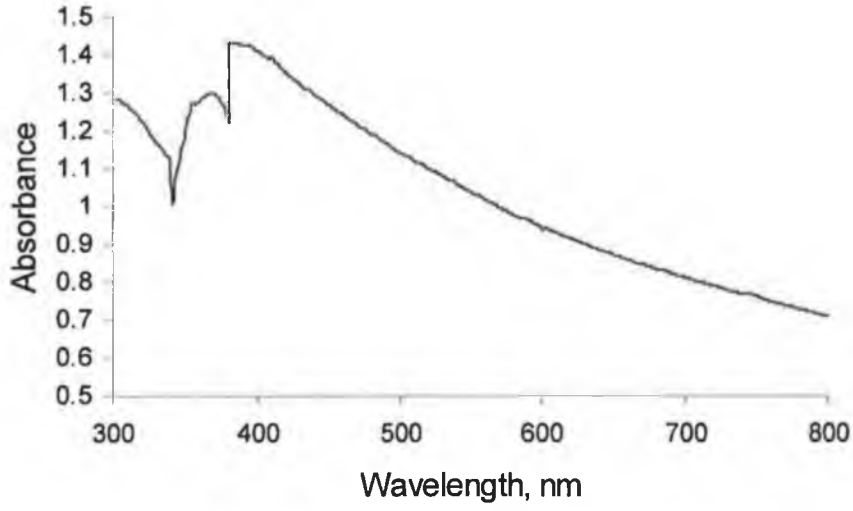

Fig. 3.11 UV/vis spectrum of (η^6-anisole)$Cr(CO)_3$ in methane matrix at 12 K

The parent peak at 1904 cm^{-1} was split, and depletion in the center of the peak was observed and there was the grow-in of a new peak at 1895 cm^{-1}. The peak at 1976 cm^{-1} which was depleted in the pure methane matrix upon photolysis with 405 nm, split in CO containing matrixes, Fig. 3.12. This can be assigned to another rotamer of the complex formed by the rotation the anisole ligand about the Cr-arene axis.

The grow-in of new peaks at 2067 and 1906 cm^{-1} in CO-methane matrixes can be assigned to the formation of the pentacarbonyl species $Cr(CO)_5(\eta^1$-O-anisole).

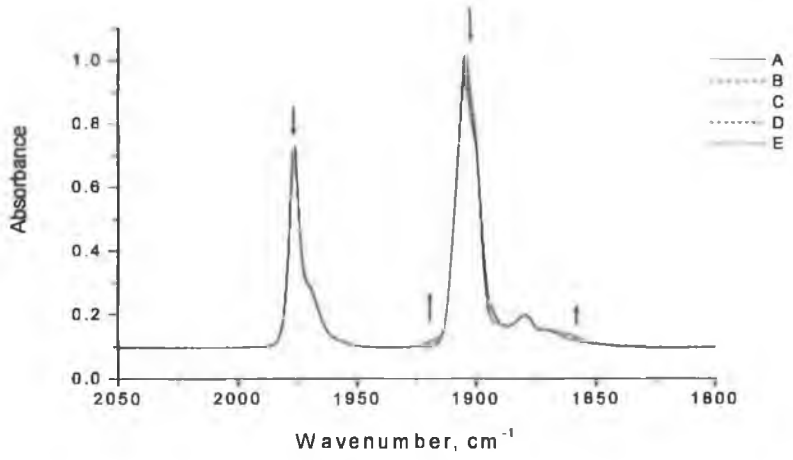

Fig. 3.12 IR spectra of (η^6-anisole)Cr(CO)$_3$ in methane matrix at 12 K recorded (A) before, B, C, D, and E after monochromatic visible irradiation λ_{exc} = 405 nm, 20, 60, 110 and 160 min respectively.

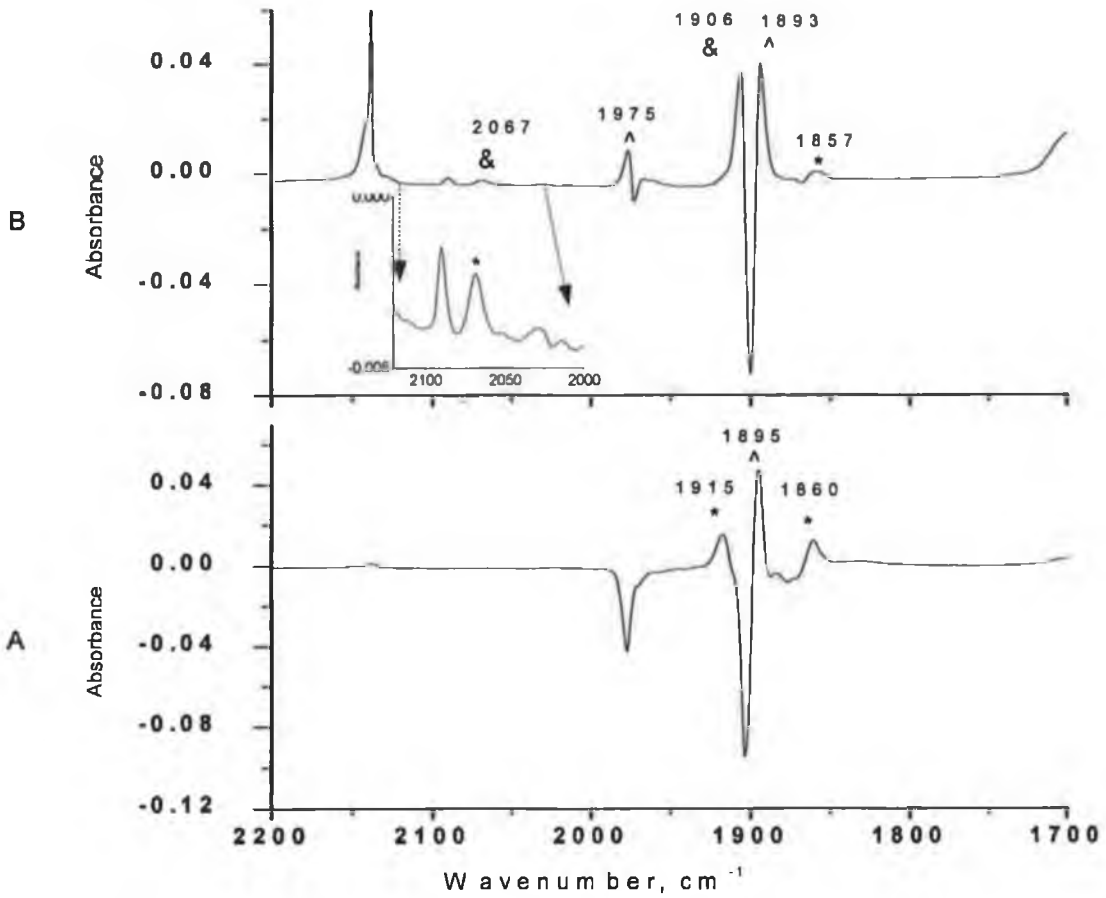

Fig. 3.13 Difference IR spectra following monochromatic photolysis of (η^6-anisole)Cr(CO)$_3$ with λ_{exc} = 405 nm (A) in methane matrix at 12 K for 160 min, (B) in 5% CO-CH_4 matrix. The bands labelled with *, & and ^ are related the complex (η^6-anisole)Cr(CO)$_2$, (η^1-O-anisole)Cr(CO)$_5$ and the rotamer (η^6-anisole)Cr(CO)$_3$ respectively.

In addition to the characteristic features of the dicarbonyl species, the photolysis with 334 nm also leads to a grow-in of new peaks at 1889 and 1832 cm^{-1} in a pure methane matrix. These did not appear in CO-methane matrixes, so we assigned the band at 1832 cm^{-1} to the formation of *fac*-$Cr(CO)_3$ (literature[21] 1957, 1841, 1833 cm^{-1}). In the presence of CO in the matrix this species will react to form the hexacarbonyl complex, Fig. 3.14. The band at 1889 cm^{-1} is assigned with caution to be one of ν_{CO} bands of the coordinatively unsaturated species (η^1-O-anisole)$Cr(CO)_3$.

Upon photolysis at 313 nm, the only product formed is the dicarbonyl species, while the photolysis with 297 nm resulted a regeneration of the parent peaks with depletion of the dicarbonyl species.

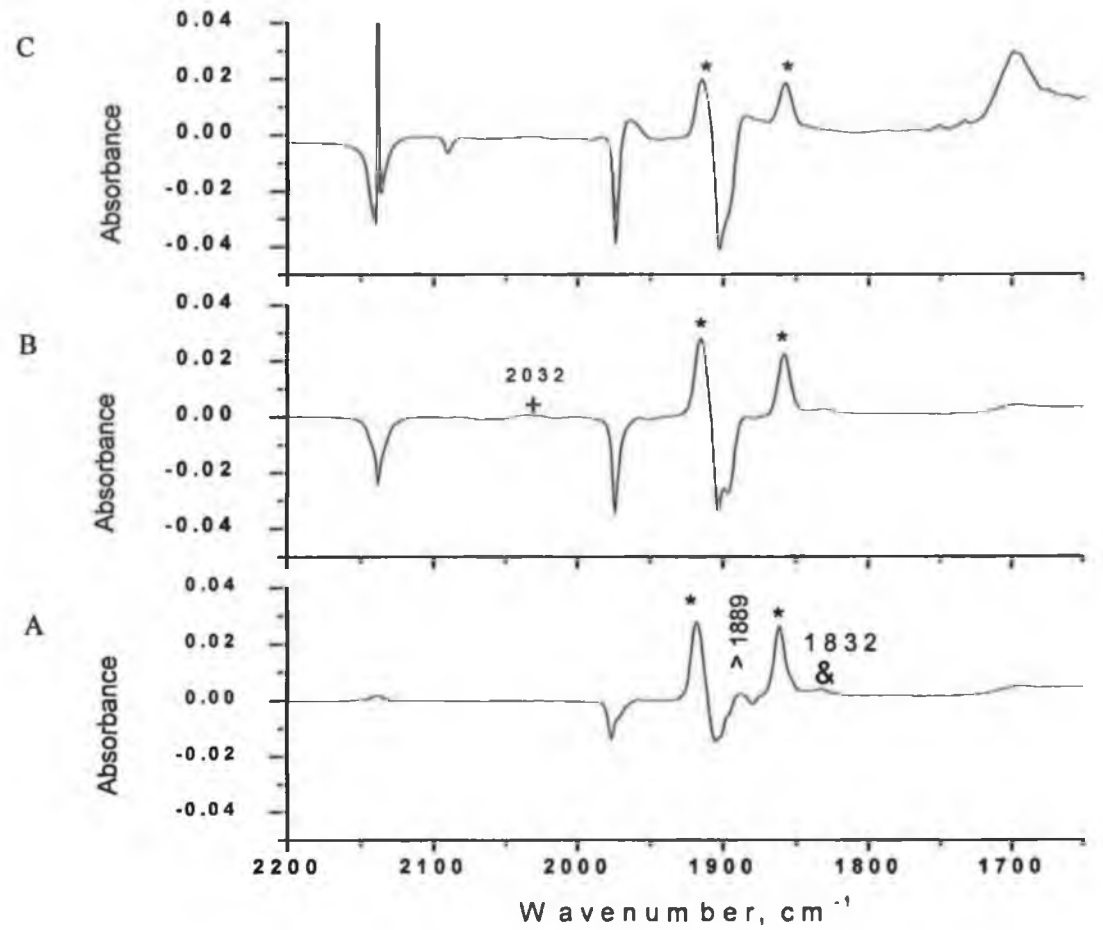

Fig. 3.14 Difference IR spectrum following photolysis with λ_{exc} = 334 nm of (η^6-anisole)$Cr(CO)_3$ at 12 K, A) for 220 min in CH_4, B) for 280 min in 2% CO-CH_4 C) for 310 min in 5% CO-CH_4. The bands labelled with *, &, ^, and + are related the complex (η^6-anisole)$Cr(CO)_2$, *fac*-$Cr(CO)_3$, (η^1-O-anisole)$Cr(CO)_3$ and (η^1-O-anisole)$Cr(CO)_5$ respectively.

Visible irradiation of (η^6-anisole)$Cr(CO)_3$ (λ_{exc} >400 nm) in the methane matrix, results in regeneration of the parent peaks with depletion of the dicarbonyl species peaks. In CO containing matrixes the formation of chromiumhexacarbonyl was indicated by the grow-in of the shoulder at 1982 cm^{-1}, Fig. 3.15.

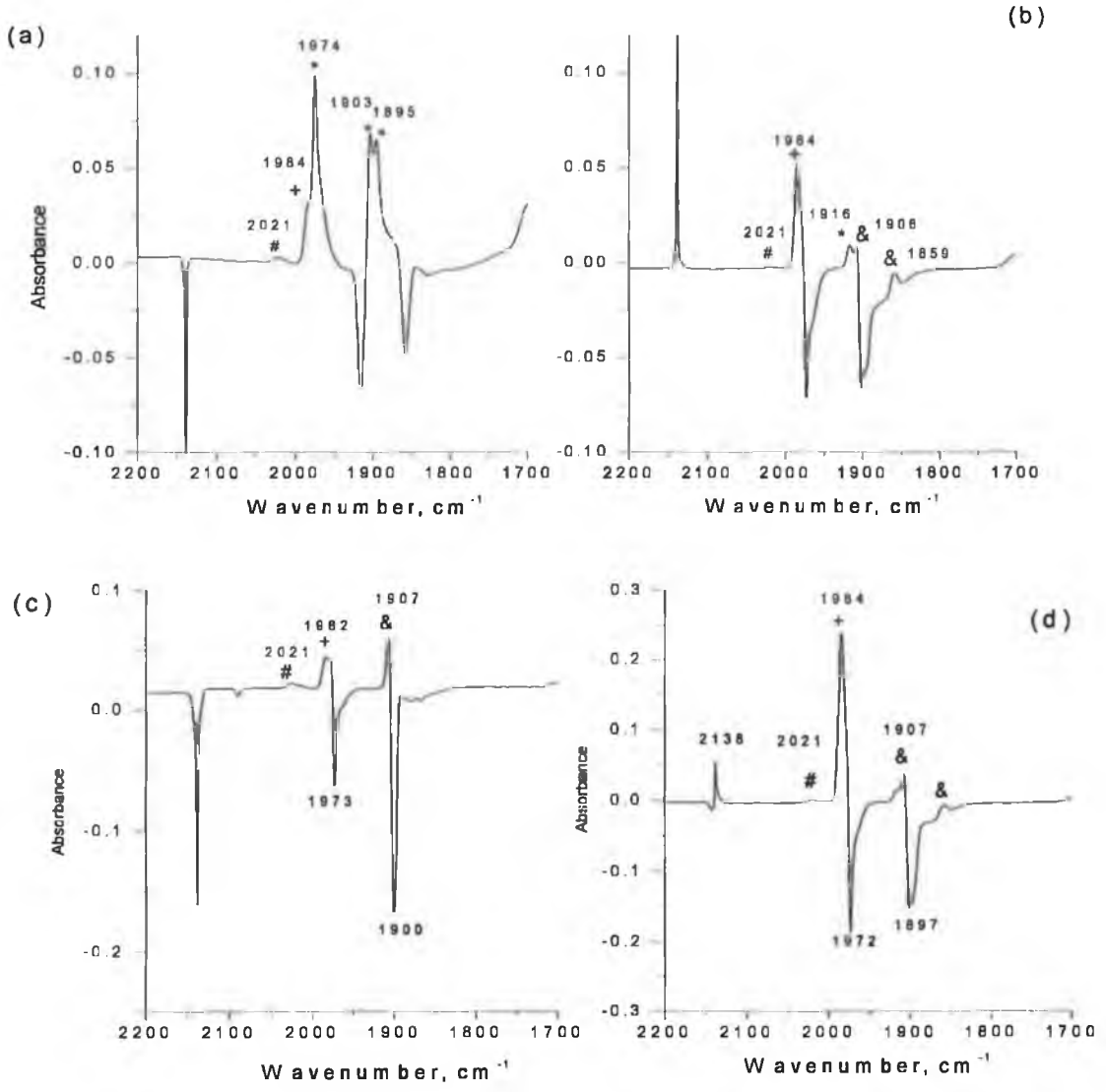

Fig. 3.15 The difference IR spectra of (η^6-anisole)$Cr(CO)_3$ in 5% CO-CH_4 matrix at 12 K following (a) visible photolysis with λ_{exc}>400 nm for 220 min (b) sample in (a) afterUV photolysis with λ_{exc} >300 nm for 180 min. (c) in separate experiment visible photolysis with λ_{exc} >400 nm for 155 min, (d) sample in (c) after UV photolysis with λ_{exc} >300 nm for 155 min. The bands labelled with *, &, # and + are related the parent tricarbonyl complex, (η^6-anisole)$Cr(CO)_2$, (η^1-O-anisole)$Cr(CO)_4$ and $Cr(CO)_6$ respectively.

In a separate experiment visible irradiation λ_{exc} >400 nm of (η^6-anisole)$Cr(CO)_3$ in 5% CO-CH_4 matrix resulted in the formation of chromium hexacarbonyl which was indicated by the grow-in of the shoulder at 1984 cm^{-1}.

Upon UV photolysis of (η^6-anisole)$Cr(CO)_3$ with >300 nm, the dicarbonyl species (η^6-anisole)$Cr(CO)_2$ formed along with the hexacarbonyl compound as indicated by the grow-in of the intense peak at 1984 cm^{-1}. The tetracarbonyl species (η^1-O-anisole)$Cr(CO)_4$ was also formed as indicated by the band at 2021 cm^{-1}, Fig. 3.15.

3.2.4 The matrix isolation photochemistry of (η^6-benzaldehyde)$Cr(CO)_3$

The IR spectroscopic data for (η^6-benzaldehyde)$Cr(CO)_3$ in the ν_{CO} region and all observed photoproducts obtained during this matrix isolation experiments are given in Table 3.4.

The photochemistry of this complex was investigated in pure methane, 2% CO-methane, 5% CO-methane matrixes at 12 K using monochromatic irritation at 436, 405, 365, 334, 313, and 297 nm, followed by irradiation at 546 and 436 nm, and lastly with broad band radiation at >410, >320, and >300 nm

COMPLEX	ν_{CO} (cm^{-1})	MATRIX
Deposition bands:		
(η^6-benzaldehyde)$Cr(CO)_3$	1995, 1940, 1927, 1909, 1704	CH_4
Photoproduct bands :		
(η^6-benzaldehyde)$Cr(CO)_2$	1948, 1896, 1680	CH_4
fac-$Cr(CO)_3$	1857, 1833, 1816	CH_4
fac-$Cr(CO)_3$ (literature [21])	1957, 1841, 1833	CH_4
$Cr(CO)_4$(η^1-O-benzaldehyde)	2032	CO/CH_4
$Cr(CO)_5$(η^1-O-benzaldehyde)	2075,1950	CO/CH_4
$Cr(CO)_5$	1960	CO/CH_4
$Cr(CO)_6$	1984	CO/CH_4

Table 3.4: Spectroscopic data for (η^6-benzaldehyde)$Cr(CO)_3$ and photoproducts observed during these matrix experiments

The ν_{CO} stretching bands of (η^6-benzaldehyde)$Cr(CO)_3$ in methane matrix are at 1995, 1940, 1927 and shoulder at 1909 cm^{-1}(The complex ν_{CO} bands are subject to matrix splitting). Upon changing the matrix to a 2% CO-methane or a 5% CO-methane matrix the band at 1940 cm^{-1} was more intense than the band at 1927 cm^{-1}

Visible photolysis ($\lambda_{exc.}$ = 436 nm) Fig. 3.16 resulted a grow-in of two bands, one at 1992, and the other at 1932 cm^{-1}, which lies between the two parent bands with concomitant depletion of the ν_{CO} of the carbonyl group at 1704 and grow-in of the band at 1707 cm^{-1}. As this change is not greatly affected by the concentration of CO in the matrix, this change seems to indicate the formation of another rotamer of (η^6-benzaldehyde)$Cr(CO)_3$.

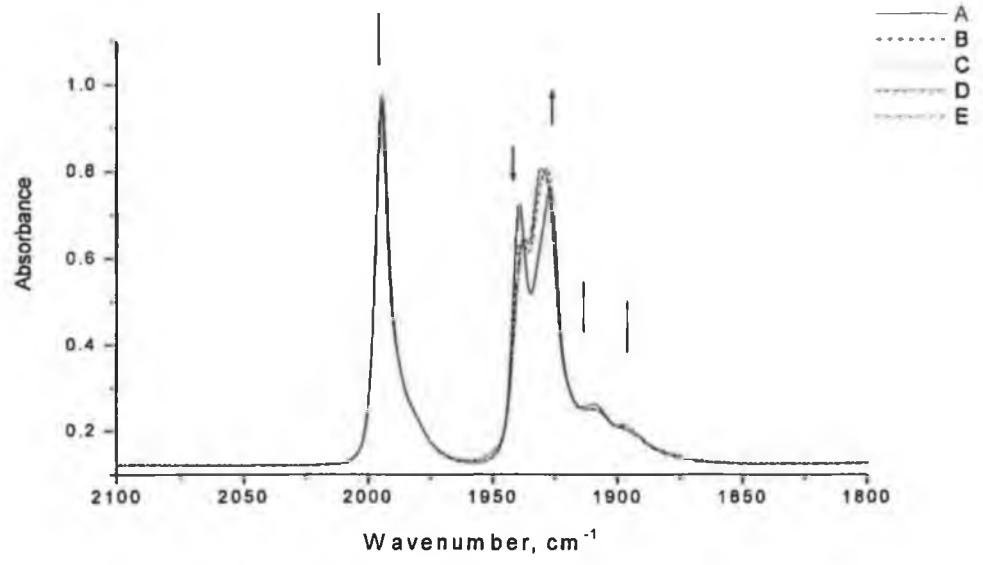

Fig. 3.16 IR spectra of (η^6-benzaldehyde)$Cr(CO)_3$ in a methane matrix at 12 K (A), after15 min. (B), after 45 min. (C), after 75 min. (D), and after 120 min (E) of photolysis by 436 nm.

The formation of the CO loss photoproduct ((η^6-benzaldehyde)$Cr(CO)_2$) is also indicated by the formation of two bands at 1896, 1948 cm^{-1} albeit with low yield.

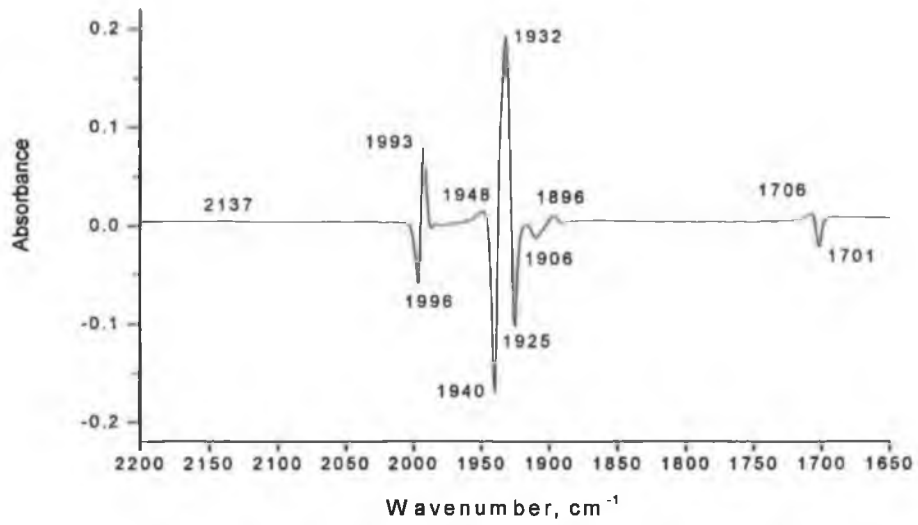

Fig. 3.17 Difference IR spectrum of a methane matrix containing (η^6-benzaldehyde)$Cr(CO)_3$ following photolysis with 436 nm for 120 min.

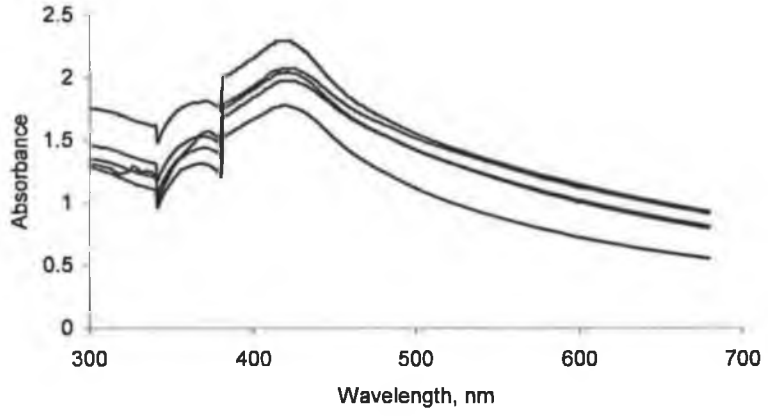

Fig. 3.18 The UV/vis spectra of (η^6-benzaldehyde)$Cr(CO)_3$ at 12 K, after15 min. , after 45 min., after 75 min., and after 120 min of photolysis by 436 nm. λ_{max} is not greatly affected by the photolysis

The photolysis of (η^6-benzaldehyde)$Cr(CO)_3$ in a methane matrix with ($\lambda_{exc.}$ = 405 nm) resulted grow-in of two bands at 1949, and 1896 cm^{-1} along with the weak feature at 2136 cm^{-1} attributable to free CO, Fig. 3.19. The bands at 1949, and 1896 cm^{-1} can be assigned to the dicarbonyl species (η^6-benzaldehyde)$Cr(CO)_2$. The frequency separation of these bands (53 cm^{-1}) is close to that of benzene analogue (54 cm^{-1}).

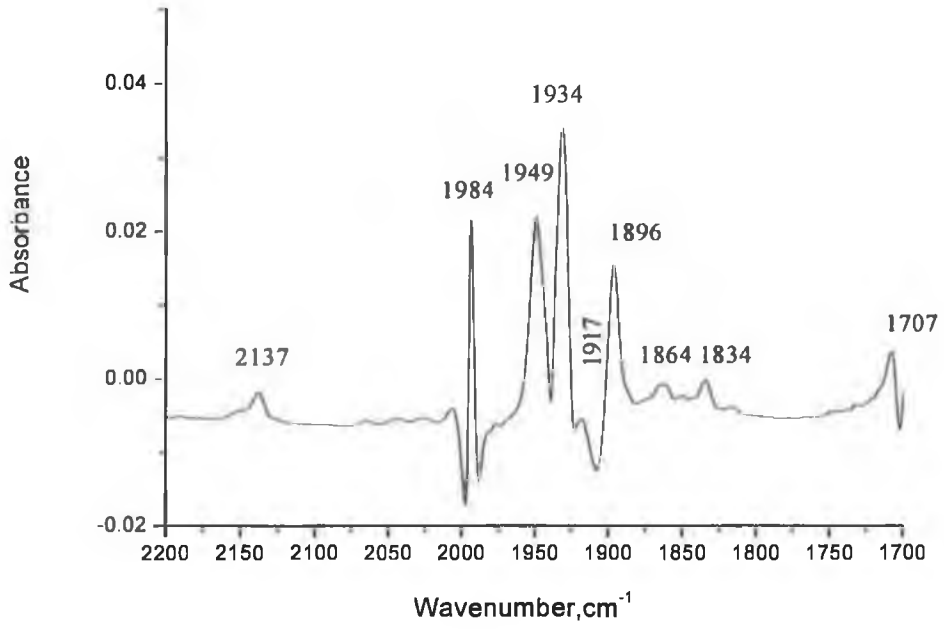

Fig. 3.19 Difference IR spectrum of (η^6-benzaldehyde)$Cr(CO)_3$ in methane matrix after photolysis with 405 nm for 300 min.

The increase of CO concentration in the matrix led to a decrease in the concentration of the dicarbonyl species with increased yield of a ring slip product as indicated by the grow-in of the two bands at 1991, 1927 cm^{-1}.

Upon photolysis with ($\lambda_{exc.}$ = 365 nm) Fig. 3.20, this wavelength seems to induce loss of CO as indicated by the grow-in of the bands at 1948, 1895 cm^{-1} and ring slippage $\eta^6 \rightarrow \eta^1$. The species is trapped by CO to form the pentacarbonyl species as indicated by the appearance of the peaks at 2032, 1961 cm^{-1} which are assigned to (η^1-O-benzaldehyde)$Cr(CO)_4$, and $Cr(CO)_5$ species respectively (some bands of both species do not appear in the spectrum because they are obscured by the parent and the dicarbonyl species peaks).

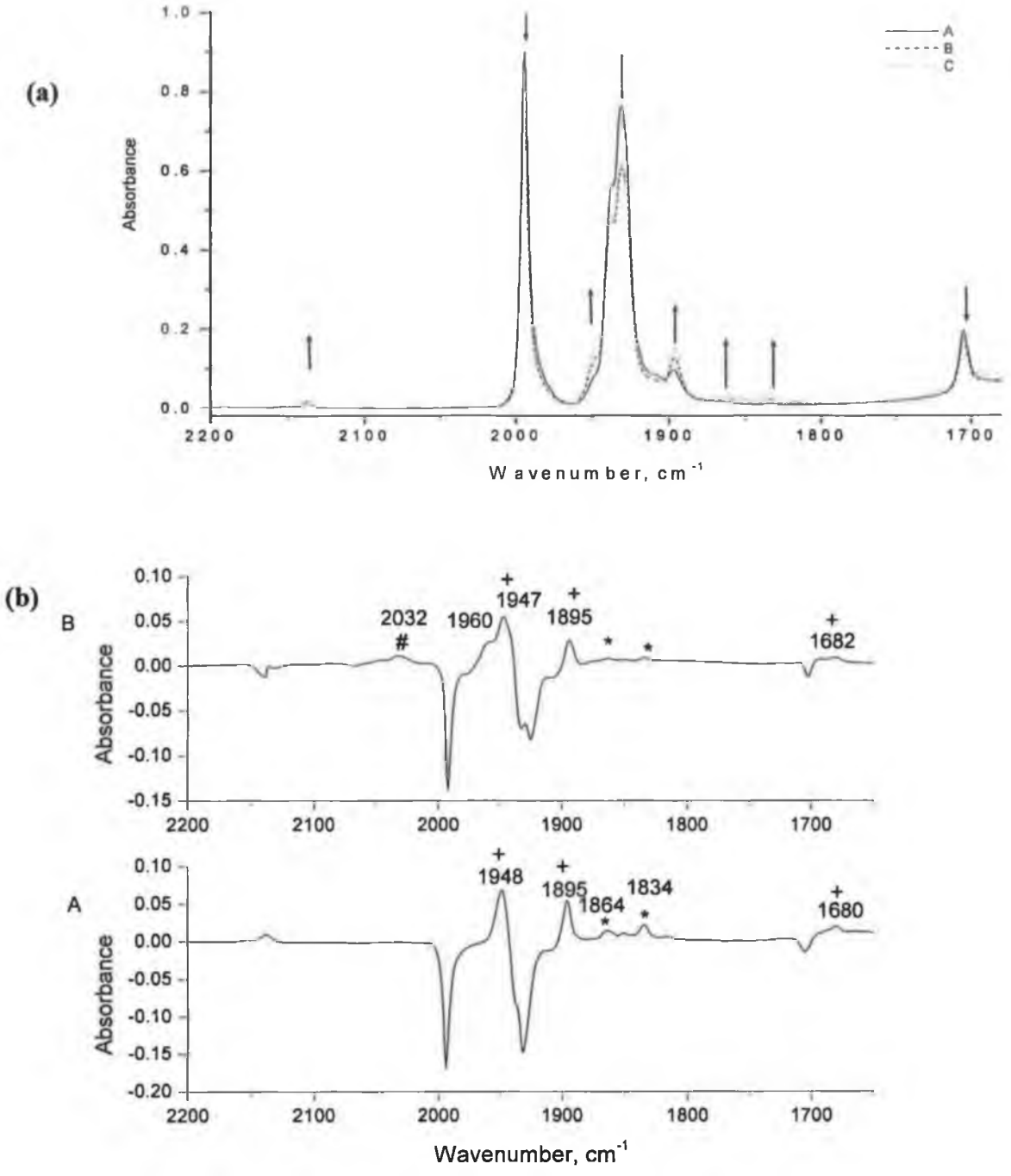

Fig. 3.20 (a) FTIR spectrum of the (η^6-benzaldehyde)$Cr(CO)_3$ in methane matrix at 12 K (A) before photolysis. (B) After 130 min. (C) after 250 min photolysis with 365 nm. (b) A) Difference IR spectrum after photolysis with 365 nm for A) 250 min in methane matrix, B) 205 min in 2% CO-CH_4 matrix. The bands labelled with +, *, and # are for the dicarbonyl species (η^6-benzaldehyde)$Cr(CO)_2$, *fac*-$Cr(CO)_3$ and (η^1-benzaldehyde)$Cr(CO)_4$ species respectively.

Upon photolysis with 334 nm, Fig. 3.21, CO loss is observed with the formation of (η^6-benzaldehyde)$Cr(CO)_2$ (ν_{CO} = 1948, 1895, 1680 cm^{-1}).

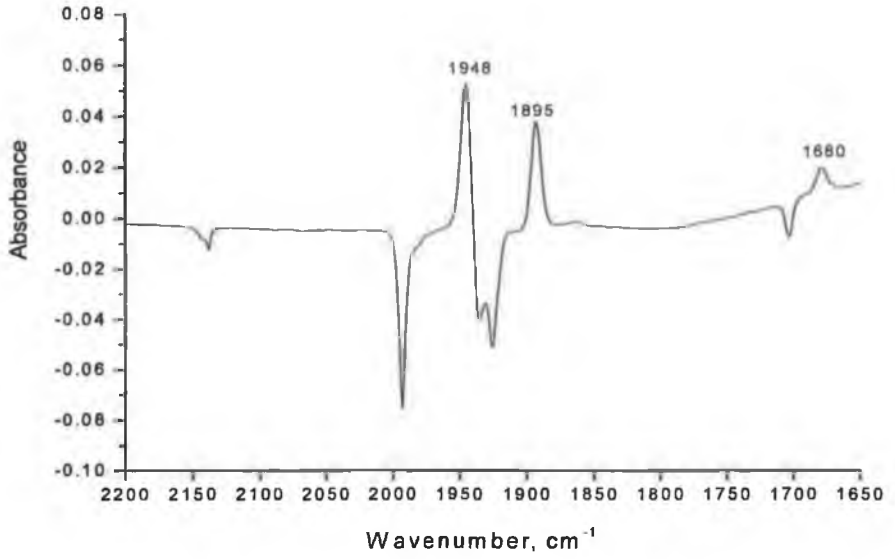

Fig. 3.21 Difference IR spectrum following photolysis of (η^6-benzaldehyde)$Cr(CO)_3$ in 2% CO-methane matrix at 12 K with 334 nm for 150 min.

Upon photolysis of (η^6-benzaldehyde)$Cr(CO)_3$ in methane matrix with 313 nm, Fig. 3.22, the characteristic bands of the dicarbonyl species again appeared. Bands at 1863, 1834 cm^{-1} were also observed and were assigned to the *fac*-$Cr(CO)_3$ moiety (the band at ca. 1957 cm^{-1} was obscured by the parent bands) (in the literature[21] the bands for *fac*-$Cr(CO)_3$ are at 1957, 1841, 1833 cm^{-1} following the photolysis of (η^6-pyridine)$Cr(CO)_3$). The gradual disappearance of these bands upon increasing the concentration of CO in the matrix give further evidence for the formation of this species (i.e. *fac*-$Cr(CO)_3$ moiety) which is trapped by CO to form the tetracarbonyl, pentacarbonyl and hexacarbonyl species, while the band at 1682 cm^{-1} is related to ν_{CO} of the free benzaldehyde.

Upon photolysis (η^6-benzaldehyde)$Cr(CO)_3$ with 297 nm, a slight change occurred with the formation of dicarbonyl species and *fac*-$Cr(CO)_3$ moiety but this change almost disappeared when the concentration of CO in the matrix was increased.

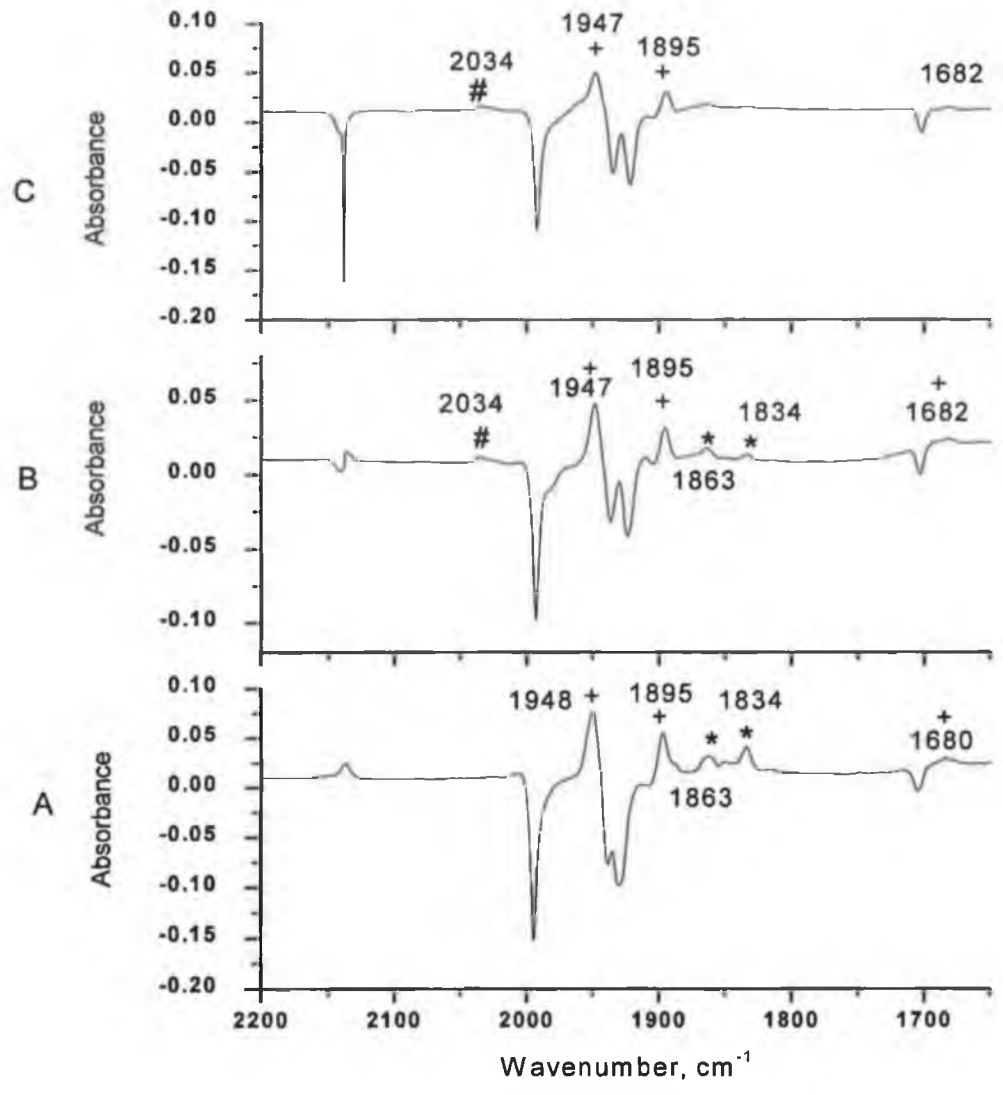

Fig. 3.22 Difference IR spectra obtained following photolysis of (η^6-benzaldehyde)$Cr(CO)_3$ with 313 nm, (A) in pure methane matrix for 405 min. (B) in 2% CO-CH_4 matrix for 275 min (C) in 5%CO-CH_4 matrix for 320 min. The bands labelled with +, *, and # are for the dicarbonyl species (η^6-benzaldehyde)$Cr(CO)_2$, , *fac*-$Cr(CO)_3$ and (η^1-benzaldehyde)$Cr(CO)_4$ species respectively.

In matrixes free of CO subsequent photolysis of (η^6-benzaldehyde)$Cr(CO)_3$ with 546 nm, Fig. 3.23, led to the regeneration of the parent complex (i.e. (η^6-benzaldehyde)$Cr(CO)_3$). However, when CO was present formation of the hexacarbonyl complex was observed as indicated by the grow-in of the band at 1985 cm^{-1}. The appearance of the bands at 2075, 1950 cm^{-1} can be assigned to the pentacarbonyl species $Cr(CO)_5$(η^1-O-benzaldehyde).

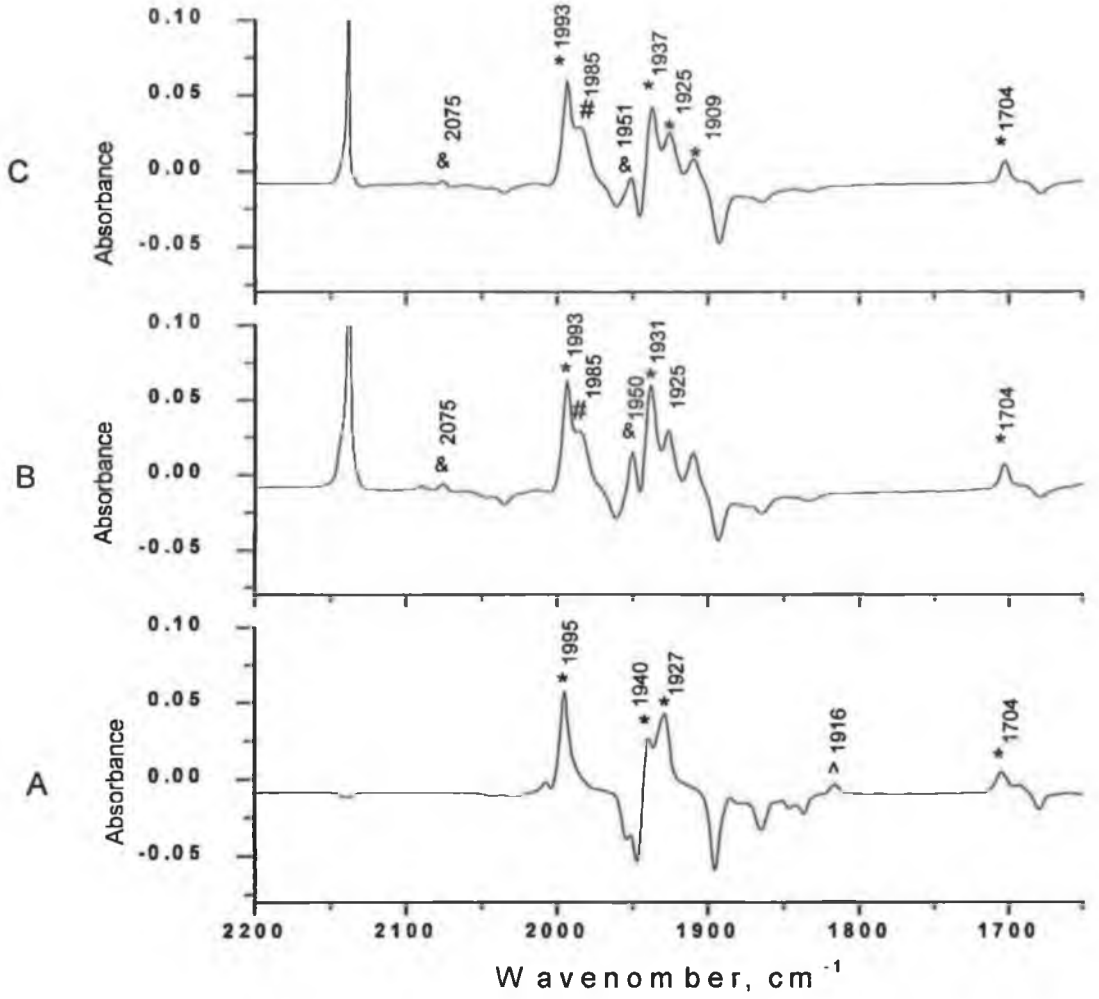

Fig. 3.23 Difference IR spectra obtained following photolysis of (η^6-benzaldehyde)$Cr(CO)_3$ with 546 nm, (A) in pure methane matrix for 120 min (B) in 2% CO-CH_4 matrix for 120 min (C) in 5%CO-CH_4 matrix for 120 min. The bands labelled with *, &, ^ and # are for the parent tricarbonyl species (η^6-benzaldehyde)$Cr(CO)_3$, $Cr(CO)_5(\eta^1$-O-benzaldehyde), *fac*-(η^1-O-benzaldehyde)$Cr(CO)_3$ and $Cr(CO)_6$ respectively.

Subsequent photolysis of (η^6-benzaldehyde)$Cr(CO)_3$ with 436 nm, Fig. 3.24, regenerated the parent complex along with the *fac*-$Cr(CO)_3$ moiety as indicated by the grow in of the bands at 1865, 1835 cm^{-1}. In the presence of CO this moiety is trapped by CO to form the hexacarbonyl compound as indicted by the band at 1982 cm^{-1}.

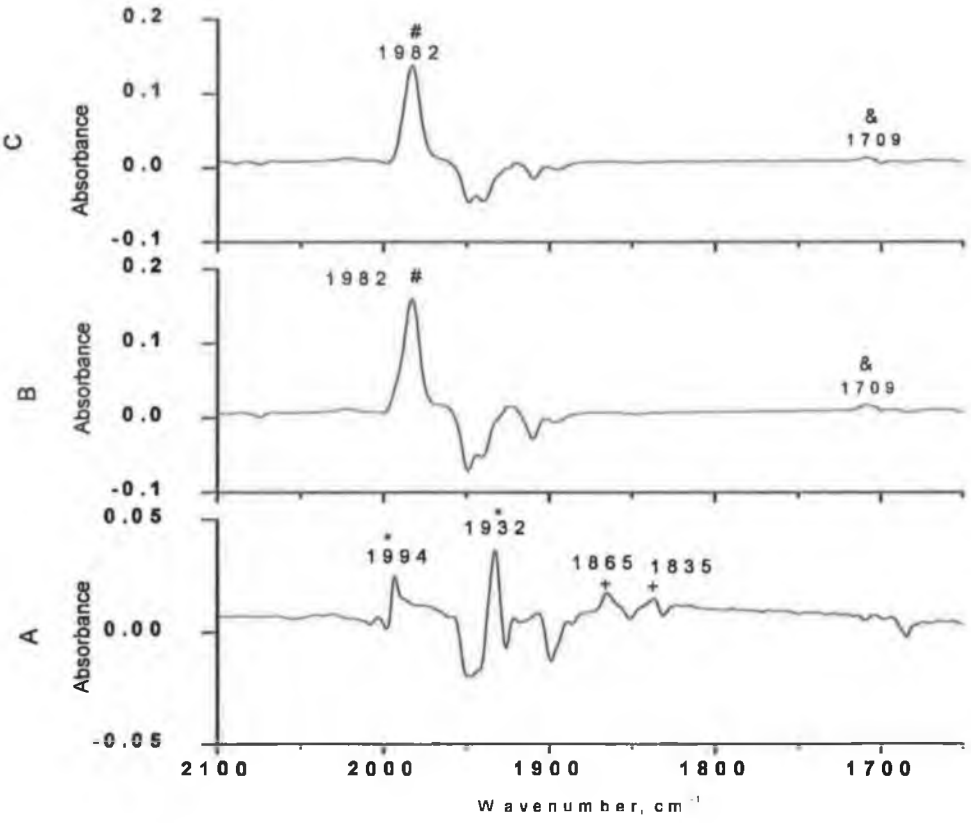

Fig. 3.24 Difference IR spectra obtained following photolysis of (η^6-benzaldehyde)$Cr(CO)_3$ with 436 nm, (A) in pure methane matrix for 90 min. (B) in 2% CO-CH_4 matrix for 90 min (C) in 5%CO-CH_4 matrix for 130 min. The bands labelled with *, +, # and & are for the parent tricarbonyl species, *fac*-$Cr(CO)_3$, $Cr(CO)_6$ and free benzaldehyde respectively.

In the absence of CO the visible photolysis of the irradiated matrix at >410 nm, Fig. 3.25, resulted a grow-in of the parent peaks at 1994, 1930, and 1705 cm^{-1} and depletion of the free CO peak at 2133 cm^{-1}, while in the presence of CO in the matrix, photolysis of the matrix induced the formation of the hexacarbonyl complex as indicated by the grow-in of the peak at 1982 cm^{-1}, along with the formation of the parent tricarbonyl complex.

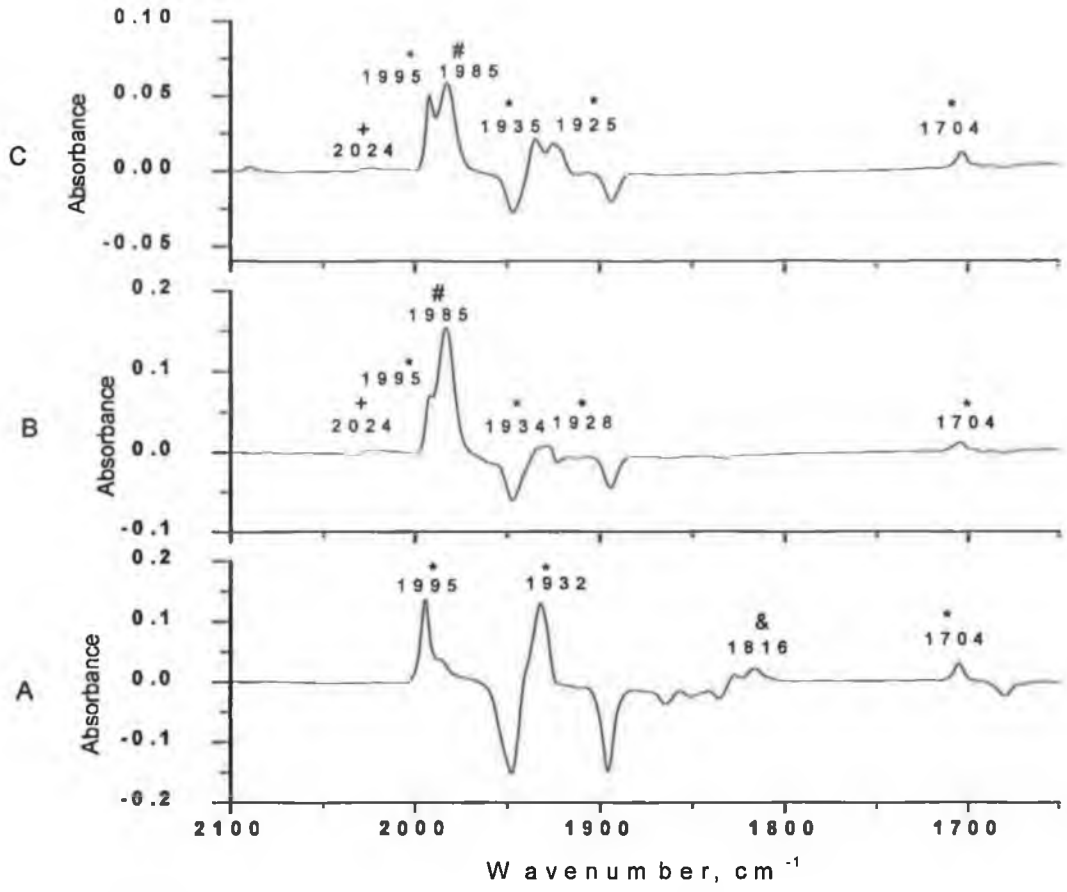

Fig. 3.25 Difference IR spectra obtained following photolysis of (η^6-benzaldehyde)$Cr(CO)_3$ after photolysis with >410 nm, A) in pure methane matrix for 90 min., B) in 2% CO-CH_4 matrix for 180 min C) in 5% CO-CH_4 matrix for 185 min. The bands labelled with *, &, +, and # are for the parent tricarbonyl species, *fac*-(η^1-O-benzaldehyde)$Cr(CO)_3$, cis-(η^1-O-benzaldehyde)$Cr(CO)_4$, and $Cr(CO)_6$ species respectively.

Upon UV photolysis of (η^6-benzaldehyde)$Cr(CO)_3$ with >320 nm, Fig. 3.26, in the absence of CO produced dicarbonyl species (η^6-benzaldehyde)$Cr(CO)_2$ (1949, 1896 cm^{-1}) and a tricarbonyl species (1857, 1833 cm^{-1}). The later is trapped with CO to form chromiumhexacarbonyl as indicated by the appearance of the band at 1984 cm^{-1} and the disappearance of the bands of the tricarbonyl species.

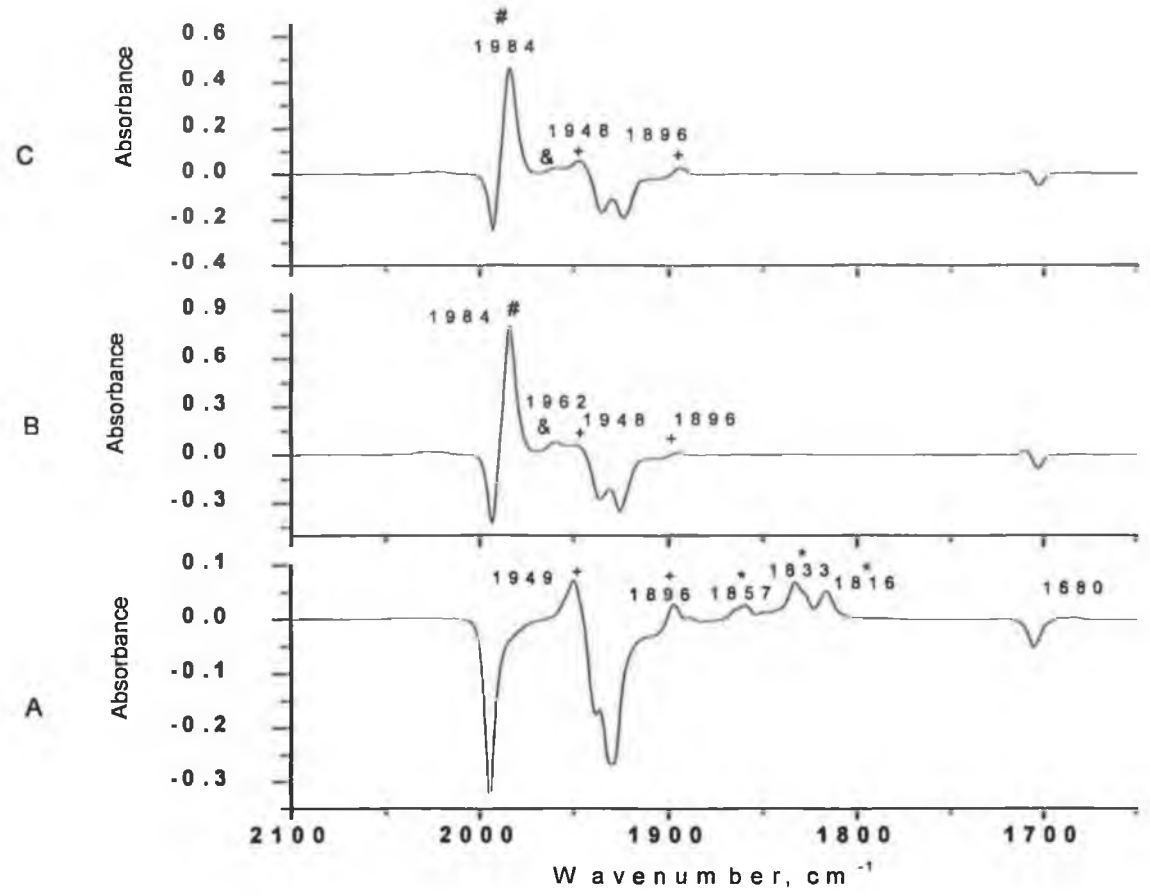

Fig. 3.26 Difference IR spectra obtained following photolysis of (η^6-benzaldehyde)$Cr(CO)_3$ with >320 nm, A) for 410 min. in pure CH_4 matrix, B) 80 min. in 2% CO-CH_4 matrix C) 80 min. in 5% CO-CH_4 matrix. The bands labelled with +, *, &, and # are for the dicarbonyl species (η^6-benzaldehyde)$Cr(CO)_2$, *fac*-$Cr(CO)_3$, $Cr(CO)_5$, (η^1-benzaldehyde)$Cr(CO)_4$, and $Cr(CO)_6$ respectively.

When CO is present the dicarbonyl species also partially trapped by CO so the intensity of the ν_{CO} bands of the dicarbonyl are reduced as the concentration of CO in the matrix is increased.

Upon photolysis of (η^6-benzaldehyde)$Cr(CO)_3$ with >300 nm, in the absence of CO in the matrix, the tricarbonyl species *fac*-$Cr(CO)_3$ was formed as indicated by grow-in in the bands at (1857, 1833 cm^{-1}). If this tricarbonyl species is trapped by CO, chromiumhexacarbonyl is formed as indicated by the appearance of the band at 1984 cm^{-1}, Fig. 3.27.

The formation of free benzaldehyde is indicated by the grow-in of the band at 1710 cm^{-1} for υ_{CO} band.

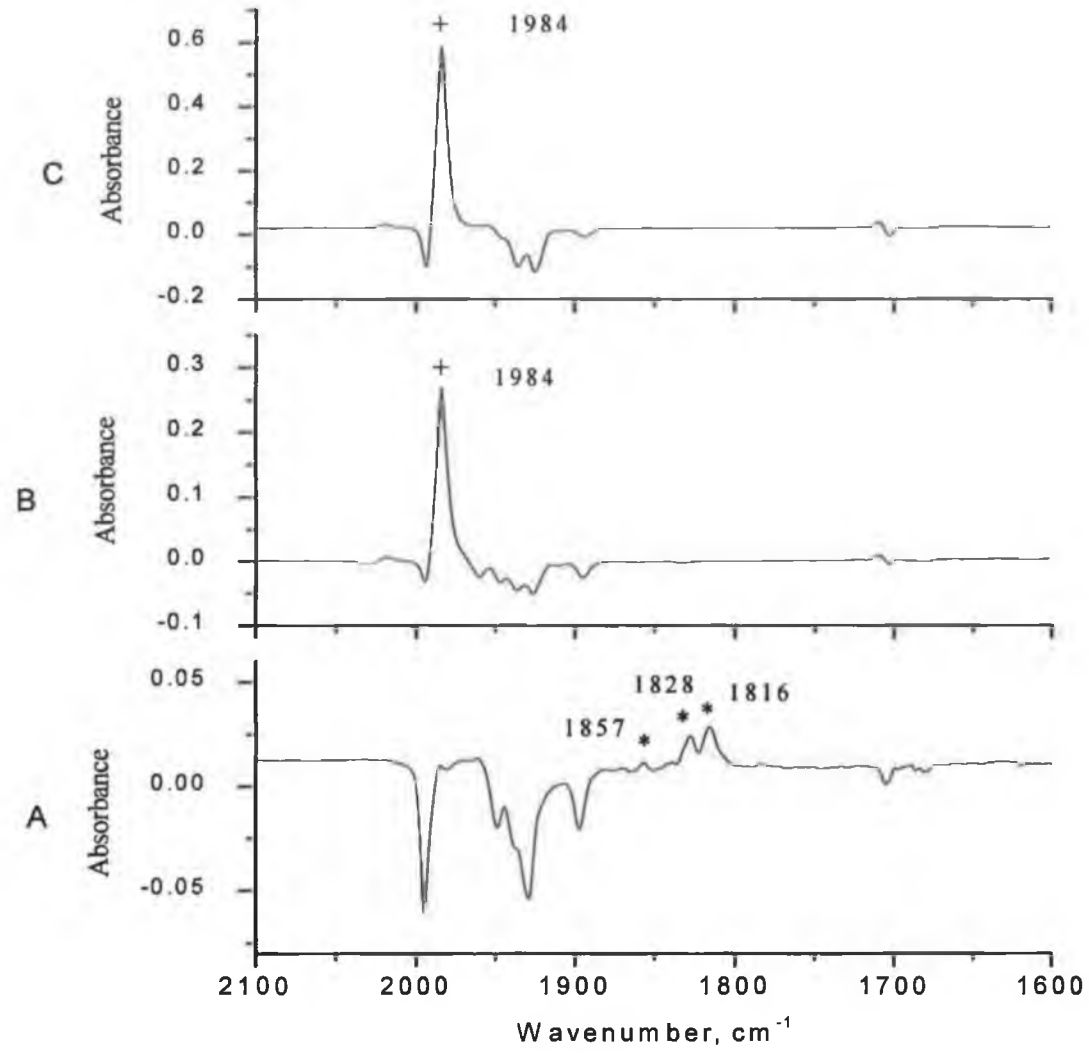

Fig. 3.27 Difference IR spectra obtained following photolysis of (η^6-benzaldehyde)$Cr(CO)_3$ with >300 nm, A) for 85 min. in pure CH_4 matrix, B) 90 min. in 2% CO-CH_4 matrix C) 90 min. in 5% CO-CH_4 matrix. The bands labelled with * and + are for *fac*-$Cr(CO)_3$, and $Cr(CO)_6$ respectively.

Generally increasing the temperature for the methane matrix lead to the regeneration of the parent complex. In addition to the regeneration of the parent tricarbonyl species as indicated by the grow-in of the bands at 1996, and 1940 cm^{-1} increasing of the temperature of CO-methane matrixes also resulted in the grow-in of some bands related to the rich CO complexes (containing $Cr(CO)_4$ and $Cr(CO)_5$ moieties), Fig. 3.28.

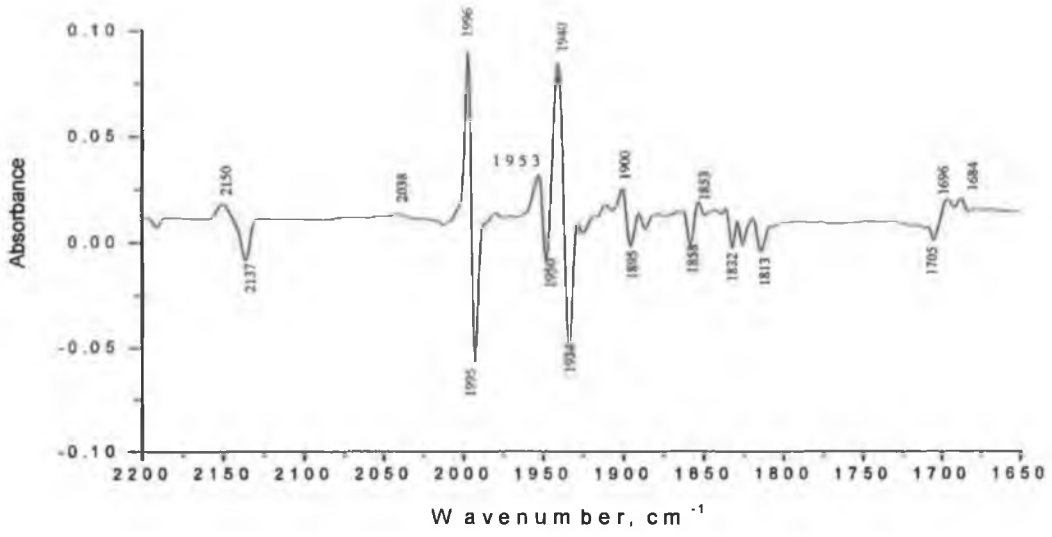

Fig. 3.28 Difference IR spectrum following annealing of the matrix after photolysis (η^6-benzaldehyde)$Cr(CO)_3$ in 5% CO-CH_4 matrix.

3.2.5 The matrix isolation photochemistry of (η^6-methylbenzoate)$Cr(CO)_3$:-

The IR spectroscopic data in ν_{CO} region for (η^6-methylbenzoate)$Cr(CO)_3$ and all photoproducts obtained during this matrix isolation experiments are given in Table 3.5.

The parent ν_{CO} peaks for (η^6-methylbenzoate)$Cr(CO)_3$ in pure methane matrix occurred at 1991, 1923, and 1735 cm^{-1}. The IR and UV/vis spectra of (η^6-methylbenzoate)$Cr(CO)_3$ are given in Fig.3.29 and 3.30 respectively.

COMPLEX	ν_{CO} (cm^{-1})	ν_{N-N} (cm^{-1})	MATRIX
Deposition bands: (η^6-methylbenzoate)$Cr(CO)_3$	1991, 1923, 1735		CH_4
Rotamer (η^6-methylbenzoate)$Cr(CO)_3$	1926		
(η^6-methylbenzoate)$Cr(CO)_2$	1943, 1890		CH_4
(η^6-methylbenzoate)$Cr(CO)_2N_2$	1955, 1912	2165	N_2
fac-(η^6-methylbenzoate)$Cr(CO)(N_2)_2$	1873	2211, 2238	N_2
$Cr(CO)_5$(η^1-O-methylbenzoate)	2037, 2024, 1959		CO/CH_4
(η^1-O-methylbenzoate)$Cr(CO)_3(N_2)_2$	2023, 1981	2217, 2251	N_2
$Cr(CO)_6$	1985		CO/CH_4

Table 3.5: IR spectroscopic data in ν_{CO} region for (η^6-methylbenzoate)$Cr(CO)_3$ and all photoproducts observed.

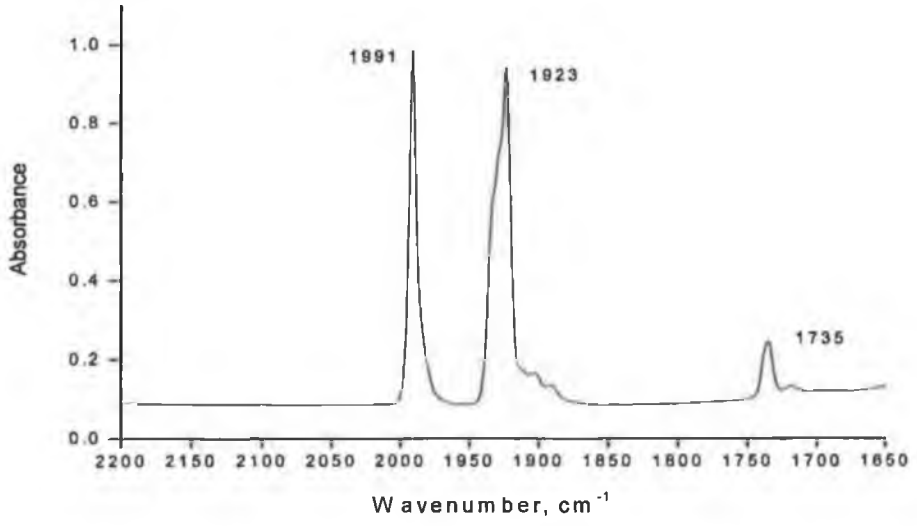

Fig.3.29 The infrared spectrum in ν_{CO} region of (η^6-methylbenzoate)$Cr(CO)_3$ in pure methane matrix.

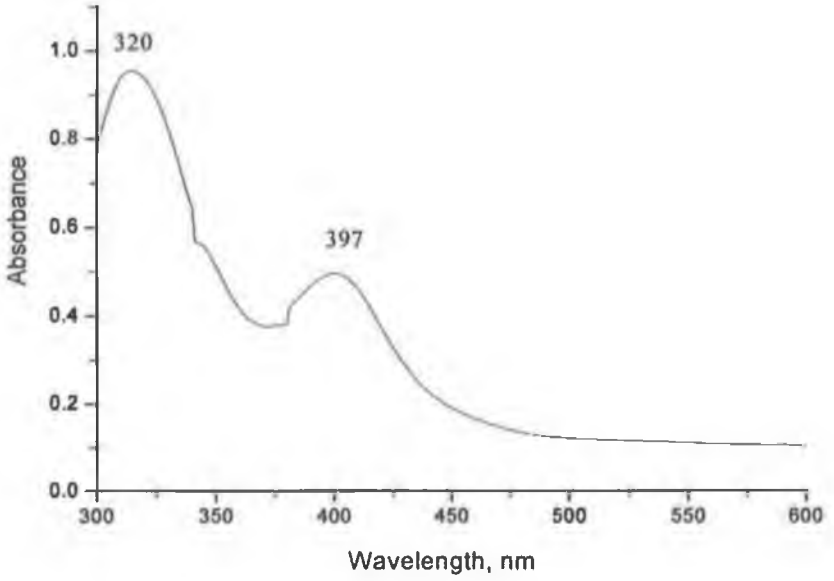

Fig 3.30 UV/visible spectrum of (η^6-methylbenzoate)$Cr(CO)_3$ in a pure dinitrogen matrix.

Photolysis by monochromatic visible irradiation (λ_{exc} = 436, or 405 nm) in a methane matrix resulted in the changes illustrated in Fig. 3.31. The spectroscopic changes have been assigned to the depletion of the parent peak at 1991 cm^{-1} with splitting of the peak at 1923 cm^{-1} to give depletion at 1932, 1921 cm^{-1} and grow in at 1926 cm^{-1}. This can be assigned to rotamer of (η^6-methylbenzoate)$Cr(CO)_3$.

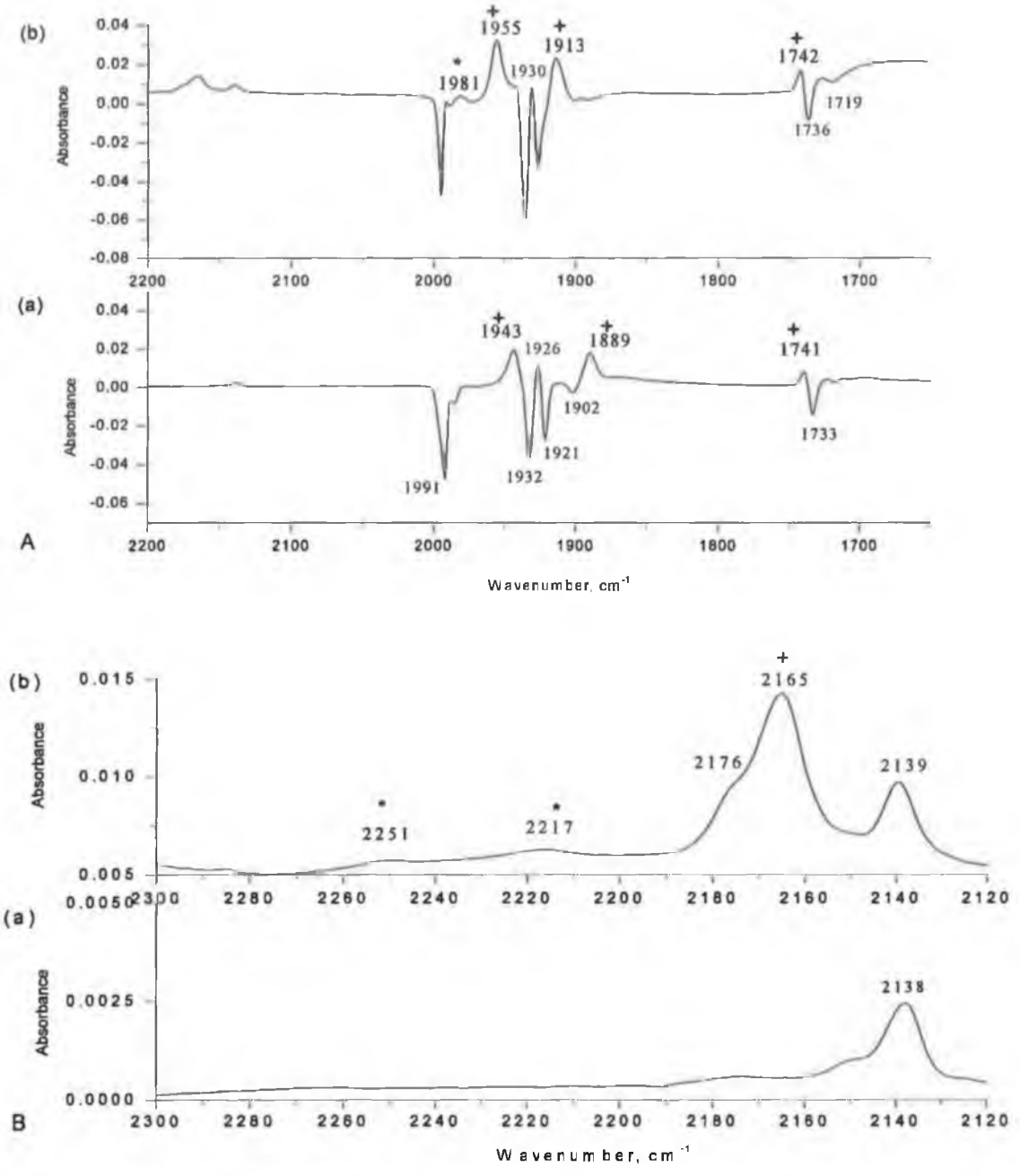

Fig. 3.31 (A) Difference spectra obtained following visible photolysis of (η^6-methylbenzoate)$Cr(CO)_3$ at 12 K (a) in methane matrix λ_{exc} = 405 nm; for 120 min, (b) in dinitrogen matrix λ_{exc} = 436 nm; for 560 min. (B) Expansion of the figures (a) and (b) shown in (A) at the range 2300-2120 cm^{-1}. The bands labelled with (+) are for (η^6-methylbenzoate)$Cr(CO)_2(N_2)$, while the bands labelled with (*) are for *fac*-(η^1-O-methylbenzoate)$Cr(CO)_3(N_2)_2$.

The grow in of the two peaks at 1943, 1889 cm^{-1} are assigned to the formation of the dicarbonyl species (η^6-methylbenzoate)$Cr(CO)_2$ because the frequency separation between the two peaks is 54 cm^{-1}, close to that for the benzene analogue. There is

also a weak feature at 2139 cm^{-1} attributable to the free CO. This was formed concomitantly with the band at 1741 cm^{-1}. This change in υ_{CO} stretching of the carboxylate group is as a result of the increase in the electron density on the arene ligand as one of the three CO ligands is lost.

Irradiation of (η^6-methylbenzoate)$Cr(CO)_3$ in a N_2 matrix at 12 K with λ_{exc} = 436 nm produced the dicarbonyl complex (η^6-methylbenzoate)$Cr(CO)_2(N_2)$ as observed from depletion of the parent bands and the growth of the bands at 1955, 1913 cm^{-1}. Two bands of similar intensity were observed in the υ_{N-N} region (2251 and 2217 cm^{-1}) indicative of cis-coordinated N_2 ligands, Fig. 3.31. The wavenumber difference between the υ_{N-N} antisymmeteric and symmetric vibrational modes (34 cm^{-1}) is similar to the differences observed for (η^1-pyridine)$Cr(CO)_3(N_2)_2$ in dinitrogen matrix (33 cm^{-1})[21], and for (η^5-C_5H_5)$Nb(CO)_2(N_2)_2$ in xenon (39 cm^{-1}) and (η^5-C_5H_5)$V(CO)_2(N_2)_2$ (32 cm^{-1}).[26] Therefore the visible irradiation of (η^6-methylbenzoate)$Cr(CO)_3$ in N_2 matrix produces *fac*-(η^1-O-methylbenzoate)$Cr(CO)_3(N_2)_2$. The appearance of new bands at 2023, 1981 cm^{-1} are for the ν_{CO} for this complex while the other band was obscured by the bands of the dicarbonyl species.

To provide greater confidence about the assignments of the dinitrogen complexes formed we undertook DFT calculations using B3LYP/LanL2DZ level of theory on, (η^6-methylbenzoate)$Cr(CO)_2(N_2)$, (η^6-methylbenzoate)$Cr(CO)(N_2)_2$ and *fac*-(η^1-O-methylbenzoate)$Cr(CO)_3(N_2)_2$ to calculate the IR active frequencies.

Tables 3.6, 3.7, and 3.8 show the comparison of ν_{CO}, ν_{N-N} for each of the complexes *vide infra*. The calculated IR frequencies are close to those observed experimentally.

Calculated*	Experimental	Assignment
1703		ν_{CO} of carboxylate
1922	1912	ν_{CO}
1957	1955	ν_{CO} symmetric
2151	2165	ν_{N-N}

* Correction factor is 1.02021

Table 3.6 IR frequencies in ν_{CO} and ν_{N-N} region of (η^6-methylbenzoate)$Cr(CO)_2(N_2)$

Calculated*	Experimental	Assignment
1701	**	ν_{CO} of carboxylate
1932	1873	ν_{CO}
2126	2211	ν_{N-N} Asymmetric
2165	2238	ν_{N-N} Symmetric

* Correction factor is 1.02021

** This band is obscured by dicarbonyl complex band

Table 3.7 IR frequencies in ν_{CO} and ν_{N-N} region of (η^6-methylbenzoate)Cr(CO)$(N_2)_2$.

Calculated*	Experimental	Assignment
1725	1742	ν_{CO} of carboxylate
1934	**	ν_{CO} Asymmetric
1946	1981	ν_{CO} Asymmetric
1996	2023	ν_{CO} Symmetric
2168	2217	ν_{N-N} Asymmetric
2215	2251	ν_{N-N} Symmetric

* Correction factor is 1.02021

** This band is obscured by dicarbonyl complex band at 1955 cm^{-1} of the dicarbonyl species.

Table 3.8 IR frequencies in ν_{CO} and ν_{N-N} region of (η^1-O-methylbenzoate)Cr$(CO)_3(N_2)_2$.

In CO-methane matrixes the photolysis of (η^6-methylbenzoate)Cr$(CO)_3$ with 436 nm produced a rotamer of the parent complex. In addition the dicarbonyl species was also formed. The formation of the tetracarbonyl and pentacarbonyl was also evidently formed by the reaction of ring-slip species with CO and was indicated by the bands at 2068, 2024, 1960 cm^{-1}, Fig 3.32. The hexacarbonyl complex could also have been produced, however its band was obscured by the rotamer bands. Also this band obscured the other bands of the pentacarbonyl and tetracarbonyl.

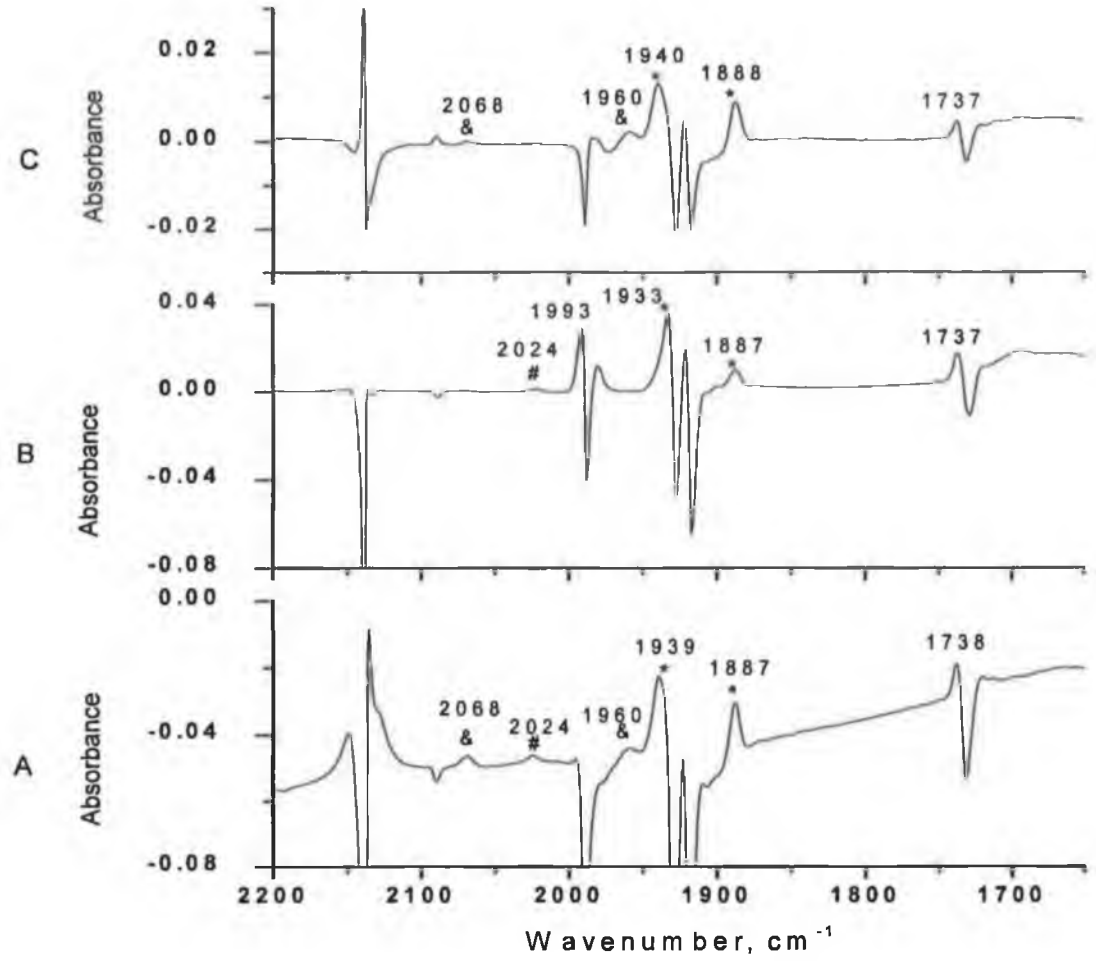

Fig 3.32 Difference IR spectra obtained following visible photolysis of (η^6-methylbenzoate)$Cr(CO)_3$ at 12 K (A) in 2% CO-CH_4 matrix with λ_{exc} = 405 nm; 330 min (B) and (C) in 5% CO-CH_4 matrix with 436 nm for 560 and 405 nm for 345 min respectively.

Photolysis with 365 and 334 nm, Fig. 3.33, led to the loss of CO to form the dicarbonyl species (η^6-methylbenzoate)$Cr(CO)_2$ as apparent from the appearance of the two peaks at 1943, and 1889 cm^{-1} in methane matrix or methane-CO matrixes. Upon the photolysis in dinitrogen matrix the dicarbonyl species is trapped by dinitrogen to form the complex (η^6-methylbenzoate)$Cr(CO)_2(N_2)$ with ν_{CO} bands at 1955, 1912 cm^{-1} and the ν_{N-N} bands at 2165 cm^{-1}.

The peak at 1918 cm^{-1} may be related to the tetracarbonyl species (η^1-O-methylbenzoate)$Cr(CO)_4$.

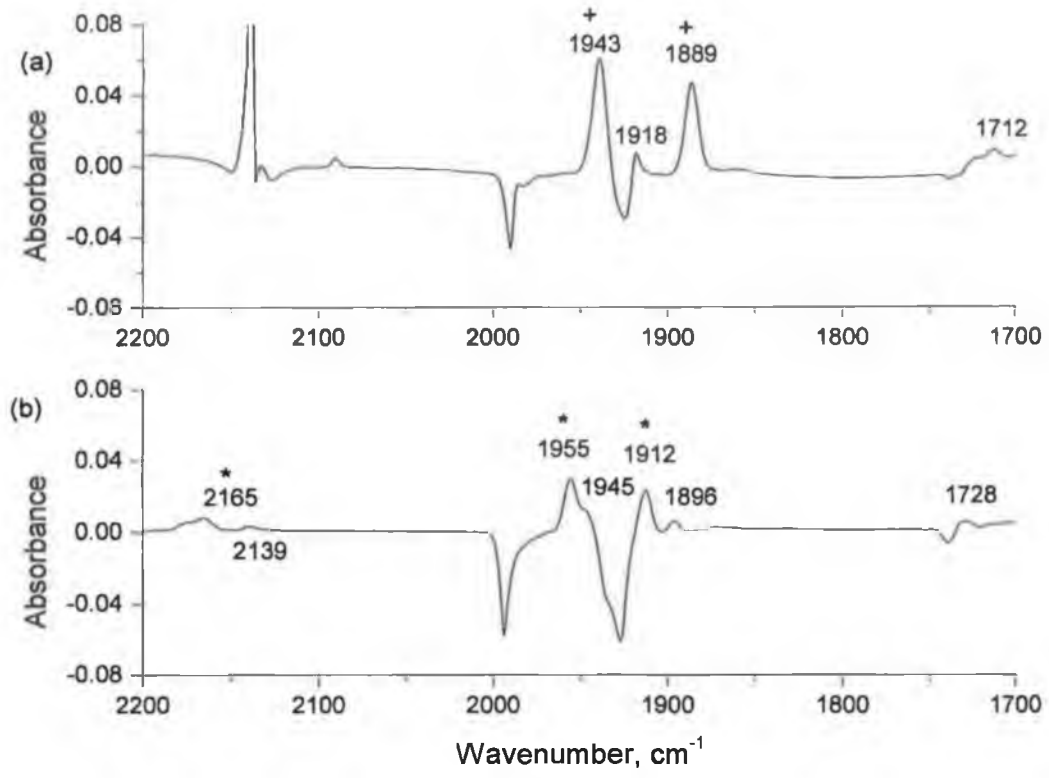

Fig. 3.33 Difference IR spectra obtained following UV photolysis λ_{exc} = 334 nm of (η^6-methylbenzoate)$Cr(CO)_3$ at 12 K, a) in 2% CO-methane matrix; for 440 min, b) in dinitrogen matrix, for 334 min.

Photolysis of (η^6-methylbenzoate)$Cr(CO)_3$ in 2 % CO/CH_4 matrix with 313 nm, Fig. 3.34, resulted the loss of CO from the parent tricarbonyl complex to form the dicarbonyl species. In addition, the grow-in of the peak at 1959 cm^{-1} in the CO-doped matrixes can be assigned to a pentacarbonyl species.

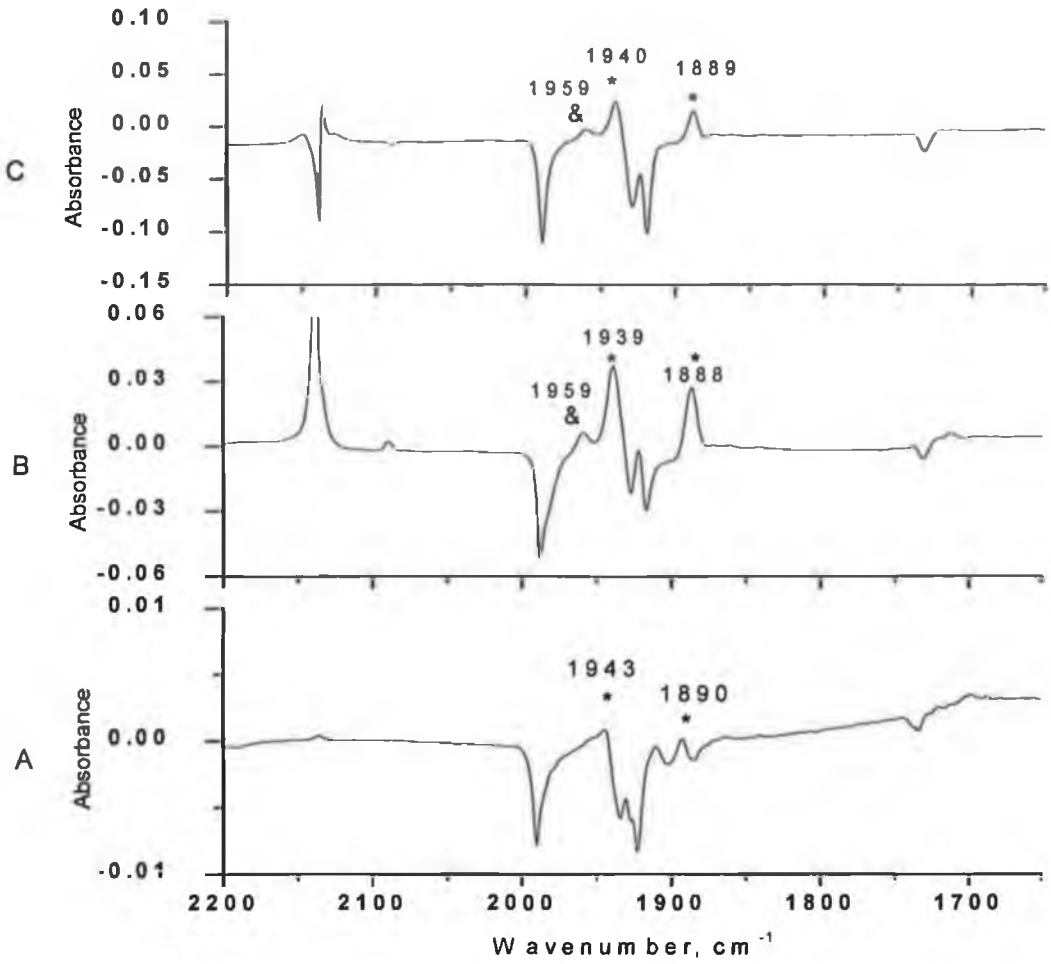

Fig. 3.34 Difference IR spectra obtained following UV photolysis λ_{exc} = 313 nm of (η^6-methylbenzoate)$Cr(CO)_3$ at 12 K, (A) in methane matrix for 75 min (B) in 2% CO-methane matrix; for 290 min, (C) in 5% CO-methane matrix; for 290 min. The bands labelled with (*) are for (η^6-methylbenzoate)$Cr(CO)_2$, while the bands labelled with (&) are for $Cr(CO)_5$ species which possibly formed during the photolysis.

In addition to the formation of the *fac*-(η^1-O-methylbenzoate)$Cr(CO)_3(N_2)_2$ and (η^6-methylbenzoate)$Cr(CO)_2N_2$ species, irradiation in a N_2 matrix with 313 nm produced another weak band at 1873 cm^{-1} and bands at 2211 and 2238 cm^{-1}, Fig. 3.35. This is indicative of another complex with cis-coordinated N_2 ligands. The wavenumber difference between the υ_{N-N} antisymmeteric and symmetric vibrational modes (27 cm^{-1}) is different to the difference observed for *fac*-(η^1-O-methylbenzoate)$Cr(CO)_3(N_2)_2$ (34 cm^{-1}). Therefore it is proposed that UV irradiation with λ_{exc} = 313 nm resulted in loss of CO from (η^6-methylbenzoate)$Cr(CO)_2(N_2)$ to form *fac*-(η^1-O-methylbenzoate)$Cr(CO)(N_2)_2$.

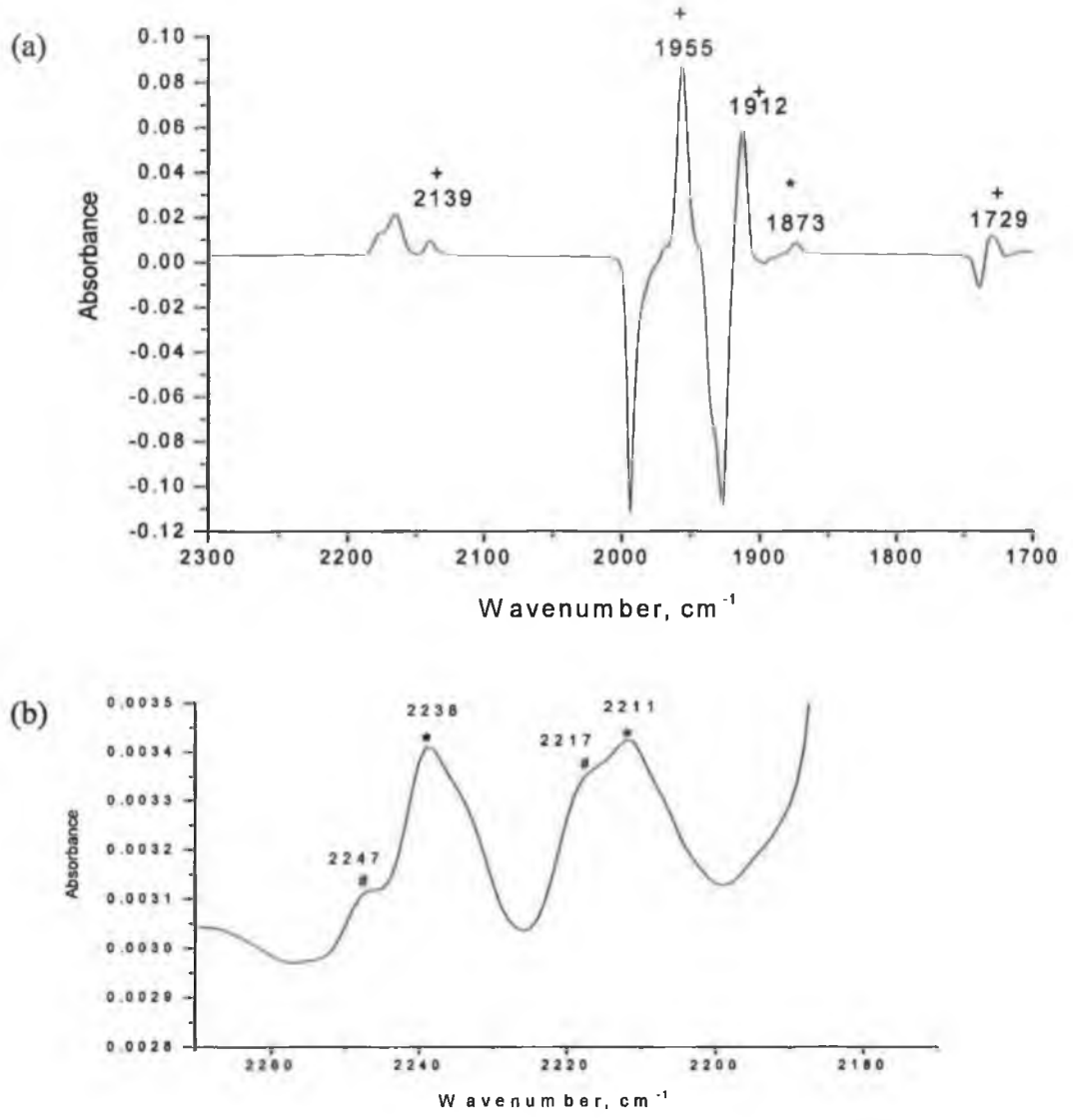

Fig. 3.35 Difference IR spectrum obtained following UV photolysis λ_{exc} = 313 nm of (η^6- methylbenzoate)$Cr(CO)_3$ at 12 K, (a) in dinitrogen matrix for 210 min (b) expansion of the bands in the range 2170-2270 cm^{-1}. The bands labelled with (+) are for (η^6-methylbenzoate)$Cr(CO)_2(N_2)$, while the bands labelled with (*) are for the complex *fac*-(η^1-O-methylbenzoate)$Cr(CO)_3(N_2)_2$, and (#) for the complex (η^6-methylbenzoate)$Cr(CO)(N_2)_2$.

UV irradiation with 297 nm lead to regeneration of the parent peaks with depletion of (η^6-methylbenzoate)$Cr(CO)_2$ species peaks.

Consequently, visible irradiation with >400 nm of (η^6-methylbenzoate)$Cr(CO)_3$ in methane matrix led to regeneration of the parent peaks with depletion of (η^6-methylbenzoate)$Cr(CO)_2$ species peaks. In CO containing matrixes, Fig. 3.36, the

formation of chromium hexacarbonyl was observed at 1985 cm^{-1}. In a separate experiment the photolysis of (η^6-methylbenzoate)$Cr(CO)_3$ in 5% CO-methane matrix with >400 nm lead to the grow-in of a peak at 1985 cm^{-1} as a result of formation of $Cr(CO)_6$.

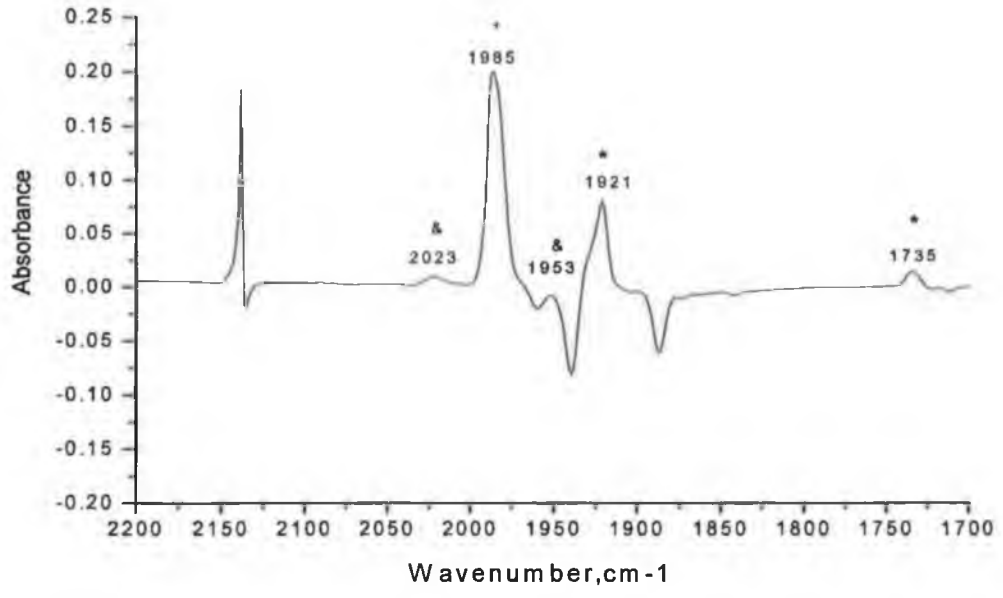

Fig. 3.36 Difference IR spectrum obtained following photolysis of (η^6-methylbenzoate)$Cr(CO)_3$ in 2% CO-methane matrix with λ_{exc} >400 nm; for 100 min at 12 K. The bands labeled with *, &, and + are for the parent tricarbonyl complex, $Cr(CO)_5(\eta^1$-O-methylbenzoate), and $Cr(CO)_6$ respectively.

Subsequent photolysis of the dinitrogen matrix ($\lambda_{exc.}$ >400 nm) mainly resulted in regeneration of the parent tricarbonyl complex and depletion of the dicarbonyl bands at 1955, 1912 and also the depletion the features at 2165 cm^{-1}, Fig. 3.37. Therefore, the photolysis with >400 nm induced the regeneration of the parent tricarbonyl complex and the formation of the ring slip complex. Furthermore, new ν_{CO} bands appeared at 2023, 1981 cm^{-1}, the $\nu_{N\text{-}N}$ bands at 2251, 2217 cm^{-1}, ν_{CO} band at 2149 cm^{-1} for the complex *fac*-(η^1-O-methylbenzoate)$Cr(CO)_3(N_2)_2$.

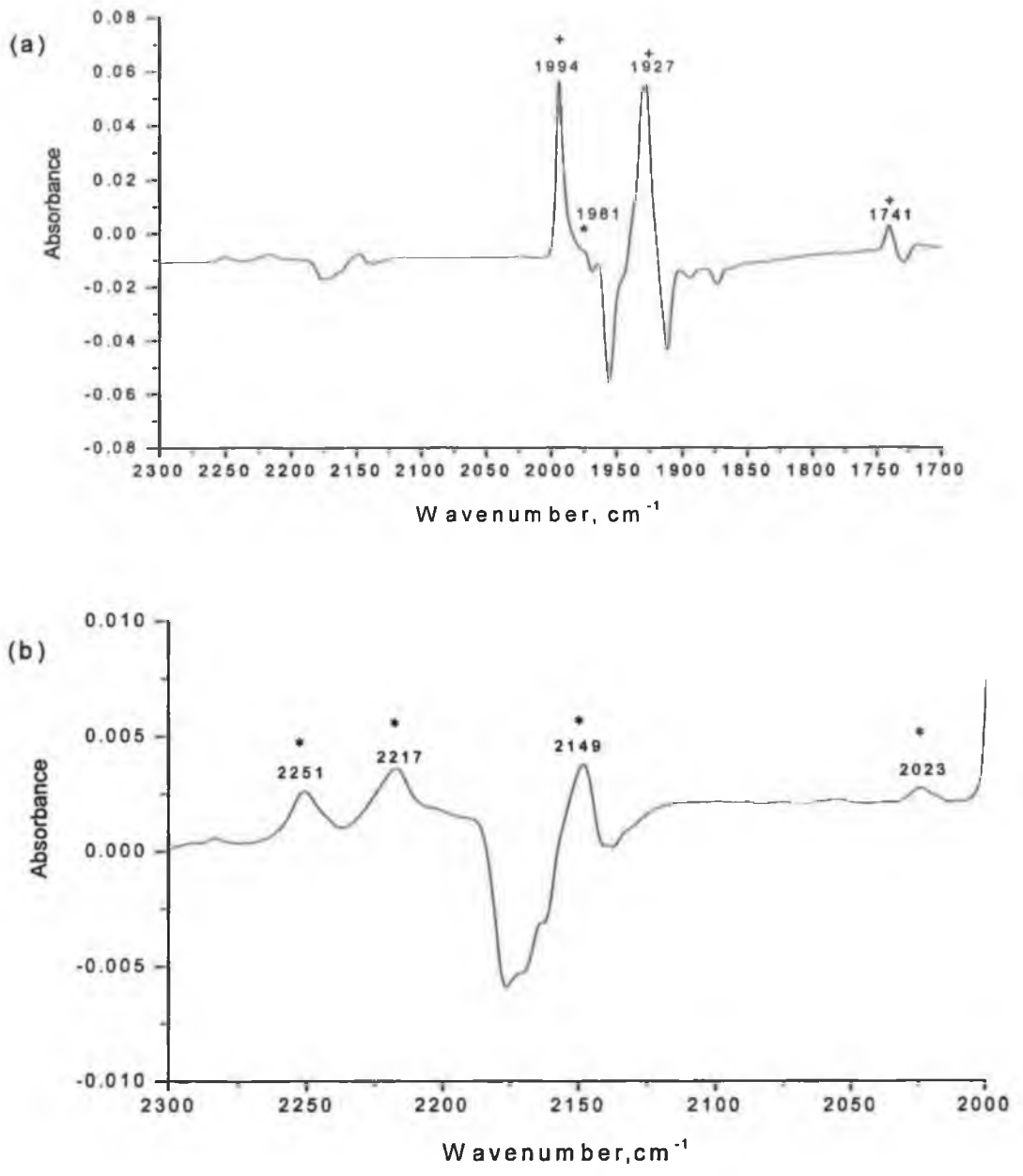

Fig. 3.37 (a) Difference IR spectra obtained following visible photolysis of (η^6-methylbenzoate)$Cr(CO)_3$ in 5% CO-CH_4 matrix at 12 K with >400 nm for 120 min (b) Expansion of the spectrum in (a) in the region 2000-2300 cm^{-1}. The bands labelled with (+) are for the parent tricarbonyl complex, while the bands labelled with (*) are for the complex *fac*-(η^1-O-methylbenzoate)$Cr(CO)_3(N_2)_2$

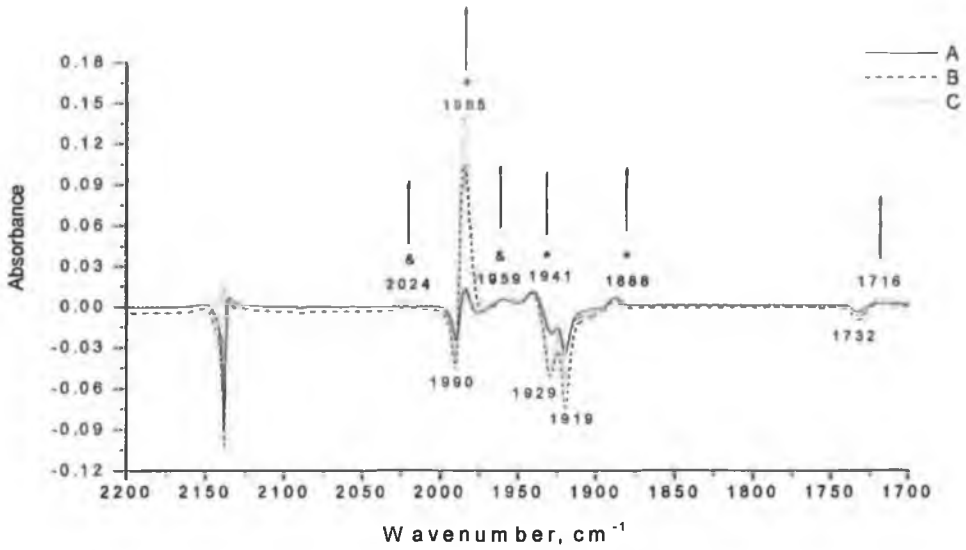

Fig. 3.38 Difference IR spectrum obtained following UV photolysis of (η^6-methylbenzoate)$Cr(CO)_3$ in 2% CO-methane matrix at 12 K, λ_{exc}>300 nm; (A) 30, (B) 120, (C) 150 min.. The bands labelled with *, &, and + are for (η^6-methylbenzoate)$Cr(CO)_2$, $Cr(CO)_5(\eta^1$-O-methylbenzoate), and $Cr(CO)_6$ respectively.

UV photolysis (λ_{exc} >300 nm) of (η^6-methylbenzoate)$Cr(CO)_3$ in 2 % CO-CH_4 or 5% CO-CH_4 matrix Fig. 3.38, resulted the formation of dicarbonyl species which is trapped by CO to form the tricarbonyl or by dinitrogen to form (η^6-methylbenzoate)$Cr(CO)_2N_2$, Fig. 3.39, and also the hexacarbonyl as indicated by the increase in the intensity of the peak at 1985 cm^{-1}.

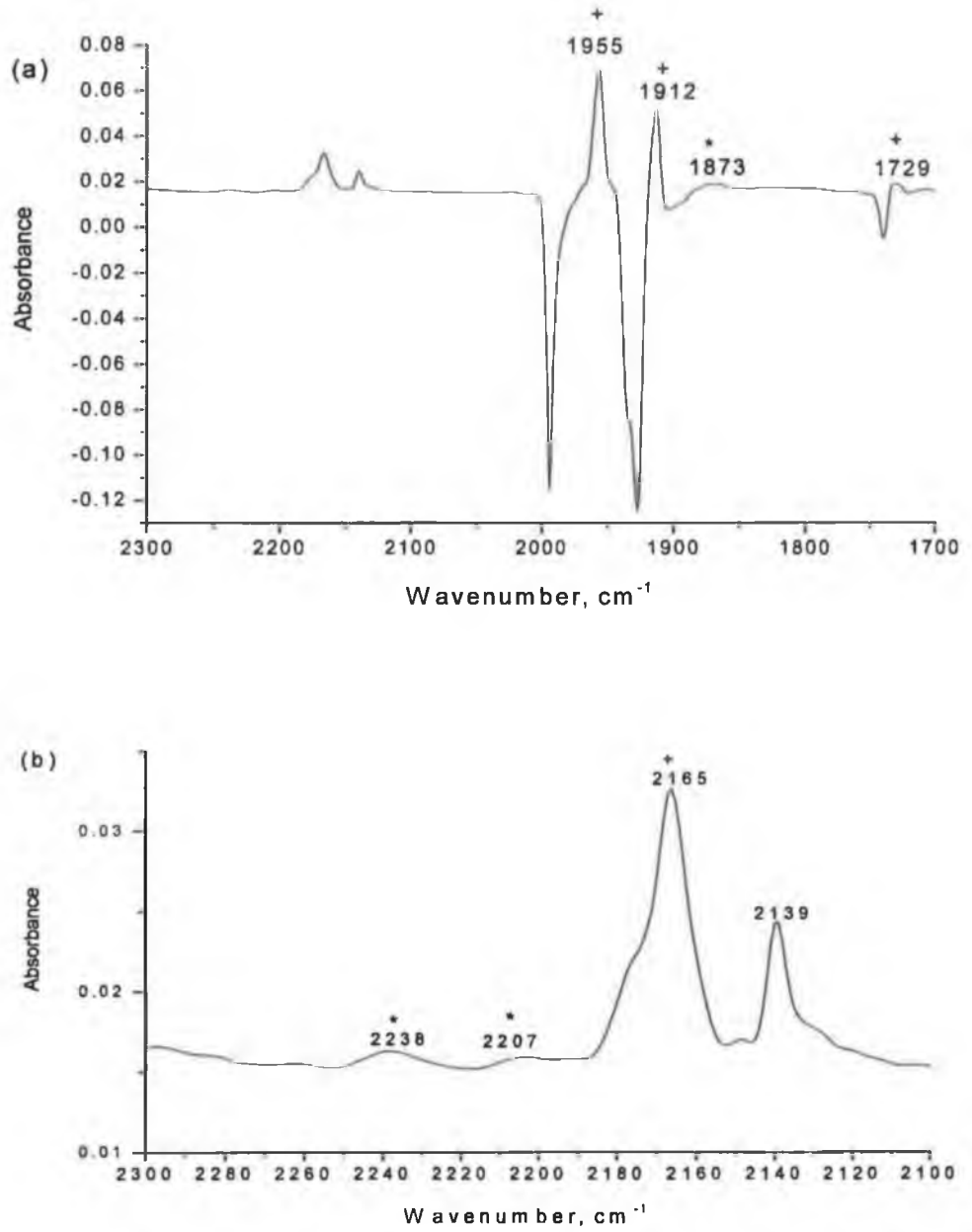

Fig. 3.39 (a) Difference IR spectrum obtained following UV photolysis of (η^6-methylbenzoate)$Cr(CO)_3$ in dinitrogen matrix at 12 K, λ_{exc}>300 nm; 150 min.(b) Expansion of the spectrum in the region 2300-2100 cm^{-1}. The bands labelled with (+) are for (η^6-methylbenzoate)$Cr(CO)_2(N_2)$complex, while the bands labelled with (*) are for the complex (η^6-methylbenzoate)$Cr(CO)(N_2)_2$. The band at 2139 cm^{-1} is free CO.

3.3 Discussion

The methodology used in these experiments was to start each experiment by using the lowest energy photolysis possible and increasing the energy of the irradiation in a stepwise fashion using the Hg lines of a Hg/Ar lamp and suitable interference filter. This involves the following wavelengths 436, 405, 365, 334, 313, and 297 nm. Subsequently, broadband irradiation with >410, >400, >320, >300 nm was used. The selection of the photolysis wavelengths depends on the UV/vis. spectrum of the sample. The photolysis times depend on obtaining a significant change in the IR spectrum of the matrix or until no further change in the spectrum is observed. Generally UV/vis spectra give little information about the products formed, so they are rarely considered in this discussion.

The matrix isolation photochemistry in CO-matrixes of (η^6-benzene)$Cr(CO)_3$ provides no information about a haptotropic shift reaction of the arene ring and results in the formation of $Cr(CO)_6$. The only products that can be detected in the 5% CO-methane matrix are the rotamer of (η^6-benzene)$Cr(CO)_3$, $Cr(CO)_6$ and the dicarbonyl species (η^6-benzene)$Cr(CO)_2$.

The photochemistry of substituted-arene complexes of the type (η^6-arene)$Cr(CO)_3$ provides more information about the haptotropic shift reaction to ultimately produce *fac*-$Cr(CO)_3$ or other CO rich moieties formed (in CO-methane matrixes). Thus many moieties can be detected in these matrixes especially in the case when the substituent is an electron-withdrawing group such as CHO or $COOCH_3$.

In these experiments evidence for two photochemical pathways in the excitation of (η^6-arene)$Cr(CO)_3$ have been obtained, one is the CO loss while the second is the haptotropic shift.

The CO-loss species (η^6-arene)$Cr(CO)_2$ coordinates to the matrix material to fill the coordination sphere even when the matrix is un-reactive like methane. The yield of the CO-loss species decreases upon increasing the concentration of CO in the matrix. In a dinitrogen matrix, the dinitrogen will trap the CO-loss species to form the dinitrogen adduct (η^6-arene)$Cr(CO)_2(N_2)$. Extending the photolysis to shorter wavelengths further CO ligand can be lost to form (η^6-arene)$Cr(CO)(N_2)_2$. To our knowledge there are no reports in the literature for the formation of these species.

The haptotropic shift of the arene from $\eta^6 \rightarrow \eta^4 \rightarrow \eta^2 \rightarrow \eta^1$ and finally loss of the arene to form *fac*-$Cr(CO)_3$ is detected. In CO-methane matrixes the ring slip intermediates can be trapped with CO to form the CO rich moieties such as cis-(η^1-arene)$Cr(CO)_4$, $Cr(CO)_5$(L) L= substituted arene, $Cr(CO)_5$, and $Cr(CO)_6$. Photolysis

of (η^6-methylbenzoate)$Cr(CO)_3$ in a dinitrogen matrix provided information on the nature of the ring slip intermediates. Thus the trapping of one of the ring slipped intermediates with N_2 formed *fac*-(η^1-O-methylbenzoate)$Cr(CO)_3(N_2)_2$.

A summary of the matrix isolation photochemistry of the complexes of the type (η^6-C_6H_5-X)$Cr(CO)_3$ is presented in Scheme 3.4. From these experiments it would appear that the two photochemical pathways (i.e. arene loss or CO loss) are wavelength dependent. Thus the arene loss is more efficient following long wavelength photolysis while the CO loss is more efficient for short wavelength photolysis.

The appearance of another rotation isomer (rotamer) in the matrix isolation studies of (η^6-C_6H_5-X)$Cr(CO)_3$ complexes upon photolysis with long wavelength (monochromatic or broad band) is not unexpected. The energy of even a long wavelength photon is higher than the rotational barrier for the rotation of the arene group around chromium to the centre of arene axis (Cr-arene).

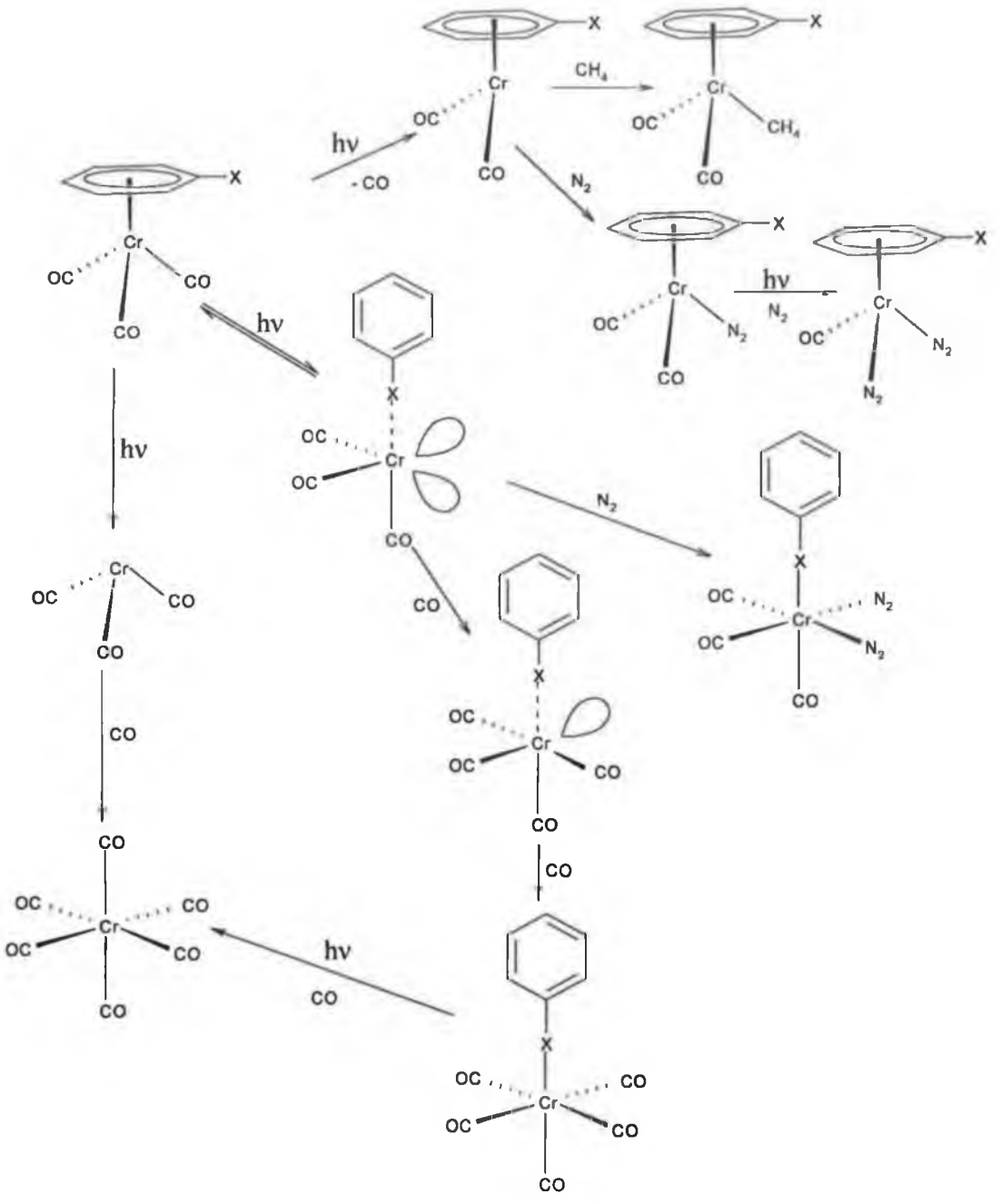

Scheme 3.4 the general schematic representation of the photochemical reactions of $(\eta^6\text{-}C_6H_5\text{-}X)Cr(CO)_3$ complexes. Some of the photoproducts have not observed in the matrix isolation experiments. Dinitrogen matrix was used in the case of the methylbenzoate complex only.

The photolysis of $(\eta^6\text{-}C_6H_6)Cr(CO)_3$ with visible broad-band light ($\lambda_{exc.}$>400 nm) results in the formation of new bands at 1982 and 1911 cm^{-1}, with the depletion of the parent bands at 1977 and 1906 cm^{-1}. As the difference between the new two bands (71 cm^{-1}) has the same value to the difference between the parent two bands, these new two bands were assigned to a rotamer. This rotamer is in eclipsed

conformation because the parent $(\eta^6\text{-}C_6H_6)Cr(CO)_3$ molecule at the matrix temperature tend to adopt the more stable staggered structure.

$$(\eta^6\text{-}C_6H_6)Cr(CO)_3 \xrightarrow{h\nu} (\eta^6\text{-}C_6H_6)Cr(CO)_2 + CO$$

$$(\eta^6\text{-}C_6H_6)Cr(CO)_3 + 3\ CO \xrightarrow{h\nu} Cr(CO)_6 + C_6H_6$$

A recent study by Brennan[22] on the quantum efficiency of arene exchange of benzene for CO to form $Cr(CO)_6$ in CO-saturated cyclohexane, has failed to detect such a reaction for the benzene complex, our matrix isolation experiments using short wavelength photolysis (λ_{exc} > 300 nm) of this complex in 5% CO-CH_4 matrix gave good evidence for the formation of $Cr(CO)_6$ as indicated by the grow-in of the band at 1984 cm^{-1}. Two important factors must be considered, firstly this molecule may show different behaviour under monochromatic irradiation than is observed under broad band photolysis (i.e. the photochemistry of $(\eta^6$-benzene$)Cr(CO)_3$ may involve multiphoton absorptions). Secondly the lifetime of the photointermediates in solution is significantly less than in a frozen matrix. This short lifetime produces reaction with added CO and cannot compete with an efficient back reaction.

The photolysis with >400 nm of the matrix isolated $(\eta^6$-aniline$)Cr(CO)_3$ in CO-methane matrix which had previously been irradiated using monochromatic irradiations produced $Cr(CO)_6$, while the irradiation of another sample which was not subjected to monochromatic irradiation failed to produce $Cr(CO)_6$. Thus it would appear that irradiation with monochromatic light produced a species such as *fac*-$Cr(CO)_3$ which upon reaction with CO under photolysis with > 400 nm finally produced $Cr(CO)_6$.

$$(\eta^6\text{-}C_6H_5\text{-}X)Cr(CO)_3 \xrightarrow{h\nu} \textit{fac}\text{-}Cr(CO)_3 + 3\ CO \longrightarrow Cr(CO)_6$$

Generally, the photolysis of $(\eta^6$-arene$)Cr(CO)_3$ in a pure CH_4 matrix which had been previously irradiated with 297 nm resulted in regeneration of the parent tricarbonyl species with depletion of the dicarbonyl species. Here we observed photolysis reaction of $(\eta^6$-arene$)Cr(CO)_2$ with CO to form the parent tricarbonyl complex. This is consistent with the laser flash photolysis study by Brennan[22] of these complexes in cyclohexane which found the formation of the band at 280 nm for the photogenerated transient $(\eta^6$-arene$)Cr(CO)_2$(cyclohexane) which thermally reacted with CO to form

the parent tricarbonyl complex. In the case of (η^6-aniline)$Cr(CO)_2$(cyclohexane) species, this also reacted with the parent tricarbonyl to form a dimeric species.[22] As the diffusion of the dicarbonyl species to the parent tricarbonyl species is not possible under the matrix conditions, the reaction with CO is the only pathway for the reaction of the dicarbonyl species (η^6-aniline)$Cr(CO)_2$ in the matrix.
Upon photolysis (η^6-benzaldehyde)$Cr(CO)_3$ with 297 nm, a slight change occurred with the formation of dicarbonyl species and *fac*-$Cr(CO)_3$ moiety. However this change was significantly reduced, with growth of the CO rich species bands when the concentration of CO in the matrix was increased.

Photolysis of complexes of the type (η^6-C_6H_5-X)$Cr(CO)_3$, X= NH_2, OCH_3, CHO, or $COOCH_3$ in a methane matrix produces the 12 electron coordinatively unsaturated *fac*-$Cr(CO)_3$ moiety with varying efficiency depending on the wavelength of the photolysis and the substituent on the benzene ring. Upon performing the experiment in various concentrations of CO in the methane matrix, the *fac*-$Cr(CO)_3$ bands gradually disappeared when the concentration of CO increased under the same conditions in the matrix. This was because the reaction of *fac*-$Cr(CO)_3$ with CO giving the hexacarbonyl complex and the other CO rich species is more efficient in the presence of higher concentrations of CO. A further species that was observed upon the photolysis of anisole and benzaldehyde complexes is the *fac*-(η^1-C_6H_5-X)$Cr(CO)_3$ species in which the oxygen atom coordination to the metal atom.

The presence of substituents on the arene results, in some instances, to a red shift in the low-lying absorption this allows the use of lower energy photolysis compared to the unsubstituted arene complexes. The photolysis of (η^6-benzaldehyde)$Cr(CO)_3$ with $\lambda_{exc.}$ = 436 nm forms another rotamer of (η^6-benzaldehyde)$Cr(CO)_3$, and a small amount of the CO loss product (η^6-benzaldehyde)$Cr(CO)_2$. So, the photolysis with this wavelength induced both arene and to a small extent CO loss. This excitation involves a mixture of both Cr-arene CT and Cr-CO CT transitions. This result is confirming by our DFT calculations, see chapter 5 for more details.
The photolysis of the benzaldehyde complex in methane matrix with long wavelength irradiation produced the tricarbonyl species *fac*-$Cr(CO)_3$ and *fac*-(η^1-O-benzaldehyde)$Cr(CO)_3$ which upon reaction with CO produced various CO-rich species such as cis-$Cr(CO)_4$, cis-(η^1-O-benzaldehyde)$Cr(CO)_4$, $Cr(CO)_5$, $Cr(CO)_5$(η^1-

O-benzaldehyde) and $Cr(CO)_6$. The appearance of one or more of these species depends on the wavelength, the concentration of CO in the matrix, the quantum efficiency, the time of the photolysis, and the stabilities of these photoproducts under the photolysis conditions.

In the absence of CO in the matrix the following reaction predominates

fac-$Cr(CO)_3$ + benzaldehyde $\longrightarrow$ *fac*-(η^1-O-benzaldehyde)$Cr(CO)_3$,

While the presence of CO in the matrix, follows the following processes.

fac-$Cr(CO)_3$ + CO $\longrightarrow$ $Cr(CO)_4 + Cr(CO)_5 + Cr(CO)_6$

fac-(η^1-O-benzaldehyde)$Cr(CO)_3$ + CO $\longrightarrow$ cis-(η^1-O-benzaldehyde)$Cr(CO)_4$ + $Cr(CO)_5$(η^1-O-benzaldehyde).

The matrix isolation of (η^6-methylbenzoate)$Cr(CO)_3$ in dinitrogen matrix resulted the coordinatively unsaturated moieties which trapped dinitrogen to form different N_2 complexes such as (η^6-methylbenzoate)$Cr(CO)_2(N_2)$, (η^6-methylbenzoate)$Cr(CO)(N_2)_2$, and the ring slip species (η^1-O-methylbenzoate)$Cr(CO)_3(N_2)_2$. The IR spectra were compared with those calculated using DFT methods to provide a correct assignment of the N-N stretching bands.

Successive loss of CO from (η^6-methylbenzoate)$Cr(CO)_3$ resulted in the two dinitrogen complexes, (η^6-methylbenzoate)$Cr(CO)_2(N_2)$, and (η^6-methylbenzoate)-$Cr(CO)_2(N_2)$ as shown below.

(η^6-methylbenzoate)$Cr(CO)_3$ $\xrightarrow[-CO]{N_2}$ (η^6-methylbenzoate)$Cr(CO)_2(N_2)$ $\xrightarrow[-CO]{N_2}$ (η^6-methylbenzoate)$Cr(CO)(N_2)_2$

The loss of two CO ligands and formation of (η^6-benzene)$Cr(CO)(N_2)_2$ was observed in the flash photolysis of (η^6-benzene)$Cr(CO)_3$ in dinitrogen gas is known in the literature [14]. Goff *et al.* [19] got this photoproduct (i.e. (η^6-benzene)$Cr(CO)(N_2)_2$) upon photolysis of (η^6-benzene)$Cr(CO)_3$ in polyethylene matrix under pressure of N_2 gas.

3.4 Conclusion

The matrix isolation studies of (C_6H_5-X)$Cr(CO)_3$ complexes, (X = H, NH_2, OCH_3, CHO, or COOMe) have been undertaken to provide information about how the electronic structure of these complexes can alter their photochemical behaviours

under the matrix conditions. The nature of the substituent on the benzene ring has been shown to affect the photochemical properties of their metal tricarbonyl complexes. Complexes with electron withdrawing substituents on the benzene ring seem to be more reactive than those with electron-donating substituents. Wavelength dependence has been found for the yields of both the CO loss and arene loss photoproducts. Different matrix gases have been used in these studies. Thus methane, dinitrogen, 2 %, 5%, or 10 % CO-methane mixtures have been used at 12 K. These studies revealed the light induced haptotropic shift of these complexes upon photolysis. The coordinatively unsaturated molecules produced are trapped with CO or N_2 to produce different photoproducts and to give indication if any of the bonding change in arene coordination mode.

3.5 References: -

1) a) Strohmeier, W.; Van Hobe, D.Z., *Z. Naturforsch., Teil B*, 1963,18, 981, b) Strohmeier, W.; Hellmann, H., *Z. Naturforsch.,Teil B*, 1963,18, 769.

2) a) Mahaffy, C.A.L.; Pausson, P.L., *J.Chem. Res.(S),* 1979,126.

b) Mahaffy, C.A.L.; Pausson, P.L., *J.Chem. Res.(M),* 1979,1752.

3) Zimmerman C.L.; Shaner S.L.; Roth S.A., Willeford B.R., *J.Chem. Res.(S*), 1980,108.

4) a) Wrighton, M, *Fortschr. Chem. Forsch.*, 65, 37,1976; b) *Chem. Rev.,* 1974, 74, 401.

5) Wrighton,M.S.; Haverty, J.L., *Z. Naturforsch.,* 1975, 30, 254.

6) Rest, A.J.; Sodeau, J. R.; Taylor, D. J. *J. Chem. Soc., Dalton Trans.*, 1978, 651.

7) Bitterwolf, E.B.; Lott, K.A.; Rest, A.J.; Mascetti, J. *J. Organomet. Chem.*, 1991, 419, 113.

8) Black J.D.; Boylan, M.J.; Braterman, P. S., *J. Chem. Soc., Dalton. Trans*, 1981, 673.

9) Gilbert, A.; Kelly, J.M.; Mbudzwait, M.; and Koerner von Gustorf, E.A., *Z. Naturforsch.,* 1976, B31, 1091.

10) McGrath I.M., *Ph.D. Thesis*, Dublin City University, 1993.

11) a) Creaven, B.S., *PhD Thesis*, Dublin City University, 1987, b) Creaven, B.S., George, M.W.; Ginzburg, A.G.; Hughes, C.; Kelly, J.M.; Long, C.; McGrath, I.M.; Ptyce, M.T., *Organometallics* 1993, 12, 3127.

12) Pryce, M. T., *PhD Thesis*, Dublin City University, 1994.

13) Trembovler, V.N.; Barenentskaya, N.K.; Fok, N.V.; Zaslavskaya, G.B.; Yavorskii, B.M.; Stekina, V.N., *J.Organomet. Chem.,* 1976,117, 339.

14) Zheng, Y; Wang, W.; Lin, J.; She, Y.; Fu, K.J., *J. Phys. Chem.*, 1992, 96, 9821.

15) Wang, W.;Jin, P.; Liu, Y., She,Y; Fu, K *Chinese Phys. Lett.*, 1991,491, 8, 9; Zheng, Y.,Wang, W.; Lin, Jingu; She, Y.; Fu, K., *J.Phys. Chem.* 1992, 96, 7650.

16) Traylor, T.G.; Stewart, K.J.; Goldberg, M.J., *J.Am. Chem. Soc.,* 1984,106, 4445.

17) Cohen, R.; Weitz, E.; Martin, J.M.L.; Ratner, M.A., *Organometallics,* 2004,23, 2315.

18) Jahr, H.C.; Nieger, M; Dötz, K.H., *Chem. Comm.*, 2003, 2866.

19) Goff, S.E.J.; Nolan, T.F.; George, M.W.; Poliakoff, M., *Organometallics*, 1998, 17, 2730.

20) Shaver, A.; Butler, I.S.; Eisenberg, A.; Gao, J.P.; Xu, H.Z.; Fong, B.; Uhm, H.; Klein, D., *Appl. Organomet. Chem.,* 1987, 383.

21) Breheny, C.J.; Draper, S.M.; Grevels, F.W.; Klotzbücher, W.E.; Long, C.; Pryce, M. T.; Russell, G., *Organometallics*, 1996, 15, 3679.

22) Brennan, P., *Ph.D. Thesis*, Dublin City University, 2003.

23) McKenna, J., *Ph.D. Thesis*, Dublin City University, 2003.

24) Boxhoorn, G.; Stufkens, J.; Oskam, A., *Inorg. Chim. Acta,* 1979, 33, 215.

25) Sellmann, D.; Muller, J. *J.Organomet. Chem.*, 1984, 277, 379.

26) George M.W.; Haward M.T.; Hameley P.A.; Hughes C.; Johnson F.P.A.; Pop V.K.; Polikoff, M., *J. Am. Chem. Soc.*, 1993,115, 2286.

Chapter 4

Matrix Isolation Experiments on Complexes of the Type (η^6-arene)$Mo(CO)_3$

Chapter 4

4.1 Literature Survey

4.1.1 The thermal chemistry of (η^6-arene)$Mo(CO)_3$ complexes: -

Thermochemical studies show that the benzene-Mo bond (284.512 $kJ.mol^{-1}$) in (η^6-benzene)$Mo(CO)_3$ is stronger than the benzene-Cr bond (221.752 $kJ.mol^{-1}$) in (η^6-benzene)$Cr(CO)_3$.[1] Kinetically, however, the situation is reversed. The metal-arene bond in (η^6-benzene)$Mo(CO)_3$ is far more labile than that of (η^6-benzene)$Cr(CO)_3$. This and the resulting difficulty in handling the Mo compounds have prevented their use in synthesis.[2]

It is well known that the molybdenum complexes of the type (η^6-arene)$Mo(CO)_3$ undergo efficient thermal substitution of the arene with donor ligands like arene, CO, phosphines, donor solvents like THF, acetone, or acetonitrile at room temperature, to afford complexes of the type (η^6-arene')$Mo(CO)_3$, $Mo(CO)_6$, $Mo(CO)_3(PR_3)_3$, $Mo(CO)_3D_3$ respectively, (D = Donor solvent).[3]

Recently the oxidative addition of the complex (η^6-toluene)$Mo(CO)_3$ to strong aromatic C-Cl bonds followed by migratory insertion of unsaturated organic compounds have been demonstrated. This reaction affords the seven-coordinate molybdenum(II) metallacycle.[4]

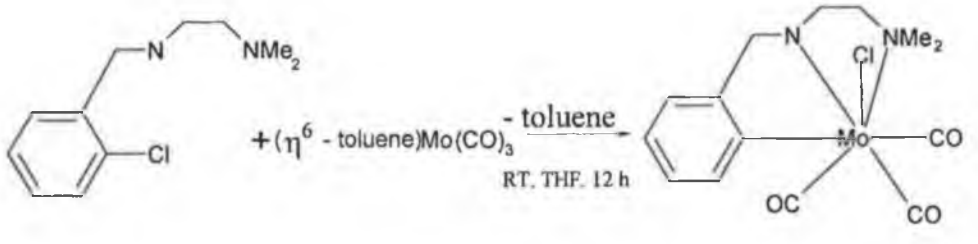

4.1.2 Photochemistry of (η^6-arene)$Mo(CO)_3$ complexes

The photolysis of (η^6-arene)$Mo(CO)_3$ complexes seems to give the CO-loss species as the primary photoproduct ((η^6-arene)$Mo(CO)_2$)[5]. This species most probably exists as a solvated intermediate. Thus the primary photochemical reaction of (η^6-1,3,5-mesitylene)$Mo(CO)_3$ can be summarized in equations 4.1, and 4.2 [6]: -

(η^6-1,3,5-mesitylene)$Mo(CO)_3$ $\xrightarrow{h\nu}$ (η^6-1,3,5-mesitylene)$Mo(CO)_2$ + CO 4.1

(η^6-1,3,5-mesitylene)$Mo(CO)_2$ $\xrightarrow{S}$ (η^6-1,3,5-mesitylene)$Mo(CO)_2$(S) 4.2

The shifts of the high and low frequency bands in the ν_{CO} region relative to parent ν_{CO} bands are similar for both chromium and molybdenum complexes. The difference between high and low frequency bands for both the tricarbonyl and dicarbonyl species is 58 and 38 cm^{-1} for the chromium system while for molybdenum the difference is 60 and 42 cm^{-1}.

Goff, *et al* [7] studied, the UV irradiation of $(\eta^6\text{-}C_6H_3Me_3)M(CO)_3$ (M = Cr, or Mo) in polyethylene matrix in the presence of N_2. Here the mono-, bis-, and tris-N_2 complexes, $(\eta^6\text{-}C_6H_3Me_3)M(CO)_{3-x}(N_2)_x$ were observed at room temperature. By contrast, irradiation of $(\eta^6\text{-}C_6H_3Me_3)M(CO)_3$ in polyethylene in the presence of H_2 only generated the mono-H_2 complexes $(\eta^6\text{-}C_6H_3Me_3)M(CO)_2(H_2)$.

4.2 Results: - The matrix isolation of (η^6-arene)Mo(CO)$_3$

The matrix isolation of (η^6-arene)Mo(CO)$_3$ complexes were performed in methane, 2% or 5% CO-methane, and/or dinitrogen matrixes. Fig 4.1 presents a representation of the parent tricarbonyl complex (1) and its photoproducts (2-12) in different matrixes.

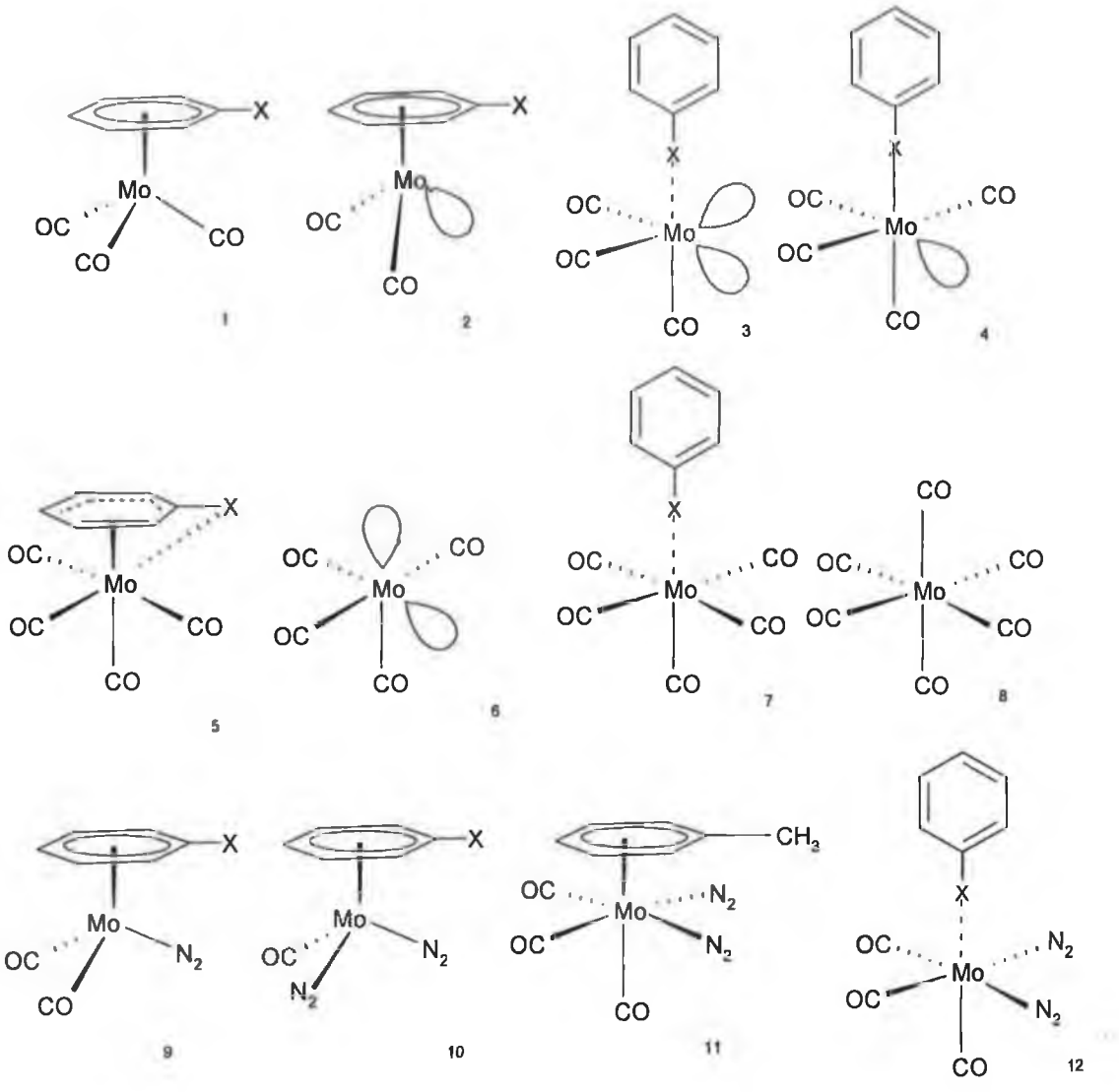

Fig. 4.1 Representation of structures of the parent tricarbonyl complex (1) and photoproducts (2-12) observed during these matrix isolation studies.

4.2.1 The matrix isolation photochemistry of (η^6-toluene)Mo(CO)$_3$: -

The IR spectroscopic data for (η^6-toluene)Mo(CO)$_3$ and all photoproducts obtained during these matrix isolation experiments are given in Table 4.1.

A sample of this complex was deposited in methane matrix at 20 K. The carbonyl stretching bands of the parent complex occur at 1980, 1972, 1907, and 1884 cm^{-1} in a methane matrix. The IR spectrum of (η^6-toluene)Mo(CO)$_3$ is given in Fig.4.2.

COMPLEX	ν_{CO} (cm^{-1})	ν_{N-N} (cm^{-1})	MATRIX
Deposition bands:			
(η^6-toluene)Mo(CO)$_3$	1980, 1972, 1907, 1884		CH_4
Photoproduct bands:			
Rotamer (η^6-toluene)Mo(CO)$_3$	1984, 1911		CH_4
Rotamer (η^6-toluene)Mo(CO)$_3$	1986, 1917		N_2
(η^6-toluene)Mo(CO)$_2$	1920, 1865		CH_4
(η^6-toluene)Mo(CO)$_2$(N_2)	1940, 1893	2153	N_2
(η^6-toluene)Mo(CO)(N_2)$_2$		2237,	N_2
fac-(η^2-toluene)Mo(CO)$_3$(N_2)$_2$		2210	N_2
Mo(CO)$_4$	2054, 1935, 1910	2252,	CO/CH_4
Mo(CO)$_6$	1984	2226	CO/CH_4

Table 4.1: Spectroscopic data for (η^6-toluene)Mo(CO)$_3$ and all its photoproducts obtained during the matrix experiments

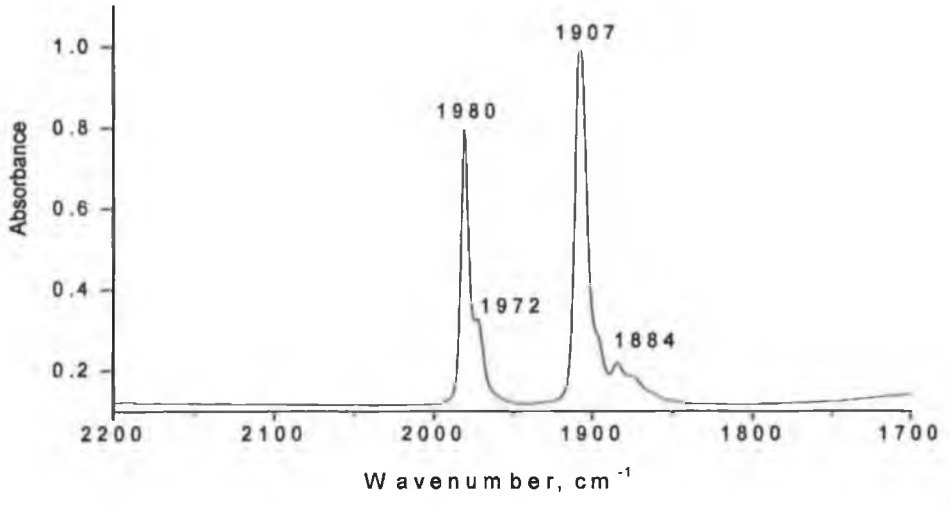

Fig 4.2 FTIR spectrum of (η^6-toluene)Mo(CO)$_3$ in a methane matrix at 12 K.

4.2.1.1 The matrix isolation photochemistry of (η^6-toluene)$Mo(CO)_3$ in Methane matrix: -

Visible photolysis of (η^6-toluene)$Mo(CO)_3$ in a methane matrix ($\lambda_{exc.}$ = 405 nm) results in the formation of new bands at 1984 and 1911 cm^{-1}, with a reduction in the parent bands at 1981 and 1907 cm^{-1}. Small features at 1920 and 1865 cm^{-1} in the IR spectrum were also observed The separation between the two bands at 1984 and 1911 cm^{-1} is similar to that of the parent peaks so these new bands have been assigned to a rotamer of (η^6-toluene)$Mo(CO)_3$. The bands at 1920, 1865 cm^{-1} with a grow-in of free CO features at 2137 cm^{-1}, which are close to those peaks observed for the complex (η^6-mesitylene)$Mo(CO)_2$ in methane matrix (1914, 1861 cm^{-1})[7], so they assigned to the dicarbonyl species (η^6-toluene)$Mo(CO)_2$, Fig 4.3.

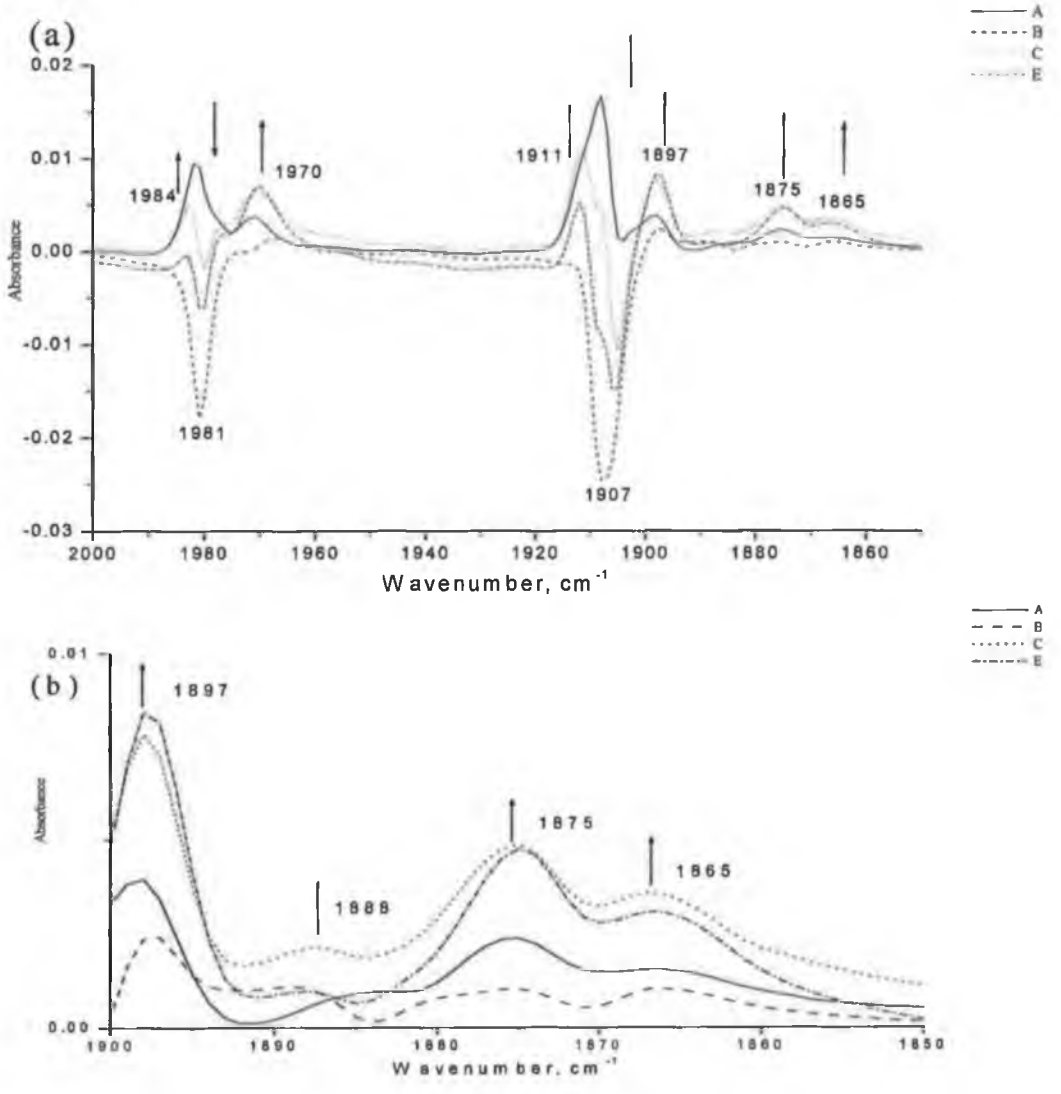

Fig 4.3 (a) IR difference spectrum of (η^6-toluene)$Mo(CO)_3$ in methane matrix at 12 K after photolysis with 405 nm for, A) 90 min, B) 150 min, C) 260 min, D) 320 min, (b) Expansion of the region at the range 1900-1850.

Photolysis of (η^6-toluene)$Mo(CO)_3$ in methane matrix at 12 K ($\lambda_{exc.}$ = 313 or 297 nm) results a grow-in of bands at 1920, 1865 cm^{-1} with free CO features at 2137 cm^{-1} these bands are assigned to (η^6-toluene)$Mo(CO)_2$. The band at 1837 cm^{-1} is assigned to ring slipped photoproduct (η^2-toluene)$Mo(CO)_3$, Fig 4.4.

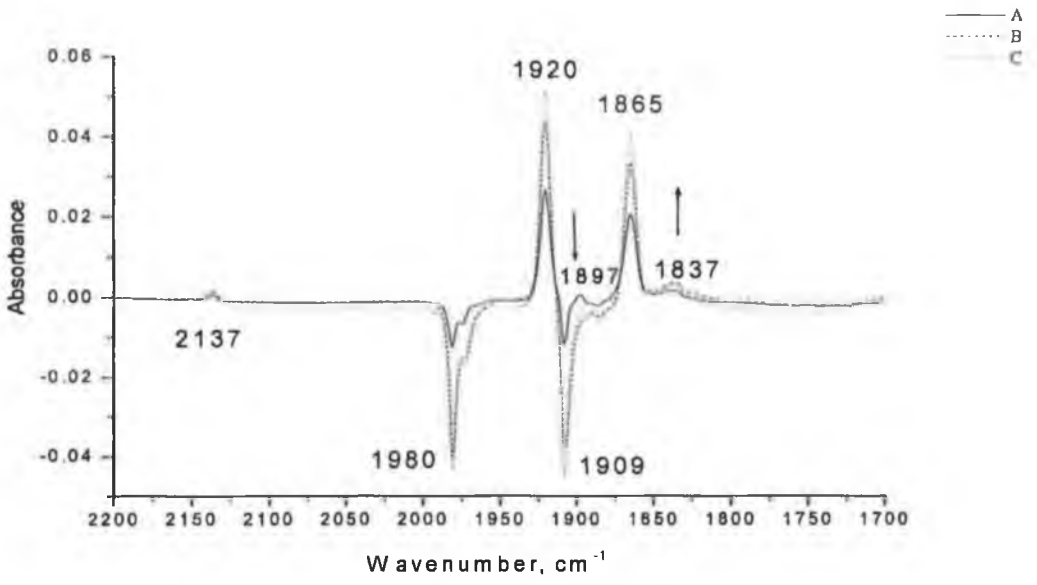

Fig 4.4 IR difference spectrum of (η^6-toluene)$Mo(CO)_3$ at 12 K after photolysis with 313 nm in methane matrix for, (A) 75 min, (B) 170 min, (C) 240 min.

The visible photolysis of (η^6-toluene)$Mo(CO)_3$ in CH_4 matrix at 12 K with $\lambda_{exc.}$ > 400 nm results in the formation of a new bands at 1976 and 1903 cm^{-1}, with a reduction in the parent bands at 1981 and 1907 cm^{-1} with small features at 1922 and 1867 cm^{-1} Fig 4.5. The separation between the two bands at 1984 and 1911 cm^{-1} is similar to that of the parent peaks so these bands have been assigned to a rotamer of (η^6-toluene)$Mo(CO)_3$.

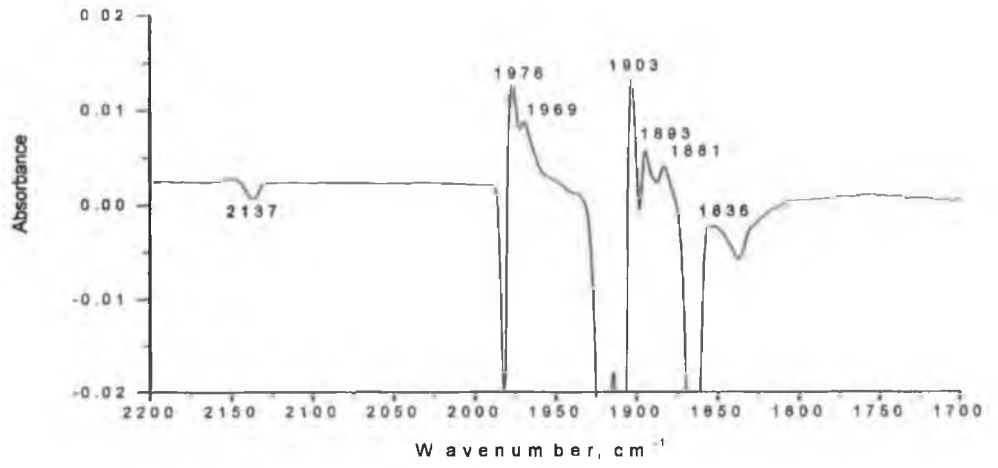

Fig 4.5 IR difference spectrum of (η^6-toluene)Mo(CO)$_3$ at 12 K after photolysis with ($\lambda_{exc.}$ > 400 nm) at 12 K in methane matrix for 100 min.

Subsequent photolysis with UV irradiation $\lambda_{exc.}$ > 300 nm of methane matrix resulted depletion of the parent tricarbonyl peaks at 1980, and 1908 cm^{-1} with the formation of dicarbonyl species (η^6-toluene)Mo(CO)$_2$ as assigned by the bands at 1920, 1865 cm^{-1} and a grow-in of free CO features at 2137 cm^{-1}, Fig 4.6.

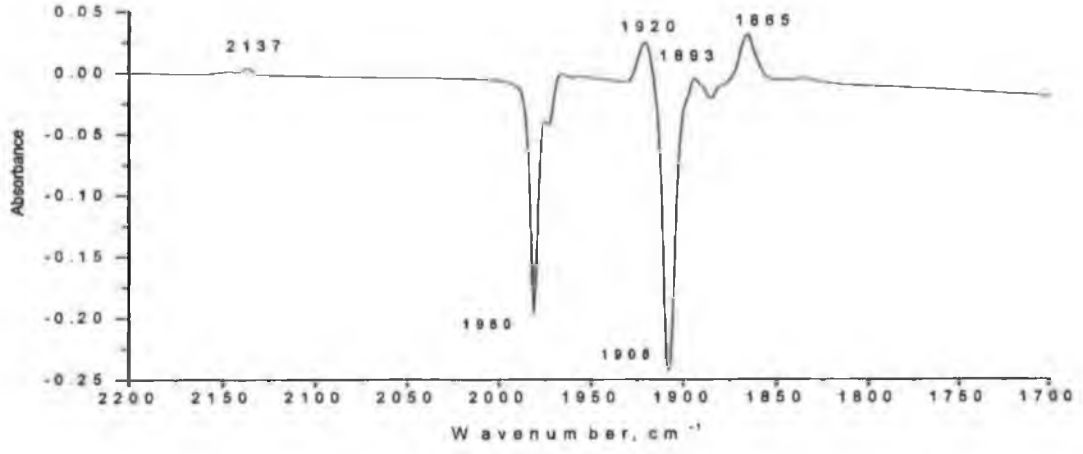

Fig 4.6 IR difference spectrum of (η^6-toluene)Mo(CO)$_3$ at 12 K after photolysis with ($\lambda_{exc.}$ > 300 nm) in methane matrix for 90 min,

4.2.1.2 The matrix isolation photochemistry of (η^6-toluene)$Mo(CO)_3$ in N_2 matrix: -

In a N_2 matrix the grow-in of the parent peaks was observed upon photolysis with 405 nm.

The photolysis (η^6-toluene)$Mo(CO)_3$ in N_2 matrix at 12 K with 313 nm produced the the dicarbonyl species (η^6-toluene)$Mo(CO)_2(N_2)$ at 1940, 1893 cm^{-1}. The bands at, 2210 and 2180 cm^{-1} which were close to that observed for (η^1-pyridine)$Cr(CO)_3(N_2)_2$ [9] and the spectral separation is 30 cm^{-1} is close to that observed for the later (33 cm^{-1}). Hence we assigned these bands to ν_{N-N} of the cis-coordinated N_2 ligands in (η^2-toluene)$Mo(CO)_3(N_2)_2$. In addition to these bands another band observed at 2237 cm^{-1} which close to that observed for (η^6-methylbenzoate)$Cr(CO)(N_2)_2$ (2211, 2238 cm^{-1}), (Chapter 3) so these bands can be assigned to (η^6-toluene)$Mo(CO)(N_2)_2$, while the other band should be obscured by the band at 2210 cm^{-1}, Fig 4.7.

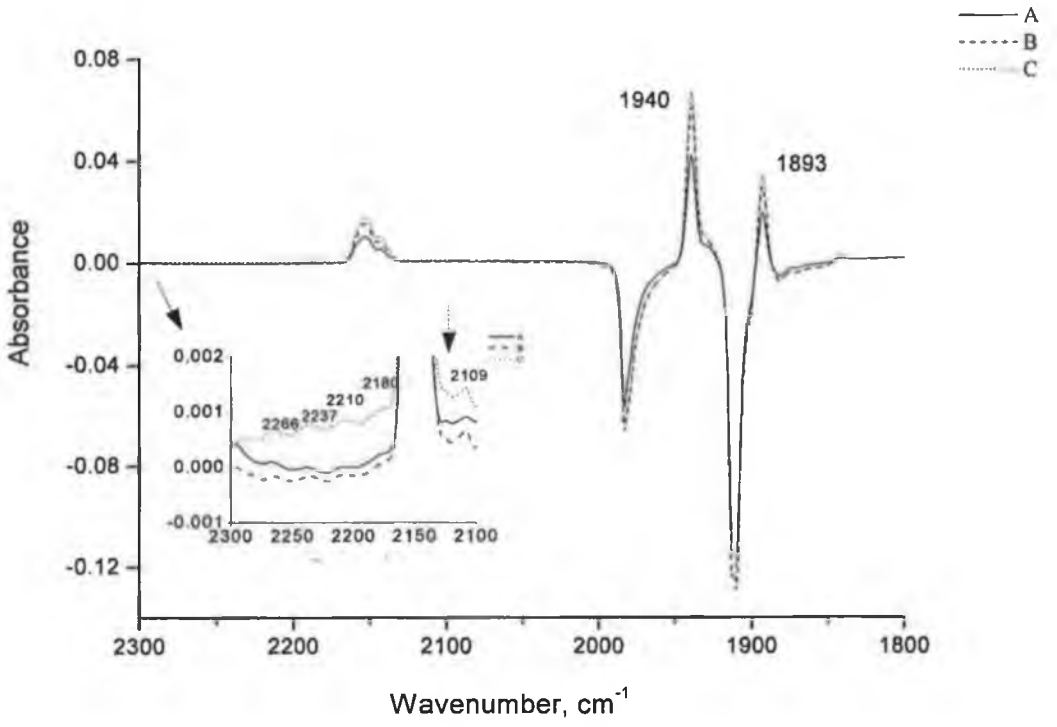

Fig 4.7 IR difference spectrum of (η^6-toluene)$Mo(CO)_3$ at 12 K after photolysis with 313 nm in dinitrogen matrix for (A) 75 min, (B) 170 min, (C) 200 min.

Further visible photolysis of this matrix with $\lambda_{exc.} > 400$ nm results in the regeneration of the parent bands at 1984, 1910 cm^{-1} Fig 4.8. Extending the photolysis

time results in depletion of these bands with grow-in of small bands at 1987, 1916 cm^{-1} a rotamer of $(\eta^6$-toluene$)Mo(CO)_3$.

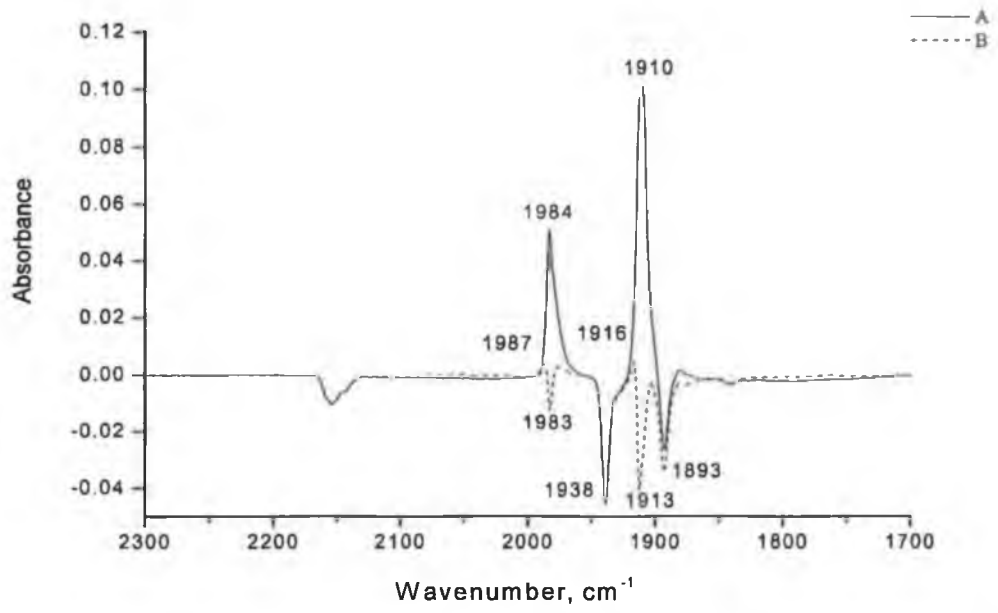

Fig 4.8 IR difference spectrum of $(\eta^6$-toluene$)Mo(CO)_3$ at 12 K after photolysis with ($\lambda_{exc.} > 400$ nm) at 12 K in dinitrogen matrix for A) 50 min, B) 100 min.

The photolysis with > 300 nm in N_2 matrix produced the dicarbonyl species at 1938, 1893, and 2153 cm^{-1} while the weak features at 2252, 2226 (ν_{N-N}), and 1764 cm^{-1} (ν_{CO}) were assigned to the ring slip photoproduct $(\eta^2$-toluene$)Mo(CO)_3(N_2)_2$. The bands at 1986, 1917 cm^{-1} were assigned to another rotamer of the parent tricarbonyl complex, Fig 4.9.

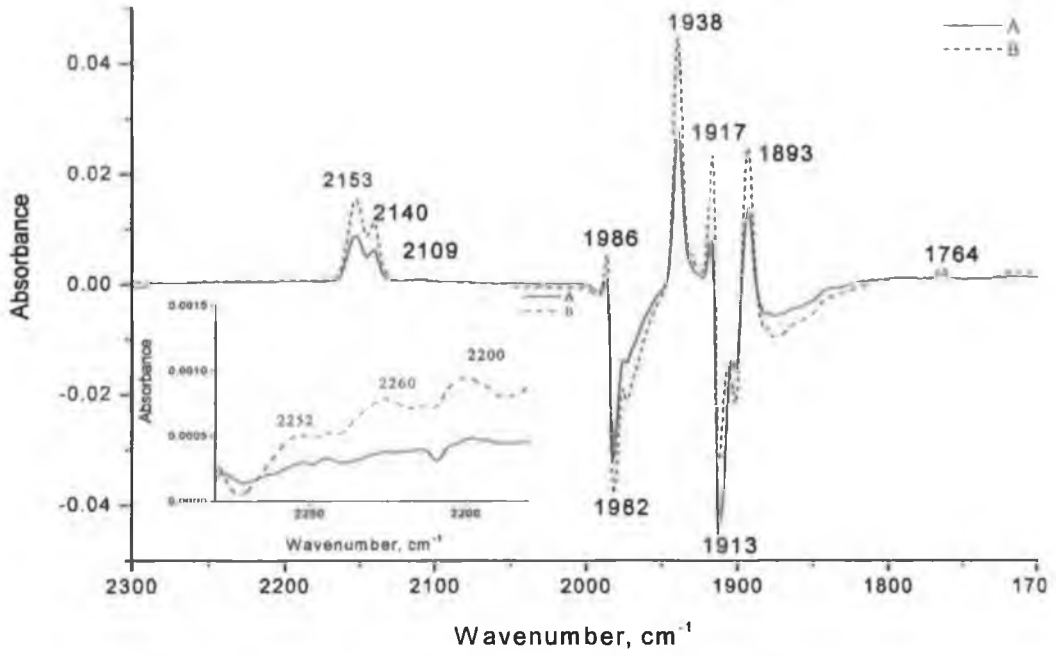

Fig 4.9 IR difference spectrum of (η^6-toluene)$Mo(CO)_3$ at 12 K after photolysis with ($\lambda_{exc.}$ > 300 nm) in dinitrogen matrix for (A) 30 min, (B) 90 min.

4.2.1.3 The matrix isolation photochemistry of (η^6-toluene)$Mo(CO)_3$ in 5% CO/CH_4 matrix: -

In a 5 % $CO\text{-}CH_4$ matrix the depletion of the parent peaks was observed upon subsequent photolysis with 405 nm without appearance of any new bands.

In addition to the formation of dicarbonyl species (1919, 1863 cm^{-1}), the photolysis with 313 nm of (η^6-toluene)$Mo(CO)_3$ in 5% CO matrix resulted in the formation of a tetracarbonyl $Mo(CO)_4$ species with low yield as indicated by the grow-in of the bands at 2054, 1935, 1910 cm^{-1}(literature 2057, 1949, 1945, 1927, 1887 cm^{-1}). The remaining peaks are obscured by the parent peaks. The appearance of the peak at 1981 cm^{-1} was assigned to the molybdenumhexacarbonyl, Fig.4.10.

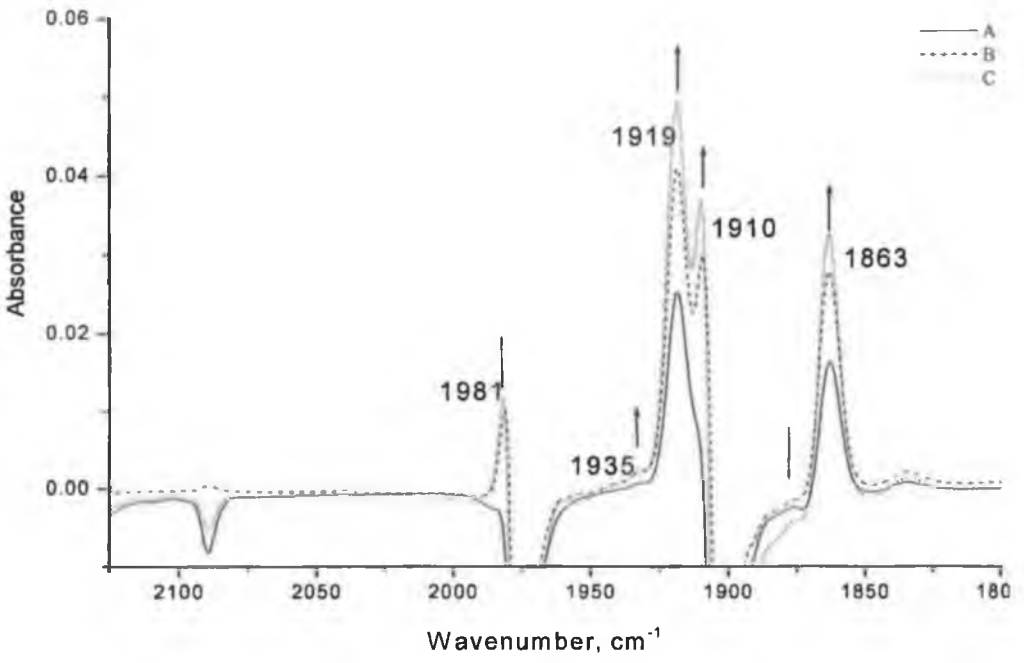

Fig 4.10 IR difference spectrum of (η^6-toluene)$Mo(CO)_3$ at 12 K after photolysis with 313 nm in 5% CO-CH_4 matrix for (A) 75 min, (B) 170 min, (C) 260 min.

The photolysis of (η^6-toluene)$Mo(CO)_3$ in 5% CO-CH_4 matrix with $\lambda_{exc.}$ = 297 nm resulted in regeneration of the parent bands along with the (η^6-toluene)$Mo(CO)_2$ species as indicated by the grow-in of the bands at 1922, 1867 cm^{-1}, Fig. 4.11.

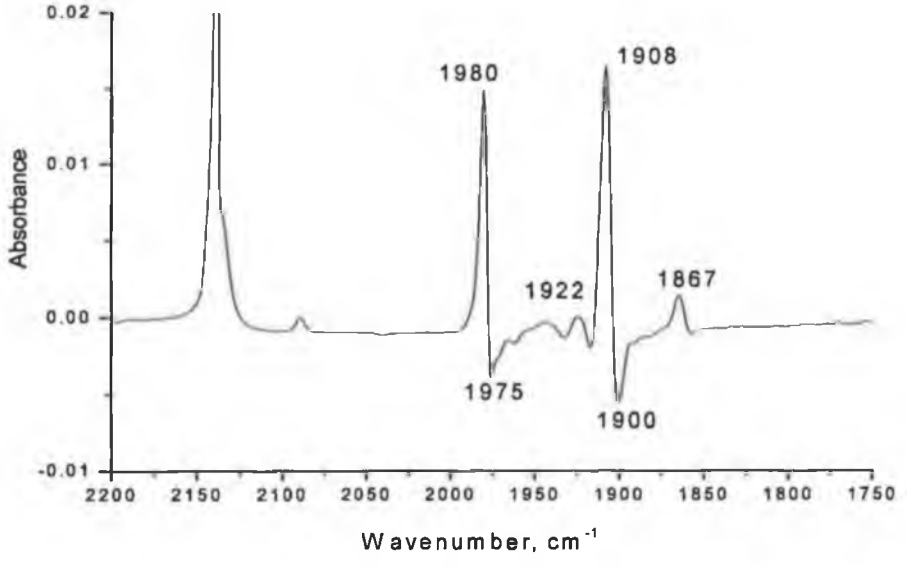

Fig 4.11 IR difference spectrum of (η^6-toluene)$Mo(CO)_3$ in 5% CO-CH_4 matrix at 12 K after monochromatic photolysis with 297 nm for 105 min.

The photolysis with $\lambda_{exc.} > 400$ nm of (η^6-toluene)$Mo(CO)_3$ in 5% CO matrix results in regeneration of the parent tricarbonyl species with the formation of the molybdenumhexacarbonyl as assigned by the grow-in of the band at 1981 cm^{-1} and weak features at 2020, and 1954 cm^{-1} which assigned to the coordinatively unsaturated tetracarbonyl photoproduct (η^2-toluene)$Mo(CO)_4$, Fig 4.12.

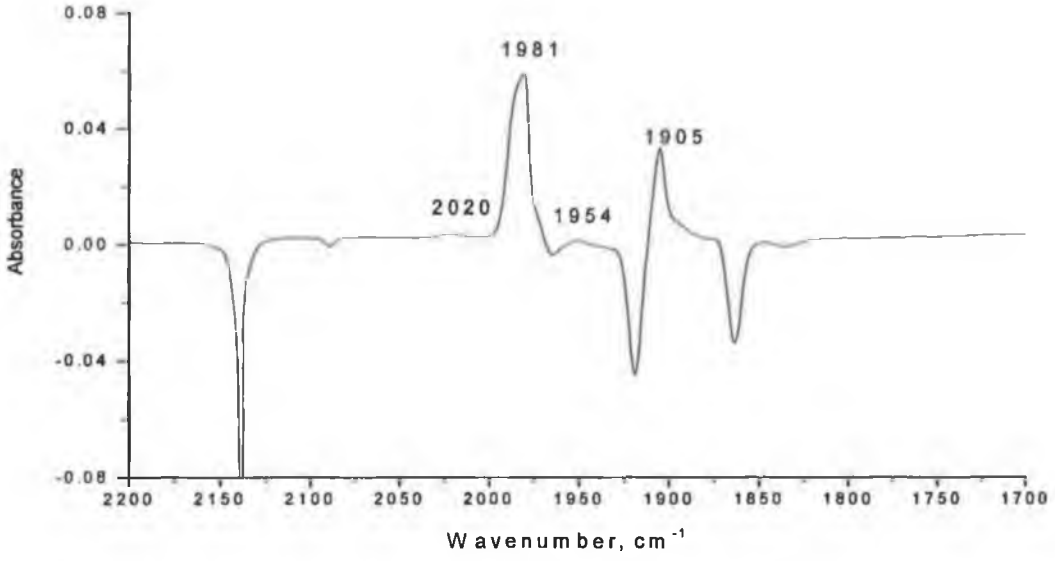

Fig 4.12 IR difference spectrum of a matrix originally containing (η^6-toluene)$Mo(CO)_3$ at 12 K after photolysis with ($\lambda_{exc.} > 400$ nm) in 5% CO-CH_4 matrix for 100 min.

In addition to the formation of dicarbonyl species (1920, 1863 cm^{-1}), the photolysis of (η^6-toluene)$Mo(CO)_3$ ($\lambda_{exc.} > 300$ nm) in 5% CO matrix results in the formation of the band at 1985 cm^{-1} which assigned to the molybdenumhexacarbonyl, Fig.4.13 and weak features at 2020, and 1954 cm^{-1} which assigned to the coordinatively unsaturated tetracarbonyl photoproduct (η^2-toluene)$Mo(CO)_4$.

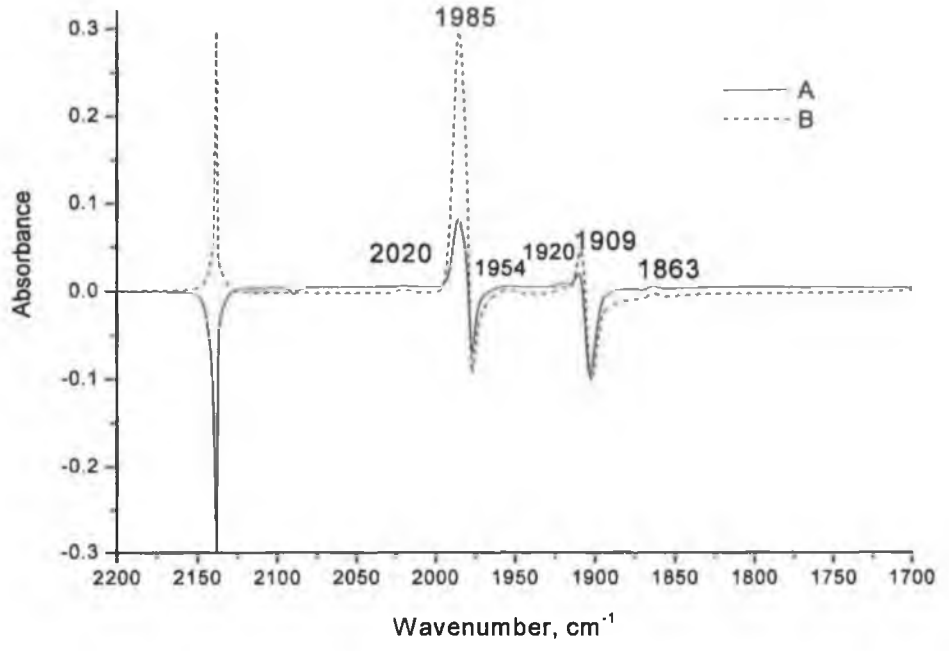

Fig 4.13 IR difference spectrum of (η^6-toluene)$Mo(CO)_3$ at 12 K after photolysis with ($\lambda_{exc.}$ > 300 nm) in 5% CO-CH_4 matrix for (A) 30 min, (B) 125 min.

4.2.2 The matrix isolation photochemistry of (η^6-anisole)$Mo(CO)_3$: -

The IR spectroscopic data for (η^6-anisole)$Mo(CO)_3$ and all photoproducts obtained during these matrix isolation experiments are given in Table 4.2.

A sample of this complex was deposited in methane matrix at 20 K. The metal carbonyl stretching frequencies of the parent complex occur at 1979, 1902, and 1877 cm^{-1} in methane matrix (the presence of the band at 1877 cm^{-1} may caused by the another isomer of this complex). The IR spectrum of (η^6-anisole)$Mo(CO)_3$ are given in Fig.4.14.

COMPLEX	ν_{CO} (cm^{-1})	ν_{N-N} (cm^{-1})	MATRIX
Deposition bands:			
(η^6-anisole)$Mo(CO)_3$	1979, 1902, 1877		CH_4
Photoproduct bands:			
Rotamer (η^6-anisole)$Mo(CO)_3$	1911, 1896		CH_4
Rotamer (η^6-anisole)$Mo(CO)_3$	1986, 1917		N_2
Rotamer (η^6-anisole)$Mo(CO)_3$	1979, 1907, 1893		5% CO/CH_4
(η^6-anisole)$Mo(CO)_2$	1919, 1862		CH_4
(η^6-anisole)$Mo(CO)_2(N_2)$	1940, 1893	2140	N_2
(η^6-anisole)$Mo(CO)(N_2)_2$	1980	2236, 2251	N_2
$Mo(CO)_4$	2052, 1932		5% CO/CH_4
cis-(η^1-O-anisole)$Mo(CO)_4$	2040		5% CO/CH_4
(η^2-anisole)$Mo(CO)_4$	2022, 1954		5% CO/CH_4
fac.-(η^1-O-anisole)$Mo(CO)_3$	2023, 2016		5% CO/CH_4
(η^1-O-anisole)$Mo(CO)_3(N_2)_2$	1795,1762	2221, 2253	CH_4
$Mo(CO)_6$	1984		N_2
			5% CO/CH_4

Table 4.2: Spectroscopic data for (η^6-anisole)$Mo(CO)_3$ and all its photoproducts.

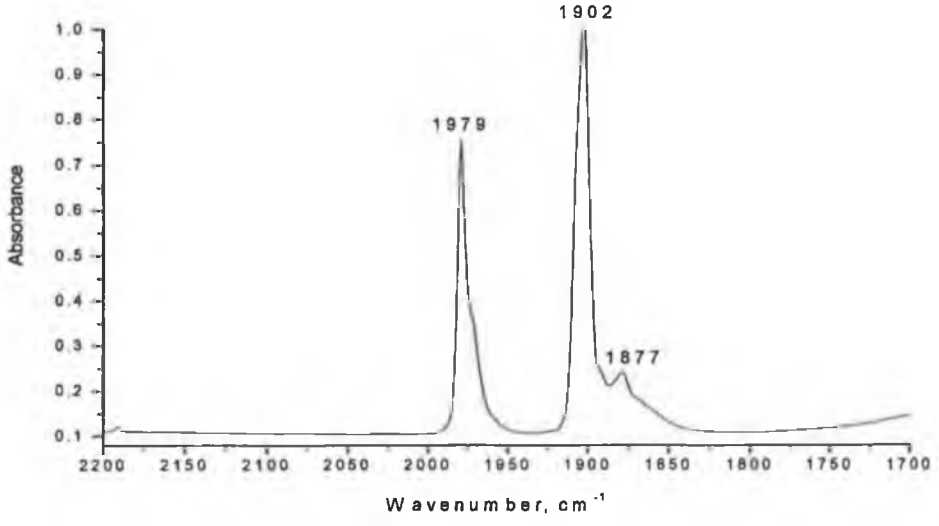

Fig 4.14 FTIR of (η^6-anisole)$Mo(CO)_3$ in methane matrix at 12 K.

4.2.2.1 The matrix isolation photochemistry of (η^6-anisole)Mo(CO)$_3$ in methane matrix: -

The photolysis of (η^6-anisole)Mo(CO)$_3$ in CH_4 matrix at 12 K with $\lambda_{exc.}$ = 436 or 365 nm results in the formation of a new bands at 1982, 1911 and 1896 cm^{-1}, with a depletion of the parent bands at 1978 and 1903 cm^{-1}, Fig 4.15. The bands at 1982, 1911, and 1896 cm^{-1} are assigned to another rotamer of (η^6-anisole)Mo(CO)$_3$.

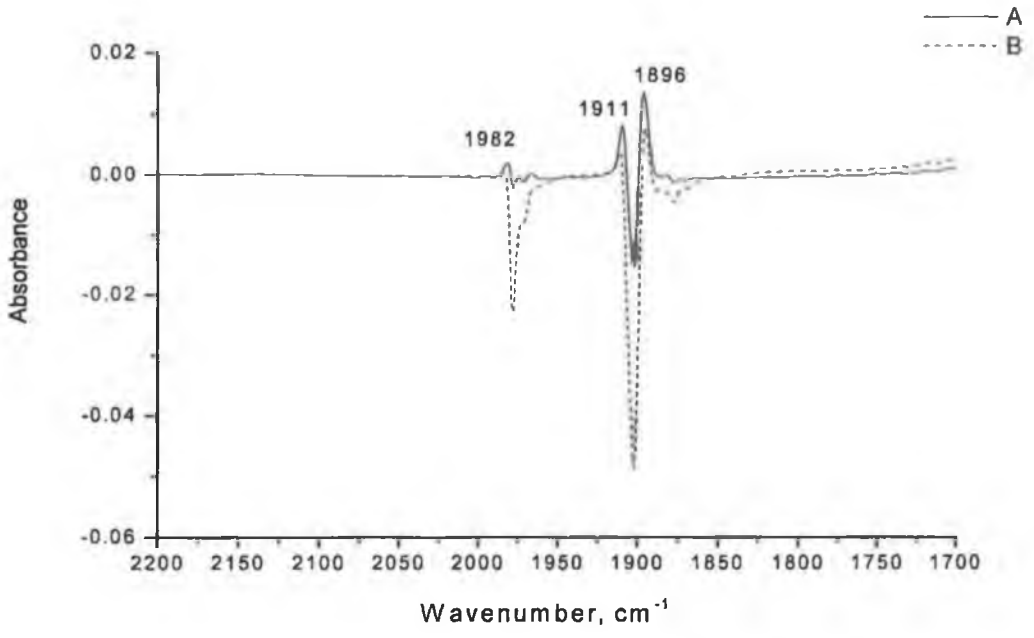

Fig 4.15 IR difference spectrum of (η^6-anisole)Mo(CO)$_3$ in CH_4 matrix at 12 K after photolysis with 365 nm for A) 90 min B) 200 min.

UV photolysis of (η^6-anisole)Mo(CO)$_3$ in CH_4 matrix at 12 K with $\lambda_{exc.}$ = 334 nm results in a depletion of the bands of the parent with concomitant formation of two bands at 1919 and 1862 cm^{-1}, Fig 4.16.

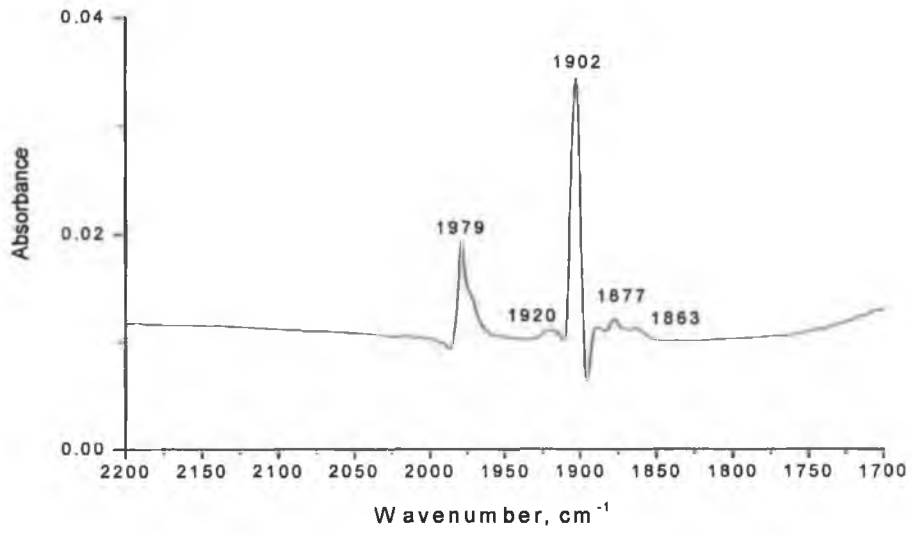

Fig 4.16 IR difference spectrum of (η^6-anisole)Mo(CO)$_3$ in CH_4 matrix at 12 K after photolysis with 334 nm for 285 min.

Subsequent UV photolysis of (η^6-anisole)Mo(CO)$_3$ in CH_4 matrix at 12 K with $\lambda_{exc.}$ = 313 or 297 nm results in a depletion of the parent bands with concomitant formation of two bands at 1919 and 1862 cm^{-1}, Fig 4.17 and assigned to the CO loss product, (η^6-anisole)Mo(CO)$_2$, for two reasons. Firstly free CO is observed in the matrix, at 2138 cm^{-1}. Secondly, spectral separation between the two peaks (57 cm^{-1}) is close to that observed for (η^6-benzene)Cr(CO)$_2$ (56 cm^{-1}).

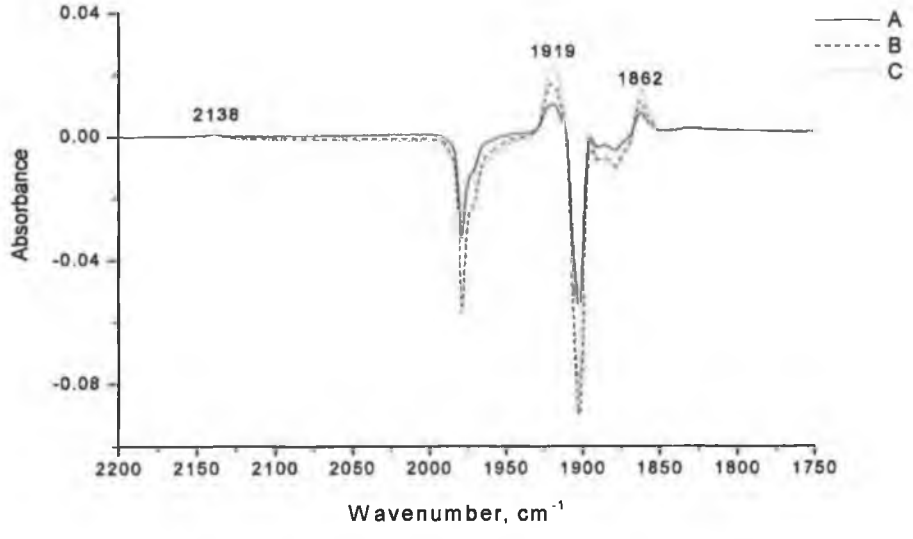

Fig 4.17 IR difference spectrum of (η^6-anisole)Mo(CO)$_3$ in CH_4 matrix at 12 K after photolysis with 313 nm for A) 75, B) 200 min C) 320 min.

The visible photolysis of (η^6-anisole)$Mo(CO)_3$ in CH_4 matrix at 12 K with $\lambda_{exc} > 400$ nm resulted in the regeneration of the parent bands at 1979, 1902 and 1877 cm^{-1}, and a depletion of the dicarbonyl bands at 1920 and 1863 cm^{-1}. New weak band at 1888 cm^{-1} in the IR spectrum were observed Fig 4.18 and assigned to (η^1-O-anisole)$Mo(CO)_3$.

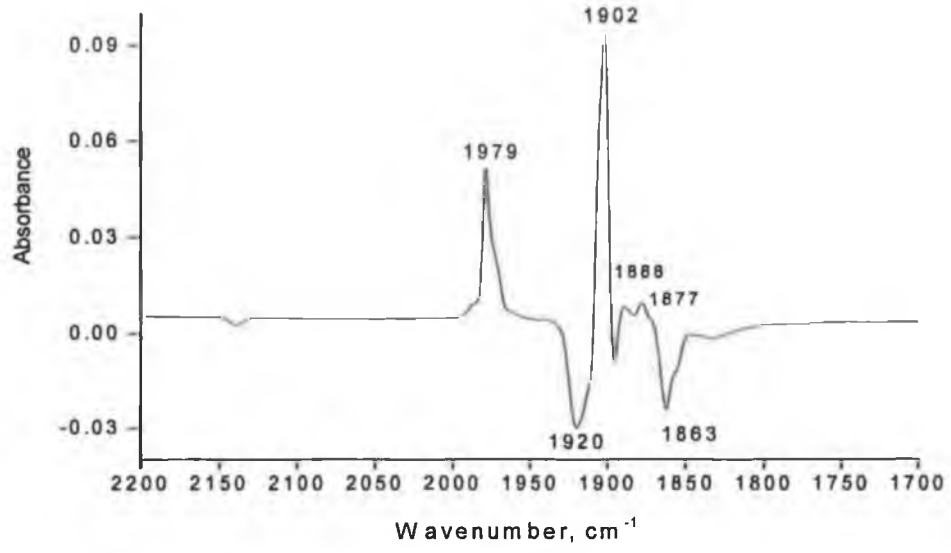

Fig 4.18 IR difference spectrum of (η^6-anisole)$Mo(CO)_3$ in CH_4 matrix at 12 K after photolysis with > 400 nm for 130 min.

Subsequent photolysis with UV irradiation $\lambda_{exc.} > 300$ nm of methane matrix containing (η^6-anisole)$Mo(CO)_3$ results in a depletion of the parent tricarbonyl peaks with grow-in of the bands at 1922 and 1863 cm^{-1} for the dicarbonyl species (η^6-anisole)$Mo(CO)_2$ in addition to free CO features at 2137 cm^{-1}, Fig 4.19.

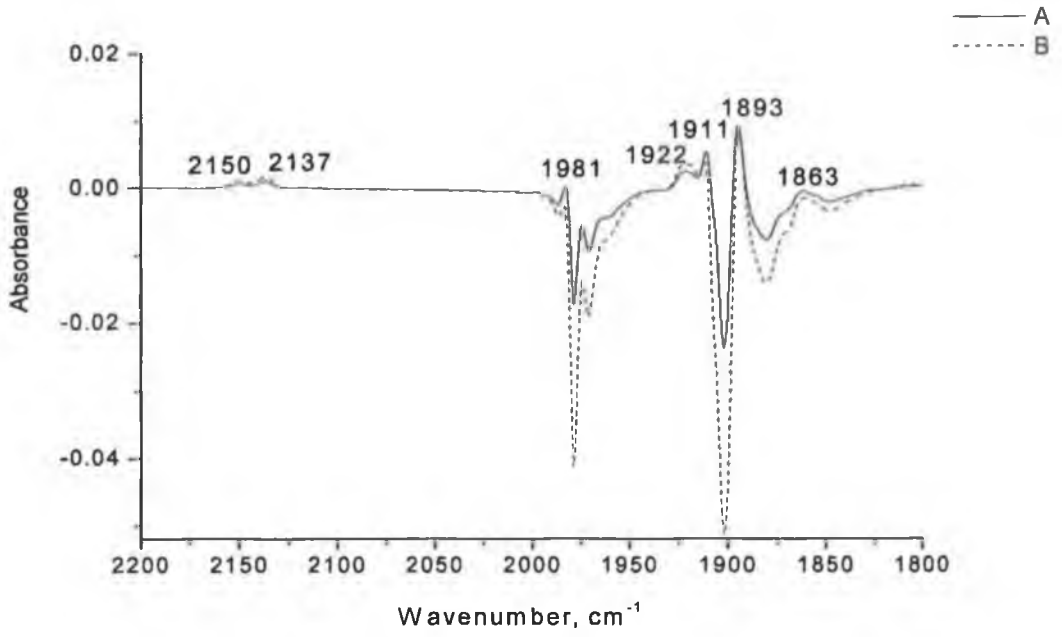

Fig 4.19 IR difference spectrum of (η^6-anisole)Mo(CO)$_3$ in CH_4 matrix at 12 K after photolysis with > 300 nm for A) 40 min, B) 120 min.

4.2.2.2 The matrix isolation photochemistry of (η^6-anisole)Mo(CO)$_3$ in N_2 matrix: -

Photolysis with visible irradiation ($\lambda_{exc.}$ = 436 nm) of (η^6-anisole)Mo(CO)$_3$ in a N_2 resulted a grow-in of the bands at 1981, 1910, 1900 cm^{-1} with depletion of the parent bands, Fig 4.20. The bands at 1981, 1910, 1900 cm^{-1} are assigned to another rotamer.

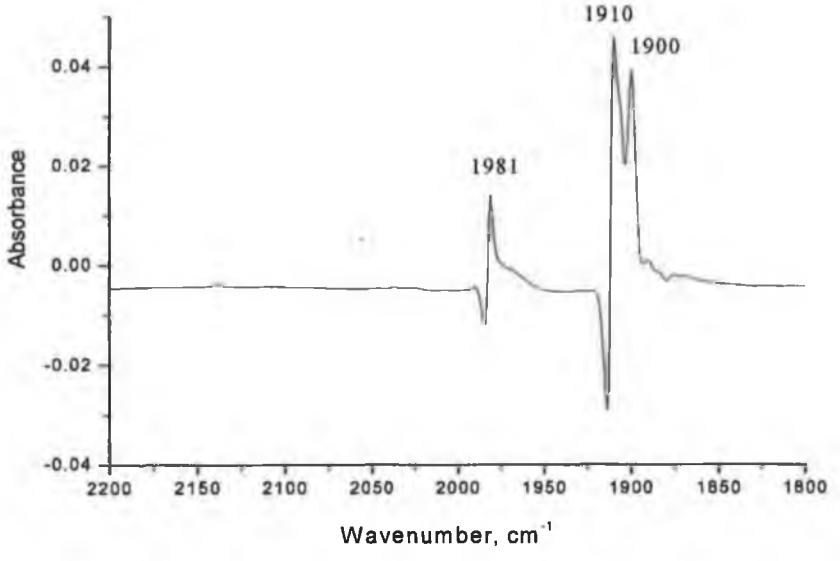

Fig 4.20 IR difference spectrum of (η^6-anisole)Mo(CO)$_3$ at 12 K after photolysis with 436 nm in N_2 matrix for 220 min.

Subsequent visible photolysis of this sample with $\lambda_{exc.}$ = 405 nm resulted in the formation of new bands at 1982, 1911 and 1904 cm^{-1}, with a depletion of the parent bands Fig 4.21, and these are assigned to another rotamer of (η^6-anisole)$Mo(CO)_3$. The shoulder at 1890 cm^{-1} can be assigned to be one of the dicarbonyl species (η^6-anisole)$Mo(CO)_2(N_2)$ bands with the free CO band at 2140 cm^{-1}.

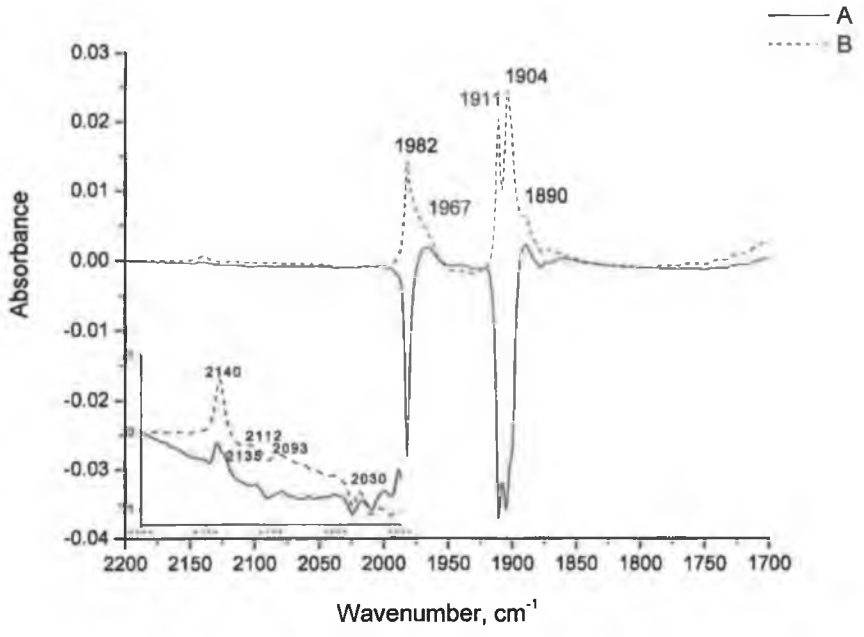

Fig 4.21 IR difference spectrum of (η^6-anisole)$Mo(CO)_3$ in N_2 matrix at 12 K after photolysis with 405 nm for (A) 180 min., (B) 240 min.

Subsequent photolysis of (η^6-anisole)$Mo(CO)_3$ in a N_2 matrix at 12 K with $\lambda_{exc.}$ = 365 nm resulted in the formation of new bands at 1937 and 1890 cm^{-1}, with a depletion of the parent bands Fig 4.22, and these were assigned to the dicarbonyl species (η^6-anisole)$Mo(CO)_2$ supported by the appearance of the free CO band at 2140 cm^{-1}.

Subsequent visible photolysis of this sample in a N_2 matrix at 12 K with $\lambda_{exc.}$ = 334 nm resulted in the grow-in of the bands at 1982, 1911 and 1904 cm^{-1}, Fig 4.23, and these bands were assigned to another rotamer of (η^6-anisole)$Mo(CO)_3$

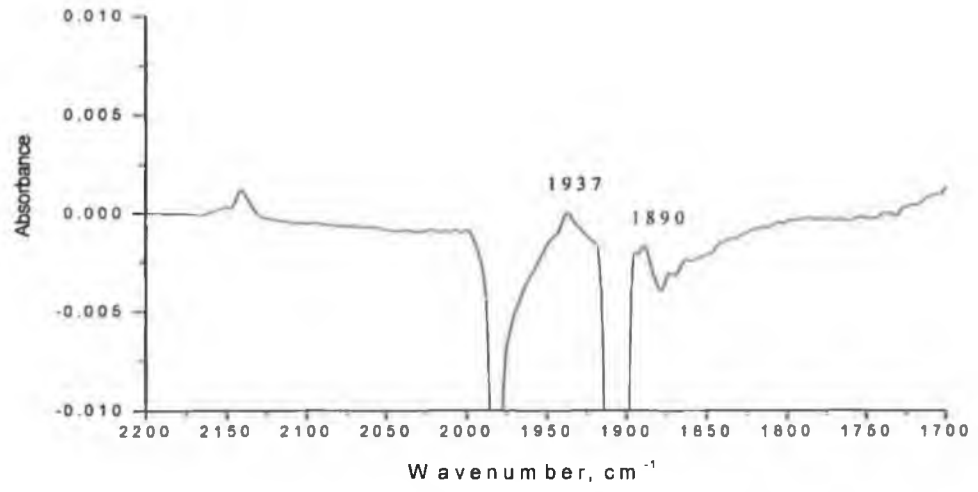

Fig 4.22 IR difference spectrum of (η^6-anisole)Mo(CO)$_3$ in N_2 matrix at 12 K after photolysis with 365 nm for 220 min.

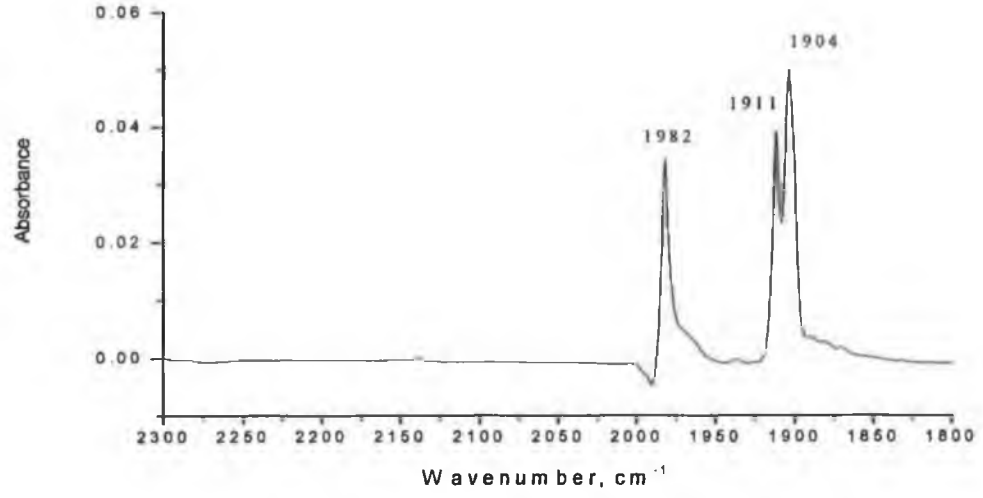

Fig 4.23 IR difference spectrum of (η^6-anisole)Mo(CO)$_3$ in N_2 matrix at 12 K after photolysis with 334 nm for 245 min.

Irradiation of a dinitrogen matrix containing (η^6-anisole)Mo(CO)$_3$ with 313 nm, resulted in a grow-in of the bands at 1937, 1889 cm^{-1} of the dicarbonyl compound which has at $\nu_{N\text{-}N}$ band at 2151 cm^{-1}, as well as weak features at 1980 cm^{-1} for (η^6-anisole)Mo(CO)$(N_2)_2$, Fig 2.24. Further evidence is observed in the matrix, at 2251, and 2236 cm^{-1} for the presence of two $\nu_{N\text{-}N}$ bands of the cis-dinitrogen ligands.

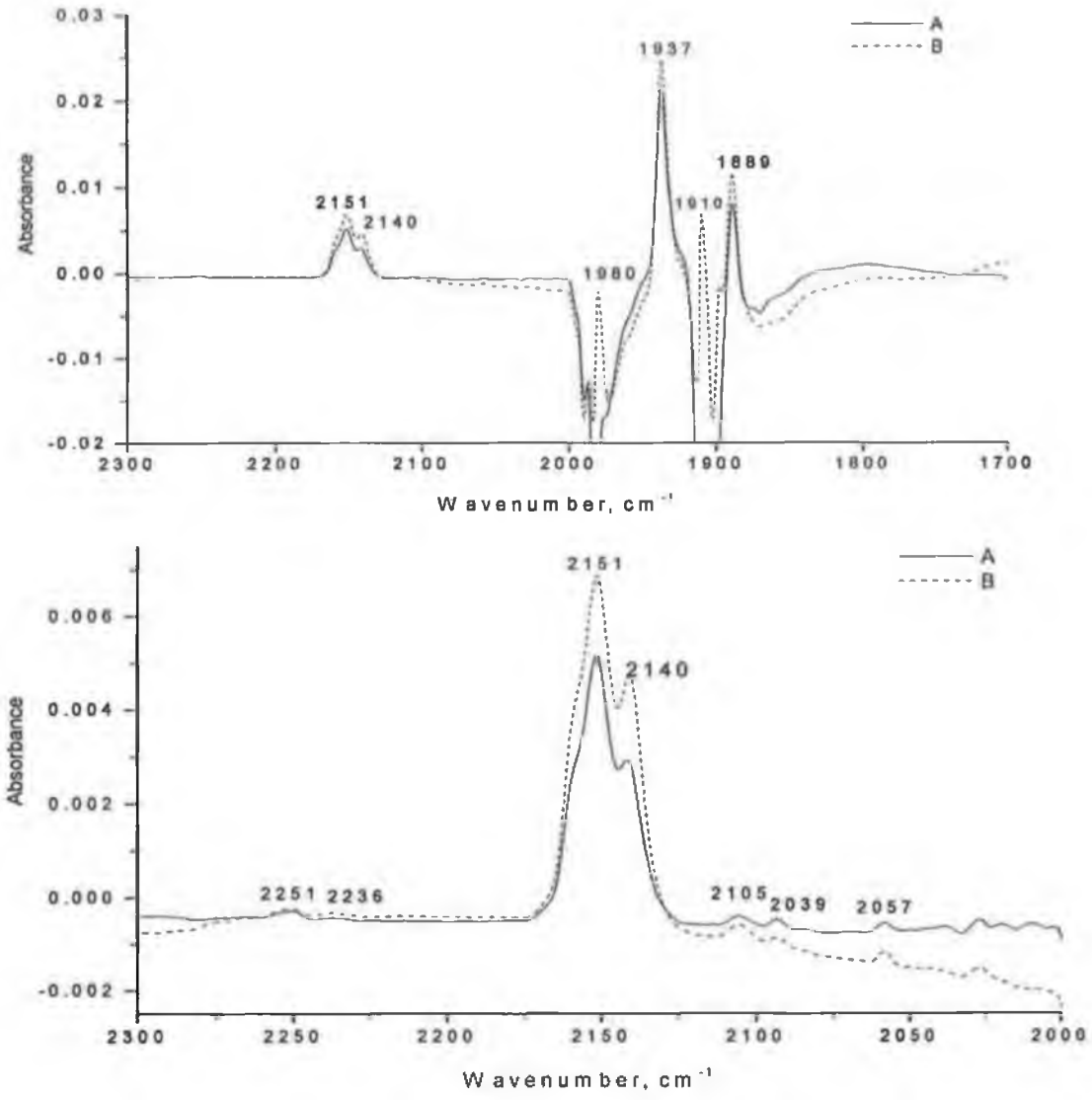

Fig 4.24 IR difference spectrum of (η^6-anisole)Mo(CO)$_3$ in N_2 matrix at 12 K after photolysis with 313 nm for A) 130 min, B) 225 min.

Irradiation of a dinitrogen matrix containing (η^6-anisole)Mo(CO)$_3$ with 297 nm, resulted in a grow-in of the dicarbonyl features at 1937 (ν_{CO}) and 2151 cm^{-1} ($\nu_{N\text{-}N}$), Fig 4.25.

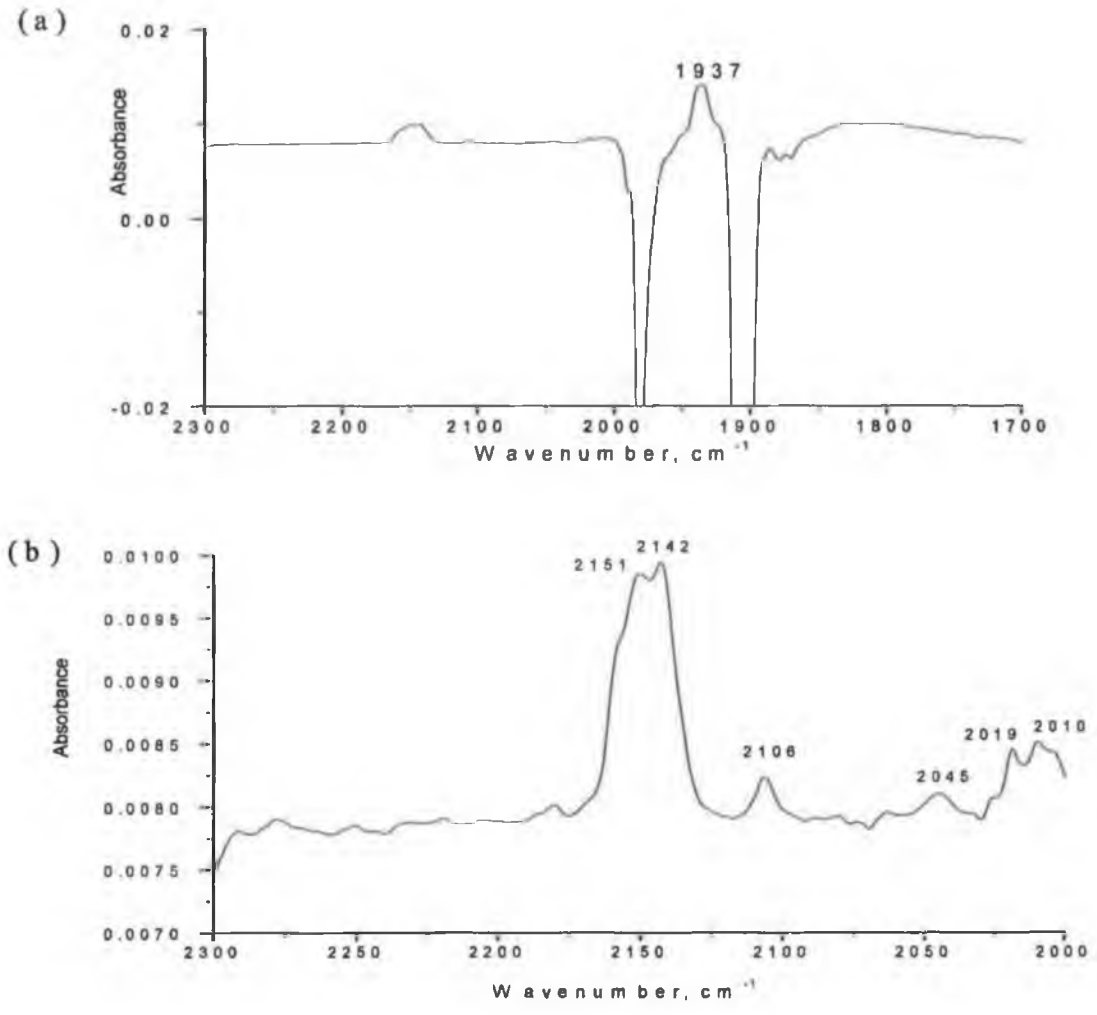

Fig 4.25 (a) IR difference spectrum of (η^6-anisole)$Mo(CO)_3$ in N_2 matrix at 12 K after photolysis with 297 nm for 120 min.(b) expansion of the spectrum in the region 2300-2000 cm^{-1}.

Subsequent irradiation of the N_2 matrix containing (η^6-anisole)$Mo(CO)_3$ with > 400 nm, resulted in a regeneration of the parent bands at 1982, 1911, and 1904 cm^{-1} with depletion of dicarbonyl, free CO and N_2 features Fig 2.26. The weak band at 1870 cm^{-1} is tentatively assigned to (η^1-O-anisole)$Mo(CO)_3$.

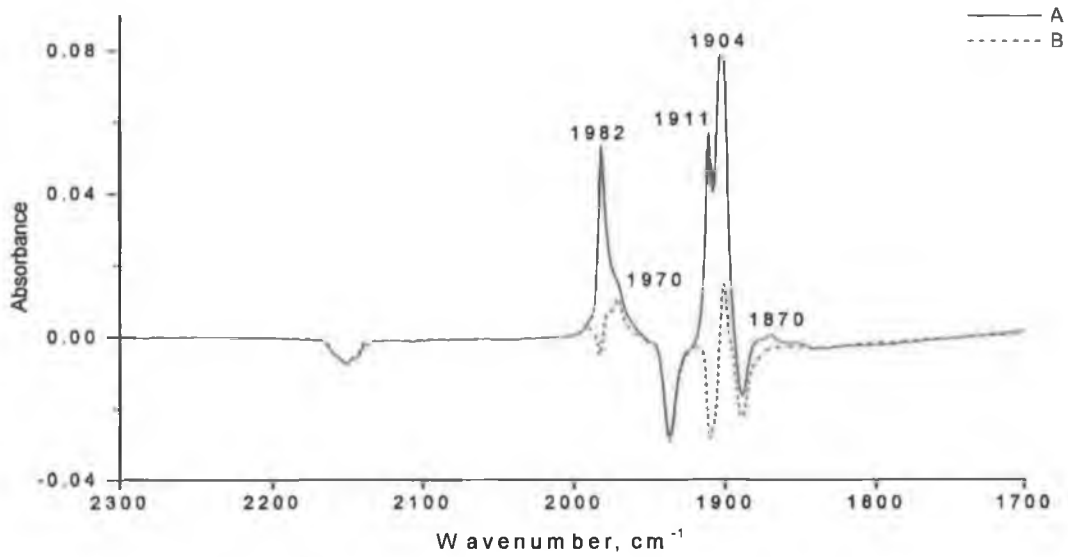

Fig 4.26 IR difference spectrum of an irradiated N_2 matrix containing (η^6-anisole)$Mo(CO)_3$ at 12 K after photolysis with >400 nm for A) 40 min, B) 95 min.

Irradiation of N_2 matrix containing (η^6-anisole)$Mo(CO)_3$ with > 300 nm, resulted in a depletion of the parent tricarbonyl bands with grow-in of a dicarbonyl species (η^6-anisole)$Mo(CO)_2(N_2)$ with bands at 1937, 1887 cm^{-1} for dicarbonyl species as which

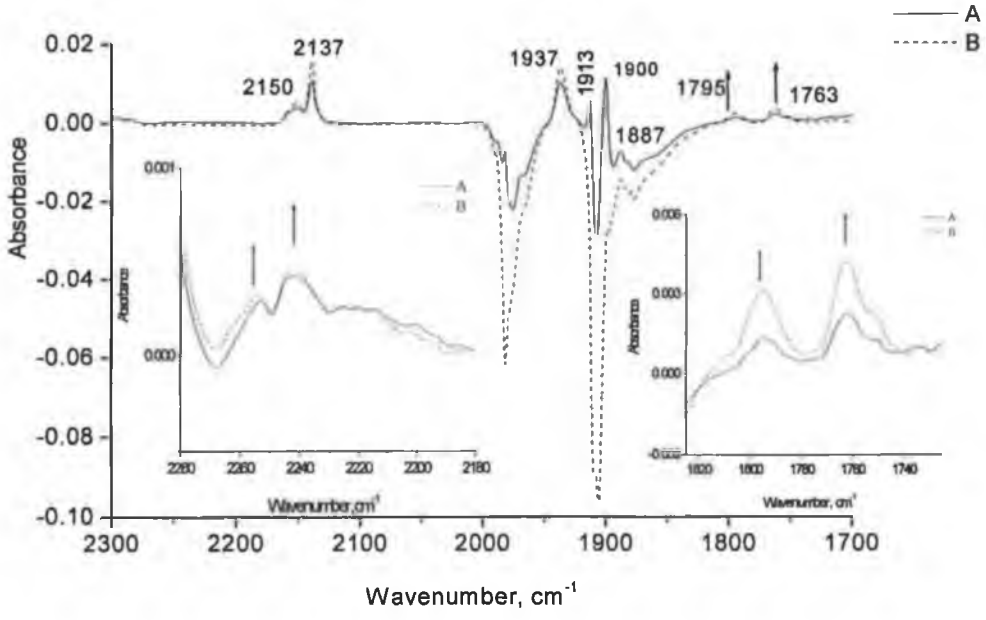

Fig 4.27 IR difference spectrum of a previously irradiated N_2 matrix containing (η^6-anisole)$Mo(CO)_3$ at 12 K after photolysis with >300 nm for A) 65 min, B) 160 min. The small figures shown are for the expansions of the regions in the range 2280-2180 cm^{-1} and 1820-1720 cm^{-1}.

also exhibited features at 2137 for free CO and N-N features at 2150 cm^{-1}. The grow-in of weak bands at 1795, 1762 cm^{-1} with concomitant grow-in of two bands at 2221 and 2253 cm^{-1}, Fig 4.27 were assigned to *fac*-(η^1-O-anisole)$Mo(CO)_3(N_2)_2$.

4.2.2.3 The matrix isolation photochemistry of (η^6-anisole)$Mo(CO)_3$ in 5% CO-CH_4 matrix: -

Photolysis with visible irradiation ($\lambda_{exc.}$ = 436 nm) of (η^6-anisole)$Mo(CO)_3$ in a 5% CO-CH_4 matrix resulted a grow-in of the bands at 1978, 1907, 1893 cm^{-1} with depletion of the parent bands, Fig 4.28. These changes are assigned to the formation of a rotamer of the tricarbonyl complex.

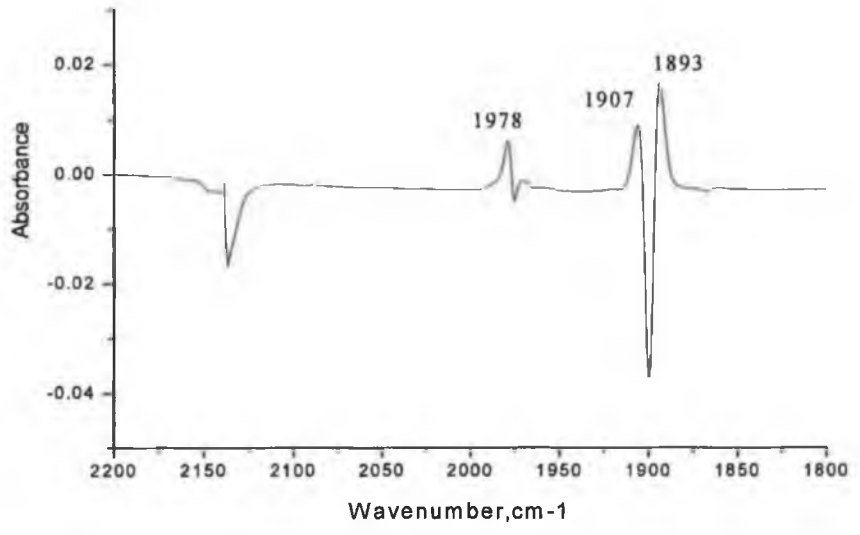

Fig 4.28 IR difference spectrum of (η^6-anisole)$Mo(CO)_3$ at 12 K after photolysis with 436 nm in 5% CO-CH_4 matrix for 220 min.

Irradiation $\lambda_{exc.}$ = 405 nm produced, in addition to the rotamer bands at 1980, 1907 cm^{-1}, further bands at 2052, and 1932 cm^{-1} which were assigned to a $Mo(CO)_4$ species (literature 2057, 1949, 1927, 1887 cm^{-1})[7] while the band 2040 cm^{-1} is assigned to cis-(η^1-O-anisole)$Mo(CO)_4$, Fig 4.29.

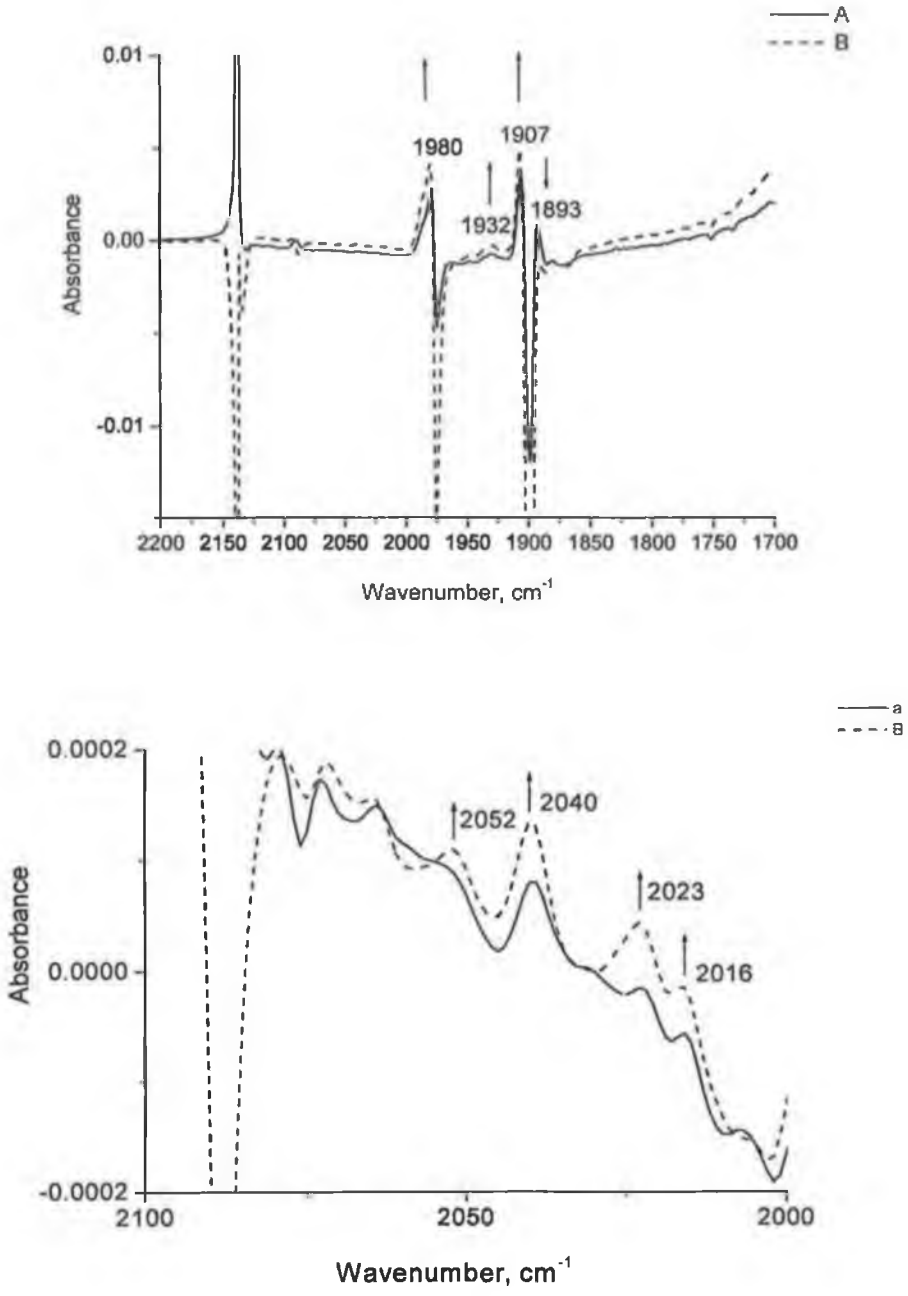

Fig 4.29 IR difference spectrum of (η^6-anisole)$Mo(CO)_3$ in 5% $CO-CH_4$ matrix at 12 K after photolysis with 405 nm for A) 150 min, B) 310 min.

Irradiation in with $\lambda_{exc.}$ = 365 nm resulted in formation of the rotamer bands at 1979, 1907, 1893 cm^{-1}, Fig 4.30.

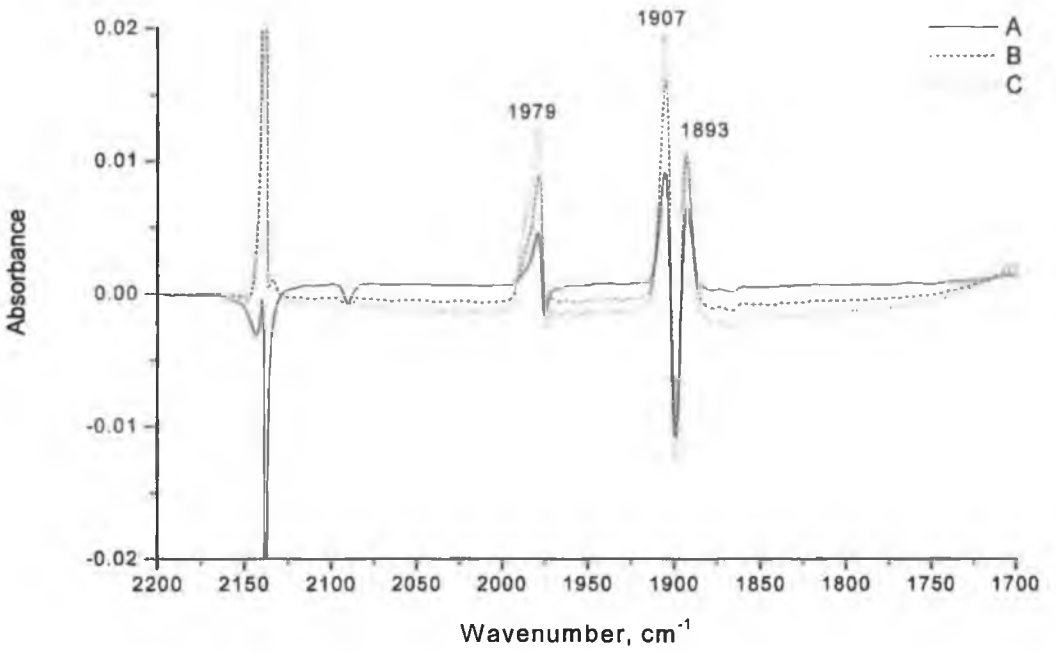

Fig 4.30 IR difference spectrum of (η^6-anisole)$Mo(CO)_3$ in 5% CO-CH_4 matrix at 12 K after photolysis with 365 nm for A) 90 min, B) 200 min, C) 280 min.

Photolysis of (η^6-anisole)$Mo(CO)_3$ in a 5% CO-CH_4 matrix with $\lambda_{exc.}$ = 334 nm resulted in the formation of the rotamer bands at 1979, 1907, 1893 cm^{-1} and a grow-in of the hexacarbonyl band at 1984 cm^{-1}, Fig 4.31.

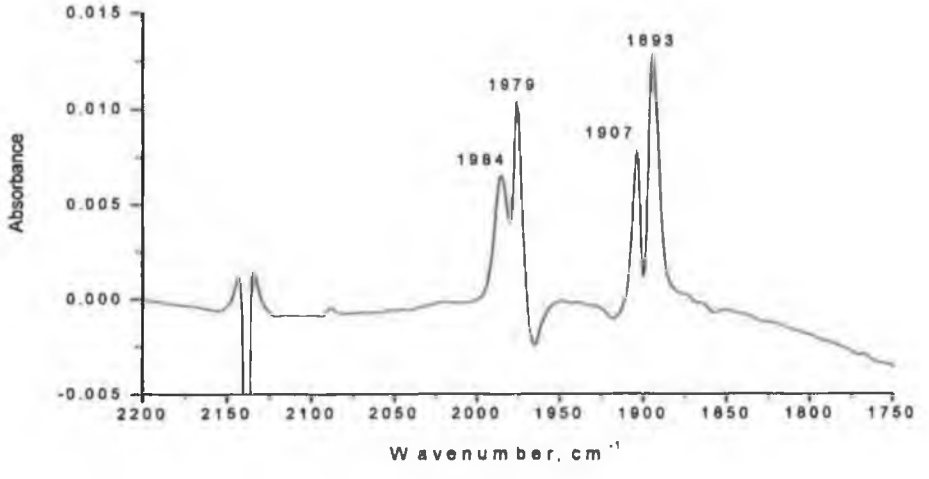

Fig 4.31 IR difference spectrum of (η^6-anisole)$Mo(CO)_3$ in 5% CO-CH_4 matrix at 12 K after photolysis with 334 nm for 215 min

Photolysis of (η^6-anisole)$Mo(CO)_3$ in a 5% CO-CH_4 matrix with a $\lambda_{exc.}$ = 313 nm resulted in a grow-in of the dicarbonyl features at 1917, and 1858 cm^{-1}, and a weak

feature at 1982 cm^{-1} assigned molybdenum hexacarbonyl, and bands at 2072, 1963, 1908 cm^{-1} for the pentacarbonyl species $Mo(CO)_5(\eta^1$-O-anisole), and a band at 2040 cm^{-1} for the coordinatively unsaturated tetracarbonyl species cis-$Mo(CO)_4(\eta^1$-O-anisole), Fig 4.32, the other expected bands for this species may obscured by the dicarbonyl species bands.

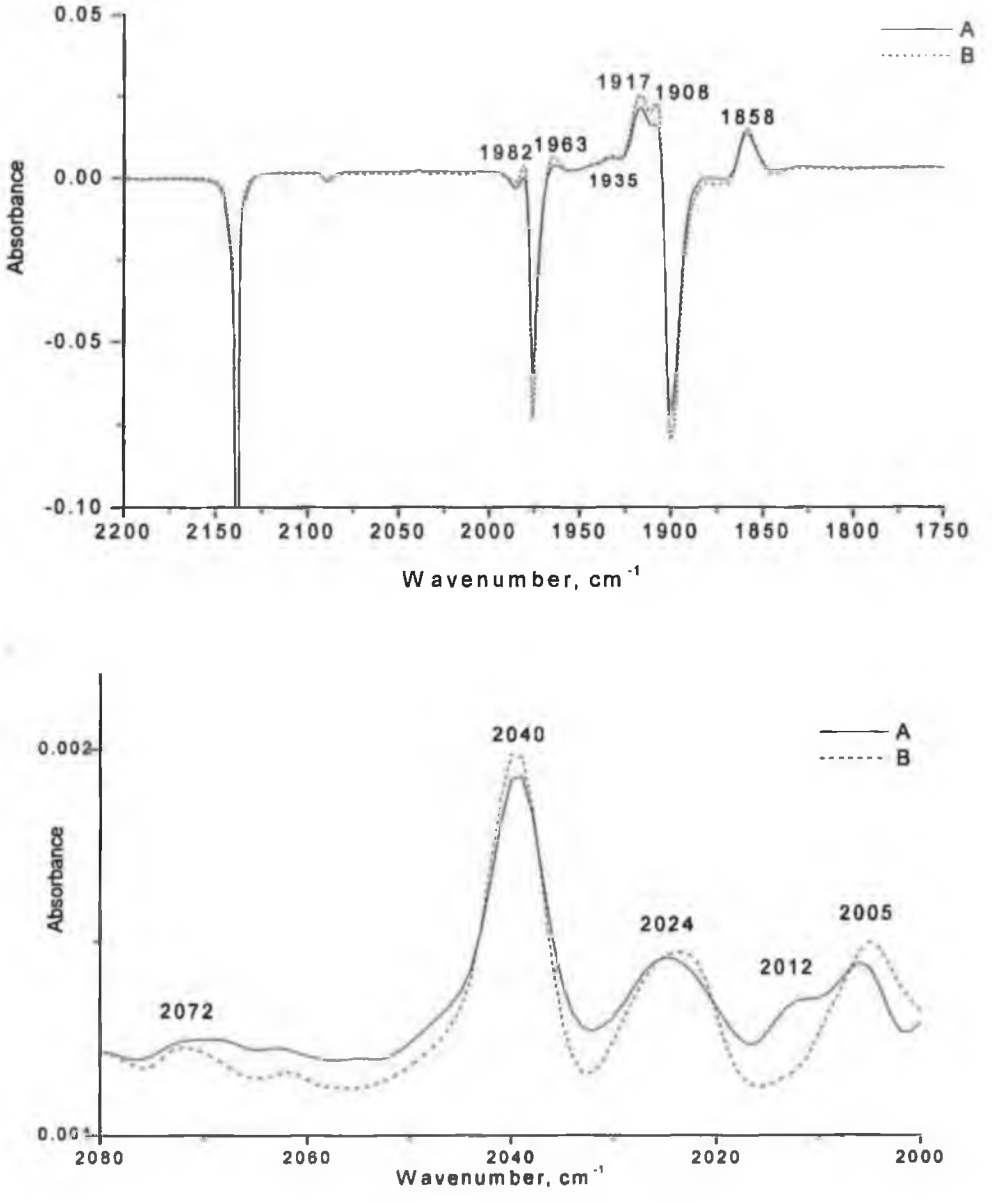

Fig 4.32 IR difference spectrum of $(\eta^6$-anisole)$Mo(CO)_3$ in 5% $CO-CH_4$ matrix at 12 K after photolysis with 313 nm for A) 210 min, B) 320 min.

Further Irradiation of the matrix at 297 nm, resulted in a grow-in of the dicarbonyl features at 1920, and 1861 cm^{-1}, and weak features at 1987 cm^{-1} for $Mo(CO)_6$, 2067 for the pentacarbonyl species $(\eta^1$-O-anisole)$Mo(CO)_5$, 2048 and 1945 cm^{-1} for the

tetracarbonyl species $Mo(CO)_4$ (literature[8] 2057, 1949, 1945, 1927, 1887 cm^{-1} (the complex ν_{CO} bands are subject to the matrix splitting therefore the number of them is higher than expected four bands); plane bands 2033, and 2013 cm^{-1} for the tetracarbonyl species with Cs symmetry (η^1-O-anisole)$Mo(CO)_4$, Fig 4.33. The remaining peaks related to these complexes may be obscured by the parent bands or the other photoproducts bands.

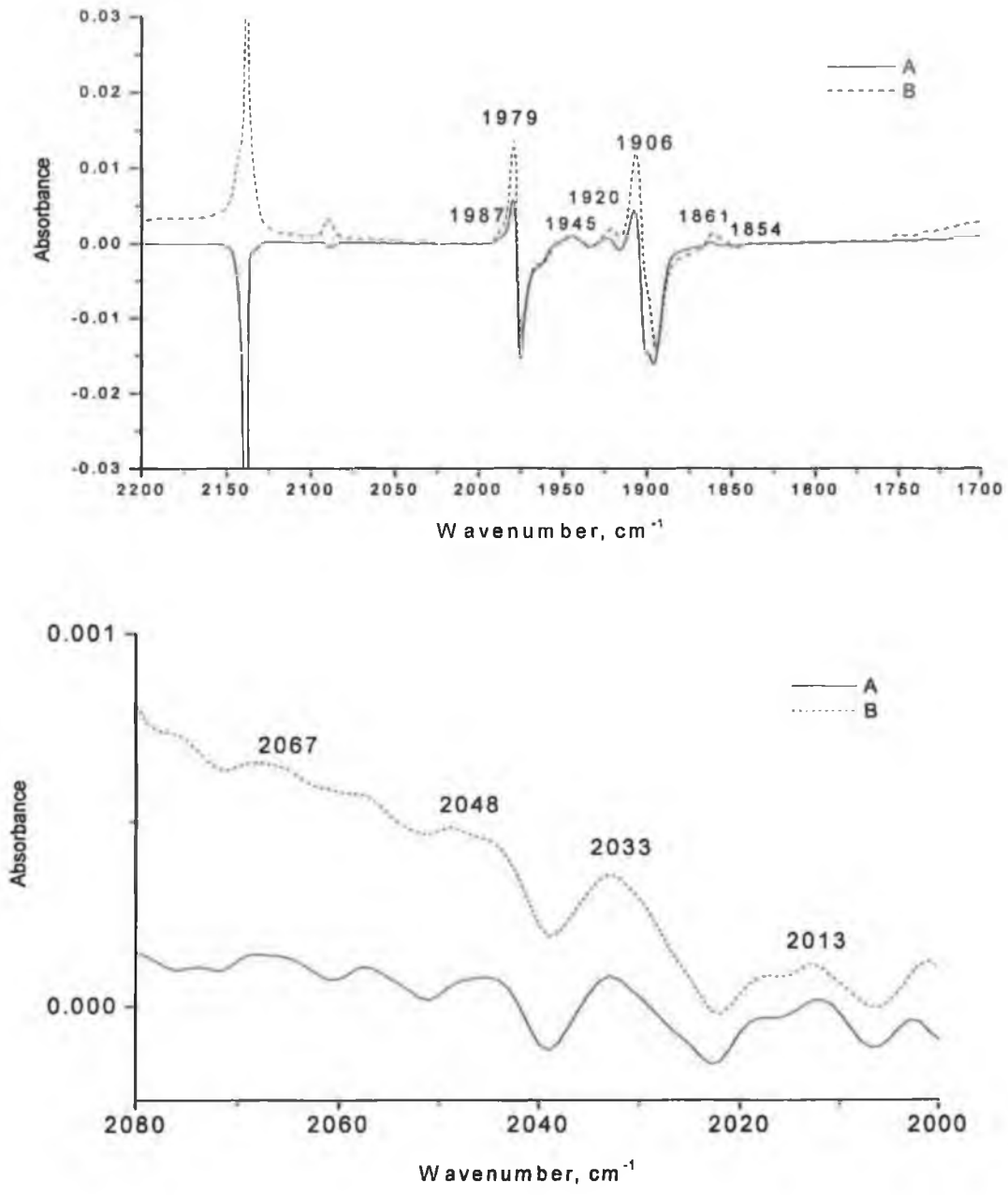

Fig 4.33 IR difference spectrum of (η^6-anisole)$Mo(CO)_3$ in 5% CO-CH_4 matrix at 12 K after photolysis with 297 nm for A) 100 min, B) 205 min.

Subsequent visible photolysis of this matrix at 12 K with $\lambda_{exc.}$ > 400 nm resulted in the regeneration of the parent bands at 1980 and 1900 cm^{-1}, with a depletion of the dicarbonyl bands at 1918 and 1860 cm^{-1} with appearance of new strong band at 1985 cm^{-1} for the molybdenum hexacarbonyl. Weak bands at 2022, 1952 cm^{-1} were also produced and which assigned to the tetracarbonyl species with Cs symmetry (η^2-anisole)$Mo(CO)_4$. Extending the photolysis time increases the yield of hexacarbonyl while more tricarbonyl complex was consumed, Fig 4.34.

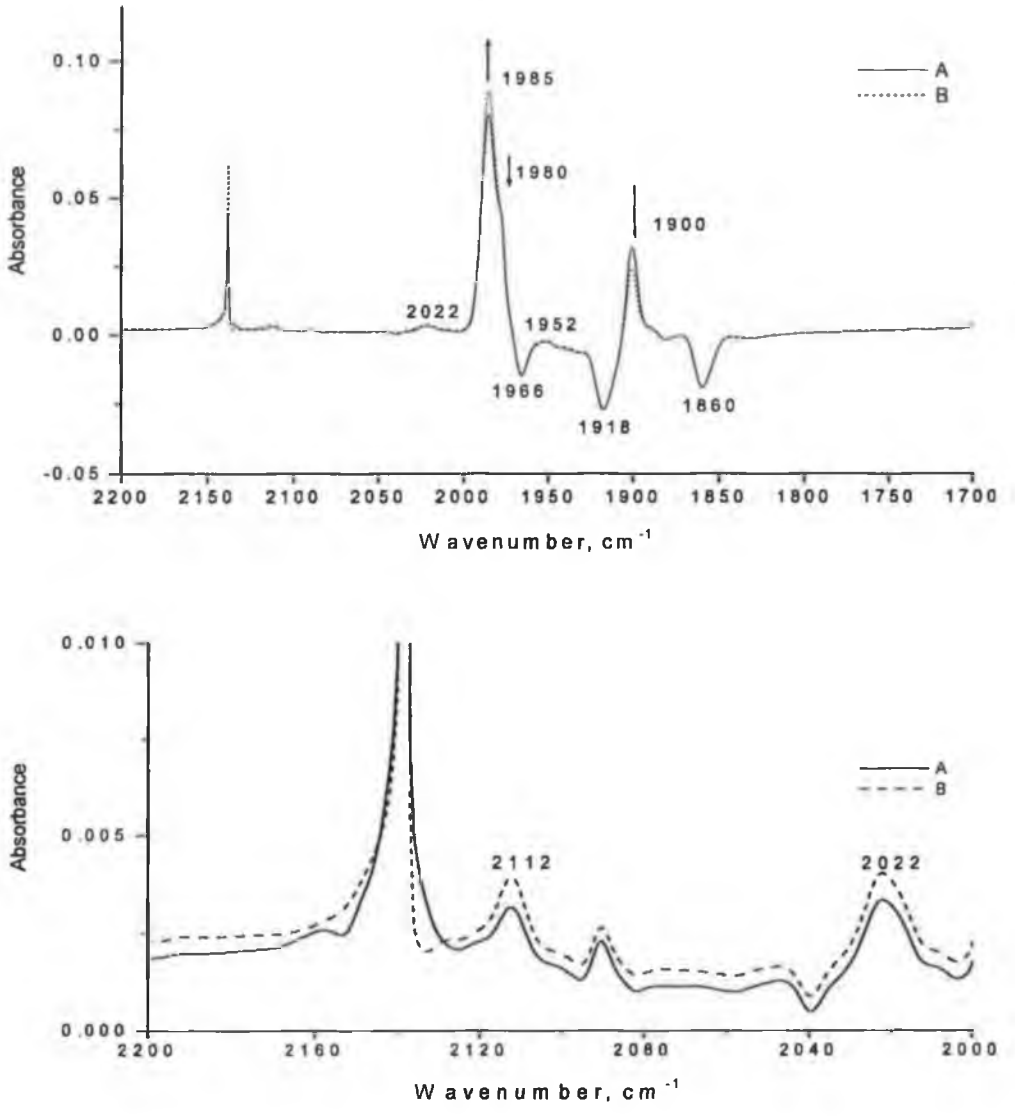

Fig 4.34 IR difference spectrum of (η^6-anisole)$Mo(CO)_3$ in 5% $CO-CH_4$ matrix at 12 K after photolysis with > 400 nm for A) 50 min, B) 80 min. The arrows represent the effect of extending the photolysis time on the bands.

Subsequent photolysis of the matrix with > 300 nm resulted in the formation of the band at 1986 cm^{-1}, which was assigned to molybdenumhexacarbonyl, Fig.4.35. Weak bands at 2020, and 1954 cm^{-1} were assigned to tetracarbonyl species with Cs symmetry namely (η^1-O-anisole)$Mo(CO)_4$.

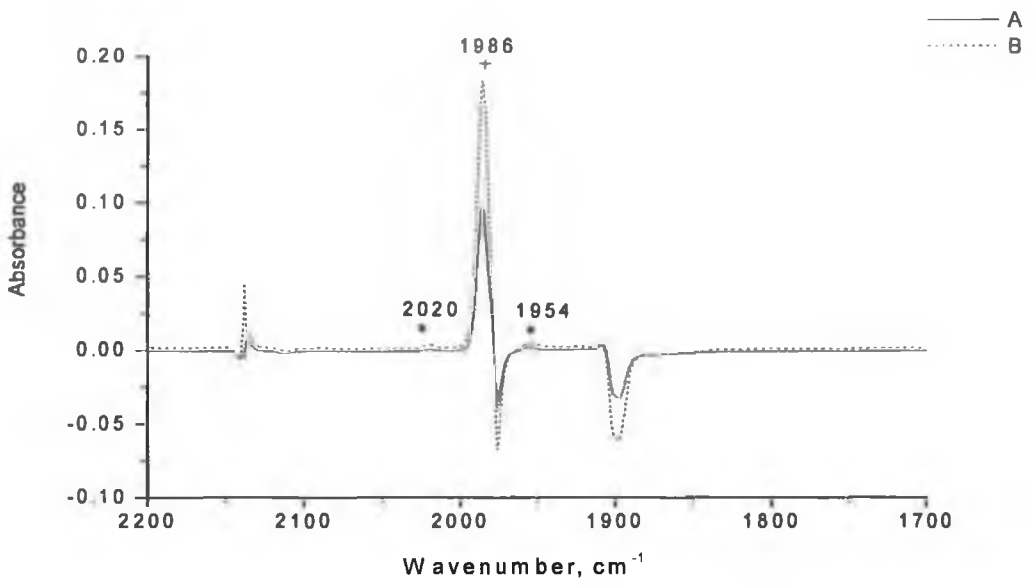

Fig 4.35 IR difference spectrum of an irradiated matrix containing (η^6-anisole)$Mo(CO)_3$ in 5% CO-CH_4 matrix at 12 K after photolysis with > 300 nm for A) 30 min, B) 60 min. The bands labelled with * and + are for (η^1-O-anisole)$Mo(CO)_4$ and $Mo(CO)_6$.

4.2.3 The matrix isolation photochemistry of (η^6-N,N-dimethylaniline)$Mo(CO)_3$:-

The IR spectroscopic data for (η^6-N,N-dimethylaniline)$Mo(CO)_3$ and all photoproducts obtained during these experiments are given in Table 4.3.

A sample of (η^6-N,N-dimethylaniline)$Mo(CO)_3$ was deposited in methane matrix at 20 K. The metal carbonyl stretching frequencies of the parent complex occur at 1969, 1893, 1885, and 1865 cm^{-1} in methane matrix. The principle IR absorption of (η^6-N,N-dimethylaniline)$Mo(CO)_3$ in the ν_{CO} region are given in Fig.4.36.

COMPLEX	ν_{CO} (cm^{-1})	MATRIX
Deposition bands:		
(η^6-N,N-dimethylaniline)$Mo(CO)_3$	1969, 1893, 1885, 1865	CH_4
Photoproduct bands:		
Rotamer (η^6-N,N-dimethylaniline)$Mo(CO)_3$	1984, 1911	CH_4
(η^6-N,N-dimethylaniline)$Mo(CO)_2$	1903, 1842	CH_4
(η^1-N,N-dimethylaniline)$Mo(CO)_3$	1816, 1914	CH_4
(η^1-N,N-dimethylaniline)$Mo(CO)_4$	2024	CO/CH_4
$Mo(CO)_4$	2061	CO/CH_4
$Mo(CO)_6$	1984	CO/CH_4

Table 4.3: Spectroscopic data in ν_{CO} region for (η^6-N,N-dimethylaniline)$Mo(CO)_3$ and all its photoproducts.

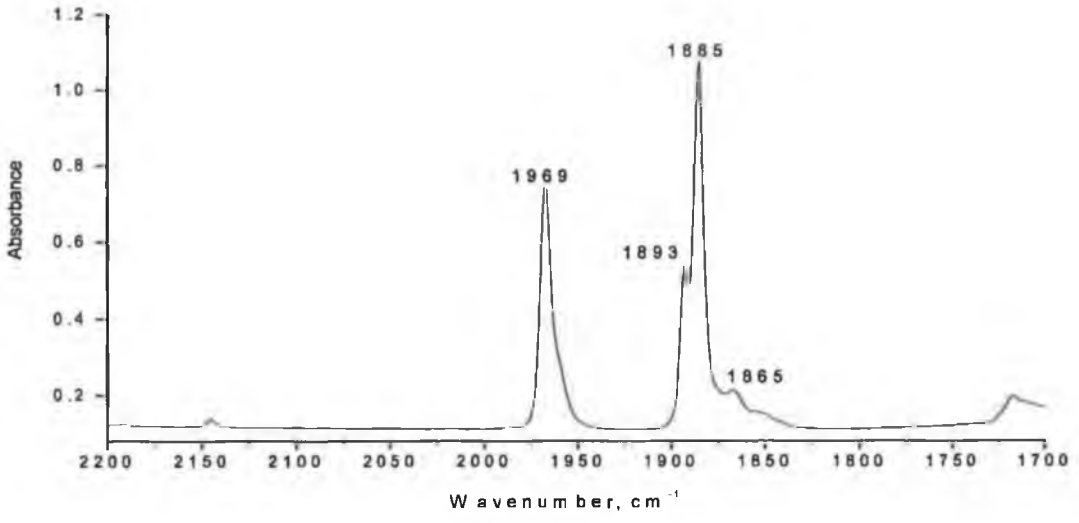

Fig 4.36 FTIR of (η^6-N,N-dimethylaniline)$Mo(CO)_3$ in methane matrix at 12 K.

Generally the photosubstitution of (η^6-N,N-dimethylaniline)$Mo(CO)_3$ is less efficient than the other tricarbonyl species in this study.

4.2.3.1 The matrix isolation photochemistry of (η^6-N,N-dimethylaniline)-$Mo(CO)_3$ in methane matrix: -

The visible photolysis of (η^6-N,N-dimethylaniline)$Mo(CO)_3$ in different matrixes at 12 K with $\lambda_{exc.}$ = 436 or 405 nm resulted a depletion of the parent bands at 1969 and 1885, 1893 cm^{-1} without appearance of any new metal carbonyl bands.

The photolysis with $\lambda_{exc.}$ = 365 nm resulted a depletion of the parent bands with a grow-in of very weak bands at 1897, 1842 cm^{-1} and free CO features at 2139 cm^{-1} these were assigned to the formation of dicarbonyl species (η^6-N,N-dimethylaniline)$Mo(CO)_2$. The remaining bands at 1959, 1870 cm^{-1} can be assigned to other rotamer of (η^6-N,N-dimethylaniline)$Mo(CO)_3$, Fig 4.37.

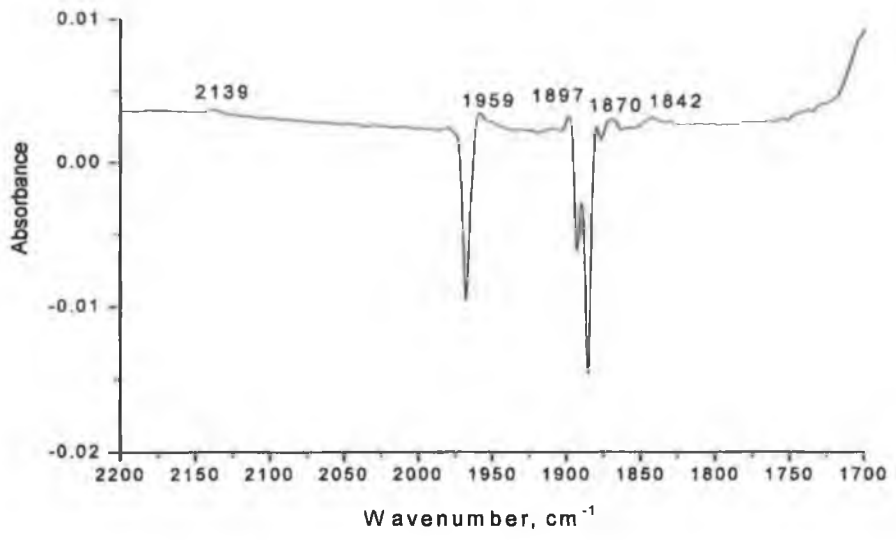

Fig 4.37 IR difference spectrum of (η^6-N,N-dimethylaniline)$Mo(CO)_3$ at 12 K after photolysis with 365 nm in CH_4 matrix for 160 min.

Subsequent UV photolysis with $\lambda_{exc.}$ = 313 nm this matrix resulted in the production of the dicarbonyl (η^6-N,N-dimethylaniline)$Mo(CO)_2$ with bands at 1903, 1842 cm^{-1} and a free CO feature at 2139 cm^{-1}. The other bands at 1816, 1914 cm^{-1}, Fig 4.38 which are not produced in similar experiments in conducted in a 2% CO-CH_4 matrix are assigned to *fac.*-$Mo(CO)_3$(η^1-N,N-dimethylaniline) which can then react with CO to form various CO rich species.

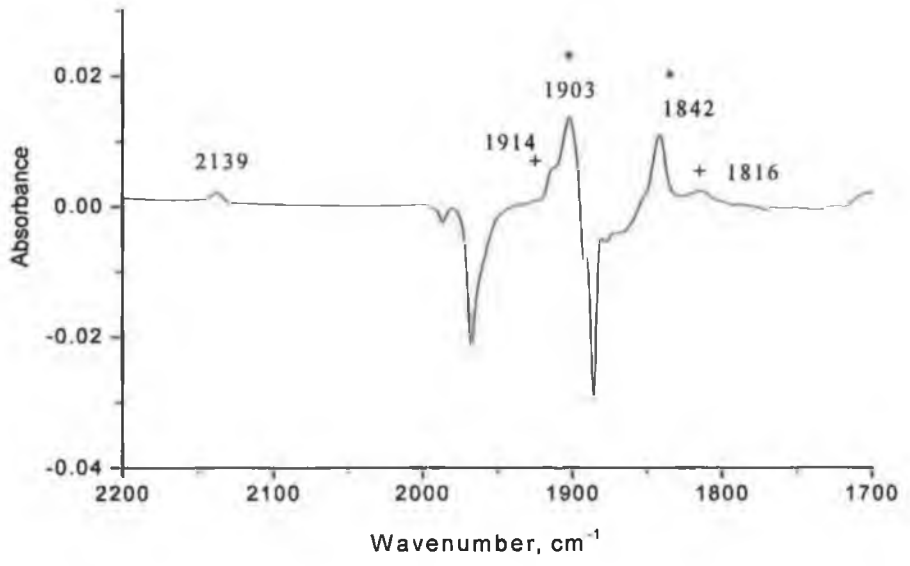

Fig 4.38 IR difference spectrum of (η^6-N,N-dimethylaniline)Mo(CO)$_3$ at 12 K after photolysis with 313 nm in CH_4 matrix for 200 min.

The visible photolysis of this sample in CH_4 matrix at 12 K with $\lambda_{exc.} > 400$ nm resulted the grow-in of the bands at 1987 and 1859 cm^{-1}, and a depletion of the parent bands. The bands at 1987 and 1859 cm^{-1} (Fig 4.39) were assigned to another rotamer of (η^6-N,N-dimethylaniline)Mo(CO)$_3$.

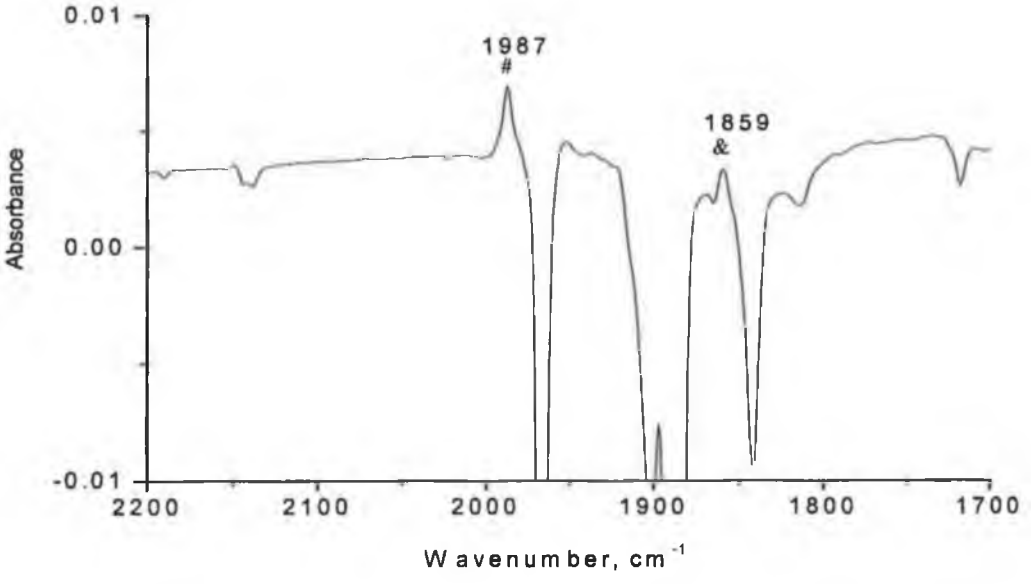

Fig 4.39 IR difference spectrum of (η^6-N,N-dimethylaniline)Mo(CO)$_3$ at 12 K after photolysis with > 400 nm in CH_4 matrix for 80 min.

Subsequent photolysis with UV irradiation $\lambda_{exc.} > 300$ nm of methane matrix containing (η^6-N,N-dimethylaniline)$Mo(CO)_3$ resulted depletion of the parent bands with the formation of a dicarbonyl species (η^6-N,N-dimethylaniline)$Mo(CO)_2$ with bands at 1904, 1845 cm^{-1}, together with free CO features at 2137 cm^{-1}, Fig 4.40. The band at 1914 cm^{-1} is related to the tricarbonyl species (η^1-N,N-dimethylaniline)$Mo(CO)_3$.

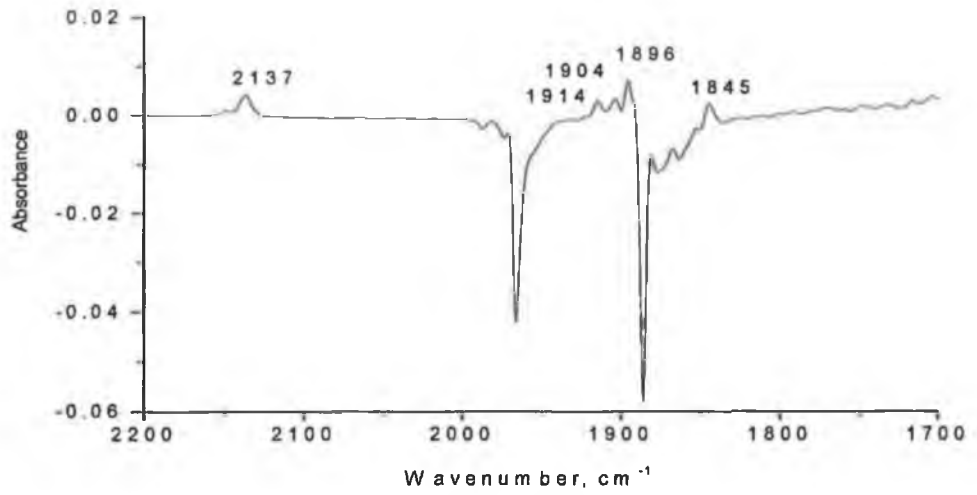

Fig 4.40 IR difference spectrum of (η^6-N,N-dimethylaniline)$Mo(CO)_3$ at 12 K after photolysis with > 300 nm in CH_4 matrix for 115 min.

4.2.3.2 The matrix isolation photochemistry of (η^6-N,N-dimethylaniline)-$Mo(CO)_3$ in 2% CO-CH_4 matrix

The photolysis of (η^6-N,N-dimethylaniline)$Mo(CO)_3$ in a 2% CO-CH_4 matrix at 12 K with $\lambda_{exc.}$ = 365 nm resulted a grow in of band at 1984 cm^{-1} which indicates formation of $Mo(CO)_6$ and the bands at 2014, 2004 cm^{-1} are assigned to the tetracarbonyl species $Mo(CO)_4$(η^1-N,N-dimethylaniline), while the bands at 1969, 1893 and 1885 cm^{-1} are assigned to a rotamer of the parent tricarbonyl species, Fig 4.41.

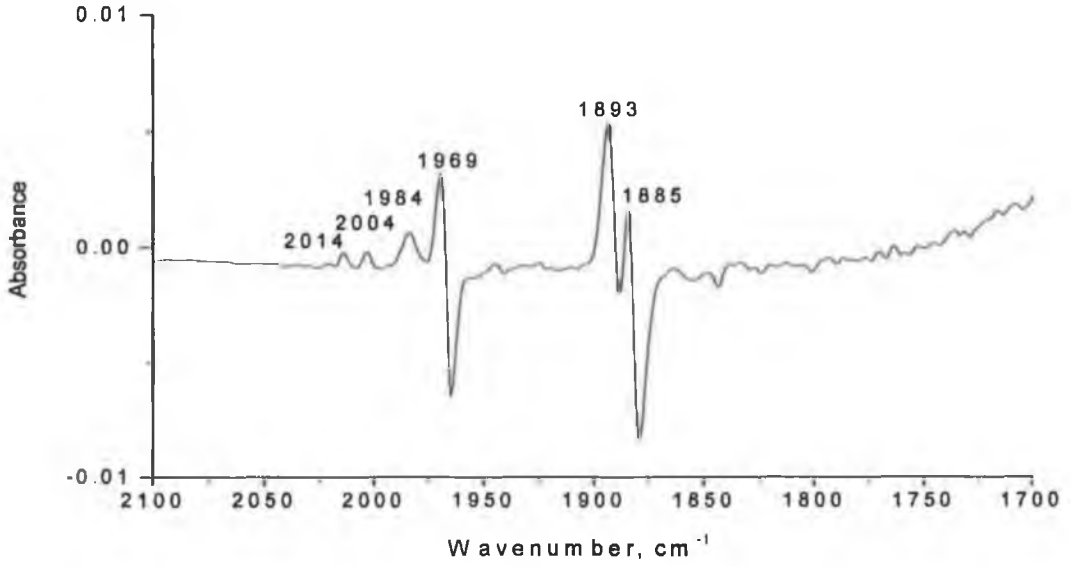

Fig 4.41 IR difference spectrum of (η^6-N,N-dimethylaniline)Mo(CO)$_3$ at 12 K after photolysis with 365 nm in 2 % CO-CH_4 matrix for 205 min.

Subsequent UV photolysis with $\lambda_{exc.}$ = 313 nm the matrix resulted in the production of the dicarbonyl (η^6-N,N-dimethylaniline)Mo(CO)$_2$ with bands at 1900, 1840 cm^{-1}, Fig 4.42.

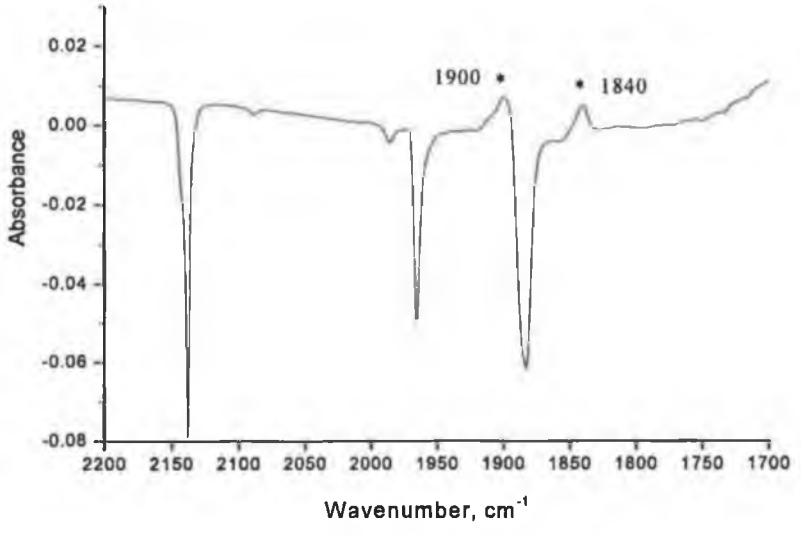

Fig 4.42 IR difference spectrum of (η^6-N,N-dimethylaniline)Mo(CO)$_3$ at 12 K after photolysis with 313 nm in 2 % CO-CH_4 for 110 min.

The subsequent photolysis of this matrix with $\lambda_{exc.}$ > 400 nm resulted in the production of the bands at 2024 and 1986 cm^{-1}, which were assigned to (η^1-N,N-dimethylaniline)Mo(CO)$_4$ with Cs symmetry and Mo(CO)$_6$ respectively, Fig. 4.43.

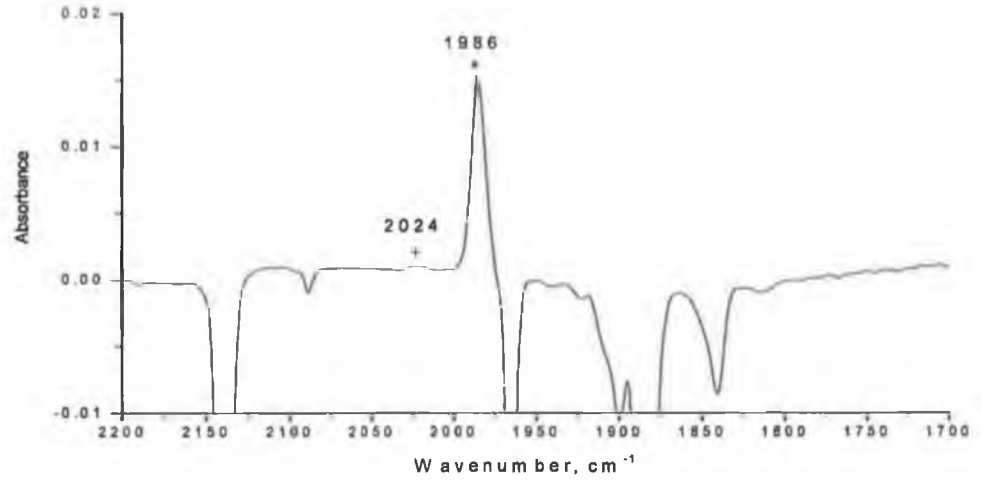

Fig 4.43 IR difference spectra of (η^6-N,N-dimethylaniline)Mo(CO)$_3$ at 12 K after photolysis with > 400 nm in 2 % CO-CH_4 matrix for 95 min.

The photolysis of this matrix with λ_{exc} > 300 nm resulted the formation of the band at 1986 cm^{-1} which assigned to the molybdenumhexacarbonyl, the band at 2021 cm^{-1} was assigned to (η^1-N,N-dimethylaniline)Mo(CO)$_4$ with Cs symmetry. The band at 1840 cm^{-1} was assigned to the dicarbonyl species (η^6-N,N-dimethylaniline)Mo(CO)$_2$, the band at 2061, 1967, and 1885 cm^{-1} which assigned to the tetracarbonyl species Mo(CO)$_4$ (literature[8] 2057, 1949, 1945, 1927, 1887), while the band at 1893 cm^{-1} can be assigned to the parent tricarbonyl complex which is partially regenerated upon this photolysis, Fig 4.44.

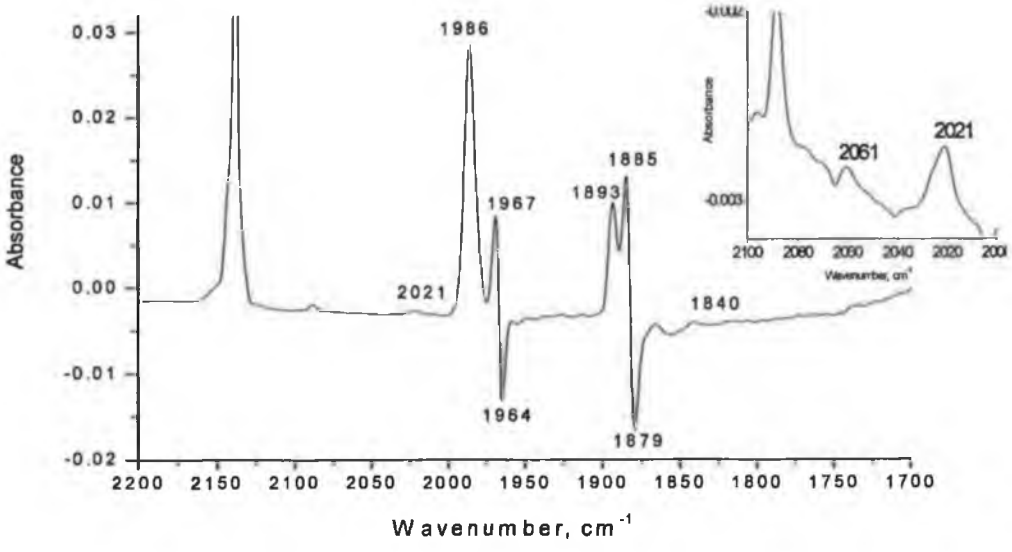

Fig 4.44 IR difference spectrum of (η^6-N,N-dimethylaniline)Mo(CO)$_3$ at 12 K after photolysis with > 300 nm in 2 % CO-CH_4 matrix for 110 min, the plot up-right this figure represent expansion of the plot in the range 2100-2000 cm^{-1}.

4.3 Discussion

The photochemistry of the molybdenum-arene tricarbonyl system is different from that of the chromium analogues. The quantum efficiencies for the arene or CO loss in molybdenum complexes appear to be lower than those of chromium analogues.

Although no evidence for the haptotropic shifts in the molybdenum-arene complexes has been obtained previously, the matrix isolation studies here give good evidence for the photoinduced haptotropic shifts of the arene to form different coordinatively unsaturated complexes. In these the arene coordinates in an η^4, η^2, or η^1 mode occurs. Thus, upon photolysis of the toluene complex (i.e. (η^6-toluene)$Mo(CO)_3$) in an active matrix like dinitrogen or CO-methane matrixes, various ring slip species have been detected.

The coordination of arene ligand through aromatic ring in a η^1, or η^2 mode is well known in the literature. Sheline and co-workers[10] studied the formation of (arene)$W(CO)_5$ produced during the photolysis of $W(CO)_6$ in hexane at -80 °C in the presence of arene (arene = benzene, toluene, *p*-xylene, mesitylene, 1,2,3-trimethylbenzene, or hexamethyl-benzene). Dobson *et al.*[11] found that (arene)$Cr(CO)_5$ complexes (arene = benzene, toluene, or halogeneted benzene) formed as transient species during flash photolysis studies of $Cr(CO)_6$ in the appropriate solvent and monitored the formation of these complexes using TRIR spectroscopy. These reports provide good evidence for this type of coordination of an arene ligand. The interaction is weak and occurs through ring-edge, ring centre or 'agostic' –C-H-M interactions, Fig. 4.45.[11]

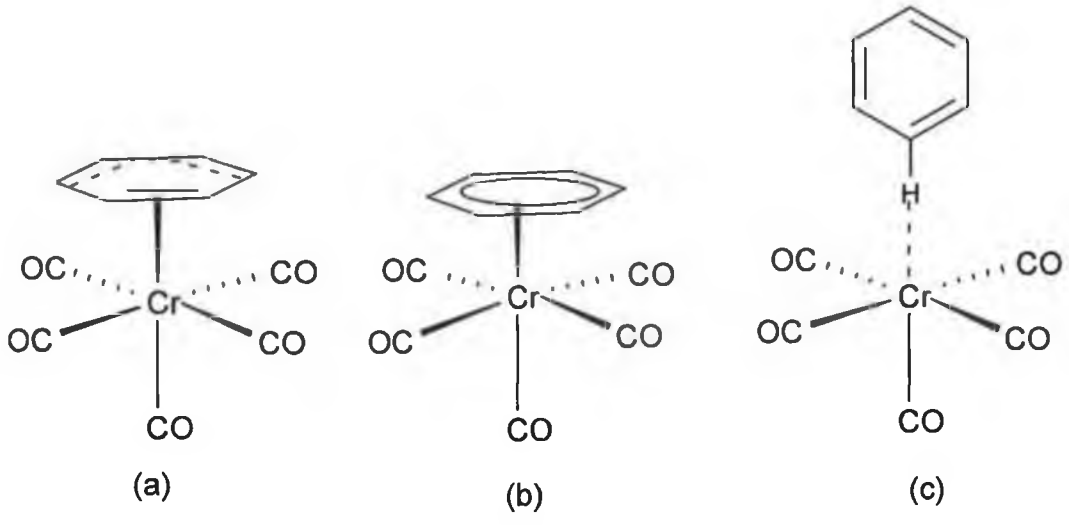

Fig 4.45 The coordination modes of the benzene and $Cr(CO)_5$ complex, a) ring-edge, b) ring centre, c) 'agostic' –C-H-M interaction.

In general the photochemistry of the complexes of the type (η^6-arene)$Mo(CO)_3$ like the analogues chromium complexes are wavelength dependent. Long wavelength photolysis induces the ring slippage while the short wavelength photolysis induces the formation the dicarbonyl complex as the main photoproduct. It seems to be that both processes contribute in the excitation with any wavelength in different percentage.

In addition to the wavelength dependence, the appearance of any photoproduct is dependent on the stability of these products and the matrix gas. In methane matrix the main products formed are *fac.*-(η^1-arene)$Mo(CO)_3$, *fac.*-(η^1-N,N-dimethylaniline)$Mo(CO)_3$.

The photolysis of the Cr-tricarbonyl complexes with 313 nm in the methane matrix induces produces *fac.*-$Cr(CO)_3$, while the photolysis of molybdenum complexes under the same conditions provided no indication for the formation of *fac.*-$Mo(CO)_3$. The presence of an electrondonating substituent on the benzene ring increases the electrondensity on the ring. This will increase the ability of the ring to coordinate to a metal centre. Such substituent may play a role in the increasing of the stability of the ring slipped intermediates. The presence of a substituent, containing an atom with a lone pair of electrons that can coordinate to the metal, will also stabilise the ring slipped photoproducts. In anisole the ethereal O-atom can coordinate to the metal while the nitrogen in N,N-dimethylaniline is sterically hindered by the two methyl groups making the coordination of the nitrogen to the metal centre more difficult, consequently coordination through the ring is also sterically stained that through the N atom. The presence of the bulky dimethyl groups will in effect hinder the ring slip process.

Scheme 4.1 outlines the general photoreactions in the matrix isolation photochemistry of the (η^6-C_6H_5-X)$Mo(CO)_3$ complexes. The loss of CO from the parent tricarbonyl produces the coordinatively unsaturated (η^6-C_6H_5-X)$Mo(CO)_2$ species which interacts with a methane molecule in the matrix to form (η^6-C_6H_5-X)$Mo(CO)_2(CH_4)$ while in a dinitrogen matrix forms the dinitrogen complex (η^6-C_6H_5-X)$Mo(CO)_2(N_2)$. Photolysis of the later with short wavelength light results in the loss of a further CO to form (η^6-C_6H_5-X)$Mo(CO)(N_2)_2$. The second pathway for (η^6-C_6H_5-X)$Mo(CO)_3$ complexes involves the haptotropic shift of the arene to form the coordinatively unsaturated photoproduct such as (η^1-C_6H_5-X)$Mo(CO)_3$. In a dinitrogen matrix this is trapped to form *fac.*-(η^1-C_6H_5-X)$Mo(CO)_3(N_2)_2$. In CO-

methane matrix the complex (η^1-C_6H_5-X)$Mo(CO)_3$ is trapped to form the CO-rich complexes (η^1-C_6H_5-X)$Mo(CO)_4$, (η^1-C_6H_5-X)$Mo(CO)_5$ and eventually complete arene loss to give $Mo(CO)_6$ as the final product.

4.3.1 Matrix isolation of (η^6-toluene)$Mo(CO)_3$: -

In the matrix isolation of (η^6-toluene)$Mo(CO)_3$ in methane matrix the photolysis with long wavelength ($\lambda_{exc.}$ = 405 nm) resulted the formation of a rotamer of the parent compound, which has higher energy ν_{CO} bands than the parent tricarbonyl complex. The other photoproduct is the dicarbonyl complex (η^6-toluene)$Mo(CO)_2$ which appears to be formed with low quantum efficiency.
In a N_2 matrix a grow-in of the parent peaks was observed upon photolysis with 405 nm (this may be because the thickness of the matrix is not the same, so intensity of the IR band will effected)

The photolysis (η^6-toluene)$Mo(CO)_3$ in N_2 matrix at 12 K with 313 nm produced both the CO loss and the haptotropic shift photoproducts (i.e. (η^6-toluene)$Mo(CO)_2(N_2)$ and *fac.*-(η^1-toluene)$Mo(CO)_3(N_2)_2$). The complex (η^6-toluene)$Mo(CO)_2(N_2)$ is photoactive under these conditions and losses a further CO ligand to form the dinitrogen complex (η^6-toluene)$Mo(CO)(N_2)_2$.

The photolysis with 313 nm of (η^6-toluene)$Mo(CO)_3$ in 5% CO matrix produced the dicarbonyl species (i.e. (η^6-toluene)$Mo(CO)_2$) along with the tetracarbonyl $Mo(CO)_4$ species and with molybdenumhexacarbonyl.

4.3.2 Matrix isolation of (η^6-anisole)$Mo(CO)_3$: -

The photolysis of (η^6-anisole)$Mo(CO)_3$ in methane or 5% CO-methane or dinitrogen matrix with $\lambda_{exc.}$ = 436 nm resulted a new rotamer of this complex, which has ν_{CO} frequencies lower than the parent tricarbonyl complex bands. The photolysis in methane with 405 nm resulted in addition to the bands of the rotamer, in the formation of another band at 1890 cm^{-1} assigned to the dicarbonyl species (i.e. (η^6-anisole)$Mo(CO)_2$). In dinitrogen matrix this photolysis produced the rotamer and the dicarbonyl species which was trapped by N_2 to form (η^6-anisole)$Mo(CO)_2(N_2)$ with a $\nu_{N\text{-}N}$ vibration at 2140 cm^{-1}. The photolysis in a 5% CO-methane matrix produced the

tetracarbonyl species $Mo(CO)_4$ with four ν_{CO} bands and also another bands which was assigned to the coordinatively unsaturated cis-$Mo(CO)_4(\eta^1$-O-anisole) species in which anisole ligand is coordinated through oxygen atom.

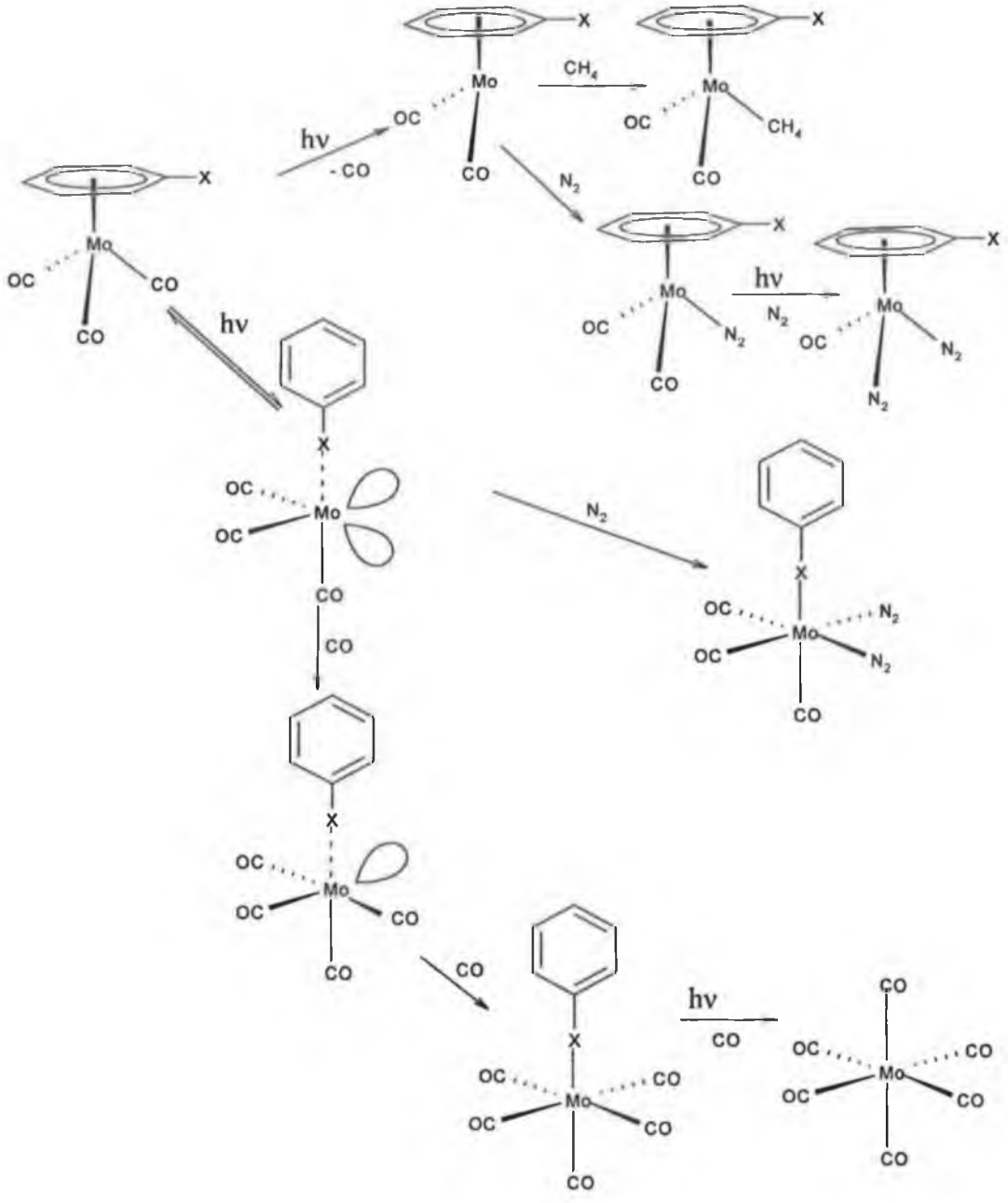

Scheme 4.1 the general schematic representation of the photochemical reactions of $(\eta^6$-C_6H_5-X)$Mo(CO)_3$ complexes. A dinitrogen matrix was used for the toluene and anisole complexes only.

The only photoproduct formed upon the photolysis of $(\eta^6$-anisole)$Mo(CO)_3$ in methane with 313 or 297 nm was the coordinatively unsaturated complex (η^6-anisole)$Mo(CO)_2$. The photolysis for the same complex with 313 nm in 5% CO-

methane matrix formed in addition to the dicarbonyl species, CO-rich species such as tetracarbonyl, pentacarbonyl and hexacarbonyl species. Thus, it seems that the irradiation with this wavelength resulted in both the loss of CO and the ring slip which traps CO to form $Mo(CO)_6$, and $Mo(CO)_5(\eta^1$-O-anisole), and the coordinatively unsaturated species cis-$Mo(CO)_4(\eta^1$-O-anisole). In a dinitrogen matrix the initially formed (η^6-anisole)$Mo(CO)_2(N_2)$ was they photosensitive forming (η^6-anisole)$Mo(CO)(N_2)_2$. Surprisingly, there was no indication of ring slipped photoproduct in dinitrogen matrixes.

Irradiation of a 5% CO-CH_4 matrix containing (η^6-anisole)$Mo(CO)_3$ at 297 nm, resulted in the formation of the dicarbonyl species, and CO-rich photoproducts $Mo(CO)_6$, the pentacarbonyl species (η^1-O-anisole)$Mo(CO)_5$, the tetracarbonyl species $Mo(CO)_4$, and cis-(η^1-O-anisole)$Mo(CO)_4$. While the photolysis with 297 nm of (η^6-anisole)$Mo(CO)_3$ in dinitrogen matrix resulted the dicarbonyl species (η^6-anisole)$Mo(CO)_2(N_2)$ and the ring slipped photoproduct cis-dinitrogen species *fac.*-$Mo(CO)_3(N_2)_2(\eta^1$-O-anisole).

Generally, the subsequent photolysis of the irradiated matrix (methane, 5% CO-methane, or dinitrogen matrix) with $\lambda_{exc} > 400$ nm resulted in the regeneration of the parent tricarbonyl complex. In addition, traces of (η^1-O-anisole)$Mo(CO)_3$ could also observed. Photolysis of the irradiated 5% CO-CH_4 matrixes also regenerated of the tricarbonyl complex, various other species were observed and the assigned to molybdenum hexacarbonyl, and the tetracarbonyl species (η^2-anisole)$Mo(CO)_4$.

Photolysis of irradiated N_2 matrixes, resulted the regeneration of the parent tricarbonyl complex, The weak band at 1870 cm^{-1} for (η^6-anisole)$Mo(CO)_3$.

4.3.3 Matrix isolation of (η^6-N,N-dimethylaniline)$Mo(CO)_3$: -

The photolysis with $\lambda_{exc.} = 365$ nm resulted the formation of dicarbonyl species (η^6-N,N-dimethylaniline)$Mo(CO)_2$ and the other photoproduct is a rotamer of (η^6-N,N-dimethylaniline)$Mo(CO)_3$. In addition to these changes the photolysis in a 2% CO-CH_4 matrix resulted the formation of $Mo(CO)_6$ and the coordinatively unsaturated tetracarbonyl species cis-$Mo(CO)_4(\eta^1$-N,N-dimethylaniline).

Subsequent UV photolysis with $\lambda_{exc.} = 313$ nm of (η^6-N,N-dimethylaniline)$Mo(CO)_3$ in CH_4 matrix resulted in the production of the dicarbonyl (η^6-N,N-dimethylaniline)$Mo(CO)_2$ and the coordinatively unsaturated ring slipped photoproduct *fac.*-$Mo(CO)_3(\eta^1$-N,N-dimethylaniline). Although those bands which

are assigned to *fac.*-$Mo(CO)_3(\eta^1$-N,N-dimethylaniline) species were not observed in 2% CO-matrix experiment which indicated that this species reacts with CO, no indication for the formation of tetracarbonyl, pentacarbonyl or hexacarbonyl species in the IR spectrum. It seems was observed that the dicarbonyl species bands obscure these bands.

Although the visible photolysis with $\lambda_{exc.} > 400$ nm in CH_4 matrix at 12 K nm resulted another in rotamer of (η^6-anisole)$Mo(CO)_3$, the photolysis with $\lambda_{exc.} > 400$ nm in 2% CO-CH_4 matrix produced both the coordinatively unsaturated cis-(η^1-N,N-dimethylaniline)$Mo(CO)_4$ and $Mo(CO)_6$.

Subsequent photolysis with UV irradiation $\lambda_{exc.} > 300$ nm of methane matrix containing (η^6-N,N-dimethylaniline)$Mo(CO)_3$ resulted the formation of (η^6-N,N-dimethylaniline)$Mo(CO)_2$ and the coordinatively unsaturated ring slipped photoproduct (η^1-N,N-dimethylaniline)$Mo(CO)_3$. Trapping of this species with CO in 2% CO matrix resulted the formation of $Mo(CO)_6$, the coordinatively unsaturated cis-(η^1-N,N-dimethylaniline)$Mo(CO)_4$, and the tetracarbonyl species $Mo(CO)_4$.

4.4 Conclusion

Chapter 4 presents the matrix isolation experiments on the complexes of the type (η^6-C_6H_5-X)$Mo(CO)_3$, (X = CH_3, OCH_3, or $N(CH_3)_2$) in methane, dinitrogen, 2 %, or 5 % CO-methane mixtures at 12 K. It would appear that the arene loss is less efficient for molybdenum than for chromium. The formation of molybdenum hexacarbonyl and (η^1-C_6H_5-X)$Mo(CO)_3(N_2)_2$ complex upon the photolysis of (η^6-C_6H_5-X)$Mo(CO)_3$ complexes in CO-methane and N_2 matrixes provides good evidence for a haptotropic shift reaction.

4.5 References: -

1) Mukerjee, S.L.; Lang, R.F.; Ju, T.; Kiss, G.; Hoff, C.D. *Inorg. Chem.* 1992, 31, 4885.

2) Kündig, E.P.; Fabritius, C.H.; Grossheimann, G.; Romanens, P., *Organometallics*, 2004, 23, 3741.

3) a) Zingales, F.; Chiesa, A.; Basolo, F., *J. Am. Chem. Soc.*, 1966, 88, 12, 2707. b) Strohmeier, W.; Mittnacht, H., *Z. Physik. Chem.* (Frankfurt), 1961, 29, 339;

Strohmeier, W.; Müller, H., *Z. Physik. Chem.* (Frankfurt), 1964, 40, 85. c) Abel, E. W.; Bennett; Wilkinson, G., *J. Chem. Soc.*, 2323, 1959.

4) Kiplinger, J.L., Richmond, T.G., *Polyhydron*, 1997, 16, 3, 409.

5) Creaven, B.S., *PhD Thesis*, Dublin City University, 1993.

6) Pryce, M. T., *PhD Thesis*, Dublin City University, 1994.

7) Goff, S.E.J., Nolan, T.F.; George, M.W.; Poliakoff, M., *Organometallics*, 1998, 17, 2730.

8) Perutz, R.N., Turner, J.J., *J. Am. Chem. Soc.*, 1975, 97, 17, 4800.

9) Breheny, C.J.; Draper, S.M.; Grevels, F.W.; Klotzbücher, W.E.; Long, C.; Pryce, M. T.; Russell, G., *Organometallics* 1996, 15, 3679.

10) Stolz, I.W.; Haas, H.; Sheline, R.K., *J. Am. Chem. Soc.*, 1965, 87, 716.

11) a) Ladogana, S.; Nayak, S.K.; Smit, J.P.; Dobson, G.R., *Inorg. Chim. Acta,* 1998, 267, 49. b) Ladogana, S.; Dobson, G.R., Smit, J.P., *Inorg. Chim. Acta,* 1998, 271, 105.

Chapter 5

Theoretical Calculations on complexes of the type $M(CO)_5L$ and (η^6-arene)$Cr(CO)_3$

Chapter 5

5.1 Literature Survey

5.1.1 Theoretical calculations of the complexes of the type $M(CO)_5L$

The theoretical approach to the photochemical substitution reactions of group 6 hexacarbonyl complexes $M(CO)_6$ (M = Cr, Mo, or W) has developed from an initial semi empirical study, proposing a central role for LF states in CO ejection to one which considers the development of states originating from MLCT character to states which are unbound to M-CO interactions. In recent years greater interest has been shown to the theoretical and photochemical studies of the substituted group 6 carbonyl complexes $M(CO)_nL_x$ (M = Cr, Mo, or W; L = amine, carbene, or phosphine, n = 6-x, x = 1-2).

As consequence, studies of the photochemical mechanisms and the dynamics of ligand loss from organometallic compounds are both intriguing and challenging, with great potential for discoveries of new phenomena and properties. In addition the simultaneous existence of distinct reactivity and relaxation pathways, together with the presence of closely-spaced disparate excited states, provides the opportunity to control the photochemical behaviour of transition metal compounds.

Zarić, *et al.*,[3] carried out ab intio calculations at the HF level to calculate the vibrational frequencies of $W(CO)_5NH_3$ in its electronic ground $^1A_1(b_2^2e^4)$ and lowest energy excited state $^3E(b_2^2e^3a_1^1)$. The calculated frequencies of the ν(CO) bands are in agreement with observed data for $W(CO)_5$(amine) molecules. The optimised geometries of the ground and the excited states show that the W-N, $W\text{-}C_{ax}$, $C\text{-}O_{eq}$ bonds lengthen and the $C\text{-}O_{ax}$ bond shortens upon excitation. The unexpected simultaneous lengthening of both $W\text{-}C_{eq}$ and $C\text{-}O_{eq}$ is due to the $C\text{-}O_{eq}$ antibonding character in the a_1 orbital, which more than offsets its loss from the e orbital.

Ehlers *et al.* [4] carried out DFT calculations to determine the equilibrium structures of the phosphinidene transition-metal complexes $M(CO)_5$-PR, with M = Cr, Mo, or W and R = H, Ph, OH, and NH_2. The free phosphinidenes P-R have a triplet ground states, but their $M(CO)_5$ complexes prefer singlet states because of the substantial stabilisation of the unoccupied phosphorus P_π acceptor orbital. These workers found that a Dewar-Chatt-Duncanson model showed that the investigated ligands are strong

π-acceptors and even stronger σ-donors. In the case of unsubstituted PH complexes, the ground state is a singlet due to strong preferential stabilisation by π-back donation into the empty phosphorous P_π orbital. When substituents are present, the singlet state is relatively stabilised in the free phosphinidene due to π-donation from the substituent. The π-back donation from the metal fragment decreases accordingly due to competition with this substituent π-donation but remains effective in further stabilising the singlet.

DFT calculations to determine the geometries and bond dissociation energies[5] of $M(CO)_5PX_3$ (M = Cr, Mo, or W; X = H, Me, F, or Cl) showed that there is no correlation between the bond lengths and bond energies of the M-P bonds. The bond dissociation energies of the phosphane ligands follow (for all metals M) the trend $PMe_3 > PH_3 > PCl_3 > PF_3$. The energy decomposition analysis indicates that the PH_3 and PMe_3 ligands are more electrostatically than covalently bonded to the metals M. The electrostatic amounts to 56-66 % of the total attractive interactions in the M-PH_3 and M-PMe_3 bonds have more σ character (65-75 %) than π character (25-35 %). The M-P bonds of the halophosphane complexes $M(CO)_5PF_3$ and $M(CO)_5PCl_3$ are nearly half covalent and half electrostatic. The π bonding contributes ~50 % to the total orbital interaction.

Morales, *et al.* [6] used DFT calculations to find ^{31}P NMR chemical shifts in the phosphine-substituted metal carbonyls of the type $M(CO)_5PR_3$ (M = Cr or Mo; R = H, CH_3, C_6H_5, F, or Cl) as well as the ^{95}Mo NMR chemical shift of $Mo(CO)_5P(C_6H_5)_3$ and $Mo(CO)_5PX_3$ (X = F or Cl). The major contribution of the chemical shift comes from the paramagnetic coupling between the occupied d_π orbitals (HOMO) and the virtual d_σ orbitals (LUMO).

Using molecular orbital calculations, Wang *et al* [7]studied four pentacarbonyl chromium-carbene complexes $(OC)_5CrC(XR')R$. The spherical electron density around the Cr atom and the d orbital populations of Cr is in accord with the crystal field theory. Orbital energies calculated from DFT are close to those measured from PES (Photo Electron Spectroscopy). The bonding characteristics of Fisher-type carbenes are as follows: - electron donating from the carbene carbon forms the Cr-$C_{carbene}$ σ bond. While, The Cr-$C_{carbene}$ π bond is actually a Cr-C-X three centre four electron π-bond having the π density largely located at both Cr and X. The same

difference in bond lengths in these carbenes between X = O and X = N is in the M – CO_{trans} bond.

Lee and Hu, [8] using DFT, examined the complexes of the type $Cr(CO)_5L$, L = N-heterocyclic carbenes (NHC), acyclic diaminocarbenes, Fischer and Schrock type carbenes and phosphines. They found that NHC-metal bonds are significantly stronger than those of phosphines. Imidazol-2-yielidenes and their C-C saturated imidazolin-2-ylidene counterparts demonstrate similar ligand-metal binding and gas phase proton affinity (PA). The CO exchange from $Cr(CO)_6$ by NHCs and carbenes is energetically favourable, while CO exchange for phosphines is unfavourable. NHC ligands facilitate carbonyl dissociation from the complexes to a larger extent than phosphines. The geometrical parameters and force constants of trans C-O in $Cr(CO)_5L$ complexes are closely related to ligand properties such as PA, electronegativity (χ) and charge transfer (ΔN). In addition They found that the nucleophilicity of ligands decreases in the order: $:C(N(I\text{-}Pr)_2)_2 > :C(NMe_2)_2 > PCy_3$, $:C(Me)(NMe_2)_2 > PPh_3$, $:C(Me)(NMe_2)_2$, $P(alkyl)_3 > PH_3$, $:C(OH)_2$, $:CH_2 > PF_3 > :CF_2$.

Goumans *et. al.*[9] explored the photochemistry of $Cr(CO)_5PH_3$ complexes using TD DFT calculations. The lowest excited states of $Cr(CO)_5PH_3$ are metal-ligand charge transfer (MLCT) in character of which the first three are repulsive for PH_3 but modestly bonding for the axial and equatorial CO ligands. The repulsive nature is due to mixing of the initial MLCT state with a ligand field (LF) state. A barrier is encountered along the dissociation coordinate if the avoided crossing between these states occurs beyond the equilibrium distance. This is the case of the expulsion of CO but for the PH_3 group as the avoided state crossing occurs within the equilibrium Cr - P distance. The nature of the phosphorus ligand in the Cr complex is only of the modest importance. Complexes containing the three-membered phosphirane or unsaturated phosphirene rings have dissociation curves for their lowest excited states that are similar to those having a PH_3 ligand. The main difference between substituted phosphines over PH_3 is their enhanced σ-donating ability. All calculations indicate that the excited $Cr(CO)_5L$ molecules (L = PH_3, $P(C_2H_5)_3$ or $P(C_2H_3)_3$) prefer dissociation of their phosphorus ligand over that of a CO ligand.

The recent study of Záliš *et al* [10] who used TD-DFT calculations to investigate the roles of the W→L and W→CO MLCT and LF excited states for $W(CO)_5(Pip)$ and $W(CO)_5(CNpy)$. They found that the molecular orbitals are largely delocalised and

the distribution of d-character is greater than predicated by simple LF arguments. With L is a strong π-acceptor (e.g. L = CNpy, Py) complexes the LUMO orbitals are predominantly located on the ligand (L) π^*-orbital. It is closely followed in energy by a set of low-lying cis CO π^* orbitals. When L is electron-saturated ligand (Pip) the complexes have a predominantly cis CO π^*-based LUMO, followed by molecular orbitals of the same cis π^*(CO) character. Orbitals with significant d (σ^*) contribution are also rather delocalised and lie at high energy, ≥7 eV above the HOMO.

So the low lying electronic transitions and excited states of $[W(CO)_5L]$ and related complexes are of a W→L and W→CO MLCT character. No LF transitions were found to occur in a spectroscopically relevant energy range up to 6-7 eV. The lowest excited states have MLCT (CO) character for weakly electron-accepting or saturated ligands L (Pip, Py) and MLCT (L) character for strongly accepting L (PyCN). Spectroscopy, photophysics and photochemistry of $[W(CO)_5L]$ and related complexes are described by the MLCT(L)/(CO) model in which the absorption, emission, and W-N bond dissociation are determined by closely lying MLCT(L) and MLCT(CO) excited states while the high-lying LF states play only an indirect photochemical role by modifying potential energy curves of MLCT(CO) states, making them dissociative.

5.1.2 Literature survey on the theoretical calculations of (η^6-arene)$Cr(CO)_3$

Fitzpatrick. [11] investigated the electronic structure of $(\eta^6\text{-}C_6H_6)Cr(CO)_3$ within an extended CNDO/2 formalism using both experimental and standard geometries. The computed trends for bond strengths and stretching frequencies and for reactivity (charge distributions) correlated with the experimental data. The extended CNDO/2 results seem more reasonable, for example the charge and the orbital populations on chromium, than are the ab intio single ξ results. A general agreement is observed between CNDO/2 and SCCC electronic structures.

Carroll and McGlynn[12], carried out charge and configuration self-consistent Mulliken-Wolfsbefg-Helmholz calculations on $(\eta^6\text{-}C_6H_5X)Cr(CO)_3$ (X = H, NH_2). The results have been used to describe the bonding in these molecules and to discuss the main features of their electronic spectra.

Brunvoll and Cyvin[13] reported the normal coordinate analysis of the whole molecule of (η^6-benzene)$Cr(CO)_3$. The calculations have revealed similar kinematic coupling phenomena to those previously described for transition metal sandwich complexes. Mean amplitudes of vibration (u), perpendicular amplitude correction coefficients (K) and selected shrinkage effects (δ) for (η^6-C_6H_6)$Cr(CO)_3$ are given which were calculated on the basis of this normal coordinate analysis. The u and δ values are compared with the corresponding quantities in related molecules, viz. free benzene, bis(benzene)chromium and chromiumhexacarbonyl.

Threshold photoelectron-photoion coincidences spectroscopy and DFT calculations have been used to investigate the dissociation kinetics of the benzene chromium tricarbonyl cation The dissociation of the [(η^6-benzene)$Cr(CO)_3$]$^+$ ion proceeds by the sequential loss of three CO and benzene ligands.

Suresh *et al*[14] studied the structural properties as well as subtle electronic effects occurring in (η^6-C_6H_5-X)$Cr(CO)_3$, X = H, NH_2, OH,CH_3, F, CHO, CN and NO_2 complexes at HF, B3LYP, and MP2 levels using the topographical properties of molecular electrostatic potential (MESP) as well as electron density. These calculations suggest that the arene ring in every system is highly deactivated, due to the complexation to chromium moiety. However, depending on the nature of the substituent, significant changes are observed in the MESP surrounding the carbonyl oxygen. These changes at the B3LYP level show good linear correlation with Hammet σ_p constants. In general, the strength of the complexation, the overall geometry of the complex, and the electron-accepting power of the $Cr(CO)_3$ moiety are connected with the electron-accepting/-releasing nature of the arene substituent.

Schleyer, *et al*, [15] used σ-π dissected nucleus independent chemical shift (NICS) calculations in the assessment of the ring currents in (η^6-benzene)$Cr(CO)_3$. Shielding contribution from the C-C(π) orbitals to the NICS values reveal that there is no quenching of ring current in benzene of (η^6-benzene)$Cr(CO)_3$. They concluded that $Cr(CO)_3$ complexation does not reduce the aromaticity of benzene.

5.2 Results

5.2.1 Computational Details

All calculations were carried out with the B3LYP density functional theory (DFT) approach as implemented in the Gaussian 98 [16] or Gaussian 03 [17] program packages using the following bases sets STO-3G, 6-31G, or LanL2DZ. A stepwise increase of the size of the bases set from STO-3G to LanL2DZ was the approach adopted for these calculations. In addition to these basis sets the more complicated bases set 6-311G(d',p') have been used in the DFT calculations of (η^6-aniline)$Cr(CO)_3$ complex . The visualisation of the results was achieved using GaussView[18] and extraction of some of the results (the contribution percentages of the orbitals of Cr, CO, and ligand are calculated) was performed by locally created Gaussum[19] software.

The DFT is found to be appropriate for chromium carbonyl chemistry as indicated by the good agreement for calculated vibration frequencies and excitation energies with experimental measurements. Geometries of the complexes $Cr(CO)_5L$, L = pyridine (Py), 4-acetylpyirdine (Acpy), 4-cyanopyridine (CNpy) and the complexes (η^6-arene)$Cr(CO)_3$, arene = benzene, aniline, anisole, benzaldehyde, or methyl benzoate were fully optimised at each model chemistry. The first three low lying excited states of the closed-shell complexes were calculated by the Time-Dependent DFT (TD-DFT).

In some cases, Haretree-Fock and restricted Haretree-Fock (HF and RHF) calculations were formed for the geometry optimisation for comparison with the results obtained with DFT calculations.

The results of geometry optimisation, vibrational frequencies, and the excitation energies of the first three low-lying excited states were then compared to the available experimental data. The Kohn-Sham density functions are expressed herein as molecular orbitals, although this not correct but this is commonly more understandable.

5.2.2 Theoretical calculations on the complexes of the type $Cr(CO)_5L$

5.2.2.1 The optimised geometries of the complexes of the type $Cr(CO)_5L$

Fig 5.1 shows the optimised structures of $Cr(CO)_5L$, L = Py, Acpy, or CNpy. The theory indicates that the complex has local C_{4v} geometry of $Cr(CO)_5$. In the

optimised structure has the angle between the plane of pyridine and the plane of the four carbonyl groups is 45 °.

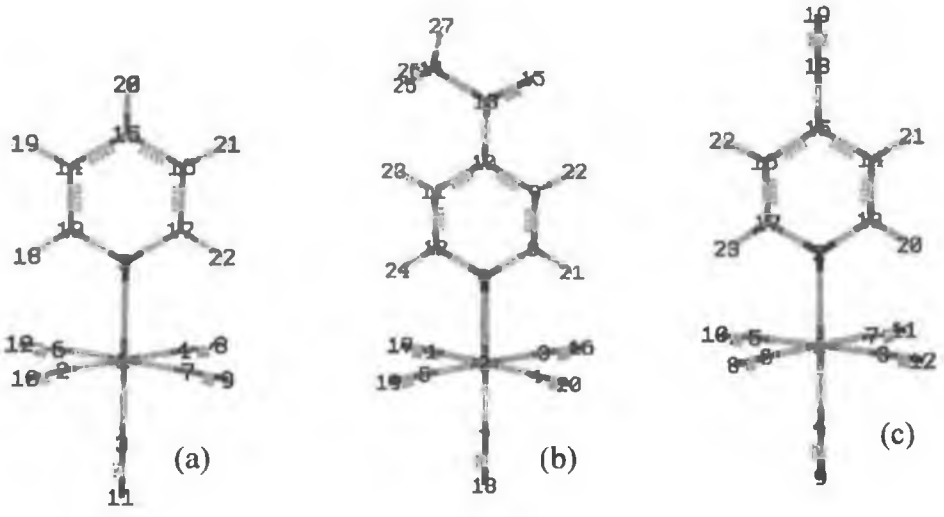

Fig 5.1 The optimised B3LYP/LanL2DZ geometry for (a) $Cr(CO)_5Py$,(b) $Cr(CO)_5Acpy$, (c) $Cr(CO)_5CNpy$.

Selected bond lengths and angles for the different theoretical methods and basis sets are summarised in Tables 5.1, 5.2, and 5.3 for pyridine acetylpyridine and cyanopyridine complexes respectively. Upon comparison of the calculated data with the experimental data, it seems that the calculations with B3LYP/LanL2DZ theory are closer to the experimental results for pyridine complex, than the results of HF/3-21G level. The trans M-C(CO) bonds are shorter than the cis-bonds for all of the complexes in the study. On the other hand C-O bonds for trans-CO ligands are longer than the cis-ligands. This gives very good indication of the back bonding between the Cr centre and trans-CO ligands is higher than cis CO ligands. This is the expected trend for substituted octahedral metal carbonyl complexes when the trans ligand is weaker π^*-acid ligand than CO.

As the acetylpyridine and cyanopyridine ligands are more π^*-acidic than pyridine ligand the Cr-N bond is shorter in these complexes than for pyridine complex.
The bond angles indicate that the four cis-CO ligands are slightly pushed out of plane.

	HF/ 3-21G	RHF/ LANL2DZ	B3LYP/ LANL2DZ	Experimental[20]	Deviation % B3LYP-Exp.
Bond lengths					
Cr1-C2or 4	1.9053(1.9054)	1.9672	1.8921	1.895, 1.902	0.16, 0.52
Cr1-C3	1.9034	1.9536	1.8567	1.824	1.79
Cr1-N5	2.2713	2.3153	2.1844	2.194	0.44
Cr1-C 6 or 7	1.9203,1.9202	1.9672	1.8921	1.905,1.906	0.68, 0.73
C-O(2,10) (4,8)	1.1421	1.1463	1.1796	1.132,1.137	4.2, 3.75
C3-O11	1.1393	1.1456	1.1832	1.153	2.62
N5C13, or 17	1.3398	1.3432	1.3645	1.403, 1.369	2.74, 0.33
C-O(6,12) (7,9)	1.1393	1.1463	1.1796	1.132, 1.137	4.20, 3.75
C-C(13,14) (16,17)	1.3776	1.3907	1.4023	1.4921,1.478	6.02, 5.12
C-H(13,18) (17,22)	1.067	1.0685	1.0831		
C-C(14,15) (15,16)	1.3825	1.3935	1.4063		
C-H(14,19)(16,21)	1.0695	1.07	1.0852		
C15-H20	1.0709	1.0713	1.0862		
Bond angles					
C2-Cr1-C3	88.8746	91.5575	89.8378	89.1	0.83
C2-Cr1-N5	91.1209	88.4388	90.1626	90.6	0.48
C2-Cr1-C6	90.194	90.7501	90.6168	90.1	0.57
C2-Cr1-C7	90.203	89.1787	89.3805	89.1	0.31
C3-Cr1-C4	88.8634	91.5621	89.8374	87.1	3.14
C3-Cr1-C6	99.8649	91.5532	89.843	87.8	2.33
C3-Cr1-C7	99.8638	91.554	89.8428	88.8	1.17
C4-Cr1-N5	91.1411	88.4417	90.1623	92.3	2.32
C4-Cr1-C6	90.1815	89.1684	89.3818	89.1	0.32
C4-Cr1-C7	90.1966	90.7336	90.6192	90.4	0.24
N5-Cr1-C6	80.1335	88.4442	90.1574	92.8	2.85
N5-Cr1-C7	80.1378	88.4486	90.1568	92.3	2.32
Cr1-N5-C13	120.8825	120.9588	121.2266	119.4	1.53
Cr1-N5-C17	120.8797	120.961	121.2265	118.8	2.04
C13-N5-C17	118.2378	118.0802	117.5469	120.0	2.04
N5-C13-C14	122.5562	122.8717	122.8799	120.6	1.89
N5-C13-H18	117.271	117.0195	116.642		
C14-C13-H18	120.1727	120.1088	120.4781		
C13-C14-C15	118.9142	118.7916	119.197	117.9	1.1
C13-C14-H19	119.7443	119.796	119.3724		
C15-C14-H19	121.3415	121.4124	121.4307		
C14-C15-C16	118.821	118.5932	118.2994	121.0	2.23
C14-C15-H20	120.5897	120.7034	120.8503		
C16-C15-H20	120.5893	120.7034	120.8503		
C15-C16-C17	118.9136	118.7917	119.197	118.6	0.50
C15-C16-H21	121.3412	121.4125	121.4307		
C17-C16-H21	119.7452	119.7959	119.3724		
N5-C17-C16	122.5572	122.8716	122.8799	119.0	3.26
N5-C17-H22	117.2695	117.0198	116.6419		
C16-C17-H22	120.1734	120.1086	120.4782		

Table 5.1 Comparisons of selected bond lengths and bond angles of $Cr(CO)_5Py$ with the experimental data obtained from Ref. (20).

	RHF/ 3-21G	RHF/ LANL2DZ	B3LYP/ LANL2DZ
Bond lengths			
Cr2-N6	2.2586	2.3151	2.174
Cr2-C1, or 5	1.7706	1.9664	1.8921
Cr2-C3, or 4	1.7343(1.756)	1.9693(1.9692)	1.8938
Cr2-C7	1.7552	1.9561	1.8589
C-O (1,17) or (5,19)	1.1707(1.1704)	1.1463	1.1794
C-O (3,16) or (4,20)	1.1719, 1.172	1.1457	1.1789
C7-O18	1.1722	1.1451	1.1824
C6-C8	1.3619	1.3445	1.3677
C8-C9	1.3822	1.3877	1.3978
C9-C10	1.3926	1.3964	1.4112
C10-C13	1.5325	1.5056	1.5104
C13-C14	1.5391	1.5102	1.5176
C13-O15	1.2216	1.2233	1.2514
C8-H21	1.0855	1.068	1.0827
C9-H22	1.0827	1.0691	1.0848
C14-H25 or 26	1.0864	1.0837	1.0982
C14-H27	1.0851	1.0786	1.0922
Bond angles			
C1-Cr2-C3	127.4824	89.1958	89.4359
C1-Cr2-C5	92.1142	90.7614	90.5507
C1-Cr2-N6	81.8807	88.4748	90.2497
C1-Cr2-C7	72.0961	91.4958	89.7587
C3-Cr2-C4	96.1321	90.7164	90.5785
C3-Cr2-N6	72.9283	88.5813	90.2736
C3-Cr2-C7	96.1653	91.446	89.7184
C4-Cr2-C5	72.1554	89.1753	89.4302
C4-Cr2-C6	136.9623	88.5741	90.272
C4-Cr2-C7	84.8097	91.4553	89.7197
C5-Cr2-C6	81.9785	88.4843	90.2508
C5-Cr2-C7	131.6214	91.4884	89.7572
C10-C13-O15	119.647	119.176	119.3924
C10-C13-C14	117.9513	119.6103	119.1187

Table 5.2 Comparisons of selected bond lengths and bond angles of $Cr(CO)_5$Acpy

	RHF/ 3-21G	RHF/ LANL2DZ	B3LYP/ LANL2DZ
Bond lengths			
Cr1-N2	2.2754	2.3191	2.1728
Cr1-C5	1.9062	1.9684	1.8935
Cr1-C4	1.9078	1.9591	1.8602
Cr1-C6 or-C7	1.9208	1.9684	1.8935
N2-C13,or -C17	1.3385	1.3419	1.3656
CO(3,12) (5,10)	1.1418	1.1459	1.1789
C4-O9	1.1382	1.1445	1.1818
CO(6,8)(7,11)	1.1391	1.1459	1.1789
CC(13,14)(16,17)	1.3773	1.3895	1.3992
CH(13,20) (17,23)	1.0665	1.0677	1.0825
CC(14,15)(15,16)	1.3856	1.3948	1.4121
CH(14,21)(16,22)	1.069	1.0694	1.0844
C15-C18	1.4278	1.4411	1.4386
C18-N19	1.1391	1.1516	1.1816
Bond angles			
N2-Cr1-C3	91.0387	88.5962	90.344
N2-Cr1-C5	91.0382	88.5977	90.3443
N2-Cr1-C6	80.4321	88.6101	90.3439
N2-Cr1-C7	80.442	88.6065	90.3432
C3-Cr1-C4	88.9616	91.403	89.6559
C3-Cr1-C6	90.1816	89.1918	89.4397
C3-Cr1-C7	90.1636	90.7407	90.5564
C4-Cr1-C5	88.9614	91.4031	89.6559
C4-Cr1-C6	99.5396	91.3947	89.6569
C4-Cr1-C7	99.5863	91.3886	89.656
C5-Cr1-C6	90.1821	90.7363	90.5552
C5-Cr1-C7	90.1628	89.1949	89.4405
Cr2-N1-C13	120.7798	120.8815	121.3252
Cr1-N2-C17	120.7803	120.8806	121.3251
C13-N2-C17	118.4399	118.2379	117.3497
N2-C13-C14	122.5853	122.895	123.1507
N2-C13-H20	117.4648	117.1662	116.6553
C14-C13-H20	119.9499	119.9388	120.1939
C13-C14-C15	118.7424	118.594	119.1225
C13-C14-H21	120.2846	120.1897	119.86
C15-C14-H21	120.973	121.2163	121.0175
C14-C15-C16	118.9046	118.7841	118.1038
C14-C15-C18	120.5478	120.6079	120.9481
C15-C16-C17	118.7424	118.594	119.1225
C15-C16-H22	120.973	121.2163	121.0175
C17-C16-H22	120.2846	120.1897	119.86
N2-C17-C16	122.5854	122.895	123.1507
N2-C17-H23	117.4648	117.1662	116.6553
C16-C17-H23	119.9499	119.9388	120.1939

Table 5.3 Comparisons of selected bond lengths and bond angles of $Cr(CO)_5CNpy$

5.2.2.2 Vibrational analysis of electronic ground state. The frequency calculation on $Cr(CO)_5L$ is primarily to check for negative frequencies which would indicate that the structure is not in the global minimum of the potential surface. All the frequencies were positive and this provides assurance that the calculated geometry in the global minimum of potential surface for that the particular model chemistry. As the theoretical results obtained for $[(Cr(CO)_5L]$ complexes have a C_{4v} local symmetry. This would indicate three IR-active ν(CO) vibrations, $2A_1 + E$. IR spectra are dominated by a strong E band. A weak A_1^2 band, which is predominantly due to an in-phase stretching vibration of the four cis CO ligands, and occurs as a weak feature at higher frequencies. The A_1^1 ν(CO) vibration, which involves mainly the trans CO ligand, manifests itself by shoulder on the low-energy side of the E band. Tables 5.4, 5.5 and 5.6 compare the experimental and calculated ν(CO) wavenumbers of $[(Cr(CO)_5Py]$, $[(Cr(CO)_5Acpy]$, and $[(Cr(CO)_5CNpy]$, respectively. The agreement between calculated is reasonable, although DFT calculations somewhat overestimated. In the actual C_{2v} symmetry of $[(Cr(CO)_5Py]$ and $[(Cr(CO)_5CNpy]$, the E-mode is split into two closely spaced modes $B_1^2 + B_2$, both of which are IR-active.

IR active band Calculated B3LYP/ LanL2DZ	Experimental (Pentane)	Assignment
481		δ(CCC) or δ(CNC) of pyridine
482		δ(CrCO)
484		δ(CCC) or δ(CNC) of pyridine+ δ(CrCO)
488		out of plane δ(CrCO)+ δ(CrCO)trans Cr-CO
558		in plane δ(CrCO)
575, 580		δ(CrCO)
656, 683		in plane δ(CCH), δ(CCC) or δ(CNC) of pyridine
696		in plane δ(CCH) of pyridine+δ(CrCO)
699, 714		δ(CrCO)
746, 805		out of plane δ(CCH), δ(CCC) or δ(CNC) of pyridine
1002		out of plane δ(CCH), δ(CCC) or δ(CNC) of pyridine
1035		ring breathing of pyridine
1074		out of plane δ(CCH), δ(CCC) or δ(CNC) of pyridine
1082		in plane δ(CCH), δ(CCC) or δ(CNC) of pyridine
1113		in plane δ(CCH), δ(CCC) or δ(CNC) of pyridine
1119		in plane δ(CCH), δ(CCC) or δ(CNC) of pyridine
1226		in plane δ(CCH) of pyridine
1288		in plane δ(CCH) of pyridine
1331		in plane δ(CCH), δ(CCC) or δ(CNC) of pyridine
1433		in plane δ(CCH), δ(CCC) or δ(CNC) of pyridine
1510		in plane δ(CCH), δ(CCC) or δ(CNC) of pyridine
1545		in plane δ(CCH), δ(CCC) or δ(CNC) of pyridine
1643		in plane δ(CCH), δ(CCC) or δ(CNC) of pyridine
1673		in plane δ(CCH), δ(CCC) or δ(CNC) of pyridine
1950		Asymmetric ν(CO)
1950		Asymmetric ν(CO) for cis CO ligands
1952	1921	Asymmetric ν(CO) for cis CO ligands
1977	1940	Asymmetric ν(CO) for cis CO ligands
2064	2069	Symmetric ν(CO)
3284		Asymmetric ν(CH)
3299		Asymmetric ν(CH)
3309		Asymmetric ν(CH)
3323		Asymmetric ν(CH)
3331		Symmetric ν(CH)

Table 5.4 IR frequencies of $Cr(CO)_5Py$ calculated from B3LYP/LanL2DZ level of theory, scaled by (1.02021).

IR active band Calculated B3LYP/ LanL2DZ	Experimental (Pentane)	Assignment
368		δ(CrCO) of cis-CO ligands in plane
410		Symmetric ν(CrC) of cis-CO ligands
416		δ(CCC)and δ(CNC) of L in plane
420		δ(CrCO) of cis-CO ligands out of plane
422		Asymmetric ν(CrCO) of cis-COs+δ(CCC), δ(CNC) of L out plane
423, 480		δ(CrCO)
482, 483		δ(CrCO) + δ(CCC) and δ(CNC) of L
486, 488		δ(CCC) and δ(CNC) of L+δ(CrCO)
552		δ(CrCO) of cis-CO ligands out of plane
557		δ(CrCO) of cis-CO ligands in plane
572, 579		δ(CrCO)
605, 636		δ(CCC) and δ(CNC)
695		δ(CrCO)+δ(CCC)and δ(CNC) of L
696		δ(CCC)and δ(CNC) in plane of L +δ(CrCO) of trans-CO
698		δ(CCC) and δ(CNC) in plane of L+δ(CrCO)
712		δ(CrCO)
776, 788, 893		δ(CCC) and δ(CNC) of L
941		δ(CCH) out of plane of L
1002		δ(HCH) of methyl group
1040		δ(CCC) and δ(CNC) of L
1040		δ(CCC) and δ(CNC) in plane of L
1061, 1093		δ(HCH) of methyl group + δ(CCH) of L
1105		δ(CCH) in plane of L
1143, 1161		δ(HCH) of methyl +δ(CCH) of L
1285, 1324		δ(CCH) in plane of L
1332		δ(CCH) of L + δ(HCH) of methyl group
1403		δ(CCH) in plane of L
1459		δ(HCH) of methyl group
1485		δ(CCH) in plane of L
1524, 1539		δ(HCH) of methyl group
1557		δ(CCH) in plane of L
1619, 1678		ν(C-C) and ν(C-N)of L+ δ(CCH) of L
1704		ν(C-O) of Acetyl group+ δ(CCH) of L
1953		Asymmetric ν(C-O) of $Cr(CO)_5$ moiety
1955		Asymmetric ν(C-O) of cis-CO ligands
1955	1926	Asymmetric ν(C-O) of $Cr(CO)_5$ moiety
1980	1942	Asymmetric ν(C-O) of cis-CO ligands
2065	2069	Symmetric ν(C-O) of $Cr(CO)_5$ moiety
3110		Symmetric ν(C-H) of methyl group
3189, 3250		Asymmetric ν(C-H) of methyl group
3303, 3307, 3326		Asymmetric ν(C-H) of pyridine ring
3332		Symmetric ν(C-H) of pyridine ring

Table 5.5 IR frequencies of $Cr(CO)_5$Acpy calculated from B3LYP/LanL2DZ level of theory, scaled by (1.02021)

IR active bands Calculated B3LYP/ LanL2DZ	Experimental in CH_2Cl_2	Assignment
217		δ(CCC) of L out of plane
232		δ(CCC) of L in plane
407		δ(CrCO) of cis-CO ligands out of plane
410		Symmetric ν(CrC) of cis-CO ligands
422, 450, 480		δ(CrCO)
482		δ(CrCO)+ δ(CCC)and δ(CNC) of L
482		δ(CrCO)
497		δ(CCC)and δ(CNC) of L
556		δ(CCC)and δ(CNC) out of plane of L
571		δ(CrCO) of cis-CO ligands in plane
575		δ(CrCO)
578		δ(CCC)and δ(CNC) of L +δ(CrCO) of trans-CO
609		δ(CrCO)+ δ(CCC)and δ(CNC) of L
694		δ(CCC)and δ(CNC) out of plane of L
698		δ(CrCO)+ δ(CCH) of L
702		δ(CrCO)
712		δ(CCC)and δ(CNC) of L
785		δ(CrCO)
812		δ(CCC), δ(CCH), and δ(CNC) in plane of L
905		δ(CCC)and δ(CNC) out of plane of L
1037		δ(CCC)and δ(CNC) in plane of L
1042		δ(CCH) out of plane of L
1108, 1158		δ(CCH) in plane of L
1263, 1297		δ(CCH) in plane of L
1317		δ(CCH), δ(CCC)and δ(CNC) in plane of L
1404, 1485		δ(CCH) in plane of L
1556		δ(CCH) in plane of L
1606, 1679		δ(CCH), δ(CCC)and δ(CNC) in plane of L
1955, 1956		Asymmetric ν(C-O) of cis-CO ligands
1958	1912	Asymmetric ν(C-O)
1981	1943	Asymmetric ν(C-O) of cis-CO ligands
2066	2070	Symmetric ν(C-O) of cis-CO ligands
2321		ν(C-N) of cyano group
3308, 3310		Asymmetric ν(C-H) of L
3331		Asymmetric ν(C-H) of L
3337		Symmetric ν(C-H) of L

Table 5.6 IR frequencies of $Cr(CO)_5CNpy$ calculated from B3LYP/LanL2DZ level of theory, scaled by 1.02021, L = CNpy.

5.2.2.3 Ground-state Electronic Structures of $Cr(CO)_5L$, L = Py, Acpy, or CNpy

The ground-state electronic structures for all complexes were calculated to determine the energies and compositions of the molecular orbitals. The orbitals are plotted according to their energies. The type of each MO was assigned on the basis of its composition and by inspection of its three-dimensional representation.

Generally, the properties of each molecular orbital for all of the three complexes are independent of the substituent on the pyridine ring, thus the orbitals of pyridine complex have the same properties as the corresponding orbitals of acetylpyridine or cyanopyridine complex. The molecular orbitals are in general stabilised upon substitution on pyridine ring by either acetyl or cyano group. The exceptions to this are the molecular orbitals H-3 and L+6 (see Section 5.3). The molecular orbitals of the cyanopyridine complex are the most stable, Table 5.7 and Fig. 5.2.

MO	Py complex	Acpy complex	CNpy complex
L+7	-0.33	-0.5	-0.64
L+6	-0.35	-0.84	-0.65
L+5	-0.87	-1.02	-1.19
L+4	-1.32	-1.46	-1.61
L+3	-1.34	-1.51	-1.64
L+2	-1.82	-2.02	-2.34
L+1	-2.04	-2.17	-2.36
LUMO	-2.28	-3.36	-3.4
HOMO	-6.35	-6.49	-6.65
H-1	-6.42	-6.57	-6.73
H-2	-6.73	-6.87	-7.02
H-3	-8.49	-7.98	-9.11

Table 5.7 The molecular orbitals of $Cr(CO)_5L$ complexes, L = Py, Acpy, or CNpy and their energies. HOMO: the highest occupied molecular orbitals and LUMO: the lowest occupied molecular orbitals. The numbering H-1 is the orbital with number of HOMO-1 and the L+1 is the orbital with number of LUMO orbital + 1 and so on.

The low energy occupied MOs H-4, H-3 (i.e. MOs number 59 and 60 respectively in pyridine complex) are mainly centred on the pyridine ligand. They correspond to the e_{1ga} and e_{1gb} orbitals of the pyridine (see Fig 1.6 in Chapter I for a description of these MOs). The orbital which corresponds to e_{1ga} in the free pyridine ligand is slightly bonding with respect to the Cr atom while the e_{1gb} orbital is nonbonding with respect to the Cr d-orbitals. It would appear that the orbital, which corresponds to the e_{1ga} assignment in pyridine, is stabilised by – 0.73 eV by this bonding relative to that with e_{1gb} assignment. Hence, these orbitals are no longer degenerate as a result of this bonding.

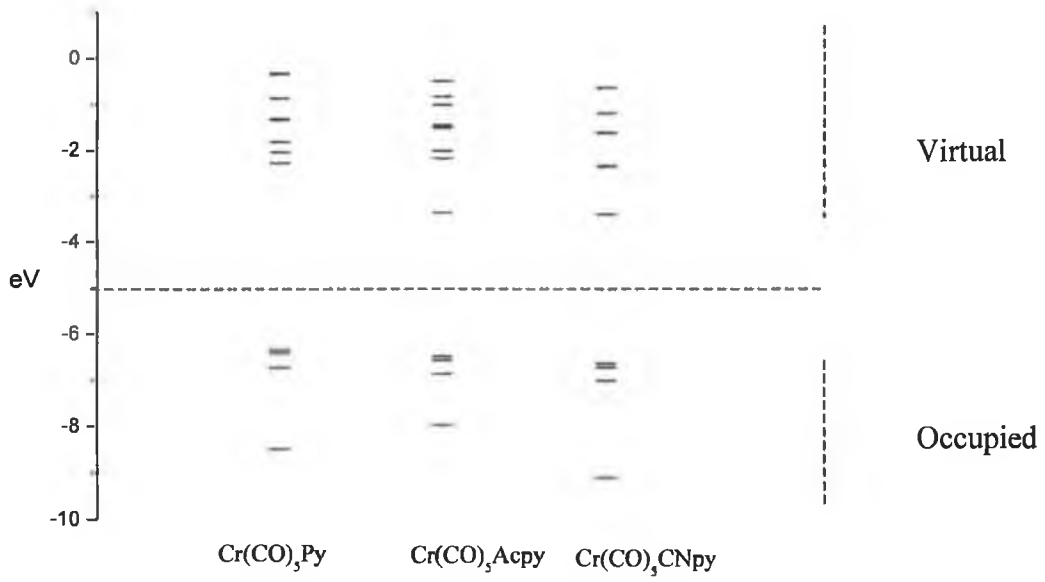

Fig 5.2 The energy level diagram of molecular orbitals of $Cr(CO)_5L$ complexes, L = Py, Acpy, or CNpy.

The H-2 orbital is a combination of 60 % chromium d-orbital and 39 % cis-CO. The other two highest occupied MOs (H-1, and HOMO) (for example 63, and 62 in pyridine complex) are mainly chromium d-orbital in character (ca. 60% character) which bonds with the trans-CO ligand, the trans-CO ligand has 20 % contribution to these orbitals and are non bonding relative to pyridine ligand, (Table 5.8). This is consistent with Záliš *et al*[10], who reported the DFT calculations of $W(CO)_5L$ and found the HOMOs were largely (60 %) metal (tungsten) d_π–orbitals in origin, yet had significant density on the cis carbonyl ligands (20%).

Our results are also in agreement with the DFT study of $Cr(CO)_5PPH_3$ by Goumans *et. al.*[9] wherein the highest occupied MOs were mainly of the metal character and were π antibonding, and with the recent studies on other substituted group 6 metal carbonyl complexes that for it is the pyridine ligands to which the metal is π antibonding, Fig 5.3, 5.4 and 5.5 .

MO no. and assignment		eV	Cr %	CO_{cis} %	CO_{trans} %	Py %
67	L+3	-1.34	4	94	1	2
66	L+2	-1.82	0	16	0	84
65	L+1	-2.04	18	78	1	3
64	LUMO	-2.28	1	2	2	96
63	HOMO	-6.35	64	20	12	4
62	H-1	-6.42	67	20	12	1
61	H-2	-6.73	61	39	0	0
60	H-3	-8.49	0	0	0	100

Table 5.8 The contribution of chromium, pyridine and CO orbitals in the complex $Cr(CO)_5Py$ for different selected molecular orbitals. The numbering H-1 is the orbital with number of HOMO-1 and the L+1 is the orbital with number of LUMO orbital + 1 and so on.

MO		eV	Cr %	CO_{cis} %	CO_{trans} %	Acpy %
78	L+3	-1.51	4	92	1	3
77	L+2	-2.02	0	14	0	85
76	L+1	-2.17	18	78	1	3
75	LUMO	-3.36	1	1	1	97
74	HOMO	-6.49	64	19	11	5
73	H-1	-6.57	68	20	12	1
72	H-2	-6.87	61	38	0	0
71	H-3	-7.98	0	0	0	100

Table 5.9 The contribution of chromium, acetylpyridine and CO orbitals in the complex $Cr(CO)_5Acpy$ for different selected molecular orbitals.

MO		eV	Cr %	CO_{cis} %	CO_{trans} %	CNpy %
73	L+3	-1.64	4	94	1	1
72	L+2	-2.34	18	78	1	3
71	L+1	-2.36	0	10	0	90
70	LUMO	-3.4	1	1	1	97
69	HOMO	-6.65	64	19	11	5
68	H-1	-6.73	68	20	11	1
67	H-2	-7.02	62	38	0	0
66	H-3	-9.11	0	0	0	100

Table 5.10 The contribution of chromium, cyanopyridine and CO orbitals in the complex $Cr(CO)_5CNpy$ for different selected molecular orbitals.

In our calculations, the LUMO has mainly pyridine π^* character. The L+1 MO shows a high localisation (ca 80 %) on the cis-carbonyl ligands with considerable contribution from Cr d-orbitals (20 %)

The L+2 M.O. is localised (84 %) on the pyridine ligand with a small contribution of cis-CO orbitals (16 %). The pyridine orbitals that contribute in the molecular orbitals

LUMO and L+2 correspond to the orbitals of the free ligand e_{2ub}, e_{2ua}. The properties of L+1 and L+2 have altered from pyridine and acetyl pyridine complex to cyanopyridine complex.

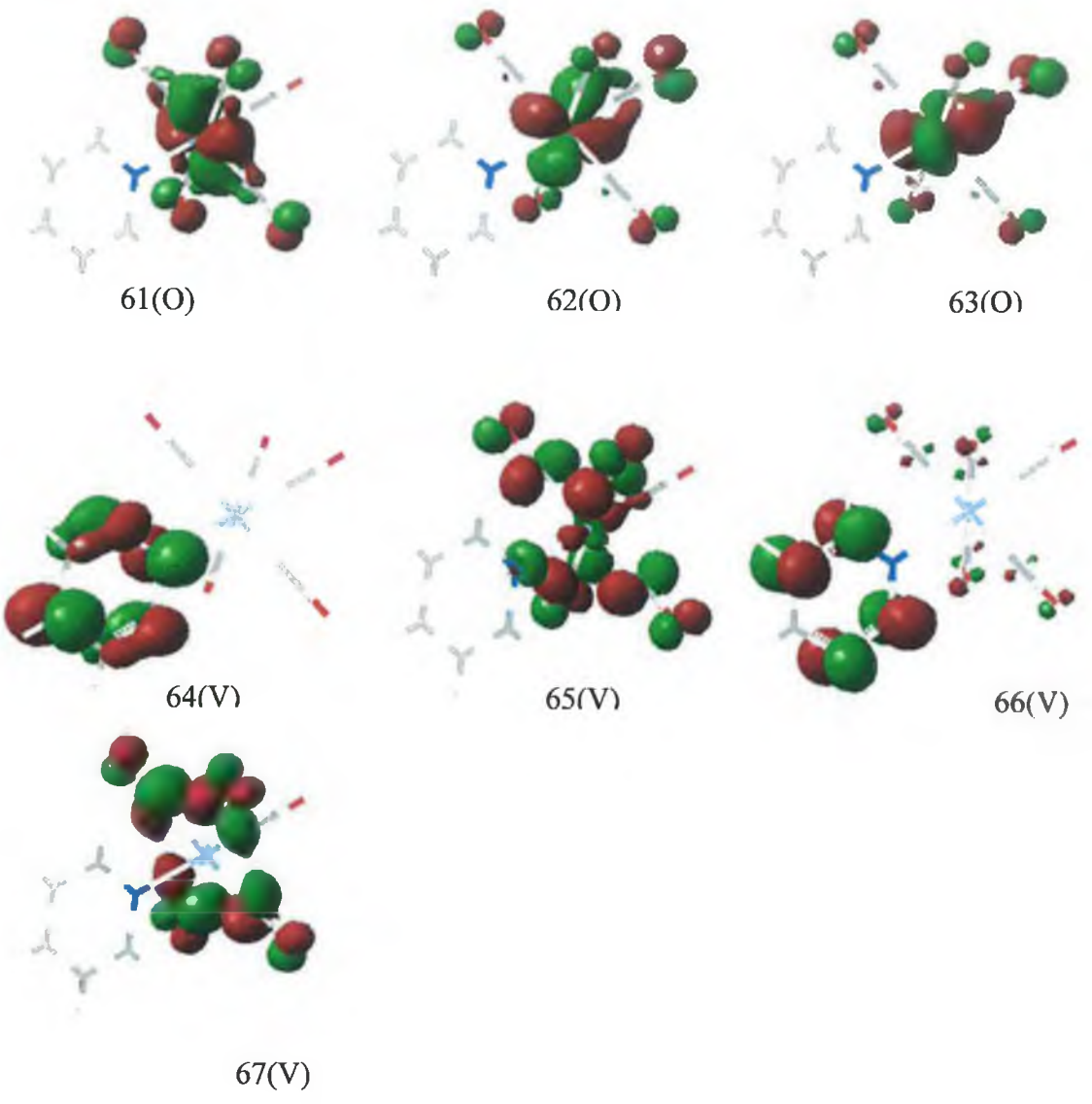

Fig 5.3 Selected molecular orbitals of $Cr(CO)_5Py$

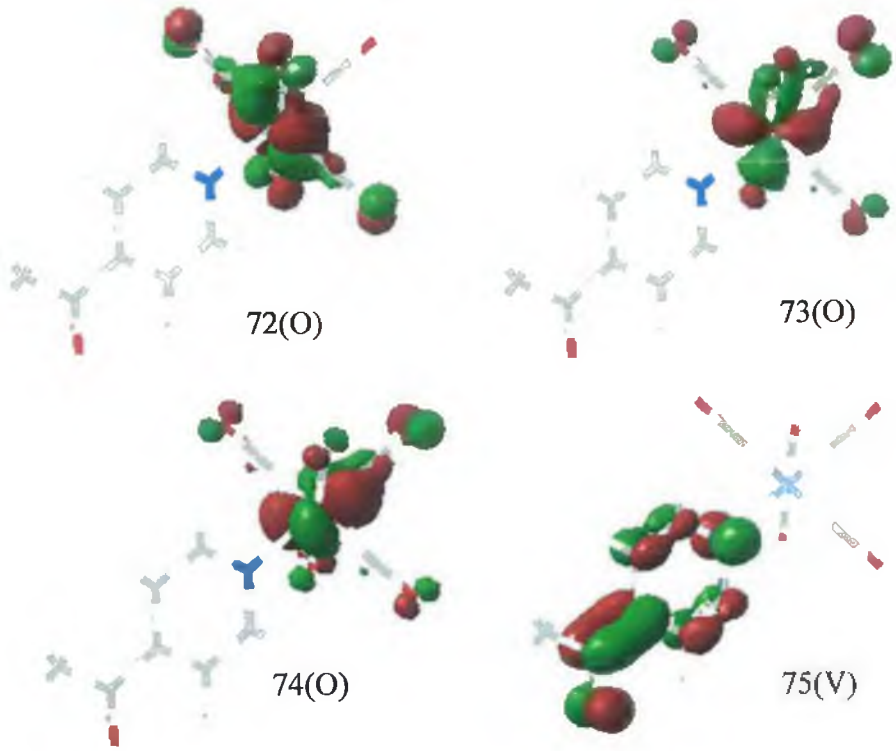

Fig 5.4 Selected molecular orbitals of $Cr(CO)_5Acpy$

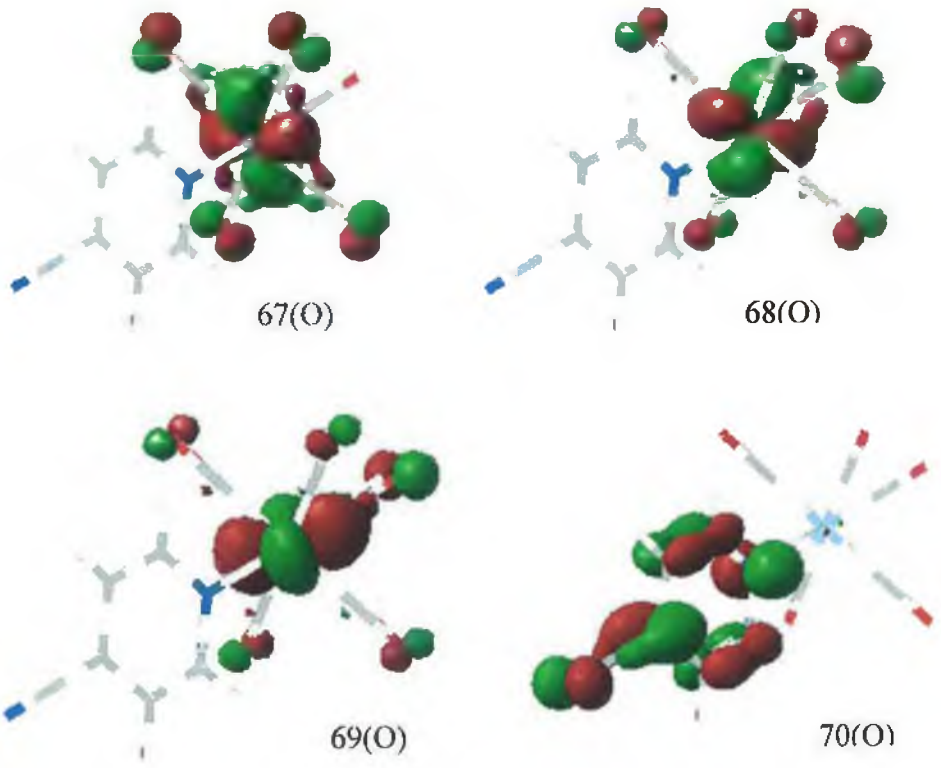

Fig 5.5 Selected molecular orbitals of $Cr(CO)_5CNpy$

The orbital e_{2ub} is stabilised by bonding with the metal relative to e_{2ua}, which cannot form a bond with the metal. This clearly is the reason for the loss of degeneracy in these molecular orbitals relative to those of the free ligand.

The orbitals are described more quantitatively in Table 5.7. From the energies listed, we note that there is HOMO-LUMO gap of 4.07, 3.13, 3.25 eV for pyridine, Acpy, and CNpy complexes respectively. The decrease in the gapes because the LUMO is mainly pyridine ring π^* in character and is effected by electron withdrawing substituents. However, HOMO is mainly chromium d-orbital in character and is relatively unaffected by substituents on the pyridine ring.

5.2.2.4 Time-Dependent DFT Calculations of singlet excited states.

Having used DFT to calculate the ground state structure of the complexes, the time-dependent calculations on $Cr(CO)_5L$ complexes, L = Py, Acpy, or CNpy were undertaken to determine the energy and the nature of the low lying excited states. The energy of each excited state is the vertical excitation energy in electron-volts (eV) from the ground state. The transitions along with the oscillator strengths are listed in Tables 5.11, 5.12, 5.13. There are some singlet-excited states with zero oscillator strengths. These states, although present in the molecule's excited-state manifold, do not contribute significantly to the compound's absorption cross-section.

A commonly used model of an excited state corresponds to excitation of an electron from an occupied to a virtual MO (i.e. a one-electron transitions). However, the excited states calculated herein demonstrate that excited-state electronic structures are best described in terms of multielectronic states, where, a linear combination of several occupied-to-virtual MO excitations comprises a given electronic transition. Assignment of the character of each excited state was based on the compositions of the occupied and virtual MOs of the dominant excitation(s) for that excited state. For example when the occupied orbital is metal-based and virtual orbital is ligand π^*-based, the transition is designated a metal-to-ligand charge transfer (MLCT). Similarly, when the occupied orbital is localized on a ligand and the virtual orbital type is ligand π^*, the transition is designated LBCT (Ligand-Based Charge Transfer, corresponding to either intra- or inter-ligand charge transfer). For the majority of the excited states calculated, such assignments can be unambiguously made. However, excited states 2 and 3 exhibit comparable LBCT and MLCT contributions; we refer to these excited states as having a mixed character.

State	E (eV) (nm)[a]	f[b]	$\Psi_o \rightarrow \Psi_v$[c]	Character[d]
1	3.1616 (392.16)	0.013	HOMO→L+1(83 %), H-2→L+3 (8%)	Cr-d_{xz}→ π^*CO_{cis}, Cr-d_{xz}→d_z^2 Cr-d_{xy}→ π^*CO_{cis}, COBCT
2	3.3247 (372.92)	0.0	H-1→LUMO (98%)	Cr-d_{yz}+trans-CO→π^*Py
3	3.3724 (367.64)	0.0289	H-2→L+1 (65%), HOMO→LUMO (28%)	Cr-d_{xy}→π^*CO_{cis}, Cr-d_{xy}→d_z^2, CO-PyCT Cr-d_{xz}→ π^*Py, CO-PyCT

Table 5.11 Selected Calculated Singlet Excited States For $Cr(CO)_5Py$.

State	E (eV) (nm)[a]	f[b]	$\Psi_o \rightarrow \Psi_v$[c]	Character[d]
1	2.5270 (490.63)	0.0000	H-1 → LUMO(99%)	Cr-d_{yz}+trans-CO→π^*Acpy, LBCT
2	2.6386 (469.88)	0.1434	HOMO→LUMO(93%)	Cr-d_{xz}→π^*Acpy, CO→AcpyCT
3	2.8421 (436.24)	0.0001	H-2→LUMO(99%)	Cr-d_{xy} →π^*Acpy, LBCT

Table 5.12 Selected Calculated Singlet Excited States For $Cr(CO)_5$ Acpy.

State	E (eV) (nm)[a]	f[b]	$\Psi_o \rightarrow \Psi_v$[c]	Character[d]
1	2.5813 (480.31)	0.0	H-1→LUMO(99%)	Cr-d_{yz}+ CO_{trans}→π^*CNpy, CO→CNpyCT
2	2.7203(455.78)	0.1525	HOMO→LUMO (92%)	Cr-d_{xz}→π^*CNpy, CO_{cis}→CNpyCT
3	2.8958 (428.15)	0.0001	H-2 → LUMO (99%)	Cr-d_{xy}→π^*CNpy, CO_{cis}→CNpyCT

[a] Energy relative to the ground state (vertical excitation), [b] Oscillator strength. [c] Occupied (Ψ_o) to virtual (Ψ_v) orbital excitation. [d] Character of excited state: metal-to-ligand charge transfer (MLCT) or Ligand based Charge transfer (LBCT, either intra-or inter-ligand charge transfer).

Table 5.13 Selected Calculated Singlet Excited States For $Cr(CO)_5CNpy$

In acetylpyridine and cyanopyridine complexes there is one designated orbital in the three calculated low lying excited states. This orbital is LUMO which is purely centred on the π^*-system of the ligand, so the expected main effect of these transitions are Cr-LCT.

HOMO→LUMO this transition appears as a pure component of the second excited state for both acetyl- and a cyano-pyridine complex while it partially contributes in the third excited state (contribution is 28%) of the pyridine complex. This transition is allowed in the three cases as shown from the comparison of the oscillator strengths of this transition. This transition is expected to be allowed because both the initial orbital d_{xz} on the metal and the designated π^*-orbital on pyridine ligand are in the same phase. As this transition involves the drift of the electrondensity from the chromium to the pyridine ligand, the expected effect of this transition is oxidising the metal centre and this will reduce the Cr-Py and Cr-CO_{trans} π-bonding resulting in the lengthening of these bonds in the excited state. So, this excited state may involve the rupture of pyridine or trans-CO ligands to form the coordinatively unsaturated $Cr(CO)_5$ or trans-$Cr(CO)_4Py$ species respectively.

HOMO→L+1 this involves mainly the transition of the electron density from the predominantly metal d_{xz} orbital (which is bonding with the trans-CO ligand) to π^*-orbitals of the four cis-CO ligands and ligand field (LF) from the d_{xz} to d_z^2 orbital which is non bonding to the four cis-CO ligands and antibonding (σ^*) to the pyridine ligand. So the expected excited state to be repulsive to pyridine ligand and will relax to form the coordinatively unsaturated species $Cr(CO)_5$ with C_{4v} symmetry.
So, this transition dominated by the M-CO_{cis} charge transfer with ca. 18 % LF transition (d_{xz} to d_z^2 transition) and some LBCT transition. This transition would labilise the cis-CO ligands and to a lesser extent the pyridine ligand.

The (H-1) to LUMO excitation which corresponds to the excited state no 2 for pyridine- and in no. 1 for both acetylpyridine- and cyanopyridine-complexes is not greatly different to the HOMO to LUMO transition (*vide supra*). H-1→LUMO (98%) in the three cases although it is represent purely (98 %) Cr-L CT to the pyridine ligand and drifting the electrondensity from Cr, which is bonding with the trans CO ligand. The expected effect is the oxidation of the metal in the excited state and ultimately the expected lablising of trans CO ligand, but as the oscillator strength for this transition is zero, is not allowed in the three cases (Pyridine, acetyl and cyanopyridine complexes). The transition is prohibited (not allowed) because both the initial orbital d_{yz} on the metal and the designated π^*-orbital on pyridine ligand are

not in the same phase (perpendicular on each other) and this will not allow the electron density to transfer between the two parts.

H-2 → LUMO this transition is appeared in the acetylpyridine and cyanopyridine complex excited states and it is very week as reflected from the comparison of the oscillator strengths of the third excited state of both complexes (0.0001). As explanation of that, the d_{xy} orbital of the metal is partially not in the same phase of the designated π^*-orbital on pyridine ligand. This transition transfers the electrondensity from d_{xy} of the chromium, which is bonding with the four cis-CO ligands to the π^*-orbital on pyridine ligand and this will reduce the bond order of the Cr-CO_{cis} and oxidise the chromium in the excited state. Lengthen of Cr-CO_{cis} bond and the excited state dynamic may expected to relax toward the loss of one of the cis-CO ligands to form $Cr(CO)_4L$ with *Cs* symmetry, but as the oscillator strength is too low the quantum yield of this photoproduct expected to be low.

H-2→L+1 this involves mainly the transition of the electrondensity from the metal d_{xy} (which is bonding to the four cis-CO ligands) to π^*-orbitals of the four cis-CO ligands and ligand field (LF) from the d_{xy} to d_z^2 orbital which is non bonding to the four cis-CO ligands and antibonding (σ^*) to the pyridine ligand. So the expected excited state to be repulsive to both pyridine and cis-CO ligands and will relax to form the coordinatively unsaturated species $Cr(CO)_5$ with C_{4v} symmetry or $Cr(CO)_4Py$ with *Cs* symmetry.

H-2→L+3 this involves the transition of the electrondensity from the metal d_{xy} (which is bonding to the four cis-CO ligands) to (L+3) which is mainly centred on π^*-orbitals of the four cis-CO ligands. So the expected excited state is repulsive to both pyridine and cis-CO ligands and will relax to form the coordinatively unsaturated species $Cr(CO)_5$ with C_{4v} symmetry or $Cr(CO)_4Py$ with *Cs* symmetry.

Experimentally the photoproducts found upon excitation of these complexes are the coordinatively unsaturated species $Cr(CO)_5$ with C_{4v} symmetry and $Cr(CO)_4L$ with *Cs* symmetry and no photoproduct resulted from the loss of trans-CO ($Cr(CO)_4L$ with C_{4v} symmetry).

5.2.3 Theoretical calculation on the complexes of the type (η^6-arene)$Cr(CO)_3$

5.2.3.1 the optimised geometries of the complexes of the type (η^6-arene)$Cr(CO)_3$

Fig 5.6 shows the optimised structures of (η^6-arene)$Cr(CO)_3$, (arene = benzene, aniline, anisole, benzaldehyde, or methylbenzoate). The theory indicates that these complexes have the local C_{3v} geometry of $Cr(CO)_3$ moiety.

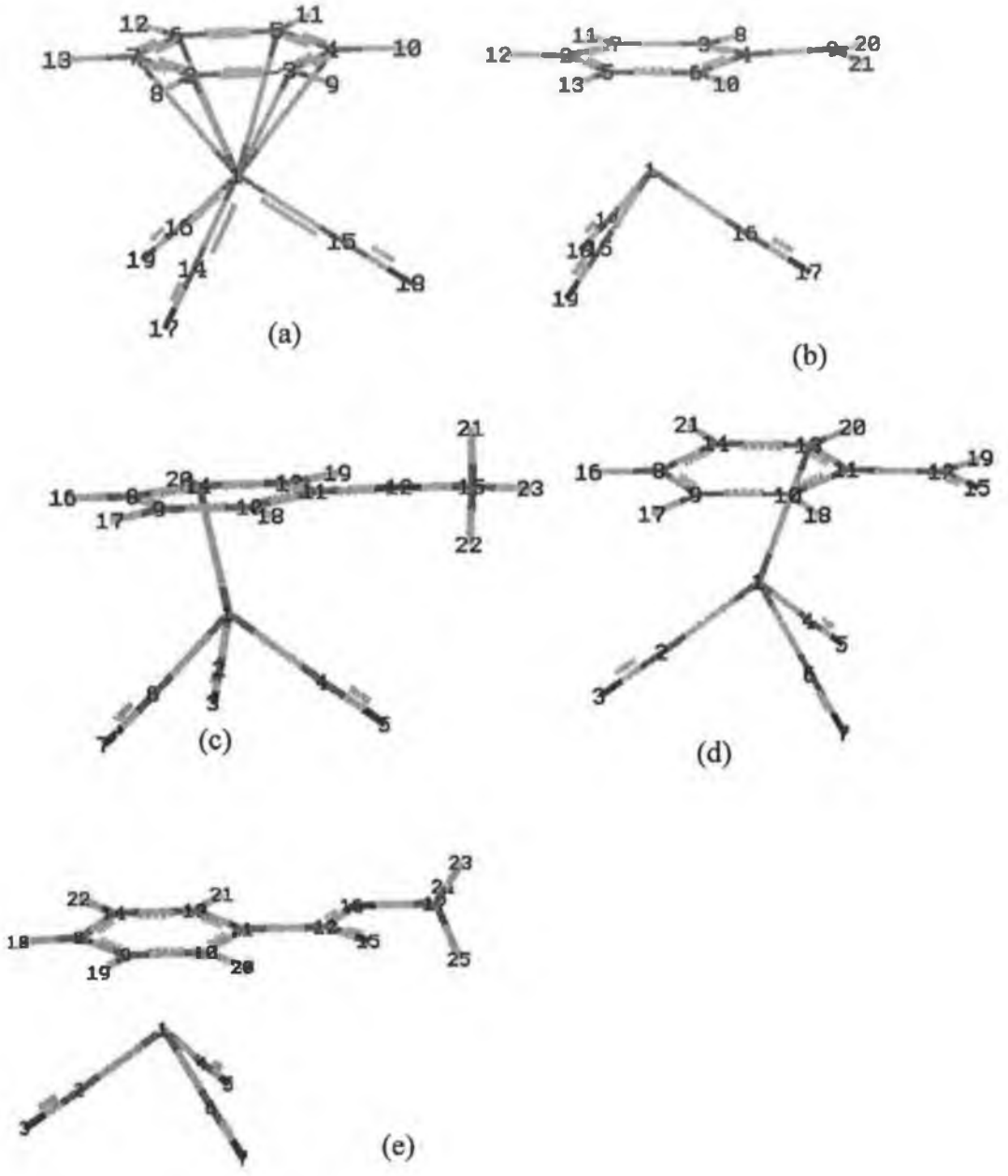

Fig 5.6 The optimised structures at the B3LYP/LanL2DZ level for (η^6-arene)$Cr(CO)_3$, where arene is (a) benzene, (b) aniline, (c) anisole, (d) benzaldehyde, (e) methylbenzoate.

The optimised structures calculated under this study are generally close to those obtained from X-ray determinations for these complexes. All the complexes have the expected three-legged piano stool structure. The benzene complex has an eclipsed structure with torsion angle of 0°, the hydrogen atoms slightly bent toward the $Cr(CO)_3$ unit. This result is supported by the microwave study by Sickafoose and co-workers [21] who found that the hydrogen atoms are bent toward the chromium atom out of the benzene ring plane by 2.8°. Similar results were obtained by neutron diffraction studies.

	RHF/ LANL2DZ	B3LYP/ LANL2DZ	Experimental	Deviation % B3LYP-Experimental
Bond lengths				
Cr1-C2 or 4 or 6	2.3824	2.3087	2.223, 2.243	3.86, 2.93
Cr1-C3 or 5 or 7	2.3938	2.3256		
C2-H8	1.0702	1.0843	1.106,1.113,1.109	2.00, 2.65, 2.28
C3-H9	1.0691	1.0833	1.106,1.113,1.109	2.10, 2.74, 2.37
Cr1-C (of COs)	1.9287	1.8317	1.845	0.73
C-O	1.1509	1.188	1.159, 1.157	2.05, 2.61
Bond angles				
C2-C3-C4	119.3492	119.3236	120.07,119.8,120.13	0.63, 0.40, 0.68
C3-C4-C5	120.6455	120.6576		
C3-C2-H8	119.6771	119.671	119.72	0.04
C2-C7-H13	120.3246	120.3279		
C2-Cr1-C5 arene	72.2852	75.9189		
C3-Cr1-C6 arene	72.2852	75.9189		
Cr1-C2-H8	125.7087	126.6694		
Cr1-C3-H9	127.1603	127.6317		
C2-C5-H11	179.16853	179.42731		
C3-C6-H12	179.75231	178.99370		

Table 5.14 Comparisons of selected bond lengths and bond angles of (η^6-benzene)$Cr(CO)_3$ with experimental values.

Complexes which have a donor substituent on the benzene ring have syn-eclipsed conformation with torsion angle of 0. While complexes containing an acceptor substituent on the benzene ring have staggered structure in which the substituent on the benzene ring does not eclipse any of the three carbonyl ligands. This is also found by other theoretical calculations and from the x-ray structure of these complexes[22]. The substituted benzene ligand is non-planar. Thus for the aniline and

anisole complexes the π-donor substituent on the ipso-carbon atoms bent away from the $Cr(CO)_3$ centre. While for benzaldehyde and methylbenzoate complexes the ipso-carbon atom bent toward the $Cr(CO)_3$ centre.

In the calculation of benzene complex, the using of both RHF/LanL2DZ and B3LYP/LanL2DZ level of calculation yielded structure parameters close to those obtained experimentally, Table 5.14.

	B3LYP/ LANL2DZ	B3LYP/ 6-31G(d',p')	Experimental	Deviation % B3LYP/6-31G(d',p') – Exp.
Bond lengths				
Cr1-C14 or 15	1.8273(1.8274)	1.8473	1.822	1.39
Cr1-C16	1.8275	1.8446	1.830	0.80
C-O (14,18 or 15,19)	1.1899	1.158	1.149	0.78
C16-O17	1.1907	1.1598	1.159	0.07
Cr1-C2	2.3092	2.2354	2.209	1.20
Cr1-C4	2.4466	2.3238	2.349	1.07
Cr1-C (3,or 6)	2.3508(2.3512)	2.2569	2.248	0.40
Cr1-C (5,or 7)	2.2903	2.206	2.188	0.82
C4-C (3 or 6)	1.4342(1.434)	1.4212		
C2-C (5or 7)	1.4237(1.4238)	1.4128		
C-C (5,6 or 3,7)	1.423(1.4229)	1.4152		
C2-H12	1.0826	1.0841		
C7-H11	1.0842	1.0855		
C4-N9	1.3771	1.3828	1.369	1.00
N-H	1.0101	1.0118	0.77	31.40
Bond angles				
Cr1-C2-C4	54.87859	52.51061		
Cr1-C3-C5	51.36696	50.06739		
C14-Cr1-C16	90.704	90.61776		
C2-C4-C9	176.82042	176.33639		
C4-N9-H20	120.62590	115.15610	113	1.91
C6-C7-H11	178.15464	177.84089		
C3-C4-C6	118.4089	118.6792		
C2-C5-C6	121.2509	121.1856		
C2-C7-C3	121.2474	121.1856		
C3-C4-N9	120.7739	120.6601	120.41	0.21

Table 5.15 Comparisons of selected bond lengths and bond angles (η^6-aniline)$Cr(CO)_3$

	B3LYP/ LANL2DZ	Experimental	Deviation % B3LYP-Experimental
Bond lengths			
Cr1-C (2,or 6)	1.8292(1.8289)	1.818, 1.823	0.62, 0.32
Cr1-C4	1.8308	1.840	0.5
C2-O3	1.1891	1.154	3.04
C-O (4,5)(6,7)	1.1888(1.1886)	1.144,1.151	3.92, 2.84
Cr1-C8	2.3143	2.225	4.01
Cr1-C11	2.3839	2.264	5.30
Cr1-C (9,or 14)	2.3051	2.203	4.63
Cr1-C (10,or 13)	2.3411(2.3418)	2.252	3.96, 3.99
C8-C (9 or 14)	1.4292(1.4188)		
C9-C (10or 14)	1.4172(1.4188)		
C11-C(10 or 13)	1.4316(1.4233)		
C8-H16	1.0828		
C-H(9,14)or (14,20)	1.084,1.0841		
C11-O12	1.3763	1.357	1.42
C15-H 21,22,or 23	1.0974, 1.0967, 1.0904		
Bond angles			
Cr1-C9-C13	52.76507		
Cr1-C8-C11	53.61717		
CCrC 2,1,6 / 4,1,6	89.4524 / 90.2261		
C9-C8-C14	118.7681		
C11-O12-C15	119.3467		
C9-C8-H16	120.5747		
C10-C9-H17	119.2708		
C11-C10-H18	118.5574		
C10-C11-C13	120.1511		
C10-C11-O12	115.2358	123.8	6.92

Table 5.16 Comparisons of selected bond lengths and bond angles (η^6-anisole)$Cr(CO)_3$

	B3LYP/LANL2DZ
Bond lengths	
Cr1-C2	1.8356
Cr1-C4	1.8375
Cr1-C6	1.8436
C2-O3	1.1857
C-O (4,5)(6,7)	1.1858 (1.1833)
Cr1-C8	2.3011
Cr1-C11	2.2982
Cr1-C9, or 14	2.3297, 2.3198
Cr1-C10, or 13	2.3081 (2.2835)
C8-C (9 or 14)	1.4317 (1.4231)
C-C(9,10or 13,14)	1.4148 (1.4241)
C11-C10 or 13	1.4355(1.4285)
C8-H16	1.0841
C-H (9,17) or (14,21)	1.0834,1.0832
C12-O15	1.2478
C12-H19	1.1066
Bond angles	
Cr1-C9-C13	51.10205
(Cr1-C8-C11	51.67219
(CCrC)2,1,6/4,1,6/2,1,4	89.3373/ 89.7063/ 89.0801
C9-C8-C14	120.7072
C11-C12-O15	123.6314
C9-C8-H16	119.5978
C10-C9-H17	120.33507
C11-C10-H18	118.1332
C10-C11-C13	119.2042
C10-C11-C12	126.5894
C11-C12-O15	123.6314
C11-C12-H19	115.382
O15-C12-H19	120.9855

Table 5.17 Comparisons of selected bond lengths and bond angles (η^6-benzaldehyde)$Cr(CO)_3$

	B3LYP/ LANL2DZ	Experimental [25]	Deviation % B3LYP-Exp.
Bond lengths			
Cr1-C2	1.8332	1.836	0.15
Cr1-C4	1.837	1.841	0.22
Cr1-C6	1.8389	1.849	0.55
C2-O3	1.1868	1.161	2.22
C-O(4,5)(6,7)	1.1858 (1.185)	1.155, 1.148	2.67, 3.22
Cr1-C8	2.3021	2.228	3.33
Cr1-C11	2.3014	2.214	3.95
Cr1-C9,or 14	2.3265, 2.3228	2.226,2.228	4.51, 9.48
Cr1-C10,or 13	2.3018 (2.2968)	2.211, 2.216	4.11, 3.65
C8-C9 or 14	1.4264 (1.4267)	1.393,1.405	2.40, 1.54
C-C(9,10 or 13,14)	1.4197 (1.4202)	1.404, 1.402	1.12, 1.30
C11-C10 or 13	1.4295 (1.4304)	1.421,1.414	0.60, 1.16
C8-H18	1.0842	1.012	7.13
C-H(9,19)or (14,22)	1.0832, 1.0833	0.906, 0.836	19.56, 29.58
C-O(12,15)(12,16)	1.2478, 1.3779	1.191, 1.336	4.77, 3.14
Bond angles			
Cr1-C9-C13	51.41295		
Cr1-C8-C11	51.78724		
(CCrC)2,1,6/4,1,6/2,1,4	89.28/ 89.43/ 89.44	88.68,87.33, 88.47	0.68, 2.41, 1.11
C9-C8-C14	120.638	119.98	0.68
C9-C8-H18	119.6759	118.87	3.09
C10-C9-H19	120.2243	116.62	3.56
C11-C10-H20	118.3172	114.25	0.04
C10-C11-C13	119.4275	119.38	0.63
C10-C11-C12	118.3922	117.65	0.20
C11-C12-O15	124.4568	124.21	1.00
C11-C12-O16	112.1604	111.05	1.07
O15-C12-O16	123.3806	124.72	

Table 5.18 Comparisons of selected bond lengths and bond angles (η^6-methylbenzoate)$Cr(CO)_3$

5.2.3.2 Vibrational analysis of electronic ground state. All elements in the Hessian matrix were positive except for one (-34 cm^{-1}) for the benzene complex The vibrational frequencies for (η^6-arene)$Cr(CO)_3$ have been calculated to test if model structure was at the global minimum on the potential energy surface. As the theoretical results obtained for (η^6-arene)$Cr(CO)_3$, complexes, arene = benzene, aniline, anisole, benzaldehyde, or methylbenzoate have a C_{3v} local symmetry, two

IR-active ν(CO) vibrations, A_1 and E. IR spectra dominated by a strong E band should be observed. Tables 5.19-23 compare the experimental and calculated ν(CO) wavenumbers of (η^6-arene)$Cr(CO)_3$ complexes.

IR active band B3LYP/ LanL2DZ	Experimental (cyclohexane)	Assignment
251		Symmetric ν(Cr-arene)
274		asymmetric ν(Cr-arene)
405		δ(CCC) and δ(CCH) out of plane of L ring
405		δ(CCC) and δ(CCH) out of plane of L ring
489		δ(CrCO) + δ(CCC) and δ(CCH) out of plane of L ring +δ(CrCO) δ(CCC) and δ(CCH) out of plane of L ring
495		δ(CrCO)
552		δ(CrCO) + δ(CCC) and δ(CCH) out of plane of L ring
622		δ(CCC) and δ(CCH) in plane of L ring + δ(CrCO)
659		δ(CrCO) +δ(CCC) and δ(CCH) in plane of L ring
672		δ(CCC) and δ(CCH) out of plane of L ring
694		δ(CrCO) +δ(CCC) and δ(CCH) out of plane of L ring
782, 873		δ(CCH) out of plane of L ring
949		δ(CCH) out of plane of L ring
981		δ(CCC) and δ(CCH) out of plane of L ring
1005		ring breathing, δ(CCC) and δ(CCH) out of plane of L ring
1047		δ(CCC) and δ(CCH) in plane of L ring
1055		δ(CCC) and δ(CCH) in plane of L ring
1055		δ(CCC) and δ(CCH) in plane of L ring
1218,1508		δ(CCH) in plane of L ring
1586		δ(CCH) in plane of L ring
1917	1918	Asymmetric ν(CO)
1980	1987	Symmetric ν(CO)
3301,3307		Asymmetric ν(CH)
3326		Asymmetric ν(CH)
3337		Symmetric ν(CH)

Table 5.19 The IR frequencies of (benzene)$Cr(CO)_3$, L = benzene, correction factor = 1.02021.

IR active band B3LYP/ LanL2DZ	Experimental In CH_2Cl_2	Assignment
253		ν(Cr-L)+δ(CCC) and δ(CCH) of L+ δ(CCrC) of carbonyl
255		ν(Cr-L)+δ(CCC) and δ(CCH) of L
316		δ(CCC) and δ(CCH) of L
380		δ(CCN), δ(CCC) and δ(CCH) of L
404		δ(CCN), δ(CCC) and δ(CCH) of L
414		δ(CCN), δ(CCC) and δ(CCH) of L
423		δ(CCN), δ(CCC) and δ(CCH) of L+ δ(CrCO)
482		δ(CCN), δ(CCC) and δ(CCH) of L+ δ(CrCO)
488		δ(CrCO) + δ(CCN), δ(CCC) and δ(CCH) of L
492		δ(CrCO) + δ(NH_2) of L
504		δ(NH_2) and δ(CCH) of L
528		δ(CCN), δ(CCC), δ(NH_2) and δ(CCH) of L+ δ(CrCO)
544		δ(CCN), δ(CCC), δ(NH_2) and δ(CCH) of L
545		δ(CCN), δ(CCC), δ(NH_2) and δ(CCH) of L+ δ(CrCO)
566		δ(CCN), δ(CCC), δ(NH_2) and δ(CCH) of L+ δ(CrCO)
632		δ(CCN), δ(CCC), δ(NH_2) and δ(CCH) of L
650		δ(CrCO) +δ(CCN), δ(CCC), δ(NH_2) and δ(CCH) of L
661		δ(CrCO) +δ(CCN), δ(CCC), δ(NH_2) and δ(CCH) of L
683		δ(CCN), δ(CCC), δ(NH_2) and δ(CCH) of L
701		δ(CrCO) +δ(CCN), δ(CCC), δ(NH_2) and δ(CCH) of L
797		δ(CCH) of L
834		δ(CCH) of L
841		δ(CCH), δ(CCN), δ(CCC) and δ(NH_2) of L
849, 931, 953		δ(CCH) of L
1021		δ(CCN), δ(CCC) and δ(CCH) of L
1045		δ(CCH), δ(CCN), δ(CCC) and δ(NH_2) of L
1045		δ(CCH), δ(CCN), and δ(CCC) of L
1132		δ(CCH), δ(CCN), δ(CCC) and δ(NH_2) of L
1214, 1219		δ(CCH) of L
1363, 1390		δ(CCH) and δ(NH_2) of L
1442, 1491		δ(CCH), δ(CCN), δ(CCC) and δ(NH_2) of L
1536, 1576		δ(CCH), δ(CCN), δ(CCC) and δ(NH_2) of L
1628		δ(CCH), δ(CCN), δ(CCC) and δ(NH_2) of L
1722		δ(NH_2) of L
1892, 1895	1875	Asymmetric ν(CO)
1960	1960	Symmetric ν(CO)
3280, 3281		Asymmetric ν(CH) of L
3295, 3298		Asymmetric ν(CH) of L
3319		Symmetric ν(CH) of L
3679		Symmetric ν(NH) of L
3815		Asymmetric ν(NH) of L

Table 5.20 The IR frequencies of (aniline)$Cr(CO)_3$ scaled with (1.02021), L = aniline.

IR B3LYP/LanL2DZ	Experimental	Assignment
325		ν(Cr-L)+δ(CCC) and δ(CCH) of L
411		ν(Cr-L)+δ(CCC) and δ(CCH) of L
423		δ(CrCO) +δ(CCC) and δ(CCH) of L
448		δ(COC) and δ(CCH) of L
484		δ(CrCO) +δ(COC) and δ(CCH) of L
492, 495		δ(CrCO)
518		δ(CCC) and δ(CCH) of L+ δ(CrCO)
549, 559, 564		δ(CrCO)+ δ(COC) and δ(CCH) of L
629		δ(CCC) and δ(CCH) of L
656		δ(CCH) of L+ δ(CrCO)
660		δ(CCH) of L+ δ(CrCO)
685		δ(CCH) of L
702		δ(CrCO) + δ(CCH) of L
787		δ(CCC) and δ(CCH) of L
812, 848		δ(CCH) of L
868, 937		δ(CCH) of L
961		δ(CCH) of L
1005		Ring breathing + ν(C-O) of O-CH_3 group
1038		δ(CCC) of L+ ν(C-O) of O-CH_3 group
1047, 1100		δ(CCH) of L
1176		δ(HCH) of methyl group
1211		δ(CCH) of L
1212, 1225		δ(CCH) of L + δ(HCH) of methyl group
1294		δ(CCC) and δ(CCH) of L + ν(C-O) of O-CH_3
1371		δ(CCH) of L
1443		ν(CC) of L
1483		δ(CCH) of L
1508, 1534		δ(HCH) of methyl group +δ(CCH) of L
1544, 1549		δ(HCH) of methyl group
1580		ν(CC) of L
1609		ν(CC) of L + δ(HCH) of methyl group
1909, 1911	1886	Asymmetric ν(CO)
1976	1967	Symmetric ν(CO)
3110		Symmetric ν(CH) of methyl group
3206		Asymmetric ν(CH) of methyl group
3270		Asymmetric ν(CH) of methyl group
3306, 3311		Asymmetric ν(CH) of L
3330, 3336		Asymmetric ν(CH) of L
3341		Symmetric ν(CH) of L

Table 5.21 The IR frequencies of (anisole)$Cr(CO)_3$ scaled with (1.02021),, L = anisole.

IR B3LYP/LanL2DZ	Experimental	Assignment
213		δ(CCO) of L
261, 273		ν(Cr-L)
307		δ(CCC) and δ(CCH) of L
415		δ(CrCO)+ δ(CCC) and δ(CCH) of L
419, 448		δ(CCC) and δ(CCH) of L
469		δ(CCC) and δ(CCH) of L+ δ(CrCO)
480		δ(CrCO)+ δ(CCC) and δ(CCH) of L
486, 491		δ(CrCO)+ δ(CCH) of L
547, 555		δ(CrCO)+ δ(CCH) of L
631		δ(CCC) of L +δ(CrCO)
642		δ(CrCO)+ δ(CCH) of L
651		δ(CrCO)+ δ(CCH) of L
667		δ(CCC) and δ(CCH) of L +δ(CrCO)
684		δ(CCC) and δ(CCH) of L +δ(CrCO)
692		δ(CCC) and δ(CCH) of L +δ(CrCO)
816, 843		δ(CCH) of L
880, 950		δ(CCH) of L
971, 995		δ(CCH) of L
1024, 1027		δ(CCH) of L
1044, 1108		δ(CCC) and δ(CCH) of L
1216, 1222		δ(CCC) and δ(CCH) of L
1265		δ(CCC) of L +ν(C-C) of phenyl-CHO
1368, 1428, 1461		δ(CCC) and δ(CCH) of L
1484, 1520		δ(CCC) and δ(CCH) of L
1575		δ(CCC) and δ(CCH) of L
1600		ν(CC)+ δ(CCH) of L
1696	1708	ν(CO) of L
1929	1931	Asymmetric ν(CO)
1938	1940	Asymmetric ν(CO)
1991	1996	Symmetric ν(CO)
3055		ν(CH) of aldehyde group
3291		Asymmetric ν(CH) of L
3306		Asymmetric ν(CH) of L
3312		Asymmetric ν(CH) of L
3325		Asymmetric ν(CH) of L
3334		Symmetric ν(CH) of L

Table 5.22 The IR frequencies of (benzaldehyde)$Cr(CO)_3$ scaled with (1.02021), L = benzaldehyde.

IR B3LYP/LanL2DZ	Experimental	Assignment
255, 270, 284		ν(Cr-L)
310		δ(COO),δ(CCC), δ(CHH) and δ(CCH) of L
370		δ(CCC) and δ(CCH) of L
414		δ(CrCO)+ δ(CCC) and δ(CCH) of L
418		δ(CrCO)+ δ(CCC) and δ(CCH) of L
449		δ(CCC) and δ(CCH) of L
478		δ(CrCO)+ δ(CCO) of L
486		δ(CrCO)+ δ(CCH) of L
490		δ(CrCO)+ δ(CCO) and δ(CCH) of L
494, 551		δ(CrCO)+ δ(CCH) of L
552		δ(CrCO) + δ(CCC) of L
634		δ(CrCO)+ δ(CCC) and δ(CCH) of L
644		δ(CrCO)+ δ(CCH) of L
657		δ(CCC) and δ(CCH) of L +δ(CrCO)
666		δ(CCC) and δ(CCH) of L
686		δ(CCC),δ(COO),δ(HCH) and δ(CCH) of L +δ(CrCO)
692		δ(CrCO) +δ(CCC),δ(COO),δ(HCH) of L
763		δ(CCC) and δ(CCH) of L
809		δ(COO) and δ(CCC) of L
828, 878		δ(CCH) of L
956		ν(C-CH_3) and δ(CCH) of L
960, 990, 1000		δ(CCH) of L
1027, 1049, 1105		δ(CCC) and δ(CCH) of L
1144,		δ(CCC) of L +ν(C-C) of phenyl-CO_2CH_3
1180		δ(HCH) of methyl group
1217, 1221, 1222		δ(HCH) of methyl group +δ(CCH) of L
1326		ν(C-C) of phenyl-CO_2CH_3 +δ(HCH) and δ(CCH) of L
1372		δ(CCH) of L
1444		ν(CC)+ δ(CCH) of L
1479		ν(CO) of L
1505		Symmetric δ(HCH)
1523		Symmetric δ(HCH)+ δ(CCH) of L
1531, 1539		Asymmetric δ(HCH)
1574, 1605		ν(CC) +δ(CCH) of L
1704		ν(CO) of L
1926, 1931	1928, 1935	Asymmetric ν(CO) of carbonyl ligands
1987	1991	Symmetric ν(CO) of carbonyl ligands
3139		Symmetric ν(CH) of methyl group
3243		Asymmetric ν(CH) of methyl group
3282		Asymmetric ν(CH) of methyl group
3305, 3315		Asymmetric ν(CH) of L
3323, 3332		Asymmetric ν(CH) of L
3341		Symmetric ν(CH) of L

Table 5.23 The IR frequencies of (methylbenzoate)$Cr(CO)_3$, L = methylbenzoate, correction factor = 1.02021.

5.2.3.3 Ground-state Electronic Structure of (η^6-arene)$Cr(CO)_3$

The ground-state electronic structure was calculated in order to determine the energies and compositions of the MO's. The orbitals are plotted according to the energies in Fig 5.7. The assignment of the type of each MO was made on the basis of its composition (Table 5.19) and by visual inspection of its three-dimensional representation (e.g. Figs 5.8, 5.9, 5.10, 5.11, and 5.12).

As a result of the existence of C_{3v} symmetry in the (η^6-benzene)$Cr(CO)_3$ complex, the ground-state electronic structure contains many degenerate orbitals. The two highest occupied MOs are mainly chromium of d-orbital (ca 61 %) character with about 27 % CO contribution. They form a π-bond with one or more of the carbonyl ligands, but the carbonyl ligands have some electron density in the anti-bonding orbitals on oxygen (Table 5.19 and Fig 5.8). The H-2 orbital in all the arene carbonyl complexes is localized on the Cr atom in mainly d_z^2 orbital with some electron density on the oxygen atoms of the three-carbonyl ligands with density on the carbon atoms, which are bonding relative to the metal orbital. The nature of this orbital does not change greatly upon changing the substituents on the benzene ring.

The HOMO and H-1 orbitals are derived from d_{xz}, and d_{yz} orbitals of the chromium atom which are bonding with one CO ligand but antibonding to the remaining two CO ligands. In the benzene complex, (Table 5.24) the orbitals H-2 and L+4 are composite non-degenerate, while the orbitals (H-5, H-6), (H-3, H-4), (HOMO, H-1), (LUMO, L+1), (L+2, L+3), and (L+5, L+6) are doubly degenerate and derive from the doubly degenerate d orbitals of the chromium atom.

This degeneracy is lost when substituents are added to the benzene ring. So some of the orbitals appear at higher energy to analogous of benzene complex. This is because, in the case of benzene complex, the chromium d-orbitals of the designated doublet degeneracy (i.e. d_{xz}, d_{yz}) face the same electrostatic field therefore they remain degenerate. The presence of the substituent on the benzene ring affects the δ-donor ability and π-acidity of the benzene ring. The ring will not bond symmetrically to the chromium atom. As the asymmetrically of the bonding of the arene to chromium increase the degeneracy will decrease. Generally the presence of the electron-withdrawing groups on the benzene ring will increase its π-acidity of the arene ligand and this will increase the π-acceptance ability. This in turn will stabilize

the molecular orbitals of the arene complex relative to the benzene complex, as shown in the Table 5.25 for the benzaldehyde and methylbenzoate complexes.

MO			eV	Cr %	CO %	Benzene %
63	L+13		1.09	94	4	2
62	L+12	}e	0.82	50	43	7
61	L+11		0.82	50	43	7
60	L+10		0.43	89	8	3
59	L+9		0.33	0	100	0
58	L+8	}e	0.29	74	20	7
57	L+7		0.29	74	20	7
56	L+6	}e	0.15	28	70	2
55	L+5		0.15	28	70	2
54	L+4		-0.52	45	53	2
53	L+3	}e	-0.83	51	42	7
52	L+2		-0.83	51	42	7
51	L+1		-1.6	4	11	85
50	LUMO	}e	-1.6	4	11	85
49	HOMO		-6.02	61	27	12
48	H-1	}e	-6.02	61	27	12
47	H-2		-6.33	73	26	2
46	H-3	}e	-9.08	11	4	85
45	H-4		-9.08	11	4	85
44	H-5	}e	-10.77	12	72	16
43	H-6		-10.77	12	72	16
42	H-7		-10.86	4	44	52

Table 5.24 The contributions of Cr, CO, and benzene in some selected the molecular orbitals of (η^6-benzene)$Cr(CO)_3$.

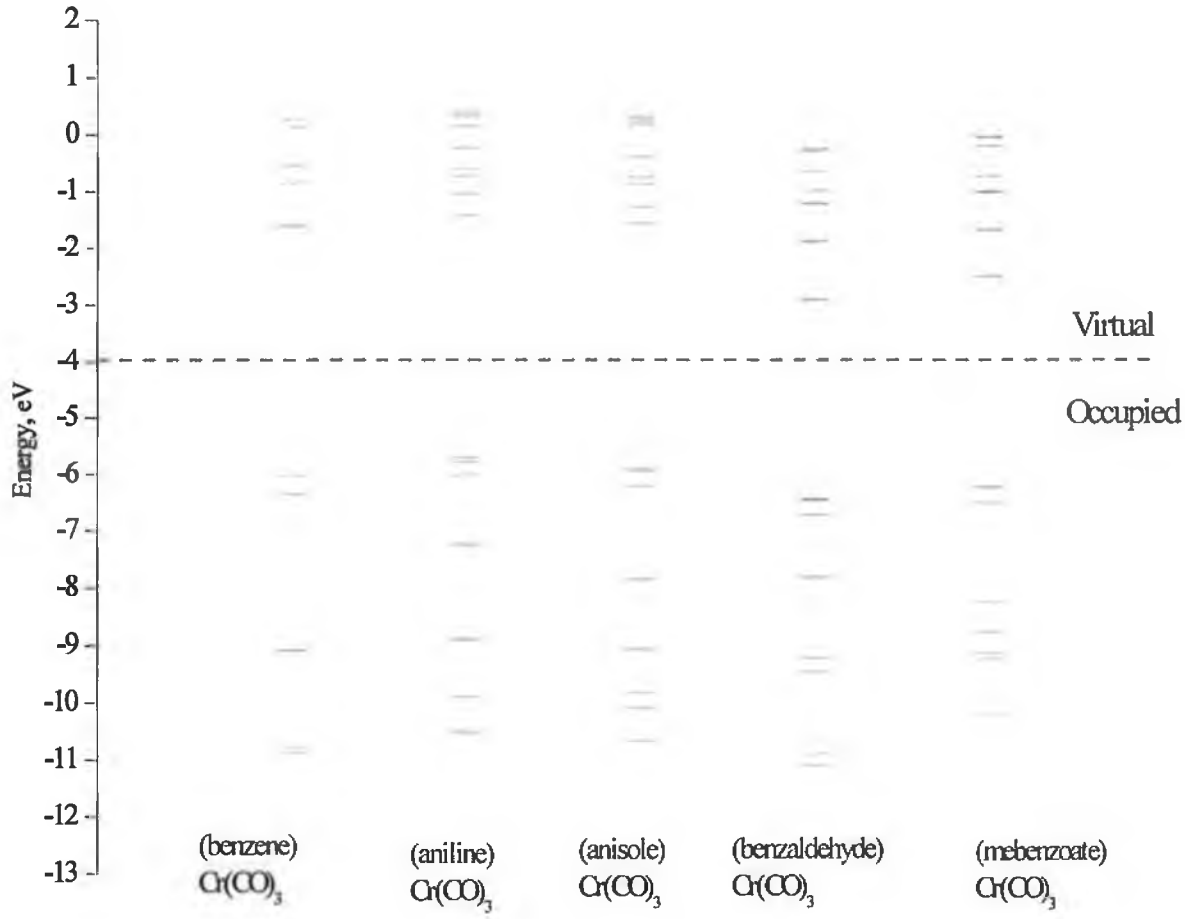

Fig 5.7 The energy level diagrams of (η^6-arene)$Cr(CO)_3$, arene = benzene, aniline, anisole, benzaldehyde, or methylbenzoate.

Conversely the presence of electron donating groups will decrease the π-acidity of the arene and hence π-bonding of the arene with the metal will decrease. As the π-acidity of the arene is more important in the formation of the molecular orbitals of (η^6-arene)$Cr(CO)_3$ complexes, a donor substituent will generally increase the energies of the molecular orbitals, as shown in Table 5.25 for the aniline and anisole complexes.

MO	Benzene complex	Aniline complex	Anisole complex	Benzaldehyde complex	Methylbenzoate complex
L+7	0.29	0.41	0.32	-0.23	-0.02
L+6	0.15	0.34	0.25	-0.27	-0.04
L+5	0.15	0.17	0.2	-0.63	-0.18
L+4	-0.52	-0.22	-0.37	-0.96	-0.71
L+3	-0.83	-0.58	-0.74	-1.18	-0.98
L+2	-0.83	-0.7	-0.84	-1.2	-1
L+1	-1.6	-1.03	-1.26	-1.87	-1.66
LUMO	-1.6	-1.41	-1.55	-2.89	-2.48
HOMO	-6.02	-5.7	-5.89	-6.43	-6.22
H-1	-6.02	-5.78	-5.94	-6.45	-6.23
H-2	-6.33	-6.01	-6.2	-6.71	-6.51
H-3	-9.08	-7.23	-7.84	-7.81	-8.24
H-4	-9.08	-8.89	-9.06	-9.21	-8.76
H-5	-10.77	-9.89	-9.82	-9.45	-9.13
H-6	-10.77	-10.48	-10.09	-10.89	-9.24
H-7	-10.86	-10.53	-10.67	-11.09	-10.19

Table 5.25 Selected calculated energy levels with their energies (in eV) for (η^6-arene)$Cr(CO)_3$ complexes.

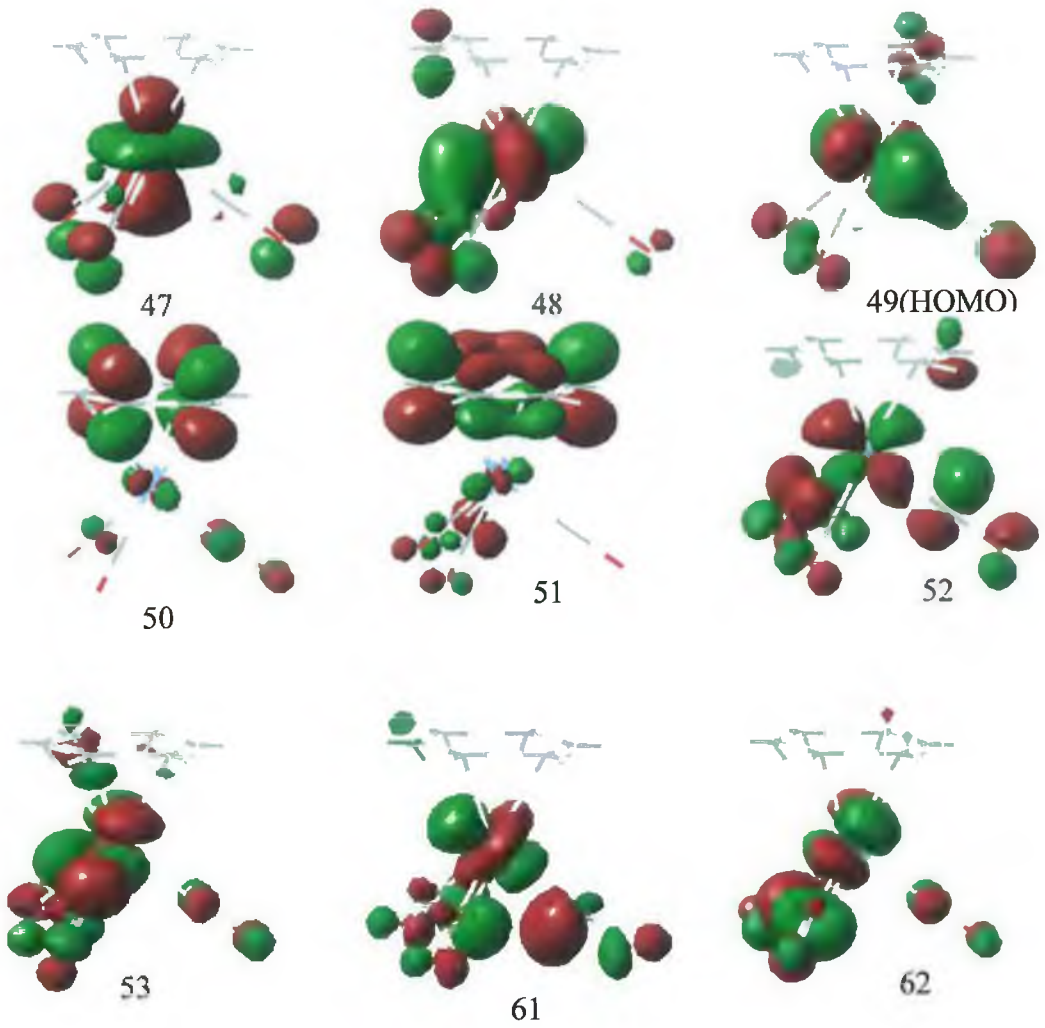

Fig 5.8 The molecular orbitals of (η^6-benzene)$Cr(CO)_3$

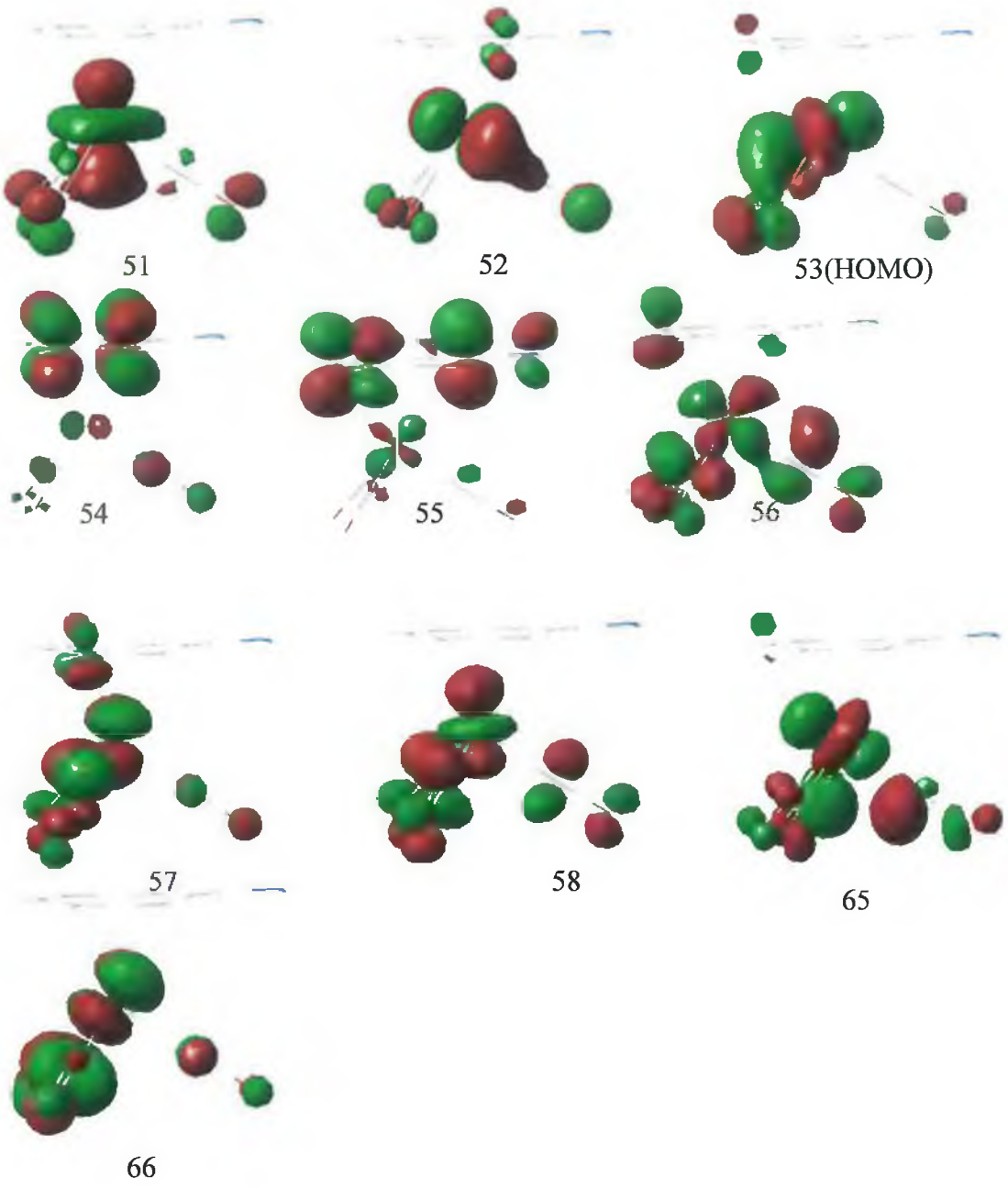

Fig 5.9 The molecular orbitals of (η^6-aniline)$Cr(CO)_3$

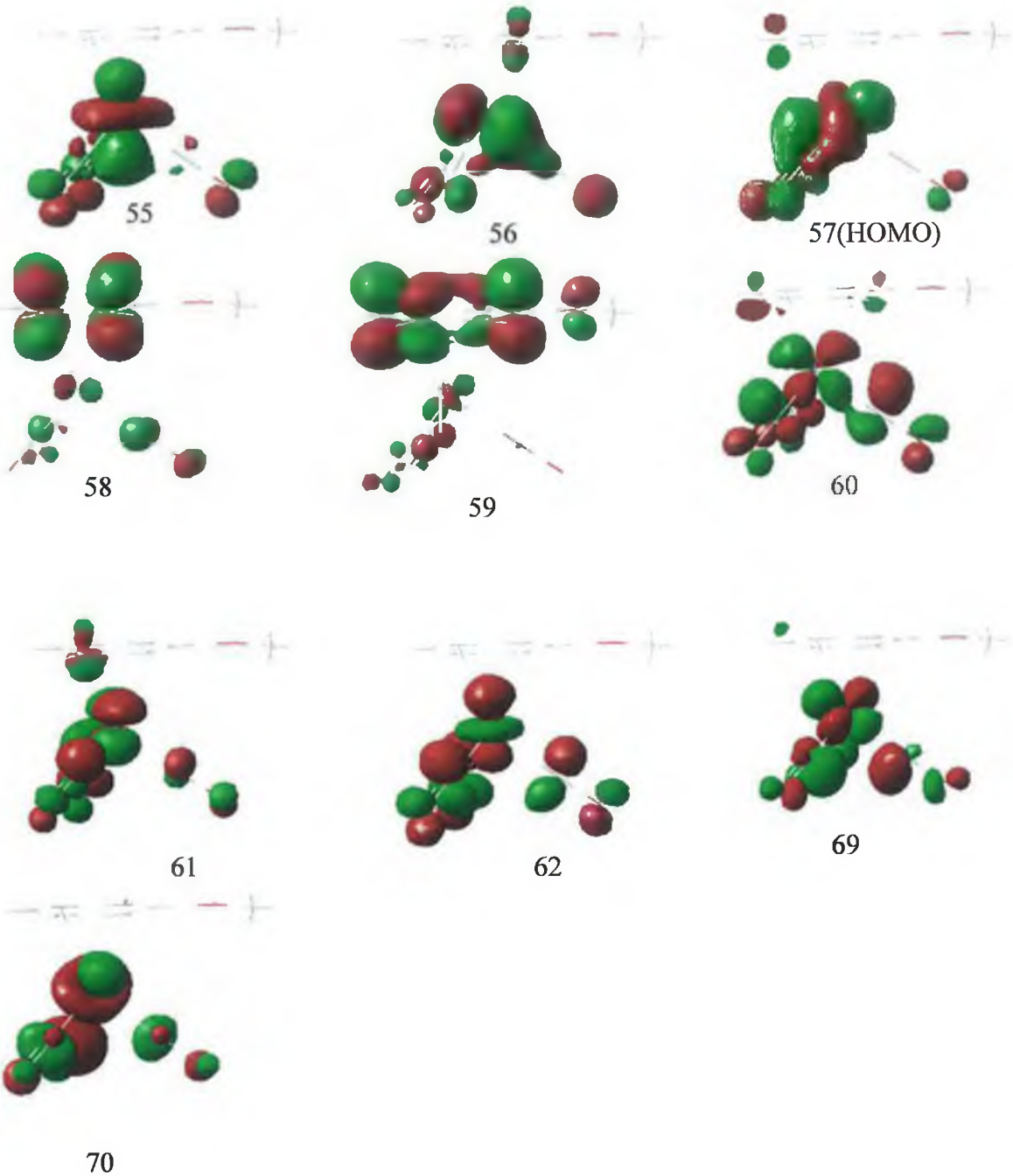

Fig 5.10 The molecular orbitals of (η^6-anisole)$Cr(CO)_3$

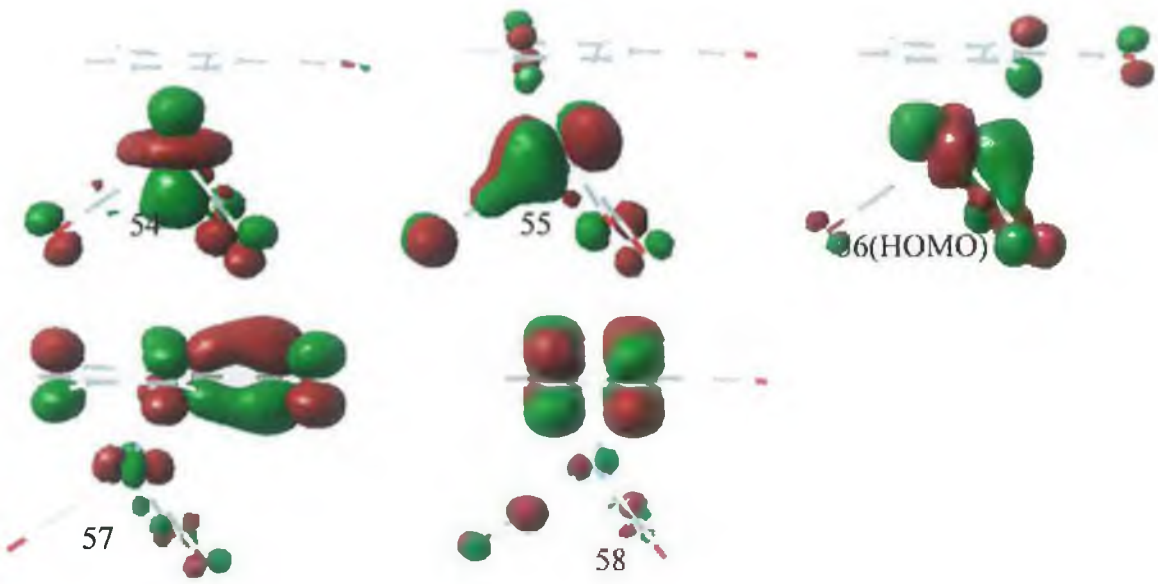

Fig 5.11 The molecular orbitals of (η^6-benzaldehyde)Cr(CO)$_3$

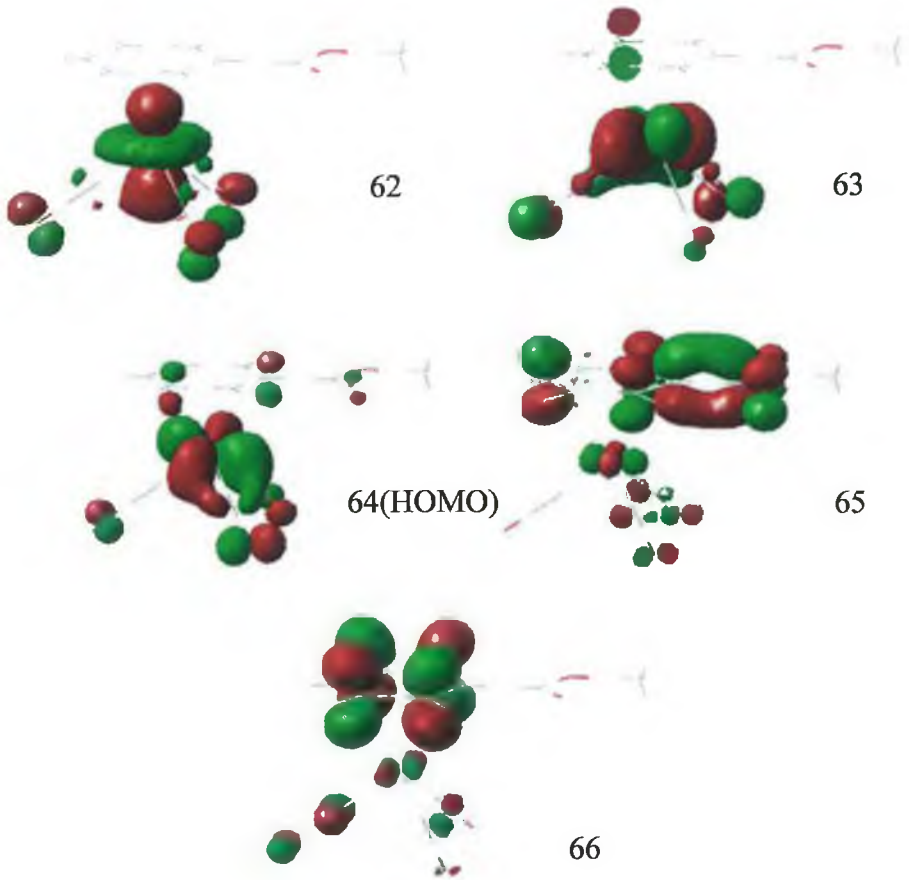

Fig 5.12 The molecular orbitals of (η^6-methylbenzoate)Cr(CO)$_3$

Another factor should be considered in the loss of degeneracy of the MOs of substituted benzenes exocyclic double bond, is the double bond orientation with respect to the arene ring (see the optimised geometries Section 5.2.2.1 for more details). This will affect, in particular the doubly degenerate orbitals d_{xz}, and d_{yz}, which face different electrostatic fields upon the substitution on the benzene ring. Thus if the exocyclic double bond is bent away from the chromium atom the repulsion between this double bond and the Cr-d_{xz} orbitals make the later appear at higher energy than d_{yz}. In the case of aniline and anisole, the d_{xz} appeared in H-1 while d_{yz} appeared in HOMO orbital. If the exocyclic substituent is bent toward the chromium atom the electrostatic field will make the Cr-d_{yz} orbitals appear at higher energy. This appeared clearly in the H-1 and HOMO orbitals of benzaldehyde and methylbenzoate complexes.

MO		eV	Cr %	CO %	Benzene %
63	L+13	1.09	94	4	2
62	L+12	0.82	50	43	7
61	L+11	0.82	50	43	7
60	L+10	0.43	89	8	3
59	L+9	0.33	0	100	0
58	L+8	0.29	74	20	7
57	L+7	0.29	74	20	7
56	L+6	0.15	28	70	2
55	L+5	0.15	28	70	2
54	L+4	-0.52	45	53	2
53	L+3	-0.83	51	42	7
52	L+2	-0.83	51	42	7
51	L+1	-1.6	4	11	85
50	LUMO	-1.6	4	11	85
49	HOMO	-6.02	61	27	12
48	H-1	-6.02	61	27	12
47	H-2	-6.33	73	26	2
46	H-3	-9.08	11	4	85
45	H-4	-9.08	11	4	85
44	H-5	-10.77	12	72	16
43	H-6	-10.77	12	72	16
42	H-7	-10.86	4	44	52

Table 5.26 The contributions of Cr, CO, and benzene in some selected molecular orbitals of (η^6-benzene)$Cr(CO)_3$.

The LUMO and L+1 orbitals are mainly localised on the arene ligand with slight electrondensities on the orbitals of two CO ligands. These chromium orbitals are

bonding respect to two CO ligands and non-bonding relative to the other. These orbitals represent e_{2ua} and e_{2ub} orbitals of the arene ring the d-orbitals of the type d_{xz}, and d_{yz}, which are bonding for both LUMO and L+1 orbitals.

The L+2 orbitals mainly localised on the three CO and chromium orbitals, which represent d_{xy} bonding relative to the CO ligands. There is also some electron density on the arene ligand, which is antibonding to the chromium orbitals.

MO		eV	Cr%	CO%	Aniline%
66	L+12	1.14	46	49	5
65	L+11	1	42	49	9
64	L+10	0.6	80	15	4
63	L+9	0.57	4	95	1
62	L+8	0.49	29	67	4
61	L+7	0.41	28	68	3
60	L+6	0.34	71	22	7
59	L+5	0.17	73	8	19
58	L+4	-0.22	51	47	2
57	L+3	-0.58	52	39	9
56	L+2	-0.7	43	46	11
55	L+1	-1.03	9	8	83
54	LUMO	-1.41	5	13	82
53	HOMO	-5.7	64	28	8
52	H-1	-5.78	60	27	13
51	H-2	-6.01	72	27	1
50	H-3	-7.23	7	2	91
49	H-4	-8.89	10	4	86
48	H-5	-9.89	5	10	85
47	H-6	-10.48	15	83	2
46	H-7	-10.53	13	82	4

Table 5.27 The contributions of Cr, CO, and aniline in some selected molecular orbitals of (η^6-aniline)$Cr(CO)_3$

MO		eV	Cr %	CO %	Anisole %
71	L+13	1.19	91	4	5
70	L+12	0.95	47	44	8
69	L+11	0.89	46	46	8
68	L+10	0.59	89	9	2
67	L+9	0.41	32	64	4
66	L+8	0.37	45	48	7
65	L+7	0.32	43	52	5
64	L+6	0.25	39	58	3
63	L+5	0.2	49	44	8
62	L+4	-0.37	46	52	2
61	L+3	-0.74	51	41	8
60	L+2	-0.84	49	44	7
59	L+1	-1.26	3	9	88
58	LUMO	-1.55	4	13	83
57	HOMO	-5.89	63	27	9
56	H-1	-5.94	61	27	13
55	H-2	-6.2	72	26	2
54	H-3	-7.84	7	2	90
53	H-4	-9.06	10	4	86
52	H-5	-9.82	1	1	97
51	H-6	-10.09	4	8	88
50	H-7	-10.67	15	83	2

Table 5.28 The contributions of Cr, CO, and anisole in some selected molecular orbitals of (η^6-anisole)$Cr(CO)_3$.

MO		eV	Cr %	CO %	Benzaldehyde %
64	L+7	-0.23	25	72	3
63	L+6	-0.27	26	71	3
62	L+5	-0.63	17	38	45
61	L+4	-0.96	26	46	28
60	L+3	-1.18	51	38	11
59	L+2	-1.2	50	39	11
58	L+1	-1.87	4	12	85
57	LUMO	-2.89	7	9	84
56	HOMO	-6.43	58	24	18
55	H-1	-6.45	62	26	12
54	H-2	-6.71	72	25	3
53	H-3	-7.81	1	0	98
52	H-4	-9.21	10	3	87
51	H-5	-9.45	11	4	85
50	H-6	-10.89	2	17	80
49	H-7	-11.09	2	16	83

Table 5.29 The contributions of Cr, CO, and benzaldehyde in some selected molecular orbitals of (η^6-benzaldehyde)$Cr(CO)_3$.

MO		eV	Cr %	CO %	Methyl benzoate%
72	L+7	-0.02	25	71	4
71	L+6	-0.04	26	71	3
70	L+5	-0.18	15	33	52
69	L+4	-0.71	34	54	12
68	L+3	-0.98	50	42	8
67	L+2	-1	51	37	12
66	L+1	-1.66	3	12	85
65	LUMO	-2.48	7	10	83
64	HOMO	-6.22	60	25	15
63	H-1	-6.23	61	26	13
62	H-2	-6.51	73	25	2
61	H-3	-8.24	0	0	100
60	H-4	-8.76	0	0	99
59	H-5	-9.13	10	3	87
58	H-6	-9.24	11	4	86
57	H-7	-10.19	0	0	100

Table 5.30 The contributions of Cr, CO, and methylbenzoate in some selected molecular orbitals of (η^6-methylbenzoate)$Cr(CO)_3$.

5.2.3.4 Time-Dependent Calculations on singlet excited states.

Following ground-state DFT calculation the time-dependent calculation on (η^6-arene)$Cr(CO)_3$ was undertaken to find the characteristics and energies of the first three low lying excited states. The energy of each excited state is the vertical excitation energy in electron-volts (eV) from the ground state. The transitions with the oscillator strengths are listed in Tables 5.31-35. There are some singlet-excited states with zero oscillator strength. These states, although present in the molecule's excited-state manifold, do not contribute significantly to the compound's absorption cross-section.

A commonly used model of an excited state corresponds to excitation of an electron from an occupied to a virtual MO (i.e. a one-electron picture). However, the excited states calculated herein demonstrate that excited-state electronic structures are best described in terms of multielectronic states, where in a linear combination of several occupied-to-virtual MO excitations comprises a given optical transition. Assignment of the character of each excited state was based on the compositions of the occupied and virtual MOs of the dominant excitation(s) for that excited state.

The nature of the substituent on the benzene ring is highly affected on the nature of the excited state, the oscillator strength of the excitation (which determine whether

the total transition is allowed or prohibited) and will determine the contribution of these excited states in photochemistry of these complexes.

For these complexes, (see Table 5.31 as example), the transition HOMO or (H-1) to LUMO or to L+1 involves the transition from an orbital, which is predominantly d-orbital in character (60 % has d_{xz} or d_{yz} properties) and is essentially bonding relative to the CO ligands to virtual orbital, which is mainly lies on π^* of the ligand and some on CO ligands. Some LF on the chromium atom also involved in this transition. So the excitation is mainly involve Cr-L charge transfer (L = benzene, aniline, anisole, benzaldehyde or methylbenzoate) and with a small LF contribution. The expected effect of this transition will lengthen Cr-CO bond in the excited state. In this excitation the metal will oxidize and this oxidation will reduce the charge drift from the metal to the ligand through π-bond and as result of that this bond will weakening and eventually resulted in the rupture of CO ligand. The result photoproduct from this excitation is the coordinatively unsaturated species $(\eta^6\text{-arene})Cr(CO)_2$. The presence of these transitions in the excited state will give the expectation that the photolysis in this band will result the CO loss from the parent tricarbonyl molecule but this also depends on the contribution of this transition in the excited state and the extension coefficient of this excitation.

The transition HOMO or H-1 to L+2, or L+3 involve the transition of electron density from orbital which is mainly d-orbital character (60 % has d_{xz} or d_{yz} properties) and bonding relative to the CO ligands to virtual orbital which mainly on the Cr d-orbitals and bonding relative to the three CO ligands in which two of these ligands bond with Cr and antibonding to the arene. So the major transitions are d-d transition (LF excitation), which involves the transition of the electrondensity from bonding orbital to antibonding orbital especially relative to the arene ligand and to lesser extent Cr-arene charge transfer. The expected effect of this transition will lengthen Cr-arene in the excited state leading to the rupture of the arene or to form the coordinatively unsaturated species $(\eta^x\text{-arene})Cr(CO)_3$ (x = 0-4).

The transition H-2 to LUMO, or L+1 involves the transition of electron density of orbital which has mainly on the Cr-d_z^2 orbital which weak bonding relative to the three CO ligands and nonbonding relative to the benzene ligand to virtual orbital which mainly lies on the arene ligand (ca. 85 %) and some on CO ligands and to small extent transition from orbital d_z^2 to one of the orbitals d_{xz} or d_{yz} (LF transition).

The transition H-2 to L+11 or L+12 involves the transition of electron density from orbital which has mainly on the Cr-d_z^2 orbital which is weakly bonding relative to the three CO ligands and antibonding to the benzene ligand to virtual orbital which mainly lies on the Cr d-orbital (which looks like the $d_{yz}+p_y$ or d_{xz} orbitals) and the three CO which, are antibonding relative to the Cr. So this transition involves the Cr d-d transition from bonding d_z^2 to antibonding $d_{yz}+p_y$ or d_{xz} on the Cr atom (LF) and Cr-CO charge transfer.

State	*E* eV, (nm)[a]	*f*[b]	$\Psi_o \rightarrow \Psi_v$[c]	Character[d]
1	3.1974 (387.76)	0.0000	H-1→LUMO (22%) H-1→L+3(24%) H-1→L+12 (22%) HOMO→L+1(24%) HOMO→L+2 (3%) HOMO→L+11(3%)	Cr d_{xz} -L CT, Cr d_{xz}-d_{yz} Cr d_{xz}-d_{yz}, Cr d_{xz} -CO CT, LBCT Cr d_{xz} -CO CT, LBCT Cr d_{yz}-L CT, Cr d_{yz}-d_{xz}, LBCT Cr d_{yz}-d_{xy}, LBCT Cr d_{yz}-($d_{yz}+p_y$), Cr d_{yz}-CO CT
2	3.2826 (377.70)	0.0014	H-2→L+2 (29%) H-2→L+1 (3%) H-2→L+11 (5%) H-1→L+1(29%) H-1→L+2(2%) HOMO→LUMO (29%) HOMO→L+3(2%)	Cr d_z^2-d_{xy}, LBCT Cr d_z^2-L CT, Cr d_z^2-d_{xz} LBCT Cr d_z^2-($d_{yz}+p_y$), Cr d_z^2-CO CT Cr d_{xz}-L CT Cr d_{xz}-d_{xy}, LBCT Cr d_{yz}-L CT, LBCT Cr d_{yz}- CO CT, LBCT
3	3.2827 (377.69)	0.0014	H-2→LUMO (3%) H-2→L+3(29%) H-2→L+12(5%) H-1→LUMO (29%) H-1→L+3(2%) HOMO→L+1(28%) HOMO→L+2 (2%)	Cr d_z^2-LCT, Cr d_z^2-d_{yz}, LBCT Cr d_z^2-d_{yz}, LBCT Cr d_z^2-d_{xz}, Cr d_z^2-CO CT Cr-L CT, Cr d_{xz}-d_{yz} Cr d_{xz}-d_{yz}, LBCT Cr d_{yz}-L CT, Cr d_{yz}-d_{xz}, LBCT Cr d_{yz}-d_{xy}, LBCT

[a] Energy above the ground state (vertical excitation), [b] Oscillator strength. [c] Occupied (Ψ_o) to virtual (Ψ_v) orbital excitation. [d] Character of excited state: Cr-to-arene charge transfer (Cr-L CT), Cr-to-CO charge transfer (Cr-CO CT) or Ligand based Charge transfer (LBCT, either intra-or inter-ligand charge transfer).

Table 5.31 Selected calculated singlet excited states for (η^6-benzene)$Cr(CO)_3$

The transition H-2 to L+4 which appeared in the aniline and anisole complexes excitation involves the transition of electron density from orbital which has mainly on the Cr-d_z^2 orbital with weak bonding relative to the three CO ligands and nonbonding or antibonding to the arene ligand to virtual orbital which mainly lies also on the CO ligands and Cr-d_z^2 orbital but it is antibonding relative to the three CO ligands. This transition involves Cr-CO CT and will lengthen the bond Cr-CO in the excited state and eventually one CO ligands will loss.

State	E eV, (nm)[a]	f[b]	$\Psi_o \rightarrow \Psi_v$[c]	Character[d]
1	3.1257 (396.67)	0.0003	H-1→L+1(4%) H-1→L+2(12%) HOMO→LUMO (65%) HOMO→L+3 (13%) HOMO→L+12 (4%)	Cr d_{yz}-L CT, Cr d_{yz}-d_{xz} Cr d_{yz}-CO CT CT, Cr d_{yz}-d_{xz}, LBCT Cr d_{xz}-L CT, LBCT Cr d_{xz}-CO CT, Cr d_{xz}-d_{yz}, LBCT Cr d_{xz}-CO CT, LBCT
2	3.1776 (390.18)	0.0017	H-2→L+1 (7%) H-2→L+2 (12%) H-2→L+4 (3%) H-2→L+11 (3%) H-1→LUMO (4%) H-1→L+3 (6%) HOMO→L+1 (22%) HOMO→L+2 (34%) HOMO→L+11 (5%)	Cr d_z^2-L CT, Cr d_z^2-d_{xz} Cr d_z^2-CO CT, Cr d_z^2–d_{xy} Cr d_z^2-CO CT Cr d_z^2-(d_{yz}+p_y), Cr d_z^2-CO CT Cr d_{yz}-L CT, Cr d_{yz}-d_{xz}, LBCT Cr d_{yz}-CO CT, LBCT Cr-L CT, LBCT Cr d_{xz}-d_{xy}, Cr d_{xz} -CO CT, LBCT Cr d_{xz}-(d_{yz}+p_y), Cr d_{xz}-CO CT
3	3.1939 (388.19)	0.0000	H-1→L+1 (14%) H-1→L+2 (24%) H-1→L+11 (4%) HOMO→LUMO (28%) HOMO→L+3 (24%)	Cr d_{yz}-L CT, Cr d_{yz}-d_{xz} Cr d_{yz}-CO CT, Cr d_{yz}-d_{xz}, LBCT Cr d_{yz}-(d_{yz}+p_y), Cr d_{yz}-CO CT Cr d_{xz}-L CT, LBCT Cr d_{xz}-CO CT, Cr d_{xz}-d_{yz}, LBCT

[a] Energy above the ground state (vertical excitation), [b] Oscillator strength. [c] Occupied (Ψ_o) to virtual (Ψ_v) orbital excitation. [d] Character of excited state: Cr-to-arene charge transfer (Cr-L CT), Cr-to-CO charge transfer (Cr-CO CT) or Ligand based Charge transfer (LBCT, either intra-or inter-ligand charge transfer).

Table 5.32 Selected calculated singlet excited states for (η^6-aniline)$Cr(CO)_3$.

State	E eV, (nm)[a]	f[b]	$\Psi_o \rightarrow \Psi_v$[c]	Character[d]
1	3.1842 (389.38)	0.0001	H-1→L+1(2%) H-1→L+2(19%) H-1→L+3(7%) HOMO→LUMO(33%) HOMO→L+2(14%) HOMO→L+3(16 %) HOMO→L+11(3 %) HOMO→L+12(2%)	Cr d_{yz} -L CT, Cr d_{yz}-d_{xz} Cr d_{yz}-d_{xy}, Cr d_{yz}-CO CT, LBCT Cr d_{yz}-CO CT, LBCT Cr d_{yz} L CT, Cr d_{xz}-d_{yz} Cr d_{xz}-d_{xy}, Cr d_{xz} -CO CT, LBCT Cr d_{xz}.d_{yz}, LBCT Cr d_{xz}-(d_{yz}+p_y), Cr d_{xz} -CO CT, LBCT
2	3.1986 (387.62)	0.0002	H-2→L+2(2%) H-2→L+3(3%) H-1→L+2(4%) H-1→L+3(4%) HOMO→LUMO(55%) HOMO→L+2(16%) HOMO→L+3(5%)	Cr d_z^2-CO CT, Cr d_z^2–d_{xy} Cr d_z^2-CO CT, Cr d_z^2–d_{yz} Cr d_{yz}-d_{xy}, Cr d_{yz}-CO CT, LBCT Cr d_{yz}-CO CT, LBCT Cr d_{yz} L CT, Cr d_{xz}-d_{yz} Cr d_{xz}-d_{xy}, Cr d_{xz} -CO CT, LBCT Cr d_{xz}.d_{yz}, LBCT
3	3.2463 (381.92)	0.0016	H-2→L+1(2%) H-2→L+2 (14%) H-2→L+4 (4%) H-2→L+11(2%) H-1→LUMO (5%) H-1→L+1 (3%) H-1→L+2(15%) HOMO→LUMO (3%) HOMO→L+1 (9%) HOMO→L+2 (18%) HOMO→L+3 (15%)	Cr d_z^2-L CT, Cr d_z^2 -d_{xz} Cr d_z^2-CO CT, Cr d_z^2–d_{xy} Cr d_z^2-(p_z+$d_{x^2-y^2}$) Cr d_z^2-(d_{yz}+p_y), Cr d_z^2-CO CT Cr d_{xz}-L CT, Cr d_{xz}-d_{yz}, LBCT Cr d_{yz} -L CT, Cr d_{yz}-d_{xz} Cr d_{yz}-d_{xy}, Cr d_{yz}-CO CT, LBCT Cr d_{yz} -L CT, Cr d_{yz} LF, LBCT Cr d_{yz} -L CT, LBCT Cr d_{yz} LF, Cr d_{yz} -CO CT, LBCT Cr d_{yz}.d_{yz}, LBCT

[a] Energy above the ground state (vertical excitation), [b] Oscillator strength. [c] Occupied (Ψ_o) to virtual (Ψ_v) orbital excitation. [d] Character of excited state: Cr-to-arene charge transfer (Cr-L CT), Cr-to-CO charge transfer (Cr-CO CT) or Ligand based Charge transfer (LBCT, either intra-or inter-ligand charge transfer).

Table 5.33 Selected calculated singlet excited states for (η^6-anisole)$Cr(CO)_3$

State	E eV, (nm)[a]	f[b]	$\Psi_o \rightarrow \Psi_v$[c]	Character[d]
1	2.6642 (465.37)	0.0004	H-1→LUMO (70%) HOMO→LUMO(26%)	Cr d_{xz}-L CT, Cr d_{xz}-d_{yz} Cr d_{yz}-L CT
2	2.9451 (420.98)	0.0001	H-2→LUMO (97%)	Cr d_z^2-LCT, Cr d_z^2-d_{yz}
3	3.0005 (413.21)	0.0439	H-1→LUMO (19%) H-1→L+1(14%) HOMO→LUMO (51%) HOMO→L+1(6%)	Cr d_{xz} -L CT, Cr d_{xz}-d_{yz} Cr d_{xz}-L CT Cr d_{yz}-L CT Cr d_{yz}-d_{xz}, LBCT

Table 5.34 Selected calculated singlet excited states for (η^6-benzaldehyde)$Cr(CO)_3$.

State	E eV, (nm)[a]	f[b]	$\Psi_o \rightarrow \Psi_v$[c]	Character[d]
1	2.4978 (496.38)	0.0006	H-1→LUMO (96%)	Cr d_{xz} -L CT, Cr d_{xz}-d_{yz}
2	2.7521 (450.51)	0.0000	H-2→LUMO (96%)	Cr d_z^2-LCT, Cr d_z^2-d_{yz}
3	2.8982 (427.79)	0.0537	H-1→L+1 (17%) HOMO→LUMO (71%)	Cr d_{xz}-L CT Cr d_{yz}-L CT

[a] Energy above the ground state (vertical excitation), [b] Oscillator strength. [c] Occupied (Ψ_o) to virtual (Ψ_v) orbital excitation. [d] Character of excited state: Cr-to-arene charge transfer (Cr-L CT), Cr-to-CO charge transfer (Cr-CO CT) or Ligand based Charge transfer (LBCT, either intra-or inter-ligand charge transfer).

Table 5.35 Selectedd Calculated Singlet Excited States For (η^6-methylbenzoate)$Cr(CO)_3$

5.3 Discussion

For decades the interpretation of the electronic spectra of the organometallic and transition metal coordination complexes have been based on the implicit of assumption that the sequence of electronic excitations should reflect the consequence of energy levels. Traditionally, the low energy transitions in the electronic spectra were assigned to be *d-d* or ligand field (LF) transitions, the highest occupied and the lowest empty orbitals were assigned as metal d orbitals[24]. These conclusions have been changed by the modern ab intio calculations for various organometallic and metal carbonyl complexes such as for $M(CO)_6$, $Mn_2(CO)_{10}$, $M(CO)_4(L_2)$ (L_2 = bidentate diimmine ligand), $Ir(Cp)(CO)_2$, $Cr(CO)_5PH_3$ and $W(CO)_5Py$. These studies assigned the main role in the low lying transitions to MLCT and M→CO CT transitions while the LF transitions lie in much higher energy level than that of MLCT or MCO CT transitions. Although the MLCT state is the low lying excited state in these complexes, for most of these complexes this excited state is nondissociative (the MLCT involves transfer of one electron from the metal to the π^* orbital of the ligand). This should increase the basicity of the ligand and the acidity of the metal centre. This would increase the σ-bonding between the two parts of the complex and can couple vibrationally with the higher energy LF excited state which is dissociative (as the case with $Cr(CO)_6$) and leads to ligand loss. However $Cr(CO)_4$(bipy) was found to have dissociative Cr-bipy CT band which leads to loss of one of the CO ligands in the femtosecound time scale (within the Frank-Condon excited state relaxation) to form the solvated species $Cr(CO)_3$(bipy)(S).[25] The oxidation of the metal in the excited state (Cr-bipy CT) resulted in lengthening of the Cr-CO bonds and leads to loss of one of CO ligands.

The TD DFT calculations were found to be very good tools for this type of complexes. This encourages us to find correlations between the calculated transitions and the photochemistry of complexes. The bonding considerations of the initial and designated orbitals are likely to be important in the fate of the excited state and ultimately the nature of the observed photochemistry.

The DFT methods were used to calculate the initial optimised geometry for the complexes. Both DFT and HF methods reproduce the experimentally observed results to a good approximation. The DFT-B3LYP method has been demonstrated to predict excellent geometries and energies. It is well known that the excitation energies from the single excitation methods are always higher than the experimental

values, while the TD DFT excitation energies have been shown to be in closer agreement with the experimental values.

Our main goal is to use the results of TD DFT calculations and the molecular orbital composition (calculated from the optimised ground state structure) to predict the photochemical behaviour of these complexes. Investigations into the role of LF or MLCT excitations in the low lying excited states and the correlation of the products observed during the photochemical studies of $M(CO)_5L$ (Chapter 2) and (η^6-arene)$Cr(CO)_3$ photochemistry (Chapter 3) are also investigated.

5.3.1 The DFT and TDDFT calculations of $Cr(CO)_5L$ complexes (L = Py, Acpy, or CNpy)

5.3.1.1 Geometry optimisation of $Cr(CO)_5L$ complexes, L = Py, Acpy, or CNpy

A comparison of the Cr-N bond lengths for the three complexes i.e. $Cr(CO)_5Py$, $Cr(CO)_5Acpy$, and $Cr(CO)_5CNpy$, the bond length in pyridine complex (2.1844 A^o) is longer than that of acetylpyridine (2.174 A^o) which in turn is longer than the cyanopyridine (2.1728 A^o). This trend follows the increase in the π-acidity of the ligand, as this will increase the bond order between the metal and the pyridine ligand. This effect is also reflected by the comparison of the bond length of $Cr\text{-}CO_{trans}$, (1.8567 A^o, L= Py; 1.8589 A^o, L= Acpy; and 1.8602 A^o, L = CNpy).

On the other hand the comparison of the $Cr\text{-}CO_{cis}$ bond lengths shows that it is shorter in pyridine complex (1.8921 A^o) and longer in the both the acetylpyridine (1.8921, 1.8938 A^o) and cyanopyridine complexes (1.8935 A^o).

In the comparison of the C-Cr-C bond angles of the $Cr(CO)_5$ moiety the four cis CO ligands are not coplanar with the metal atom, being pushed away from the pyridine ligand. The pyridine ligand bisects the C-Cr-C bond angle. The interaction between the pyridine ligand and the four cis-CO ligands results in their being slightly away from the ring plane. This makes the four cis-CO ligands to have the C_{2v} symmetry instead of C_{4v}. This effect is also observed in the acetylpyridine and cyanopyridine complexes.

5.3.1.2 The molecular orbitals of $Cr(CO)_5L$ complexes, L = Py, Acpy, or CNpy

As mentioned in the results section, the consequence of the properties of each molecular orbital for all of the three $Cr(CO)_5L$ complexes are independent on the substituent on the pyridine ring. The exceptions of this are H-3 and L+6 orbitals. The orbital H-3 is centred on the acetyl group of acetylpyridine complex while it is centred on the π-orbital of the pyridine ring for the pyridine or cyanopyridine complexes, Fig. 5.13. So the energy of this orbital in the acetylpyridine complex appears in higher than those of pyridine and cyanopyridine complexes. This shows that the molecular orbitals of the ring are more stable than those on the substituent.

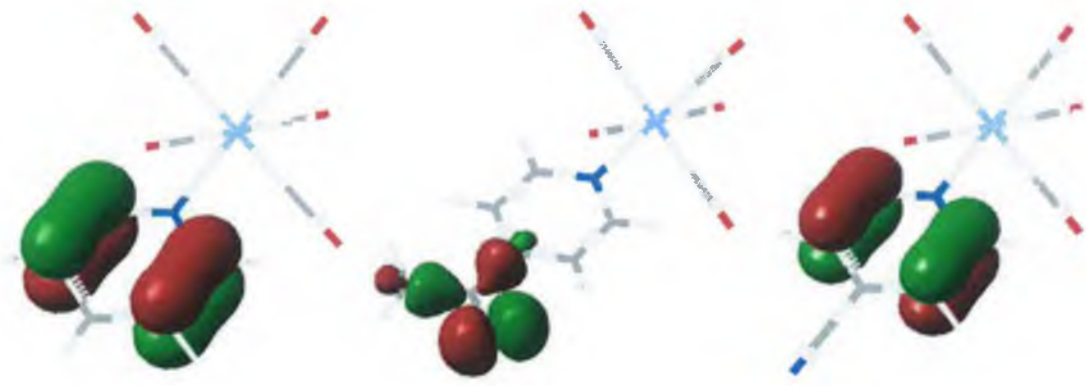

(a) (b) (c)

Fig. 5.13 The H-3 orbitals of (a) $Cr(CO)_5Py$, (b) $Cr(CO)_5Acpy$, (c) $Cr(CO)_5CNpy$.

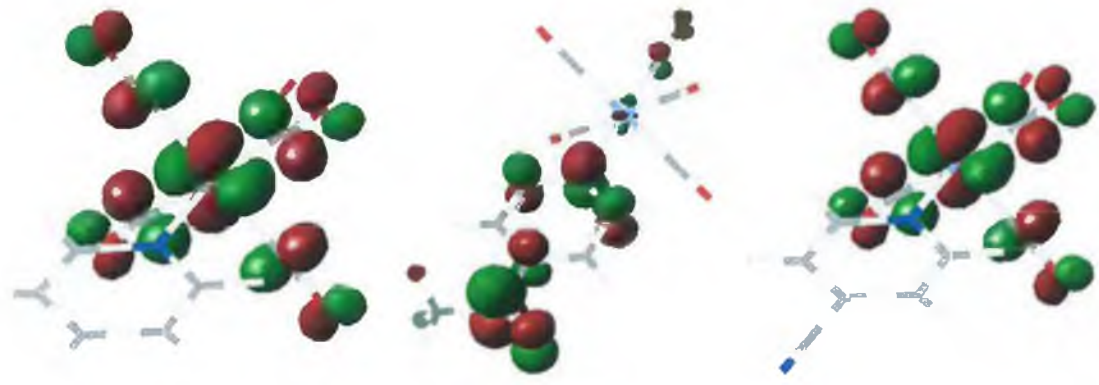

(a) (b) (c)

Fig. 5.14 The L+6 orbitals of (a) $Cr(CO)_5Py$, (b) $Cr(CO)_5Acpy$, (c) $Cr(CO)_5CNpy$.

While L+6 orbital of acetylpyridine complex is at lower energy than that of pyridine and cyanopyridine complexes. The orbital L+6 is centred predominantly on the acetylpyridine ligand with some density on trans-CO and Cr atom. It mainly has the π^*-orbital of the four cis-CO ligands and is antibonding relative to the chromium atom for the pyridine or cyanopyridine complexes, Fig. 5.14.

Generally the molecular orbitals are stabilised by the addition of substituents to the pyridine ring, the molecular orbitals of the cyanopyridine complex being the most stable, Table 5.7 and Fig. 5.2.

Kanis *et al* [26] found by studying the acceptor properties of the various pyridine or substituted pyridine complexes $Cr(CO)_5L$ that as the substituents become stronger acceptor, the energy of the pyridine π^* orbital is reduced (-1.07 eV for NH_2, -1.39 eV for H, -2.15 eV for COH). Since the LUMO is largely π^*-centred, the energy of the LUMO is extremely sensitive to 4-position derivatisation. Neither the energy of the d_{xz} fragment orbital nor the energy of the metal-based molecular HOMO are sensitive to 4-postion derivatisation. Thus the HOMO-LUMO gap is sensitive to the derivatisation and correlates well with observed trends in λ_{CT} (wavelength excitation of charge transfer band). ZINDO calculations on $Cr(CO)_5$(pyridine) or $Cr(CO)_5$(formylpyridine) found that in the pyridine complex 0.88 electrons are transferred from the metal fragment (originates in the chromium d_{xz} orbital) to the pyridine ring in the MLCT transition. The charge transfer picture for (4-formylpyridine)$Cr(CO)_5$ is similar in that the metal fragment donates extensive electron density (1.00) to the coordinated ligand. Surprisingly, "the acceptor substituent" (formyl group) receives only 0.26 of the electron density transferred to the pyridine ring.

The HOMO of the pyridine fragment interacts only weakly with the appropriate filled d_π metal orbital (d_{xz}) to raise its energy above that of the other two d_π orbitals, thereby forming the HOMO of the molecule. This molecular orbital is 93 % d_{xz}, 5% pyridine π, and 1% pyridine π^*, displaying near-negligible covalent character. Since the π^* LUMO of the pyridine fragment does not strongly interact with any metal orbitals, it becomes the LUMO of the molecule (~94% pyridine π^* and only 2% metal d_{xz}). Due to poor π-coupling between interacting fragments, the HOMO of the molecule is predominantly metal based and the molecular LUMO is primarily ligand based. The MLCT (represented by a HOMO→ LUMO excitation) involves significant charge transfer (promotion of an electron to a ~93% ligand based orbital).

The calculations on the Cr-pyridine or substituted pyridine complexes are consistent with the results obtained by Záliš *et al.*[10] for the pyridine and cyanopyridine complexes of tungsten. They found that all the molecular orbitals are largely delocalised, the d-character being distributed among more MOs than predicted by simple LF arguments. The tungsten 5d orbitals have higher energy than the chromium 3d orbitals and this according to ligand field (LF) theory will lead to higher splitting for 5d orbitals upon exposure to an octahedral field than for Cr 3d orbitals. Although the Cr 3d orbitals are lower in energy this will not effect on the position of the MLCT band. Thus the ligand field (LF) transitions still appear at higher energy for the two metals. This consistent with the recent picture of the photochemistry of the organometallic complexes in which generally the low-lying excitation is involve a MLCT transition.

5.3.1.3 Time Dependent Density Functional Theory (TD DFT) calculations and the correlation of these results with the photochemistry of $Cr(CO)_5L$, L = pyridine, acetylpyridine, and cyanopyridine

The low-lying excited states of these complexes have mainly MLCT and LBCT properties. Although these excitations are more likely to the non-dissociative, MLCT transition can take part in the population to LF excitation. These are more likely, to be dissociative with respect to pyridine ligand or CO ligands. In order to explain the observed photochemistry of these complexes, which undergoes both CO and unique ligand loss, we can expect two classes of LF states, one which is responsible for the loss of the pyridine ligand and the other loss of CO. Thus we can explain the wavelength dependency of the photochemistry of $Cr(CO)_5L$ complexes. Direct excitation with visible light will populate the lowest energy (mainly MLCT or M-CO CT and LBCT) states and these in turn populates the low energy LF state and to a smaller extent the high energy LF state, which results in pyridine ligand loss and to a lesser extent loss of CO respectively.

The presence of an electron withdrawing substituent on the pyridine ligand changes the low lying excited state from Cr-CO CT to one which is more Cr-L CT in character. An explanation for the highly efficient pyridine loss from $Cr(CO)_5Py$ upon excitation with visible light into the low lying excited state (i.e. which is mainly Cr-CO CT band) is as a result of oxidation of the metal which decreases the back donation to the pyridine ligand.

$Cr(CO)_5L$	Calculated UV/vis bands (nm)	Excited state properties	Photoproduct produced
$Cr(CO)_5Py$	392.16	Cr-CO CT	Py loss
	372.92	Cr-CO CT	Py loss
	367.64	MLCT, LBCT	Py+CO loss
$Cr(CO)_5Acpy$	490.63	MLCT, LBCT	Acpy loss
	469.88	MLCT, LBCT	Acpy loss
	436.24	MLCT, LBCT	CO loss
$Cr(CO)_5CNpy$	480.31	MLCT, LBCT	CO loss
	455.78	MLCT, LBCT	CNpy loss
	428.15	MLCT, LBCT	CO loss

Table 5.36 The calculated, experimental, and the properties of the low energy absorption bands of $Cr(CO)_5L$, where L = Py, Acpy, or CNpy. The experimentally observed photoproducts (which produced upon excitation of the complex under the absorption band) are also indicated.

5.3.1.3.1 TD DFT calculations and the correlation of these results with the photochemistry of $Cr(CO)_5Py$: -

Fig. 5.15 shows the positions of the three low-lying excited states relative to the experimental UV/vis absorption spectrum of $Cr(CO)_5Py$ in cyclohexane. These excited state are close to the position of λ_{max} of the pyridine complex. This means that these excitations contribute significantly to the overall absorptivity of the complex.

The first low-lying excited state in $Cr(CO)_5Py$ involves the transitions HOMO-(L+1) (83 %) and (H-2)-(L+3) (8 %) and these are predominantly the Cr-π^*CO CT. The HOMO-(L+1) transition also involves a LF transition (Cr d_{xz} - d_z^2 transition). As a result of these two processes (i.e. Cr-π^*CO CT and LF) the chromium atom will oxidised in the excited state so the main effect will be weakening the Cr-Py π^*-bonding and Cr-CO π^*-bonding. The most effected groups in this transition are Py and trans CO ligand (which is π-bonded to Cr d_{xz}), but these transitions will labialise the pyridine ligand for two reasons: -

1) The pyridine ligand is the weaker π-bonded to the metal.

2) The LF transition involved the transition to d_z^2 orbital which antibonding σ^* Cr-Py bond.

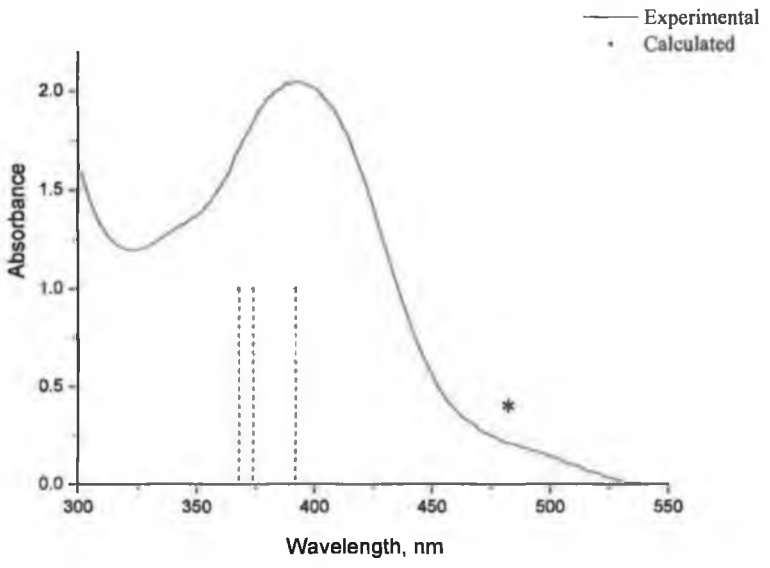

Fig. 5.15 The positions of the three low-lying excited states (vertical lines) relative to the experimental UV/vis absorption spectrum of $Cr(CO)_5Py$ in cyclohexane. * The low energy shoulder, which observed experimentally and not predicted by TD DFT can be assigned to singlet-triplet coupling.

So the excitation with band at 392 nm will result in the lablisation of Cr-Py bond, which results in pyridine loss to form the coordinatively unsaturated species $Cr(CO)_5$.

The second low-lying excited state in $Cr(CO)_5Py$ involves the transition (H-1)-LUMO and these are predominantly by the Cr-π^*Py CT. The chromium atom will be oxidised in the excited state so the main effect will be weakening the Cr-CO π^*-bonding and Cr-π^*Py CT. For the Cr-Py although this transition will weaken Cr- Py π-bonding, it will increase the Cr- Py σ-bonding. This transition will tend to labialise the trans-CO ligand because the transition involved taken an electrondensity from the bond Cr-CO_{trans} π^*-bonding to π^*-orbital on the pyridine ligand which is nonbonding relative to the trans-CO ligand. So the expected effect will be the loss of trans-CO ligand from the parent complex to form the coordinatively unsaturated species C_{4v}-$[Cr(CO)_4Py]$.

The third low-lying excited state in $Cr(CO)_5Py$ involves the transition (H-2)-(L+1) (65 %) and HOMO-LUMO and these are predominantly the Cr-π^*CO_{cis} CT and Cr-

π^*Py CT respectively, in addition to CO-Py CT. As the first transition involves the transition of the electrondensity from Cr d_{xy} which is bonding with respect to the four cis-CO ligands to the π^*-orbital of the pyridine ligand, the main effect will be labilisation of Cr-CO_{cis} bond leading to loss the CO ligand. This transition also involves a LF transition (Cr d_{xy} - d_z^2 transition). As a result of these two processes (i.e. Cr-π^*CO CT and LF) the chromium atom will oxidised in the excited state so the main effect will be weakening the Cr-Py π^*-bonding and Cr-CO π^*-bonding. The most affected groups in this transition are Py and cis CO ligand (which is π-bonded to Cr d_{xy}). The second transition involves Cr-π^*Py CT from Cr d_{xy} orbital which is bonding to the trans CO ligand to π^* which is centred on the pyridine ligand. This will labile the Cr-CO bonding.

The total effect will be the loss of pyridine ligand and to a lesser extent loss of one of the cis-CO ligands to form the coordinatively unsaturated species $Cr(CO)_5$ and Cs-$[Cr(CO)_4Py]$.

So TDDFT results provides an explanation of the experimental observations of the substitution reactions of the complexes in this study and also an explanation for the observed the wavelength dependency in the photochemistry of these complexes.

Experimentally, the excitation with visible monochromatic or broadband light with >400 or 405 nm involves the efficient loss of the pyridine ligand and less efficient loss of CO. Increasing the energy of irradiation light increases the efficiency of CO loss and decreases the efficiency of the loss of the ligand L.

5.3.1.3.2 TD DFT calculations and the correlation of these results with the photochemistry of $Cr(CO)_5$Acpy and $Cr(CO)_5$CNpy: -

The TDDFT results of these complexes are simpler than those of pyridine complex and they predict predominantly Cr-CO or Cr-L charge transfer transitions. Figs. 5.16 and 5.17 show the positions of the three low-lying excited states relative to the experimental UV/vis absorption spectrum of $Cr(CO)_5L$, L = Acpy, or CNpy in cyclohexane or toluene. These excited state are close to the position of $\lambda_{max.}$ of the acetylpyridine complex, in other words the complex in this area has a good absorptivty. While the transitions in the $Cr(CO)_5$CNpy complex are close to the shoulder of the observed absorption band.

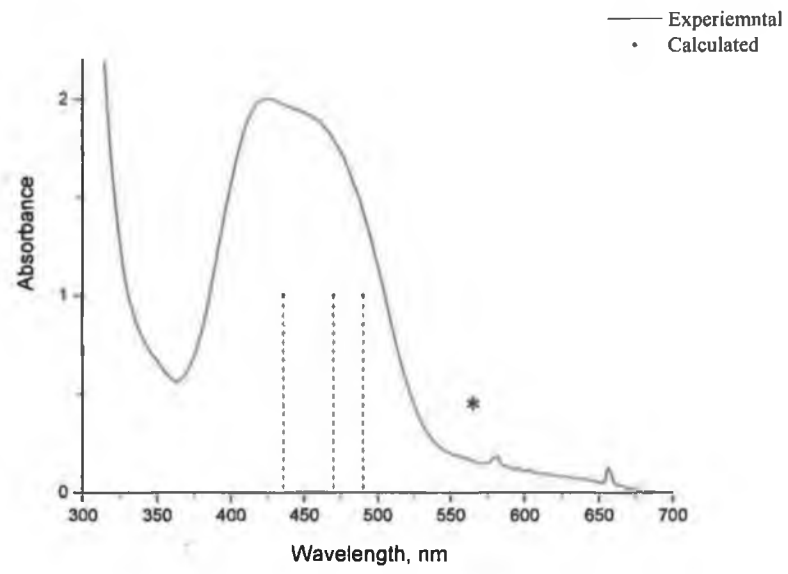

Fig. 5.16 The positions of the three low-lying excited states (vertical lines) relative to the experimental UV/vis absorption spectrum of $Cr(CO)_5$Acpy in cyclohexane. * The low energy shoulder, which observed experimentally and not predicted by TD DFT can be assigned to singlet-triplet coupling.

The first low-lying excited state in $Cr(CO)_5$Acpy involves the transition (H-1)-LUMO and is predominantly by the Cr-π^*Acpy CT. This excited state is similar to the second excited state of the pyridine complex. The chromium atom is oxidised in this excited state so the main effect will be weakening the Cr-CO π^*-bonding and Cr-π^*Acpy CT. For the Cr-Acpy although this transition will weaken Cr- Acpy π-bonding, it will increase the Cr- Acpy σ-bonding.

This transition will labialise the trans-CO ligand because the transition involved taking electrondensity from the bond Cr-CO_{trans} π^*-bonding to π^*-orbital on the acetylpyridine ligand which is nonbonding relative to the trans-CO ligand. So the expected effect will be the loss of trans-CO ligand from the parent complex to form the coordinatively unsaturated species C_{4v}-$[Cr(CO)_4L]$.

The second excited state in acetylpyridine complex involves the transition HOMO-LUMO which is dominated by Cr-π^*L CT from Cr d_{xz} orbital and which is bonding to the trans CO ligand to a π^* which is centred on the acetylpyridine ligand. This will labilise the Cr-CO bond and will eventually result in the loss of trans-CO to form the coordinatively unsaturated species C_{4v}-$[Cr(CO)_4L]$.

The third excited state is (H-2)-LUMO As the first transition involves the transition of the electrondensity from Cr d_{xy} which is bonding to the four cis-CO ligands to the π^*-orbital of the pyridine ligand, the main effect will be labilisation of Cr-CO_{cis} bond which will lengthen and may loss the CO ligand. The expected effect of this transition is the lengthening of Cr-CO bond which will resulted in the loss of a CO ligand to form the coordinatively unsaturated species Cs-$[Cr(CO)_4L]$.

Our photochemical studies on both of these complexes revealed that the loss of the unique ligand (L) the main photochemical process upon photolysis with long wavelength and increasing the energy of the photolysis light will increase the formation CO loss photoproduct. The TD DFT calculations give the expectation that the Cr-L CT as the lowest excited state in these complexes, so the expected effect of this excitation is the oxidation of the metal in the excited state and this will lengthen Cr-CO bond leading to the dissociation of this bond to form the coordinatively unsaturated photoproduct $Cr(CO)_4L$. As explanation for that difference between the theory and the experiment, it is expected to give the main role to the equilibrium between the lowest excited state with Cr-CO CT excited state or the lowest LF excited state. Under this consideration it is possible to explain the presence of unique ligand loss photoproduct upon excitation under Cr-L CT excited states.

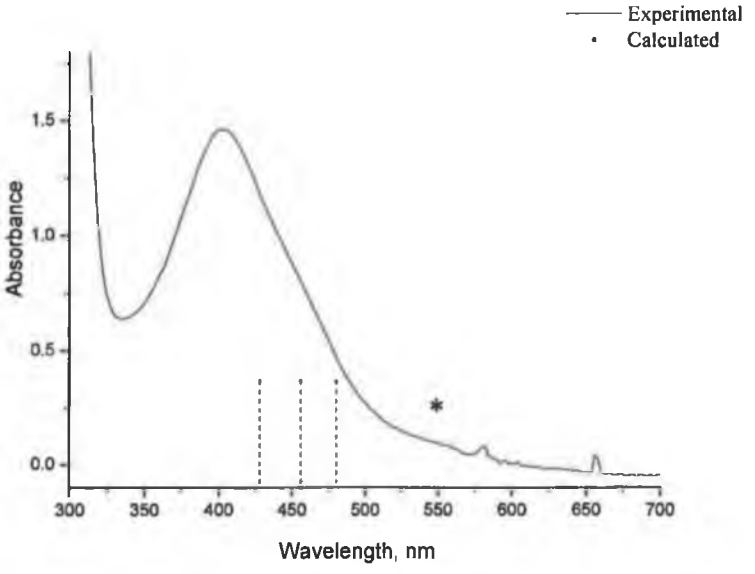

Fig. 5.17 The positions of the three low-lying excited states (vertical lines) relative to the experimental UV/vis absorption spectrum of $Cr(CO)_5(CNpy)$ in toluene. * The low energy shoulder, which observed experimentally and not predicted by TD DFT can be assigned to singlet-triplet coupling.

5.3.2 The DFT and TDDFT calculations of (η^6-arene)$Cr(CO)_3$ complexes

The benzene complex (i.e. (η^6-benzene)$Cr(CO)_3$) is the most symmetrical one amongst the selected set of arene complexes. Therefore it contains some energy levels, which have the same energy because they face a symmetrical electrostatic field of the benzene ligand. Thus we expect many of the orbitals to be doubly degenerate and these are essentially formed from the doubly degenerate orbitals d_{xz}, and d_{yz} as the incoming benzene ligand approaching along the z-axis while the orbital d_{xy} is singly degenerate. This degeneracy is lost when the benzene ring is monosubstituted by NH_2, OCH_3, CHO, or $COOCH_3$. The splitting of the originally degenerate orbitals of the benzene complex upon substitution is due to the following reasons: -

1) The substituted benzene complexes are less symmetric than the benzene complex. The d-orbitals are exposed to inhomogeneous ligand field.
2) The exo-carbon atom of the substituted benzene will either bend toward or away from the $Cr(CO)_3$ moiety. This provides another asymmetric influence on the metal orbitals.
3) The structure of complex which has electrondonating substituent on the benzene ring (as the case with aniline and anisole complexes) will has eclipsed syn structure while the complex with electron withdrawing substituent on the benzene ring (as the case with benzaldehyde and methylbenzoate complexes) will has staggered anti conformation.

The degeneracy of some of the benzene complex orbitals results in excited states having a variety of transitions for different orbitals, many of which have the same properties. While the complexes with substituted benzenes the transitions are simpler and as the substituent effect increases these transitions appear simpler.

The contribution of the arene orbitals in the low lying excited states is mainly to the lower two excited states which occur in the visible region of the spectrum.

The calculated optimised structures of (η^6-arene)$Cr(CO)_3$ complexes are consistent with the literature[14, 15, 21] structures as determined by X-ray diffraction. Thus the benzene complex has an eclipsed structure and the hydrogen atoms bent toward the $Cr(CO)_3$ moiety. While for substituted benzene with electron donor substituents the structure has a syn-eclipsed conformation while electron-withdrawing substituent prefers anti- staggered conformation.[27]A recent theoretical study by Suresh *et. al.* [14]

used Gaussian 94 package, investigated the structure and reactivity of these complexes.

In the comparison the electronic structure of (η^6-benzene)$M(CO)_3$ complex calculated in our study with that observed in Fig. 1.8 (Chapter 1), the HOMO is doubly degenerate. This is expected, as the benzene ligand faces the degenerate orbitals d_{xz}, d_{yz} so the HOMO and H-1 orbitals appeared doubly degenerate. While the orbital H-2 is singly degenerate because it is formed from the Cr-d_z^2 orbital which is nonbonding to the benzene ring but it is bonding to CO ligands. The HOMO degeneracy is lost when the benzene ring is substituted, and the Cr 3d orbitals will face an symmetric field upon bonding with the arene ligand. The degree is affected by the electronic and structural nature of the substituent.
The oscillator strength increases when the benzene ring substituted with either electron-withdrawing groups or electron-donating groups.

5.3.2.1 Time Dependent Density Functional Theory (TD DFT) calculations and the correlation of the electronic transitions with the photochemistry of (η^6-arene)$Cr(CO)_3$ complexes.

For the most symmetric molecule in this set benzene complex has various transitions for the same excited state as a result of the degeneracy. As the substituent effects increases the excitation appears simpler as a result of the difference in energy for the orbitals so just those orbitals that have specifically the energy of the transition are taken part in the transition.

5.3.2.1.1 TD DFT calculations and the correlation of the electronic transitions with the photochemistry of (η^6-arene)$Cr(CO)_3$ complexes. arene = benzene, aniline, or anisole.

Figs. 5.18-20 show the positions of the three low-lying excited states relative to the experimental UV/vis absorption spectra of (η^6-arene)$Cr(CO)_3$, arene = benzene, aniline, or anisole in cyclohexane. These excited states are close to the low absorption side of the absorption spectrum of the arene complex.
The first excited state in this complex involved the transition HOMO or (H-1) (d_{yz} properties) is bonding to the CO ligands to LUMO or to L+1 orbital, which is

predominantly lies on π^* of the ligand and some on CO ligands. Some LF on the chromium atom also involved in this transition. So the excitation is mainly involve Cr-L charge transfer (L = benzene, aniline, anisole) and with a small LF contribution. The expected effect of this transition will lengthen Cr-CO bond in the excited state. The result photoproduct from this excitation is the coordinatively unsaturated species (η^6-arene)$Cr(CO)_2$. The presence of these transitions in the excited state will give the expectation that the photolysis in this band will result the CO loss from the parent tricarbonyl molecule but this also depends on the contribution of this transition in the excited state.

The transition HOMO or H-1 to L+2, or L+3 involves the transition of electron density from HOMO or H-1 orbital which is mainly d-orbital character (60 % d_{xz} or d_{yz} character) and is bonding to the CO ligands, to a virtual orbital which mainly on the Cr d-orbitals and bonding relative to the three CO ligands in which two of these ligands bond with Cr and antibonding to the arene. So the major transitions are d-d transitions (LF excitation), which involves the transition of the electrondensity from bonding orbital to antibonding orbital especially relative to the arene ligand and to less extent Cr-arene charge transfer. The expected effect of this transition will lengthen Cr-arene in the excited state leading to the rupture of the arene to form the coordinatively unsaturated species (η^x-arene)$Cr(CO)_3$ (x = 0-4).

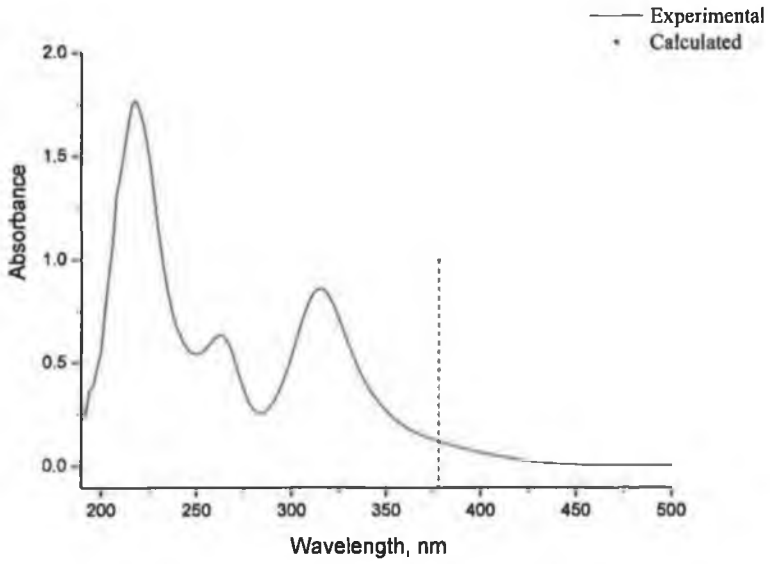

Fig. 5.18 The positions of the three low-lying excited states (vertical lines) relative to the experimental UV/vis absorption spectrum of (η^6-benzene)$Cr(CO)_3$ in cyclohexane.

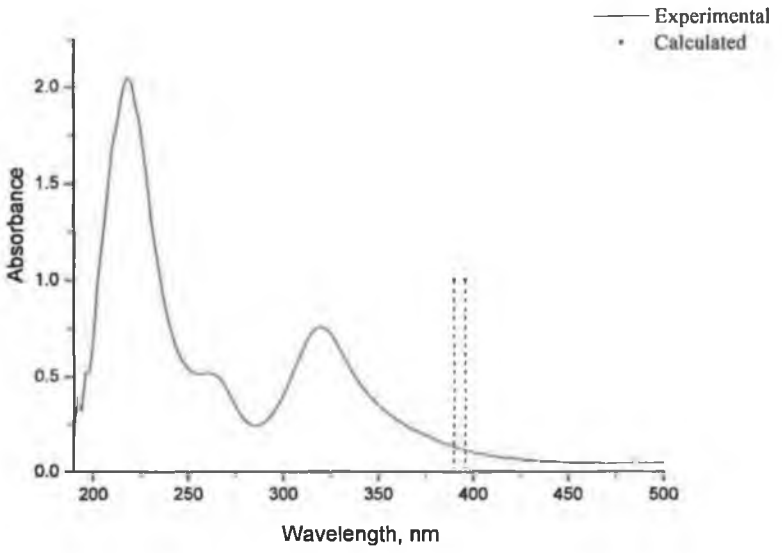

Fig. 5.19 The positions of the three low-lying excited states (vertical lines) relative to the experimental UV/vis absorption spectrum of (η^6-aniline)$Cr(CO)_3$ in cyclohexane.

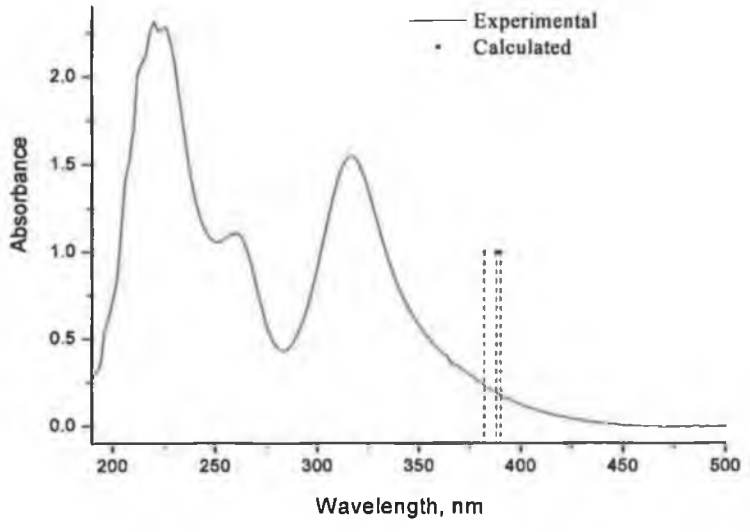

Fig. 5.20 The positions of the three low-lying excited states (vertical lines) relative to the experimental UV/vis absorption spectrum of (η^6-anisole)$Cr(CO)_3$ in cyclohexane.

In addition to transitions from the HOMO and H-1, which mentioned above the second excited state involves the transition H-2 to LUMO, or L+1. This involves the transition of electron density of orbital which has mainly on the Cr-d_z^2 orbital which weakly bonding to the three CO ligands and nonbonding to the benzene ligand to LUMO orbital which mainly lies on the arene ligand (ca. 85 %) and some extent on the CO ligands and to small extent transition from orbital d_z^2 to one of the orbitals d_{xz} or d_{yz} (LF transition). So this transition is mainly (Cr-CO) to arene CT and will

lablise the Cr-CO bond to form the coordinatively unsaturated species (η^6-arene)$Cr(CO)_2$.

The transition H-2 to L+11 or L+12 involves the transition of electron density from orbital which has mainly on the Cr-d_z^2 orbital which weakly bonding relative to the three CO ligands and nonbonding to the benzene ligand to a virtual orbital which mainly lies on the Cr d-orbital (which looks like the $d_{yz}+p_y$ or d_{xz} orbitals) and the three CO's which, are antibonding relative to the Cr. So this transition involves the Cr d-d transition from bonding d_z^2 to antibonding $d_{yz}+p_y$ or d_{xz} on the Cr atom (LF) and Cr-CO charge transfer. So this transition will involve the labialisation of Cr-arene bond and Cr-CO bond.

(η^6-arene)$Cr(CO)_3$ where arene is	Calculated UV/vis bands	Excited state properties	Photoproduct Experimentally
benzene	377.69 377.70	Cr-arene CT, Cr-CO CT, LF, LBCT	Arene and CO loss
aniline	390.18 396.67	Cr-areneCT, LBCT, LF	CO loss
anisole	381.92 387.62 389.38	Cr-arene CT, Cr-CO CT LF, LBCT	CO loss, and arene loss
benzaldehyde	413.21 420.98 465.37	Cr-arene CT, LF, LBCT	CO loss, and arene loss
methylbenzoate	427.79 496.38	Cr-arene CT, LF, LBCT	CO loss, and arene loss

Table 5.37 The calculated, experimental, and the properties of the low energy absorption bands of (η^6-arene)$Cr(CO)_3$, where arene = benzene, aniline, anisole, benzaldehyde, or methylbenzoate. The experimentally observed photoproducts (which were produced upon excitation of the complex under the absorption band) are also notified.

5.3.2.1.2 TD DFT calculations and the correlation of the electronic transitions with the photochemistry of (η^6-arene)$Cr(CO)_3$, arene = benzaldehyde or methylbenzoate: -

Figs. 5.21-22 shows the positions of the three low-lying excited states relative to the experimental UV/vis absorption spectra of (η^6-arene)$Cr(CO)_3$, arene = benzaldehyde, or methylbenzoate in cyclohexane. The excited states of these complexes appeared to be similar. All the transitions represent Cr-arene charge transfer as the main component of these excited states. In some cases they are mixed with LF transitions. The main effect of these transitions is the labialisation of CO, so the Cr-CO bond will tend to lengthen in the excited state and eventually will lead to the loss of CO. On the other hand the LF transition will labilise Cr-arene bond and eventually will lead to the loss of the arene ligand. As both of these operations are present in the first excited state, both processes are expected to be present upon photolysis of these complexes under this excitation.

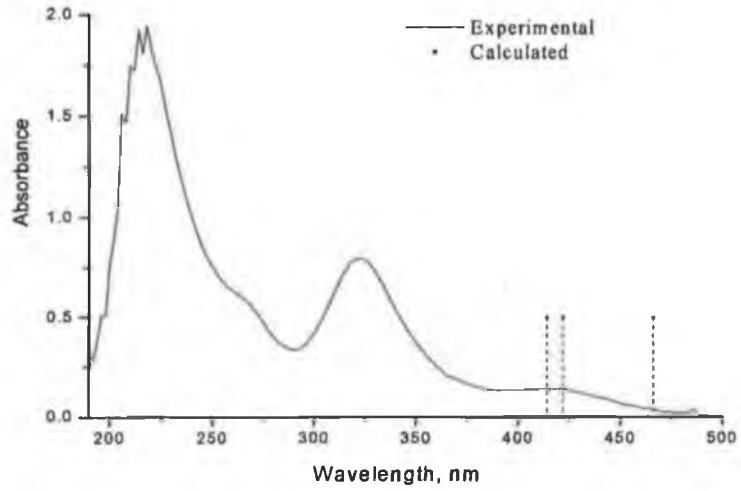

Fig. 5.21 The positions of the three low-lying excited states (vertical lines) relative to the experimental UV/vis absorption spectrum of (η^6-benzaldehyde)$Cr(CO)_3$ in cyclohexane.

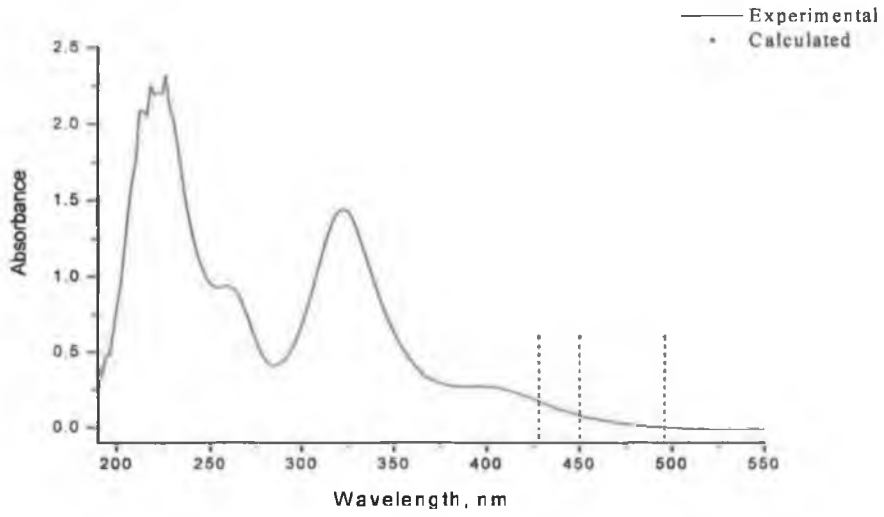

Fig. 5.22 The positions of the three low-lying excited states (vertical lines) relative to the experimental UV/vis absorption spectrum of (η^6-methylbenzoate)$Cr(CO)_3$ in cyclohexane.

Experimentally, the excitation with visible monochromatic or broadband light with >400 or 405 nm involves the efficient loss of the arene ligand and less efficient loss of CO. Increasing the energy of irradiation light will increase the efficiency of CO loss and decrease the efficiency of the loss of the arene.

5.4 Conclusion

5.4.1 The DFT studies on the complexes of the type $Cr(CO)_5L$, L = Py, Acpy or CNpy.

Our DFT studies on the complexes of the type $Cr(CO)_5L$, L = Py, Acpy or CNpy give very good match for the calculated optimised geometries and the available experimental data. The molecular orbital diagrams and the orbital composition for each orbital of these complexes were investigated. The molecular orbitals are stabilised upon substitution on the pyridine ring with electron withdrawing substituents. The general trend of the stability of the molecular orbitals follows the order $Cr(CO)_5CNpy > Cr(CO)_5Acpy > Cr(CO)_5Py$.

TD DFT calculations for the first three low lying excited states on this set of complexes generally reveals that these excitation involve transition of electron from the highest occupied molecular orbitals (HOMO) which carried ca 60 % Cr-d properties to the lowest unoccupied molecular orbitals (LUMO) which highly located

on the pyridine or CO ligands. So the low lying excited state for pyridine complex is not significantly different than that of acetyl- or cyano-pyridine complexes, and carries a high Cr-Py CT or Cr-CO CT character.

5.4.2 The DFT studies on the complexes of the type $(C_6H_5\text{-}X)Cr(CO)_3$, X = H, NH_2, OCH_3, CHO, or COOMe.

The molecular orbital diagrams and the orbital composition for each orbital of these complexes were calculated using DFT methods. Many molecular orbitals are degenerate in benzene. This degeneracy is lost upon substitution however. The electron donating substituents on the benzene ring destabilised the molecular orbitals, while the electronwithdrawing substituents stabilised them. Complexes with donor substituents tend to stabilise the d_{xz} orbital and destabilise the d_{yz} orbital and the reverse is true with electron drawing substituents. This was explained by considering geometry and substituent effects.

TDDFT calculations on the three lowest lying excited states of these complexes reveal that the lowest-energy transitions occurs from the high occupied molecular orbital which are localized on chromium d-orbitals to the low lying unoccupied molecular orbital localized on the arene or CO ligands and higher energy transition contain considerable chromium d-orbital character. So the excitations are mixture of mainly Cr-arene CT, Cr-CO CT and with a smaller contribution LF (Cr d-d transition).

5.5 References: -

1) a) Farrell, I.R.; Slageren, J.; Záliš, S.; Vlček, A. J., *Inorg. Chim. Act.*, 2001, 315, 44. b) Farrell, I.R.; Hartl, F., J.; Záliš, S.; Wanner, M.; Kaim, W; Vlček, A. J., *Inorg. Chim. Act.* , 2001, 318, 143. c) Záliš, S.; Farrell, I.R.; Vlček, A. J., *J.Am.Chem.Soc.*, 2003, 125, 4580.

2) Vlček, A. J., *Coord. Chem. Rev.,* 2002, 230, 225.

3) Zarić, S.; County, M.; Hall, M. B., *J. Am. Chem. Soc.,* 1997, 119, 2885.

4) Ehlers, A.W.; Lammertsma, K.; Baerends, E.J., *Organometllics,* 1998, 17, 2738,.

5) Frenking, G.; Wichmann, K.; Fröhlich, N.; Grobe, J.; Golla, W.; Van, D.L.; Krebs, B.; Läge, M., *Organometllics,* 2002, 21, 14, 2921.

6) Morales, Y. R.; Ziegler, T, *J. Phys. Chem. A,* 1998, 102, 3970.

7) Wang, C.C.; Wang, Y, Liu H. H.J.; Lin, K.J.; Chou, L.K.; Chan, K.S., *J.Phys. Chem. A,* 1997, 101, 8887.

8) Lee, M.T.; Hu, C.H., *Organometallics,* 2004, 23, 976.

9) Goumans, T.P.M., Ehlers, A.W.; van Hemert, M.C.; Rosa, A.; Baerends, E.J.; Lammertsma, K, *J.Am.Chem.Soc.*, 2003, 125, 3558.

10) Záliš, S.; Busby, M.; Kotrba, T.; Matousek, P.; Towrie, M.; Vlček, A. J. *Inorg. Chem.*, 2004, 1723, 43, 5.

11) Fitzpatrick, N.J., *J. Organomet. Chem*, 1977, 127, 325.

12) Carroll, D.G.; McGlynn, S.P., *Inorg. Chem.,* 1968, 7, 7, 1285.

13) Brunvoll ,J.; Cyvin, S. J., *J. Organomet. Chem.,* 1972, 36, 143.

14) Suresh, C.H.; Koga, N.; Gadre, S.R., *Organometallics*, 2000, 19, 3008.

15) Schleyer, P.R.; Kiran, B.; Simion, D.V.; Sorensen, T.S., *J. Am. Chem. Soc.*, 2000, 122, 510.

16) Frisch, M.J.; Trucks, G.W.; Schlegel, H.B.; Scuseria, G.E.; Robb, M. A.; Cheeseman, J.R.; Zakrzewski, V.G.; Montgomery, J.A., Jr.; Stratmann, R.E.; Burant, J.C.; Dapprich, S.; Millan, J..M.; Daniels, A.D.; Kudin, K.N.; Strain, M. C.; Farkas, O.; Tomasi, J.; Barone, V.; Cossi, M. ; Cammi, R.; Mennucci, B. ; Pomelli, C. ; Adamo, C.; Morokumma, K.; Malick, D. K. ; Rabuck, A. D.; Raghavachari, K.; Foresman, J. B.; Cioslowski, J.; Ortiz, J.V.; Baboul, A.G.; Stefanov, B.B.; Liu, G. ; Liashenko, A.; Piskorz, P.; Komaromi, I.; Gomperts, Y.; Nanayakkaara, A.; Gonzalez, C.; Challacombe, M.; Gill, P. M. W.; Johnson, B.; Chen, W.; Wong, M. W.; Andres, J. L.;

Gonzalez, C.; Head-Gordon, M.; Replogle, E. S.; Pople, J. A *Gaussian 98, revision A. 7*; Gaussian. Inc.; Pittsburgh, PA, 1998.

17) Frisch, M. J.; Trucks, G. W.; Schlegel, H. B.; Scuseria, G. E.; Robb, M. A.; Cheeseman, J. R. Montgomery, J. A. Jr.; Vreven, T. K. N. Kudin, J. C. Burant, J. M. Millam, S. S. Iyengar, J. Tomasi, V. Barone, B. Mennucci, M. Cossi, G. Scalmani, N. Rega, G. A. Petersson, H. Nakatsuji, M. Hada, M. Ehara, K. Toyota, R. Fukuda, J. Hasegawa, M. Ishida, T. Nakajima, Y. Honda, O. Kitao, H. Nakai, M. Klene, X. Li, J. E. Knox, H. P. Hratchian, J. B. Cross, C. Adamo, J. Jaramillo, R. Gomperts, R. E. Stratmann, O. Yazyev, A. J. Austin, R. Cammi, C. Pomelli, J. W. Ochterski, P. Y. Ayala, K. Morokuma, G. A. Voth, P. Salvador, J. J. Dannenberg, V. G. Zakrzewski, S. Dapprich, A. D. Daniels, M. C. Strain, O. Farkas, D. K. Malick, A. D. Rabuck, K. Raghavachari, J. B. Foresman, J. V. Ortiz, Q. Cui, A. G. Baboul, S. Clifford, J. Cioslowski, B. B. Stefanov, G. Liu, A. Liashenko, P. Piskorz, I. Komaromi, R. L. Martin, D. J. Fox, T. Keith, M. A. Al-Laham, C. Y. Peng, A. Nanayakkara, M. Challacombe, P. M. W. Gill, B. Johnson, W. Chen, M. W. Wong, C. Gonzalez, and J. A. Pople, *Gaussian 03, Revision A.1*, Gaussian, Inc., Pittsburgh PA, USA, 2003.

18) GaussView 3.0, Gaussian Inc., Pittsburgh PA, 2003. For more information see the Gaussian Wbsite http://www.gaussian.com/.

19) Gaussum, It is written by Noel O'Boyle, a member of Prof. Han Vos' research group at Dublin City University. This software is used to extract useful information from Gaussian programme. This includes the progress of the SCF cycles, geometry optimisation, UV-Vis/IR/Raman spectra, MO levels, MO contributions and more.

20) Cotton, F.A.; Darensbourg, D.J.; Fang, A.; Kolthammer, B.W.S.; Reed, D.; Thompson, J.L., *Inorg. Chem.*, 1981, 20, 4090.

21) Sickafoose, S.M.; Breckenridge, S.M.; Kukolich, S.G., *Inorg.Chem.*, 1994, 33, 5176.

22) Hunter, A.D.; Shilliday, L., *Organometallics*, 1992, 11, 1550.

23) Sailard, P.J.Y.; Grandjean, D., *Act.Cryst.*, 1976, B32, 2285.

24) Richards, W. G.; Cooper, D. L., *Ab intio molecular orbital theory*, Hehre, W. J.; Radon, L.; Schlayer, P. V. R; Pope, J. A., chapter 5, p 210.

25) Vlček, A. J.; Grevels, F. W.; Snoeck, T. L.; Stufkens, D. J., *Inorg. Chim. Acta*, 1998, 278, 83.

26) Kanis, D. R.; Lacroix, P. G.; Ratner, M. A.; Marks, T. J., *J. Am. Chem. Soc.*, 1994, 116, 10089.

27) Muetterties, E.L.; Bleeke, J. R.; Wucherer, E. J.; Albright, T. A., *Chem. Rev.*, 1982, 82, 499, Todres, Z. Y.; Ionina, E. A., *J. Org. Chem.*, 1993, 453, 197.

Chapter 6

Experimental

Chapter 6

Experimental

6.1 Reagents

Cyclohexane and toluene were of spectroscopic grade and were used without further purification. HPLC grade pentane was used as received without further purification. THF was distilled from sodium-benzophenone[1]. Heptane was distilled from potassium metal[1]. Diethylether and dibutylether were stored over sodium wire for 24 hours before use. Triphenylphosphine was recrystalized from diethylether before use, 4-acetylpyridine was distilled under reduced pressure and anisole was distilled under reduced pressure from P_2O_5 before use. N, N-dimethyl aniline was purified by standard procedures[1]. $(\eta^6\text{-}C_6H_6)Cr(CO)_3$ and $(\eta^6\text{-}C_6H_5COOCH_3)Cr(CO)_3$ (Aldrich Chemicals) were used as received without further purification. All other chemicals were obtained from Aldrich and used without further purifications. Air products and BOC supplied the argon and carbonmonoxide gasses

All reactions were carried out under an inert atmosphere of oxygen free dry argon or nitrogen.

6.2 Instrumentation

Infrared spectra were recorded on a Perkin Elmer 2000 FT-IR spectrometer using a 0.1 mm sodium chloride solution cell. Infrared were generally recorded in spectroscopic grade solvents as pentane, cyclohexane, and dichloromethane. NMR spectroscopy was carried out on a Burker model AC 400 NMR Spectrometer. The peaks were referenced to residual solvent peaks. U V-visible spectra were recorded on Hewlett Packard 8452A photodiode array spectrometer using quartz cells of 1 cm path length.

6.3 Synthesis of the complexes

6.3.1 The synthesis of $M(CO)_5L$; M=Cr, or W; L = Py, Acpy, CNpy, or PPh_3

These complexes were prepared via the photogenerated $M(CO)_5$ (THF) (M = Cr or W) THF = Tetrahydrofuran by use of standard literature methods[2]. Their purity was verified by infrared and UV.Vis spectroscopy.

[cis-$W(CO)_4(Acpy)_2$] complex was prepared by the thermal reaction of the 4-acetylpyridine and tungsten hexacarbonyl in toluene as a solvent.

Tetrahydrofuran pentacarbonyl-chromium(0) and -tungsten(0): - In a quartz reactor equipped with a magnetic stirrer, a gas inlet, a cooling mantle and a mercury high pressure immersion lamp, 1 mmole or of the metal hexacarbonyl (0.22 g of $Cr(CO)_6$ and 0.351 g of $W(CO)_6$) was dissolved in 125 ml of tetrahydrofuran and irradiated with stirring for ca. 2 hours. This solution was used with out further purification for the preparation of the complexes $M(CO)_5L$ (L = Py, Acpy, CNpy, or PPh_3) by addition of the appropriate ligand as indicated in the literature [3,4]

6.3.1.1 The synthesis of Pyridine pentacarbonyl-chromium(0) and tungsten(0): The THF solution of $[M(CO)_5THF]$ prepared as in (6.3.1), was transferred, under argon, to a round bottom flask containing 0.0791 g (1 mmole) of pyridine dissolved in 5 ml of THF. The solution was stirred at room temperature for 30 min. The solvent was removed under reduced pressure. The excess hexacarbonyl in the sample was removed by washing with small portions of cold pentane at ca. –80 C (3 x 5 ml). The yellow compounds were purified by recrystalization from n-pentane at –80 °C. The solid was then subjected to dynamic pumping for 2 hours for chromium complex, and 5 hours for tungsten complex at room temperature.
The yellow crystals were characterized as $[M(CO)_5Py]$ (M=Cr or W) by IR, and ^{1}H-nmr, spectroscopy, ν_{CO} bands (pentane) $[Cr(CO)_5Py]$ 2069,1940.5,1921.6 cm^{-1}.
$[W(CO)_5Py]$ 2072, 1935, 1922.5 cm^{-1} , ^{1}H-NMR:8.73(1 H), 7.73(1 H), 7.22(2 H).

6.3.1.2 The synthesis of 4-Acetylpyridine pentacarbonylchromium(0): The THF solution of $[M(CO)_5THF]$ prepared as in (6.3.1) was transferred under argon to a flask containing 0.0941 g (1 mmole) of 4-acetylpyridine dissolved in 5 ml THF. The solution was stirred for 30 min at room temperature. The solvent was removed under reduced pressure. The excess hexacarbonyl in the sample was removed by washing with small portions of cold pentane at ca. –100 C (3 x 5 ml). The yellow compound was purified by recrystalization from n-pentane at ca. –80 °C.
The yellow crystals were characterized as $[Cr(CO)_5$ Acpy] by its IR ν_{CO} bands (pentane) 2069.5,1940.5,1921.7,1709 cm^{-1}-(CH_2Cl_2) 2069.5, 1937.5,1703

6.3.1.3. The synthesis of 4-Acetylpyridine pentacarbonyltungsten (0): - The THF solution of $[W(CO)_5THF]$ which prepared in (6.3.1) was transferred under argon to 250 ml round bottom flask containing 0.0941 g of 4-Acetylpyridine dissolved in 5 ml THF. The solution was stirred for 30 min. The solvent was removed under vacuum. The excess hexacarbonyl impurities in the complex were

released by washing with cold n-pentane at ca. –100 °C (3x10 ml). The orange solid was dissolved in 20 ml of diethyl ether and the resulting solution purified by shaking with 5 g of alumina and the resulting solution was pumped dry, the complex was further purified by recrystalization from n-pentane at ca. –80 °C.

The orange crystals was identified as [$W(CO)_5$Acpy] by it's IR, ^{1}H-nmr, ν_{CO} bands in CH2Cl2:- 2074, 1932,1898 cm^{-1}. ^{1}H-NMR:8.97(2 H), 7.62(2 H), 2.62(3H)

6.3.1.4 The synthesis of 4-Cyanopyridine pentacarbonylchromium(0): - The THF solution of [$Cr(CO)_5$THF] which prepared in (6.3.1) was transferred under argon to 250 ml round bottom flask containing 0.1041 g (1 mmole) of 4-cyanopyridine dissolved in 5 ml THF. The solution was stirred for 30 min. The solvent was removed under vacuum. The excess hexacarbonyl impurities in the complex were released by washing with n-pentane (3x10 ml). The solid was dissolved in diethyl ether and purified by chromatography on silica gel. The orange band was collected and pumped dry under reduced pressure to afford the product as orange crystals. ν_{CO} bands [$Cr(CO)_5$Cnpy] (CH_2Cl_2) 2070,1942,1907 cm^{-1}

6.3.1.5 The synthesis of 4-Cyanopyridine pentacarbonyltungsten(0): - The THF solution of [$W(CO)_5$THF] which prepared as in (6.3.1) was transferred under argon to 500 ml flask containing 0.1041 g (1 mmole) of 4-cyanopyridine dissolved in 5 ml THF. The solution was stirred for 30 min. The solvent was removed under reduced pressure. The excess hexacarbonyl in the material were removed by washing with cold n-pentane (3x10 ml) and the resulting solid was dissolved in diethyl ether. The compound was purified by chromatography on silica gel using toluene as eluent. The yellow band was collected, the solvent removed under reduced pressure and pumped dry at 30 °C under reduced pressure to afford yellow crystals of [$W(CO)_5$Cnpy] ν_{CO} bands (CH_2Cl_2) 2075,1934.5,1903 cm^{-1}. ^{13}C-NMR 198, 157, 127.

6.3.1.6 The synthesis of Pentacarbonyl triphenylphosphine – chromium(0), and -tungsten(0): -

The THF solution of [$M(CO)_5$THF] prepared in (6.3.1) was transferred under argon to 500 ml flask containing 0.262 g (1mmole) of triphenylphosphine dissolved in 5 ml THF. The solution was magnetically stirred at room temperature for 30 min. The solvent was removed under reduced pressure. The excess hexacarbonyl in the sample was removed by washing with small portions of cold pentane at ca. –100 °C (3 x 5

ml). The yellow solid was purified by recrystalization from n-pentane at ca. –80 °C. The yellow crystals were characterised as $[M(CO)_5PPh_3]$ (M = Cr or W) by IR ,^{1}H-nmr,and ^{13}C-nmr spectroscopies, literature [1,2]. IR spectrum in pentane: -ν_{CO} bands (CH_2Cl_2) $[Cr(CO)_5PPh_3]$ 2064,1940 cm^{-1}.

$[W(CO)_5PPh_3]$ 2072, 1939, cm^{-1}. ^{1}H-NMR 7.37 (5H of phenyl groups).

6.3.1.7 The synthesis of *cis*- bis(4-acetylpyridine) tetracarbonyltungsten (0): -This complex was prepared for the first time in this work by heating to reflux temperature a solution containing $[W(CO)_6]$ (0.1 g, 0.284 mmole) and 4-acetylpyridine (0.07g, 0.583 mmole) in 20 ml toluene for 1.5 hr.The maroon precipitate was collected by filtration washed with hot n-hexane (3x20ml) washed and dried under reduced pressure. The maroon crystals was characterized by there IR, NMR spectroscopy as cis-$W(CO)_4(4\text{-Acpy})_2$, ν_{CO} bands 2008, 1934, 1881.4, 1838.4, 1702

^{1}H-NMR: 8.83(2H), 7.55(2 H), 2.523(3H), ^{13}C-NMR 195, 156, 143, 123, 27

6.3.2 The synthesis of [(η^6- arene)$M(CO)_3$], M = Cr; arene = aniline, anisole, or benzaldehyde; M = Mo, arene = N,N-dimethylaniline, anisole , or toluene

In the synthesis of arene complexes, except [(η^6-anisole)$Mo(CO)_3$], 25 ml flask fitted with simple reflux condenser and magnetic follower.

In the case of the benzaldehyde complex the aldehydic carbonyl group was protected by converting it to diethyl acetal prior to synthesis. (η^6-anisole)$Mo(CO)_3$ was prepared by the reaction of $[Mo(CO)_3Py_3]$ and $BF_3.OC_2H_5$

in the presence of anisole.

6.3.2.1 The synthesis of [(η^6-anisole)$Cr(CO)_3$]:- This complex was prepared by applying the procedure published in the literature (5)

$[Cr(CO)_6]$ (0.4 g,1.8 mmol), $C_6H_5OCH_3$(2.8 g, 25.9 mmol), Dibutyl ether (12 ml) and freshly distilled THF(1 ml). After purging the reaction flask with nitrogen, a reflux condenser was fitted with nitrogen bubbler so as to carry out the reaction under inert atmosphere. The mixture is heated at reflux for 24 hr. The yellow solution is cooled and filtered through celite on sintered-glass filter. The solvent was removed under vacuum at room temperature and the yellow solid washed with cold pentane.

ν_{CO} bands (CH_2Cl_2) 1967, and 1886 cm^{-1}.

6.3.2.2 The synthesis of [(η^6-aniline)$Cr(CO)_3$]: - This complex was prepared by applying the procedure published in the literature (5) [$Cr(CO)_6$] (0.4 g,1.8 mmol), $C_6H_5NH_2$(2.4 g, 24.73 mmol), Dibutyl ether (12 ml) and freshly distilled THF(1 ml). The flask and the condenser were thoroughly outgassed with nitrogen. After purging the reaction flask, a reflux condenser was fitted with nitrogen bubbler so as to carry out the reaction under inert atmosphere. The mixture is heated at reflux for 24 hr. The yellow solution is cooled and filtered through celite on sintered-glass filter. The solvent was removed under vacuum at room temperature and the yellow solid washed with cold pentane

ν_{CO} bands (cyclohexane) 1967, 1893, and 1888 cm^{-1}; (CH_2Cl_2) 1960, 1876 cm^{-1}

6.3.2.3 The synthesis of benzaldehyde diethyl acetal: - A literature procedure (6) was used. A mixture of –benzaldehyde (11 g, 0.104 mole), ethyl orthoformate (15.1 g, 0.102 mole), and 2 drops of concentrated sulphuric acid in 25 ml conical flask was magnetically stirred for 24 hours. Sodium carbonate 0.2 g-was added to neutralize. The solution was filtered and distilled under reduced pressure to afford 11.75 g (64 %) of benzaldehyde diethyl acetal, B.P. 96-99 °C/11-15 mm Hg. ^{1}H-NMR 7.33, 7.163, 5.37, 3.46

6.3.2.4 The synthesis of [(η^6-benzaldehydediethylacetal)$Cr(CO)_3$]: - A modification of a literature procedure(6,7) was used. [$Cr(CO)_6$] (0.4 g,1.8 mmol), benzaldehyde diethyl acetal (2.4 g, 24.73 mmol) in dioxane (12 ml). The flask and the condenser were thoroughly outgassed with nitrogen. After purging the reaction flask, a reflux condenser was fitted with nitrogen bubbler so as to carry out the reaction under inert atmosphere. The mixture is heated at reflux for 10 hr. The yellow solution was cooled and filtered through celite on sintered-glass filter. The solvent was removed under vacuum at room temperature and the yellow solid washed with cold pentane. The crude product was used for the preparation of benzaldehyde chromium tricarbonyl without further purification. The compound was characterized by IR spectrum

ν_{CO} bands (pentane): 1981, 1914 cm^{-1}.

6.3.2.5 The synthesis of [(η^6-benzaldehyde)$Cr(CO)_3$]:- To 0.27 g of (η^6-benzaldehydediethylacetal) chromium tricarbonyl in 40 ml ethanol 30 ml of 0.5 M HCl was added after 4 hr of stirring 150 ml of diethyl ether was added. The red ether

phase was separated. More ether was added to the aqueous phase was added and separate again. The two ether portions were collect together and the ether was evaporated at 12 torr and the rest was dried at 0.5 torr and 25 °C. The solid was dissolved in diethyl ether and passed through a pad of ciliate and pumped dry. The solid was recrystalized from pentane to give orange crystals of [(Benzaldehyde)$Cr(CO)_3$]. ν_{CO} bands(cyclohexane): 1995 , 1940, and 1931 cm^{-1} and 1707 cm^{-1}, ^{1}H-NMR 9.392 (1H), 5.887, 5.872 (2H), 5.627 (1H), 5.242, 5.226, 5.21(2H)

6.3.2.6 The synthesis of [(η^6-N,N-dimethylaniline)$Mo(CO)_3$]:- This complex was prepared following a literature procedure (8) but pentane was used instead of isopropyl ether for recrystalization. Hexacarbonylmolybdenum (0.3 g, 0.001 mole) was heated under reflux with N,N-Dimethyl aniline (0.6 g, 0.0045 mole) in heptane (30 ml) for 10 hr. The mixture was filtered to remove finally divided metal, and the solvent evaporated under reduced pressure at room temperature. The excess of the metal hexacarbonyl was sublimed under reduced pressure at 30 C and the residue recrystalized from pentane at –78 C. The pale yellow crystals are very sensitive to air and light. ^{1}H-NMR 5.838(2H), 5.063(3H) of arene, and 2.78(6H) of methyl groups

6.3.2.7 The synthesis of [(η^6-toluene)$Mo(CO)_3$]:- This complex was prepared following a literature procedure (9). Hexacarbonylmolybdenum (0.3 g, 0.001 mole) and 43 ml toluene was heated under reflux at 125 C for 24 hr. The solvent was removed under reduced pressure and the oil residue shake with 15 ml of cold pentane and decant. The solid was dried under high vacuum at 50 °C to remove the reminding [$Mo(CO)_6$]. The residue was dissolved in diethyl ether filtered under nitrogen through celite. Diethyl ether was removed to give yellow crystals of [(η^6-toluene)$Mo(CO)_3$]. ^{1}H-NMR 5.65(2H), 5.31(3H) of arene, and 2.178(6H) of methyl group

6.3.2.8 The synthesis of [$Mo(CO)_3(Py)_3$]: - This complex was prepared following a literature procedure (10). Hexacarbonylmolybdenum (0.4 g, 1.515 mmol) was reacted with pyridine (10 ml) by heating at 80 °C for 1hr and at 130 °C for additional 2 hr. The reaction mixture became dark red and was allowed to cool without stirring. Crystal formed, and adding pentane and cooling with an ice bath

completed precipitation. The mixture was filtered, and the product was washed with pyridine and pentane to afford a yellow, crystalline solid.

ν_{CO} bands (CH_2Cl_2) 1907, 1777 cm^{-1}.

6.3.2.9 The synthesis of [(η^6-anisole)Mo(CO)$_3$]: - This complex was prepared following a literature procedure (11). 4.5 mmol of $BF_3.O(C_2H_5)_2$ was added dropwise with stirring to 1.5 mmol of finely dispersed [$Mo(CO)_3(Py)_3$] and 1.5 mmol of anisole in 50 ml of ether. After 2 hr stirring at room temperature the reaction mixture was diluted with 100 ml of hexane. The ethereal hexane solution was washed with cold water (3 x 100 ml), dried over Na_2SO_4 and evaporated until starting crystallization. The solution was allowed to stand for several hours in the dry ice and the solvent was decanted. The crystals produced were washed with cold pentane and dried under vacuum. If necessary repeated crystallization from hexane was performed. IR spectrum in cyclohexane ν_{CO} 1981, 1907 cm^{-1}

6.4 Steady state photolysis

The samples were prepared as for laser flash photolysis. For steady state photolysis with NMR monitoring the samples were prepared in a degassable NMR tube in the deutrated cyclohexane. The solution was then subject to three freeze-pump-thaw procedures. Great care was necessary because the quartz in the NMR tube was very thin and could crack very easily. The sample was protected from light with aluminium foil. The sample was liquid pumped and atmosphere of Ar is then placed over the sample. A NMR spectrum was obtained of the starting compound, then the solution was placed in front of an air cooled 275 watt xenon arc lamp, with a UV/vis filter (λ> 500 nm), and turned manually for a prescribed time period.

6.5 Laser Flash Photolysis

6.5.1 Sample Preparation

Laser Flash Photolysis samples are prepared in a especially designed, sealable degassing bulb attached to fluorescence cell. By dissolution in appropriate spectroscopic grade solvent (cyclohexane or toluene), such that the absorbance at λ_{exc} was between 0.6-1.2 AU. The sample was degassed by three cycles of freeze-pump-thaw procedure to pressure of 10^{-3} torr. Subsequently, liquid pumping of the sample is carried out to ensure that traces impurities such as water are removed. The

atmosphere of interest, either CO or Ar is then placed over the sample .The pressure of gas admitted into the flash photolysis cell at this point was varied to control the concentration of CO .The solubility of the CO in cyclohexane was taken to be $9.0x10^{-3}$ M in 1atm CO. Spectra were recorded before and after degassing the sample to ensure that no changes had been taken place. Additionally, spectra were recorded through out the flash photolysis experiments in order to monitor spectral changes, should they occur.

6.5.2 The setting of Laser flash photolysis for UV-visible detection

The schematic diagram of the flash photolysis instrumentation is shown in Fig. (6.1), which contains a laser source for excitation (Nd: YAG)(neodymium yttrium aluminium garnet) laser and operates at fundamental frequency of 1064 nm; the Nd atoms about 1 % in the YAG host which has very good thermal conductivity to remove wasted heat. With the use of non-linear optics, the fundamental frequency can be doubled, tripled or quadrupled to generate a second, third or fourth harmonic at 532, 354.7 and 266 nm respectively. This gives the choice to select excitation of different photochemical processes within the system under study .The energy of the pulse is typically approximately 55 mJ, 45 mJ, and 25 mJ respectively.

The circular laser pulse is directed on to the sample cuvette .As the pulse passes through the power meter, situated directly before the sample, the oscilloscope is triggered. The monitoring light source is an air-cooled Applied Photophysics medium pressure xenon arc lamp (300 nm). This is arranged at right angle to the laser beam. The monitoring beam passes through the sample and is directed to the entrance slit of an Applied Photophysics f/3 monochromatic via a circular lens. Generally UV/vis filters (Corning) are used to block higher energy photons, thus preventing excessive photo-degradation of the sample, and allowing wavelength selection. A Hamatsu 5 stage photomultiplier tube operating at 850 V was placed at the exit slit of the monochromator. A transient digitiser via a variable load resister measured the changes in absorbance. The digitiser, a Hewlett Packard HP54510A oscilloscope was interfaced to a personal computer. The signals were recorded and analysed using a purpose designed software program, which has been previously described[12].

By recording transient signals over a range of wavelengths, the absorbance spectrum may be calculated at any time after the flash to generate difference absorption spectra of the transient species. Spectra are obtained as a result of point-by-point build up

manually changing the wavelength of the monochromator. It is necessary that the solution is optically transparent for the monitoring light beam; hence solvent like cyclohexane, toluene, which is spectroscopically transparent, is used.

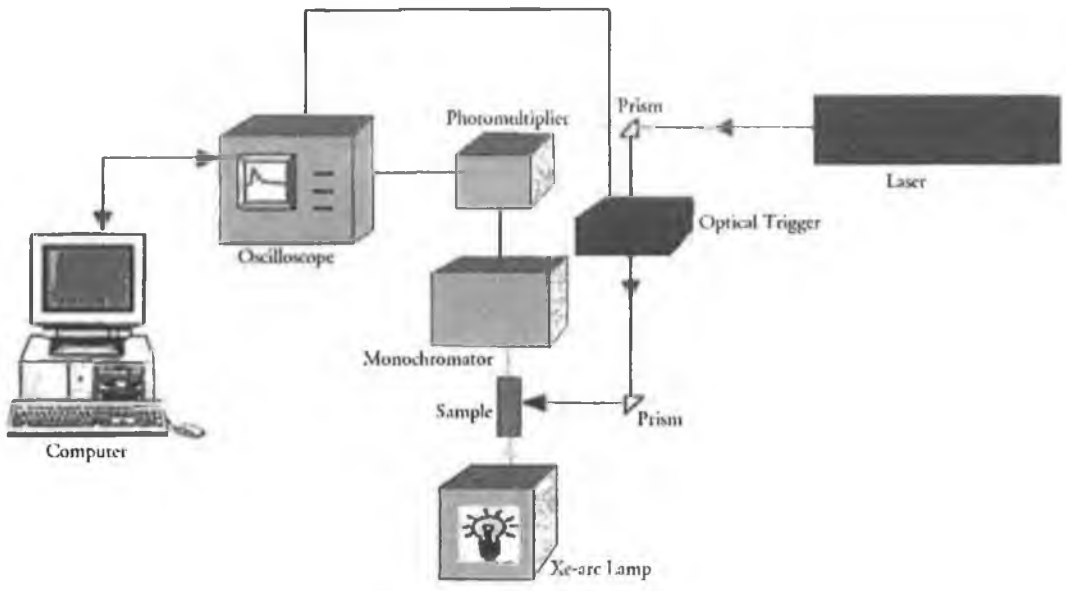

Fig. 6.1 Schematic diagram of UV/vis. Laser flash photolysis system.

6.6 Matrix Isolation

6.6.1 Sample Preparation[12, 13]

The sample was prepared for matrix isolation by transferring to a glass side arm, which was then attached to the lower part of the matrix shroud .The system is brought to the required vacuum (approximately 10^{-6} torr.) and deposition temperature (20 K). A specific volume of the required matrix gas is allowed into the gas handling line. This is then co-condensed onto the cold window with the sample, this technique called the slow spray-on technique. A gauge on the gas handling controls the rate of deposition of the matrix gas. Varying the temperature of the sample in the side arm controls the rate of sample deposition. The amount of sample deposition was periodically monitored using IR spectroscopy, until the maximum absorbance of the sample was 0.8 and 1.0 AU in the carbonyl region.

For matrix isolation studies equipment essential for construction of a system is as follows:

- Refrigeration system
- Vacuum chamber
- Vacuum pumping system

- Sample holder
- Gas handling system
- Method for generation of the species of interest e.g. UV lamp
- Method for analysis of species generated.

6.6.2 The refrigeration system

The refrigerator consists of a compressor unit connected to a compact expander unit or head module by high pressure (feed) and low pressure (return) helium. The head module is small and lights enough to be incorporated into matrix cells for use with a wide variety of instrumentation. The helium is compressed and then allowed to expand within the head module. The expansion of the helium causes the cooling effect. The choice of coolant gas and choice of host gas control the temperature limits of the matrix system. A cryostat from APD Cryogenics Inc. was used in the experiments described.

6.6.3 The vacuum chamber; the shroud.

With the matrix sample held at 12 K, it needs to be enclosed in a vacuum chamber, the shroud. The shroud must have the following features:

- At least one inlet port to facilitate deposition of matrix must be provided
- External windows appropriate to the spectroscopic technique being used
- The shroud should fit into the sample compartment of the spectrometer being used
- The interior of the shroud should be conveniently accessible at standard pressure, to facilitate cleaning of the sample window and surrounding parts
- The head module should be attached to the shroud using a seal, which can be rotated, allowing the sample window to be rotated within the shroud
- The shroud must be connected the vacuum system.

6.6.4 The vacuum system.

The shroud enclosing the head module of the refrigerator must be evacuated to insulate the cold sample from warming by convection and conduction (Dewar vacuum). Pressures around 10^{-3} millibarr are sufficient to provide an efficient

vacuum, however to minimise contamination, the highest achievable vacuum is required. A vacuum system of about 10^{-7} torr inside the sample chamber, when the cold window is at its experimental temperature (12 K), is required in all experiments. This vacuum was achieved by using an oil diffusion pump backed by a 5 stage rotary pump from Edwards High Vacuum International.

6.6.5 The sample holder

The sample holder is connected to the lower heat station of the refrigerator. It is crucial that the sample holder is made of a material that will be a good conductor at very low temperatures. Copper is the most cost-effective material for the metal part of the sample holder. In these experiments the window onto to which the matrix is deposited was made from CaF_2. Other materials used are CsBr, CsI, NaCl or KBr.

6.6.6 Gas handling system

The gases used were of very high purity from standard metal cylinders, supplied by Cryoservice Ltd. These were connected to regulators suitable for high purity gases, fitted with a flow control valve on the outlet, also supplied by Cryoservice Ltd. This allowed deposition of the matrix host at a controlled rate. Gas mixtures may be made up using a subsidiary gas handling line, increasing the risk of error, but greatly reducing the preparation time.

6.6.7 Generation of coordinatively unsaturated species

Photolysis was the chosen for generation of the coordinatively unsaturated species. This photolysis is achieved using either an Oriel 300 Watt Xe-arc lamp or 200-Watt Hg/Xe lamp. The first one used in combination with interference filters with λ_{exe}= 546, 436, 405, 365, 334, 313, and 297 nm to select particular wavelengths. The Hg/Xe lamp in combination with broad band filters with λ_{exe}>520, >410 nm, >390, >320 nm, and >300 nm to afforded broad band irradiation.

6.6.8 Analysis of species generated

In this study, IR and UV-vis spectroscopes were used to analyse the species generated. The infrared spectra recorded on a Perkin Elmer Spectrum One spectrometer. While the UV.vis spectra were recorded using Perkin Elmer Lambda EZ 201 spectrophotometer.

6.6.9 Preparation of typical sample

The samples were either solids or oils. Solid samples can be placed directly into the glass side arm, or alternatively they can be dissolved in a minimum of spectroscopic grade pentane and transferred a glass side arm. The solvent then being removed under reduced pressure. The side arm was then attached to the lower part of the shroud, close to the cold window. The spray-on gas line is then connected to the shroud. The system is brought to the required vacuum (~10^{-5} torr.) and deposition temperature (20 K). A specific volume of the required matrix gas is allowed into the gas handling line. This is then co-condensed onto the cold window with the sample. A gauge on the gas handling line mentors the rate of deposition of the matrix gas, which is controlled using a needle valve. Varying the temperature of the sample in the side arm controls the rate of sample deposition. The amount of sample deposition was monitored periodically, using IR spectroscopy, until the maximum absorbance of the sample was between 0.8 and 1.0 AU in the carbonyl region. Table 3-1 shows the conditions of the deposition of the complexes in this study.

Complex	Heating medium	Cell type	Deposition Temperature °C
$Cr(CO)_5Acpy$	Electric heating tape	L-type cell	22
$Cr(CO)_5Py$	Water bath*	L-type cell	25
(η^6-aniline)$Cr(CO)_3$	Electric heating tape	Linear cell	46
(η^6-anisole)$Cr(CO)_3$	Electric heating tape	Linear cell	28
(η^6-methylbenzoate)$Cr(CO)_3$	Water bath	L-type cell	31
(η^6-benzene)$Cr(CO)_3$	Water bath	L-type cell	15
(η^6-benzaldehyde)$Cr(CO)_3$	Water bath	L-type cell	24
(η^6-anisole)$Mo(CO)_3$	Electric heating tape	Linear cell	27
(η^6-toluene) $Mo(CO)_3$	Water bath	L-type cell	30
(η^6-N,N-dimethylaniline) $Mo(CO)_3$	Electric heating tape	Linear cell	59

* Water bath used in small Dewar.

Table (6.1) (The matrix deposition conditions of the complexes under the matrix isolation study)

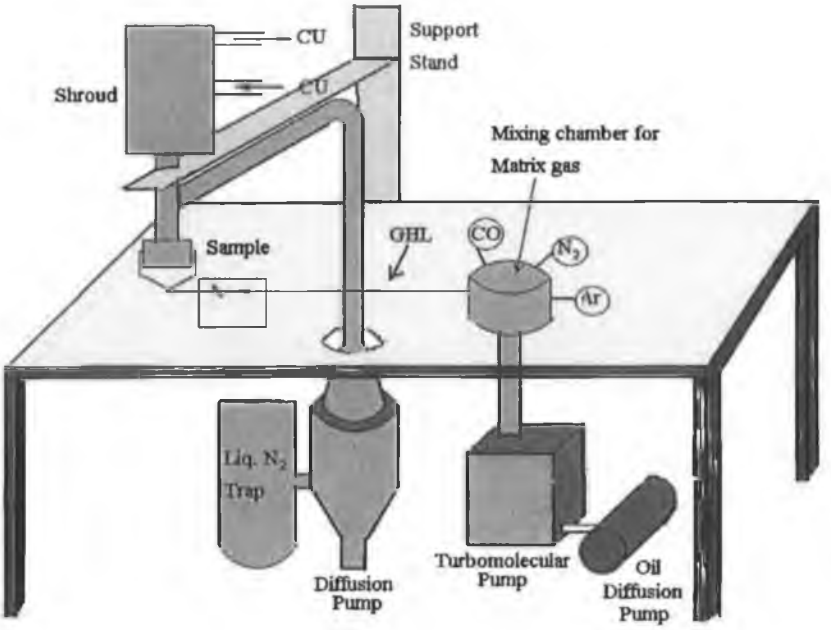

Fig. 6.2 Schematic diagram of Matrix instrumentation. CU is Compressor Unit. GHL is Gas Handling Line. Pirani and other pressure gauges are not shown.

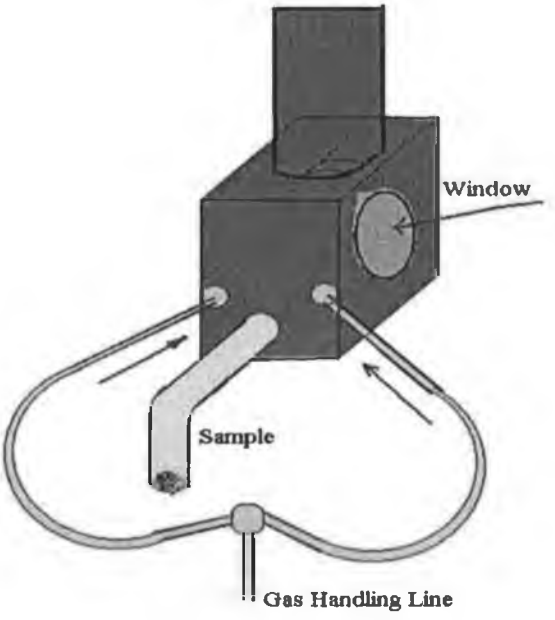

Fig 6.3 Schematic diagram of the matrix isolation cold cell.

6.7 Suggestions for future work

Photochemistry of $M(CO)_5L$ complexes: Extending the photochemical studies on this type of complexes by changing the substituent on the pyridine ring to involve non conjugated electron with drawing group like flouro or CF_3 and studying of these systems by DFT calculations for the evaluation of the experimental results.

Photochemistry of $(\eta^6$-arene$)Cr(CO)_3$: Extending the theoretical and photochemical studies on this type of complexes by changing the arene to pyridine ring with substitution on the pyridine ring by electron with drawing group like flouro or CF_3 and compare the resulting results with those observed for the complexes involved in this study. The theoretical and photochemical investigations of the mechanism of the haptotropic reaction.

6.8 References: -

1) Armarego, W.L.F., Perrrin, D.D., *Purification of laboratory chemicals*, 4th edition, Butterworth Heinemann, Oxford, 1996.

2) (a) Herrmann, W.A., *Synthetic Methods of Organometallic and Inorganic Chemistry*, Vol. 1, 119. (b) Strohmeier, W., Muller, F.J., *Chem. Ber.,* 1969,102, 3608.

3) Lees, A. J.; Adamson, A. W., *J. Am. Chem. Soc.,* 1980, 102, 6876.

4) Wrighton, M.S.; Abrahamson, H. B.; Morse, D. L., *J.Am.Chem.Soc*, 1978, 4105, , 17,1, 147.

5) Mahaffy, C.A.L.; Pauson, P.L.; *Inorg. Synth.,* 1974, 19, 154.

6) Rausch, M. D.; Moser, G. A.; Zaiko, E.J.; Lipman, A. L. *J. Organometal. Chem.,* 1970, 23, 185.

7) Drehfahl, G.;Horhold, H.H.; Kuhne, K, *Chem. Ber.*, 1965, 98, 1826.

8) Pidcock, A.; Smith, J.D.; Taylor, B.W., *J. Chem. Soc., A*, 1967,

9) Strohmeier, W., *Chem Ber*, 1961, 94, 3337.

10) Pearson, A.J.; Scoffers, E., *Organometallics,* 1997, 16, 24, 5365.

11) Nesmeyanov; A.N.; Krivykh, V.V.; Kaganovich, R. M.I., *J.Organomet. Chem.*, 1975, 102, 185.

12) Crocock B., *Ph.D. Thesis*, Dublin City University, 1994.

13) Dunkin, I.R., *Matrix Isolation Techniques, A practical Approach*, Oxford University Press, New York, 1998.